UNIVERSITAT DE BARCELONA

Subtypes in Parkinson's disease and Dementia with Lewy bodies: MRI and neuropsychological profiles

Anna Inguanzo Pons

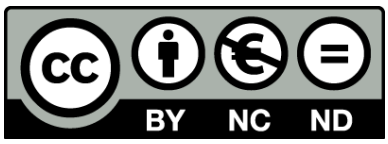

Doctoral Thesis

Subtypes in Parkinson's disease and Dementia with Lewy bodies: MRI and neuropsychological profiles

Anna Inguanzo Pons

Medical Psychology Unit
Department of Medicine
Faculty of Medicine
and Health Sciences

Universitat de Barcelona
2021

Subtypes in Parkinson's disease and Dementia with Lewy bodies: MRI and neuropsychological profiles

Thesis presented by:

Anna Inguanzo Pons

To obtain the degree of Doctor from Universitat de Barcelona in accordance with the requirements of the international PhD diploma

Supervised by:

Dra. Carme Junqué i Plaja and Dra. Bàrbara Segura Fàbregas

Medicine and Translational Research Doctoral Program

Medical Psychology Unit, Department of Medicine

Faculty of Medicine and Health Sciences

University of Barcelona

2021

Les llavors són invisibles, dormen en el secret de la terra
fins que a alguna li ve la fantasia de despertar-se.

Antoine de Saint-Exupéry. El Petit Príncep.

Als meus pares

Als meus avis

Barcelona, 5th July 2021

Dr. Carme Junqué i Plaja and Dr. Bàrbara Segura Fàbregas, professors at the University of Barcelona,

CERTIFY that they have guided and supervised the doctoral thesis entitled 'Subtypes in Parkinson's disease and Dementia with Lewy bodies: MRI and neuropsychological profiles' presented by Anna Inguanzo Pons. They hereby assert that this thesis fulfils the requirements to present her defense to be awarded the title of doctor.

Signatures,

Carme Junqué Plaja
Signat digitalment per Carme Junqué Plaja
Data: 2021.07.05 17:17:21 +02'00'

Dr. Carme Junqué

CPISR-1 C BARBARA SEGURA FABREGAS
Firmado digitalmente por CPISR-1 C BARBARA SEGURA FABREGAS
Fecha: 2021.07.05 20:23:31 +02'00'

Dr. Bàrbara Segura

This Thesis has been undertaken in the Medical Psychology Unit, Department of Medicine, Faculty of Medicine and Health Sciences, University of Barcelona. The group is part of the *Institut d'Investigacions Biomèdiques August Pi i Sunyer* (IDIBAPS) and the *Institute of Neurosciences of the University of Barcelona.*

The present work has been financially supported by a PhD fellowship from the *Universitat de Barcelona, Ajuts de personal Investigador predoctoral en formació* (APIF 2017-2018). In addition, the studies were sponsored by the *Spanish Ministry of Economy and Competitiveness* (PSI2013-41393-P; PSI2017-86930-P), by the *Generalitat de Catalunya* (2014SGR98, 2017SGR748) and by the *Fundació La Marató de TV3 in Catalunya* (20142310).

CONTENTS

FOREWORD

This Thesis, presented to obtain the degree of Doctor by the University of Barcelona, is the result of different studies carried out over a three-year period at the Medical Psychology Unit, Department of Medicine, Faculty of Medicine and Health Sciences, University of Barcelona. The Thesis follows the published papers format and includes two published peer-reviewed papers and a third paper, which is currently under review.

Study 1

Inguanzo A, Sala-Llonch R, Segura B, Erostarbe H, Abos A, Campabadal A, Uribe C, Baggio HC, Compta Y, Marti MJ, Valldeoriola F, Bargallo N, Junque C.

Hierarchical cluster analysis of multimodal imaging data identifies brain atrophy and cognitive patterns in Parkinson's disease. Parkinsonism & Related Disorders. 2021; 82: 16-23.

IF (2019): 3.926. Clinical Neurology: 50/204 (Q1).

Study 2

Inguanzo A, Segura B, Sala-Llonch R, Monte-Rubio G, Abos A, Campabadal A, Uribe C, Baggio HC, Marti MJ, Valldeoriola F, Compta Y, Bargallo N, Junque C.

Impaired Structural Connectivity in Parkinson's Disease Patients with Mild Cognitive Impairment: A Study Based on Probabilistic Tractography. Brain Connectivity. 2021; 11(5): 380-392.

IF (2019): 5.263. Neurosciences: 49/272 (Q1).

Study 3

Inguanzo A, Poulakis K, Mohanty R, Schwarz CG, Przybelski SA, Diaz-Galvan P, Lowe VJ, Boeve BF, Lemstra AW, van de Beek M, van der Flier W, Barkhof F, Blanc F, de Sousa PL, Philippi N, Cretin B, Demuynck C, Nedelska Z, Hort J, Segura S, Junque C, Oppedal K, Aarsland D, Westman E, Kantarci K, Ferreira D.

MRI data-driven clustering reveals different subtypes of Dementia with Lewy bodies. *Under review.*

RELATED ACADEMIC WORK

List of additional publications of the candidate that are the result of collaborative work with other projects, but are not included in the Thesis:

Campabadal A*, **Inguanzo A***, Segura B, Serradell M, Abos A, Uribe C, Gaig C, Santamaria J, Compta Y, Bargallo N, Junque C, Iranzo A. Cortical gray matter progression in idiopathic REM sleep behavior disorder and its relation to cognitive decline. NeuroImage Clinical. 2020; 28: 102421.

* **These authors contributed equally to the manuscript.**

Penades R, Segura B, **Inguanzo A**, Garcia-Rizo C, Catalan R, Masana G, Bernardo M, Junque C. Cognitive remediation and brain connectivity: A resting-state fMRI study in patients with Schizophrenia. Psychiatry Research: Neuroimaging. 2020; 303: 111140.

Oltra J, Segura B, Uribe C, Monte-Rubio G, Campabadal A, **Inguanzo A**, Pardo J, Marti MJ, Compta Y, Valldeoriola F, Iranzo A, Junque C. Sex differences in brain atrophy and cognitive impairment in Parkinson's disease patients with and without probable rapid eye movement sleep behavior disorder. Journal of Neurology. Journal of Neurology. 2021.

Oltra J, Uribe C, Segura B, Campabadal A, **Inguanzo A**, Monte-Rubio G, Pardo J, Marti, MJ, Compta Y, Valldeoriola F, Junque C. Brain atrophy pattern in Parkinson's Disease with probable rapid eye movement sleep behavior disorder and its association with cognitive performance. *Under review.*

LIST OF ABBREVIATIONS

AD Alzheimer's disease
AxD Axial diffusivity
ANOVA Analysis of variance
AUC Area under the ROC Curve
BDI Beck Depression Inventory
BNT Boston naming test
BOLD Blood-Oxygen-Level Dependent
CF Cognitive fluctuations
COMT Catechol-O-methyltransferase
CSF Cerebrospinal fluid
CTh Cortical thickness
DAN Dorsal attention network
DaTSCAN Dopamine transporter imaging
DGM Deep grey matter
DLB Dementia with Lewy bodies
DMN Default mode network
DTI Diffusion tensor imaging
DWI Diffusion-weighted imaging
FA Fractional Anisotropy
FC Function connectivity
FDG Fluorodeoxyglucose
fMRI Functional MRI
FOV Field of view
FRT Facial Recognition Test
GM Grey matter
HC Healthy controls
H&Y Hoehn and Yahr
JLO Judgement of Line Orientation
LEDD L-DOPA daily dose, in mg/day
MAO Monoamine oxidase
MCALT Mayo Clinic Adult Lifespan Template
MCI Mild cognitive impairment
MD Mean Diffusivity
MMSE Mini-Mental State Examination
MNI Montreal Neurological Institute
MoCA Montreal Cognitive Assessment
MRI Magnetic Resonance Imaging
MS Multiple Sclerosis
NBS Network-based statistics
NOS Number of streamlines
NPI Neuropsychiatric Inventory
PD Parkinson's Disease
PDD Parkinson's Disease dementia
PET Positron emission tomography
PiB Pittsburgh Compound B
PIGD Postural instability and gait difficulty
RAVLT Rey Auditory Verbal Learning Test
RBD REM sleep behaviour disorder
RD Radial diffusivity
RF Random Forest
ROC Receiver operating characteristic
ROI Region of interest
SDMT Symbol digit modalities test
SN Substantia Nigra
SPECT Single photon emission computed tomography
TBSS Tract-based spatial statistics
TE Echo time
TFCE Threshold-free cluster enhancement
TFNBS Threshold-free network-based statistics
TIV Total intracranial volume
TMT Trail making test
TR Repetition time
UPDRS Unified Parkinson's disease rating
UPSIT University of Pennsylvania smell identification test scale
VBM Voxel-based morphometry
VFD Visual Form Discrimination Test
VH Visual hallucinations
WM White matter
WMH White matter hyperintensities

SUMMARY

INTRODUCTION: Parkinson's disease (PD) and Dementia with Lewy bodies (DLB) appear as neurodegenerative disorders with a wide range of symptomatology that differs among patients, among which are different levels of cognitive impairment. For instance, mild cognitive impairment (MCI) in PD contributes to a specific clinical profile with a higher risk of developing dementia. Looking at PD and DLB together provides evidence of the existence of different subtypes within both diseases. In recent years, complex imaging techniques, such as magnetic resonance imaging (MRI), have been used to study pathologies of the brain. MRI measures can be used to better characterize the brain basis of PD and DLB symptomatology, such as MCI. The reconstruction of the whole-brain connectome is a complex approach that can help to describe the heterogeneous symptomatology in neurodegenerative disorders. In addition, MRI in combination with new data-driven methods, such as cluster analysis, has been used to group patients according to their similarities, which allows subtypes to be identified. Until now, most studies in PD have described subtypes based on clinical and neuropsychological data, and just a few have used MRI measures to identify subtypes with different brain patterns. As DLB research is still in a relatively early stage, no cluster analyses have been yet performed based on MRI data.

OBJECTIVES AND HYPOTHESES: Given this context, the current Doctoral Thesis focuses on the heterogeneity that characterizes PD and DLB. The main objectives were to identify subtypes based on structural MRI measures in PD and DLB, as well as to characterize the structural brain connectivity of PD associated with MCI. We hypothesized that there would be PD subtypes with different patterns of grey and white matter alterations that would be associated with particular clinical and cognitive profiles. We also hypothesized that there would be DLB subtypes characterized by different grey matter (GM) patterns, and that these patterns would explain specific symptomatology of the disease and would be differentially associated to concomitant brain changes seen in cerebrovascular and Alzheimer's diseases. Finally, we expected that PD-MCI would present a characteristic

pattern of impaired structural connectivity. In order to examine and clarify these issues, the current Doctoral Thesis is presented as a compendium of three studies.

METHODS: In Study 1, to identify subtypes in PD, we performed a hierarchical cluster analysis based on multimodal imaging using the Ward's linkage method. We performed the analysis in a sample of 62 PD patients. GM volumes of cortical and subcortical brain regions as well as fractional anisotropy (FA) white matter (WM) measures were combined. Once the subtypes were identified, voxel-based morphometry (VBM) and tract-based spatial statistics (TBSS) analyses were carried out in order to compare the pattern of GM and WM of the PD subtypes to the 33 healthy control group. Demographical, clinical and neuropsychological data were used to characterize the subtypes.

In Study 2, the sample consisted of 27 PD-MCI and 35 PD without MCI, as well as 51 healthy controls. In this study we applied threshold-free network-based statistics (TFNBS), a novel technique based on whole-brain probabilistic tractography data useful to study structural connectivity. We complemented the analysis with TBSS and graph theory analyses (global and local measures).

Study 3 included 165 DLB subjects from the Mayo Clinic and 3 centres from the European DLB consortium (E-DLB). We performed a cluster analysis based on GM volumes using a random forest method, and characterized the subtypes based on GM volumes, clinical, demographical data as well as tau, β-amyloid and cerebrovascular biomarkers. Additionally, we characterized cognitive trajectories of the subtypes in a 3-year follow-up.

RESULTS: In Study 1, we identified 3 PD subtypes which mainly differed in GM patterns, while WM involvement appeared to be more limited. PD1 (24%) was characterized by temporo-parieto-occipital GM atrophy and subcortical atrophy, as well as FA reductions mainly affecting fronto-occipital WM tracts. This subtype was the oldest and had the worse neuropsychological profile. The second subtype, PD2 (34%), was characterized

by GM atrophy limited to frontal and temporal cortical regions, and a third subtype, PD3 (42%), with non-detectable GM atrophy or WM impairment, and preserved cognitive profile.

In Study 2, we found that PD patients had fewer streamlines (NOS) compared with healthy controls. Structural connectivity impairments were present in PD with and without MCI. However, the pattern and degree of connectivity impairment were different. PD-MCI showed a higher number of abnormal connections, primarily involving those between deep GM structures and cortical regions and posterior cortico-cortical connections, mainly in the temporal and occipital regions. PD without MCI showed fewer altered connections, and unlike PD-MCI, they were mainly located in the bilateral prefrontal cortex. What is more, the logistic regression and ROC curve analysis showed that the decreased NOS in the impaired connections characteristic of PD-MCI, were able to discriminate between both PD groups with high accuracy. The TBSS analysis revealed that only PD-MCI had reduced FA values compared to controls. The graph theory analysis showed PD groups differed in local graph measures.

In Study 3, three DLB subtypes with the same disease evolution were identified based on their GM volumes. The cortical predominant subtype (30%) was characterized by widespread reduced cortical GM, older age, worse cognition at baseline and faster cognitive decline over 3 years. The second subtype, the fronto-occipital subtype (46%), had lower GM volumes in frontal and occipital regions. Finally, the subcortical predominant subtype (24%) was characterized by the greatest GM volumes, and relatively low GM volumes in the basal ganglia, as they were the only brain regions where the 3 subtypes had equivalent GM volumes. The subcortical predominant subtype was also characterized by the highest frequency of cognitive fluctuations.

CONCLUSIONS: Our overall findings support the existence of different PD and DLB subtypes that can be identified by means of cluster analyses based on MRI data, which are in turn associated with specific cognitive profiles, and that cognitive impairment in PD is also associated to a specific pattern of structural connectivity impairment. These

results contribute to clarifying the basis of heterogeneity in DLB and PD and give further information about which characteristics could be considered biomarkers of worse prognosis, with the final aim of approaching a more personalized medicine.

RESUM EN CATALÀ

Subtipus dins de la malaltia de Parkinson i de la Demència amb cossos de Lewy: IRM i perfils neuropsicològics

INTRODUCCIÓ: La malaltia de Parkinson i la Demència amb cossos de Lewy són malalties neurodegeneratives que es presenten amb una àmplia varietat de símptomes, els quals difereixen entre pacients. El deteriorament cognitiu lleu, per exemple, és un possible símptoma de la malaltia de Parkinson que contribueix en un perfil clínic concret amb un elevat risc de desenvolupar demència. Tot plegat aporta evidència de l'existència de diferents subtipus (grups) dins d'ambdues malalties. En els últims anys, s'han utilitzat tècniques d'imatge complexes, com la imatge per ressonància magnètica (IRM), per estudiar les malalties que afecten al cervell. Les diferents mesures obtingudes de la IRM, es poden utilitzar per caracteritzar les bases de la simptomatologia de la malaltia de Parkinson i de la Demència amb cossos de Lewy, com per exemple el deteriorament cognitiu lleu. La reconstrucció del connectoma de tot el cervell és una aproximació complexa que pot ajudar a descriure la simptomatologia heterogènia de les malalties neurodegeneratives, a més, la IRM en combinació amb noves tècniques guiades per les dades, com els anàlisis de clúster, s'han utilitzat per agrupar els pacient d'acord a les seves similituds, el que permet trobar subtipus de pacients. Fins ara, la majoria dels estudis en la malaltia de Parkinson han trobat subtipus basant les anàlisis en dades clíniques i neuropsicològiques, i només escassos treballs s'han basat en dades derivades d'IRM. En la Demència amb cossos de Lewy, degut a que la recerca es troba en fases més primerenques que no pas la recerca en la malaltia Parkinson, encara no s'ha realitzat cap anàlisis de clúster basat en dades d'IRM.

OBJECTIUS I HIPÒTESIS: Donat aquest context, la Tesi Doctoral que aquí es presenta es centra en l'heterogeneïtat que caracteritza la malaltia de Parkinson i a la Demència amb cossos de Lewy. Els objectius principals han estat identificar subtipus basats en dades d'IRM en Parkinson i Demència amb cossos de Lewy, així com caracteritzar la connectivitat cerebral a nivell estructural del deteriorament cognitiu lleu en la malaltia

de Parkinson. Hem hipotetitzat que hi haurien subtipus en la malaltia de Parkinson que presentarien diferents patrons d'alteració de la substància grisa i la substància blanca que s'associarien amb un perfil clínic i cognitiu específic. En aquesta línia també hem hipotetitzat que hi haurien subtipus dins de la Demència amb cossos de Lewy que es caracteritzarien per diferents patrons d'alteració de la substància grisa, i que aquests patrons, podran explicar diferències en la simptomatologia de la malaltia i es trobaran diferencialment associats a marcadors biològics d'altres processos degeneratius associats a l'envelliment, com els canvis que es troben en processos cerebrovasculars i en la malaltia d'Alzheimer. Finalment, esperaríem que el deteriorament cognitiu lleu en la malaltia de Parkinson presentés un patró característic de connectivitat estructural alterada. Amb la intenció de donar resposta a aquestes qüestions, l'actual Tesi Doctoral es presenta com un compendi de 3 estudis.

MÈTODES: En l'estudi 1, per tal d'identificar subtipus en la malaltia de Parkinson, es va dur a terme un anàlisis de clúster jeràrquic aglomeratiu, utilitzant dades multimodals d'IRM. L'anàlisi es va dur a terme en una mostra de 62 pacients i es van combinar volums de substància grisa de regions corticals i subcorticals amb mesures d'anisotropia fraccional de la substància blanca. Un cop identificats els subtipus, es va dur a terme una morfometria basada en vòxels (voxel-based morphometry (VBM), en anglès) i una estadística espacial basada en tractes (Tract-based spatial statistics (TBSS), en anglès) per tal de comparar els patrons de substància grisa i blanca amb un grup de 33 controls sans. A més, vam utilitzar dades demogràfiques, clíniques i neuropsicològiques per caracteritzar els subtipus.

A l'estudi 2, la mostra consistia en 27 pacients amb malaltia de Parkinson i deteriorament cognitiu lleu i 35 pacients sense deteriorament cognitiu, així com de 51 controls sans. En aquest estudi vam aplicar una tècnica nova que en anglès rep el nom de *threshold-free network-based statistics (TFNBS),* aquesta tècnica resulta útil per estudiar la connectivitat estructural i la vam utilitzar amb dades de tractografia probabilística de tot el cervell. A més, vam complementar l'anàlisi amb TBSS i mesures globals i locals de graf.

A l'estudi 3, vam incloure 165 pacients amb Demència amb cossos de Lewy que procedien de la Clínica Mayo i de 3 centres que formen part del consorci europeu de Demència amb cossos de Lewy, abreviat com a E-DLB. Vam realitzar un anàlisi de clúster basat en *random forest* en el que hi vam introduir volums de substància grisa de regions corticals i subcorticals de tot el cervell. En conseqüència, els subtipus els vam caracteritzar en base als volums de substància grisa, però també en base a dades clíniques, demogràfiques i de biomarcadors de tau, β-amiloide i malaltia cerebrovascular. A més, vam caracteritzar les trajectòries cognitives dels subtipus amb un seguiment de 3 anys.

RESULTATS: A l'estudi 1, vam definir 3 subtipus en la malaltia de Parkinson que principalment diferien en substància grisa, mentre que la implicació de la substància blanca era molt baixa. El primer subtipus (PD1, 24%) es caracteritzava per presentar atròfia de la substància grisa a nivell de còrtex temporal, parietal i occipital així com en regions subcorticals. A més, presentava reduccions de l'anisotropia fraccional principalment en tractes fronto-occipitals de substància blanca. Aquest subtipus, el PD1, incloïa als pacients de més edat amb el pitjor perfil neuropsicològic. El segon subtipus (PD2, 34%) es caracteritzava per atròfia de la substància grisa en regions frontals i temporals. El tercer subtipus (PD3, 42%), no presentava alteracions detectables ni a nivell de substància grisa ni de blanca, i presentava un perfil cognitiu preservat.

En l'estudi 2, vam trobar que els pacients amb malaltia de Parkinson presentaven menor número de fibres en nombroses connexions cerebrals en comparació amb controls sans. Es van trobar alteracions en la connectivitat estructural tant en pacients amb deteriorament cognitiu lleu com sense deteriorament cognitiu, tot i així, el patró i grau de les alteracions en connectivitat estructural eren diferents entre grups de pacients. Els pacients amb deteriorament cognitiu lleu presentaven major número de connexions alterades, les quals principalment involucraven connexions corticals en regions temporals i occipitals així com connexions entre l'escorça cerebral i els nuclis grisos de la base. Els pacients amb malaltia de Parkinson però sense deteriorament cognitiu, presentaven menys connexions alterades que, a diferència dels pacients amb

deteriorament cognitiu lleu, es localitzaven principalment en regions bilaterals del còrtex prefrontal. A més, la regressió logística i la corba ROC van mostrar que el número reduït de fibres en les connexions alterades que caracteritzaven el grup de pacients amb deteriorament cognitiu lleu, permetien la discriminació entre els dos grups de pacients amb una precisió elevada. L'anàlisi de TBSS va mostrar que només el pacients amb deteriorament cognitiu lleu presentaven reduccions en l'anisotropia fraccional en comparació al grup de controls sans, i l'anàlisi de graf va mostrar que els 2 grups de pacients diferien en mesures locals.

En l'estudi 3, es van identificar 3 subtipus dins de la Demència amb cossos de Lewy en base als volums de substància grisa. El subtipus amb predominança cortical (30%) es caracteritzava per una reducció generalitzada dels volums corticals de substància grisa, incloïa els pacients de més edat, pitjor cognició global i deteriorament cognitiu més ràpid en el transcurs de 3 anys. El segon subtipus, el fronto-occipital (46%), presentava menors volums de substància grisa en regions frontals i occipitals. Finalment, el subtipus amb predominança subcortical (24%), es caracteritzava per majors volums de substància grisa en regions corticals i volums relativament baixos en estructures subcorticals, donat que eren les úniques estructures en les que no hi havia diferències entre els 3 subtipus. Aquest últim subtipus amb predominança subcortical, també es caracteritzava per una major freqüència de pacients amb fluctuacions cognitives.

CONCLUSIONS: En conjunt, les troballes presentades en aquesta Tesi Doctoral donen suport a l'existència de diferents subtipus, tant en la malaltia de Parkinson com en la Demència amb cossos de Lewy, que poden ser identificats mitjançant anàlisis de clúster basats en dades d'IMR. A més, aquests subtipus reflecteixen perfils cognitius específics. El deteriorament cognitiu en la malaltia de Parkinson també es troba associat a un patró concret d'alteracions en connectivitat estructural. Així, aquests resultats contribueixen a aclarir les bases de l'heterogeneïtat descrita en la malaltia de Parkinson i en la Demència amb cossos de Lewy, i aporten informació rellevant sobre quines característiques podrien ser considerades com biomarcadors de pitjor pronòstic, amb l'objectiu final d'apropar-nos a una medicina més personalitzada.

CHAPTER 1

Introduction

1.1. A BIT OF HISTORY

In 1817 the doctor James Parkinson published "An Essay on the Shaking Palsy", in which, based on the observation of 6 patients, he described a nervous disorder characterized by a trembling of the limbs at rest, decreased muscular power and a stooped posture associated with a festinating gait (Goetz et al., 2011 for a review).

Six decades after Parkinson's essay, Jean-Martin Charcot (Goetz et al., 2011 for a review) named the disease and disentangled certain important aspects, such as the fact that it did not necessarily course with tremor and that the slowness of movement, known as bradykinesia, was a cardinal feature. Interestingly, he and his students also described two variants of the disease - tremorous and rigid/akinetic. Nowadays Parkinson's disease is defined as bradykinesia in combination with either rest tremor, rigidity, or both (Postuma et al., 2015 for a review).

In 1912, Fritz Heinrich Lewy described the depositions of protein that characterize PD in brain regions outside the substantia nigra. About 7 years later, another researcher found similar aggregates in the substantia nigra, which he called Lewy bodies. However, it was not until the mid-1980s, when immunocytochemical methods were developed, that α-synuclein was identified as the protein forming the Lewy bodies (Obeso et al., 2017 for a review). The clinical progression of PD was described later by Hoehn and Yahr (H&Y) in what became a well-known international scale. The five-stage scale consisted of unilateral (stage I) and bilateral disease (stages II to V) and the development of postural reflex impairment (stage III) as a key turning point in PD (Hoehn and Yahr 1967).

In 1990, in the context of the Lewy body diseases, the researcher Kenji Kosaka pointed out the difference between autopsied cases with younger onset and presence of parkinsonism before dementia, and cases with dementia preceding parkinsonism. In 1995, in the first international workshop to approach this disease, the term Dementia

with Lewy bodies (DLB) was established as well as its pathological guidelines, making possible, from that moment, the diagnosis of DLB (Kosaka, 2014 for a review).

Figure 1: Timeline of the main events in the history of Parkinson's disease

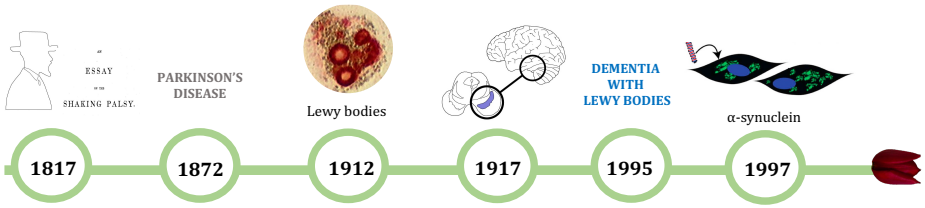

(Lewy bodies image extracted from Levin et al., 2016
and α-synuclein drawing extracted from Mehra et al., 2019.)

1.2. DIAGNOSIS AND TREATMENT OF PARKINSON'S DISEASE & DEMENTIA WITH LEWY BODIES

1.2.1. Diagnosis and symptomatology

Clinical diagnosis of PD is based on the presence of parkinsonism, specifically, the presence of bradykinesia in combination with rest tremor, rigidity, or both (Table 1). The UK Parkinson's Disease Society Brain Bank (Gibb and Lees, 1988) and the International Parkinson and Movement Disorder Society have established the criteria for clinical and research diagnosis (Postuma et al., 2015). The motor manifestations of PD can be evaluated with section III of the Unified Parkinson's disease rating scale (UPDRS) (Fahn and Elton, 1987), as well as its revised version by the Movement Disorders Society (MDS-UPDRS) (Goetz et al., 2008).

Table 1: Motor and non-motor symptomatology of Parkinson's disease

Symptom	**Definition or main features**
CORE MOTOR SYMPTOMATOLOGY	
Bradykinesia	Slowness of movement and reduction in speed or amplitude as the voluntary movement is continued. It can involve reduced facial expression (hypomimia), low voice (hypophonia), and slowness in everyday activities.
Rigidity	Increase in muscle tone when the patient is in a relaxed position. It specifically refers to "lead-pipe" resistance which implies consistent resistance to passive movement.
Rest tremor	Tremor that takes place in a frequency between 4 to 6 Hz in the limbs at rest.

NON-MOTOR SYMPTOMATOLOGY	
Hyposmia/Anosmia	Decreased/absent sense of smell
Sleep dysfunction	REM sleep behaviour disorder (RBD) Daytime sleepiness Sleep-maintenance insomnia
Autonomic dysfunction	Constipation Delayed gastric emptying Urinary urgency and frequency Orthostatic hypotension Blood pressure variability
Psychiatric disturbances	Depression Anxiety Apathy Psychosis
Cognitive impairment	Mild cognitive impairment (MCI) or dementia often initially affecting attention, executive and visuospatial functions.
Others	Hypophonia (softening of the voice) Fatigue Sialorrhea (drooling or excessive salivation) Trouble swallowing

It is well-known that PD is also accompanied by a wide range of non-motor features that can appear decades before the motor symptomatology (Figure 2).

Figure 2: Clinical symptoms associated with Parkinson's disease progression

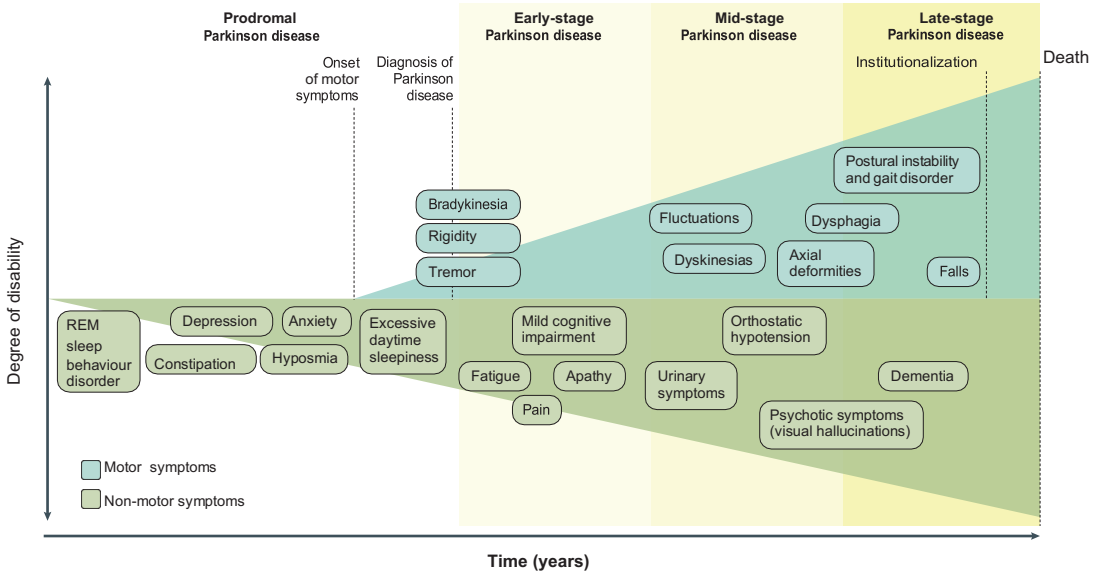

(Extracted from Poewe et al., 2017)

Additional non-motor symptoms can appear after the diagnosis and develop with the disease progression. The non-motor symptomatology includes olfactory impairment, REM sleep behaviour disorder (RBD), gastrointestinal dysfunction, depression, and cognitive impairment that can lead to dementia, among others (Pfeiffer et al., 2016).

When well-established PD patients develop dementia, we use the term Parkinson's disease dementia (PDD), which shares many characteristics with DLB. However, the temporality of the events is the main key in differentiating them, as DLB should be diagnosed when dementia occurs before or concurrently with parkinsonism (McKeith et al., 2017) (Panel 1).

Panel 1: Criteria for the clinical diagnosis of probable and possible DLB

(McKeith et al., 2017)

Essential for a diagnosis of DLB is dementia, defined as a progressive cognitive decline of sufficient magnitude to interfere with normal social or occupational functions, or with usual daily activities. Prominent or persistent memory impairment may not necessarily occur in the early stages but is usually evident with progression. Deficits on tests of attention, executive function, and visuoperceptual ability may be especially prominent and occur early.

Core clinical features *(The first 3 typically occur early and may persist throughout the course.)*

- Fluctuating cognition with pronounced variations in attention and alertness.
- Recurrent visual hallucinations that are typically well formed and detailed.
- RBD, which may precede cognitive decline.
- One or more spontaneous cardinal features of parkinsonism: bradykinesia, rest tremor, or rigidity.

Supportive clinical features

Severe sensitivity to antipsychotic agents; postural instability; repeated falls; syncope or other transient episodes of unresponsiveness; severe autonomic dysfunction, e.g., constipation, orthostatic hypotension, urinary incontinence; hypersomnia; hyposmia; hallucinations in other modalities; systematized delusions; apathy, anxiety, and depression.

Indicative biomarkers

- Reduced dopamine transporter uptake in basal ganglia demonstrated by SPECT or PET.
- Abnormal (low uptake) ^{123}iodine-MIBG myocardial scintigraphy.
- Polysomnographic confirmation of REM sleep without atonia.

Supportive biomarkers

- Relative preservation of medial temporal lobe structures on CT/MRI scan.
- Generalized low uptake on SPECT/PET perfusion/metabolism scan with reduced occipital activity ± the cingulate island sign on FDG-PET imaging.
- Prominent posterior slow-wave activity on EEG with periodic fluctuations in the pre-alpha/ theta range.

Probable DLB can be diagnosed if:

a. Two or more core clinical features of DLB are present, with or without the presence of indicative biomarkers, or **b**. Only one core clinical feature is present, but with one or more indicative biomarkers.

Probable DLB should not be diagnosed on the basis of biomarkers alone.

Possible DLB can be diagnosed if:

a. Only one core clinical feature of DLB is present, with no indicative biomarker evidence, or **b.** One or more indicative biomarkers is present but there are no core clinical features.

DLB is less likely:

a. In the presence of any other physical illness or brain disorder including cerebrovascular disease, sufficient to account in part or in total for the clinical picture, although these do not exclude a DLB diagnosis and may serve to indicate mixed or multiple pathologies contributing to the clinical presentation, or **b**. If parkinsonian features are the only core clinical feature and appear for the first time at a stage of severe dementia.

In research studies in which distinction needs to be made between DLB and PDD, the existing **1-year rule** between the onset of dementia and parkinsonism continues to be recommended.

1.2.2. Imaging biomarkers

The heterogeneous symptomatology of PD and DLB overlaps with other neurodegenerative disorders, sometimes making an accurate diagnosis difficult (Abdo et al., 2010 for a review). In this context, imaging techniques, such as positron emission tomography (PET) and single-photon emission computed tomography (SPECT), which use ionising radioactive ligands to quantify receptors, transporters, or enzymes; and magnetic resonance imaging (MRI), which uses different sequences and contrasts to study the structure of the brain and its function, are proposed as complementary tools for differential diagnosis (Blamire, 2018 for a review).

Imaging with PET and SPECT focused on the dopaminergic function, uses as common targets the vesicular monoamine transporter type 2 (VMAT2); L-aromatic amino acid decarboxylase (L-AAAD), an enzyme that converts L-DOPA to dopamine; and the dopamine transporter (DAT) (Pagano et al., 2016 for a review). Specifically, DAT SPECT imaging, which employs the ^{123}I-FP-CIT ligand and is commercially known as DaTSCAN, is commonly used in clinics to diagnose PD. Molecular imaging in PD can detect a marked signal loss in the posterior putamen, being frequently asymmetric and contralateral to the most clinically affected side of the body (Pagano et al., 2016 for a review; Poewe et al., 2017 for a review).

In DLB, as well as in PD, the DaTSCAN is also used for differential diagnosis as it presents with reduced uptake in basal ganglia, which allows differentiating between DLB and AD (McKeith et al., 2017 for a review). Moreover, ^{18}F-fluorodeoxyglucose (FDG), a radiotracer used in PET that reflects the uptake of glucose, which in turn correlates with the metabolism of the tissue, has provided supportive biomarkers for DLB. Occipital hypometabolism of FDG-PET has been correlated to neuropathology of the visual cortex and, additionally, the relative preservation of the posterior cingulate, called the cingulate island, has been described as a useful radiological sign of DLB (McKeith et al., 2017 for a review).

PET imaging is also used to quantify other relevant biomarkers. The radiotracer Pittsburgh compound B (PiB), which quantifies β-amyloid, is appropriate for AD diagnosis as well as PDD diagnosis. Tau deposits can also be captured with fluorine 18-labeled AV-1451 ([^{18}F]AV-1451) (Saeed et al., 2017 for a review).

MRI appears to be useful in identifying cerebrovascular lesions, which allows differentiating between idiopathic PD and vascular parkinsonism. In addition, accurate methods for measuring the thickness of human cerebral cortex, the volume of grey matter (GM) in cortical and subcortical structures, white matter (WM) integrity and brain activity appear as powerful tools to study neurodegenerative disorders (Panel 2). MRI has been described as a suitable technique to discern between PD, Multiple System Atrophy (MSA) and Progressive Supranuclear Palsy (PSP) as they course with different patterns of reduced fractional anisotropy (FA) (Cochrane and Ebmeier, 2013 for a review; Ota et al., 2013) as well as different patterns of atrophy (Ota et al., 2013). In addition, the preservation of the medial temporal lobe can help to differentiate DLB from AD (McKeith et al., 2017 for a review).

Although nuclear imaging as well as MRI has been an invaluable tool in research for decades and has showed their potential in elucidating the mechanisms underlying PD, there are only a few biomarkers supported in clinics. Further research, as well as longitudinal analyses, are still required to extrapolate all the evidence found in research to the clinical setting (Strafella et al., 2018 for a review).

Panel 2: MRI techniques

STRUCTURAL MRI

*Cortical thickness (**CTh**):* Measurement of the distance between the boundary that separates the WM from the pial surface. The distance between these two surfaces gives the thickness of the cortical GM.

*Voxel-based morphometry (**VBM**):* Technique that estimates the amount of GM in a voxel through its signal intensity (Whitwell, 2009). Unlike cortical thickness, it also allows to study subcortical structures, as their volumes can also be estimated.

*Diffusion tensor imaging (**DTI**):* Technique sensitive to the microdiffusion of water molecules, that allows to characterize WM integrity and architecture.

(Please see sections "DTI metrics, fibre tracking and structural connectivity", page 70).

Detailed explanation of the structural MRI techniques can be found in the Methods Chapter.

FUNCTIONAL MRI

The fMRI allows measurement of brain activity by detecting low frequency fluctuations in the blood oxygen level-dependent (BOLD) signal (Lee et al., 2013). There are two modalities: resting-state and task-based fMRI. In resting-state fMRI the participants must remain awake without thinking in anything in particular (keeping the mind blank); while task-based fMRI requires the participants to perform a specific task, such as a visual perception assignment. Functional connectivity is defined as the temporal dependency of neuronal activation patterns of anatomically separated brain regions (van den Heuvel and Hulshoff Pol, 2010).

1.2.3. Pharmacological treatment

PD treatment consists mainly of managing the motor symptomatology with drugs that increase dopamine concentrations or that stimulate the dopamine receptors. The most common drugs are levodopa (or L-DOPA), which is the precursor of dopamine; dopamine agonists, as well as monoamine oxidase type B inhibitors (MAO-B), and catechol-O-methyltransferase (COMT) inhibitors, which block the enzyme that breaks down dopamine, and the one that methylates it, respectively (Jankovic and Tan, 2020 for a review).

Levodopa is the most efficient treatment to manage the motor symptomatology of PD; however, its long-term use is related to motor complications including dyskinesia (involuntary muscle movements resembling tics), 'wearing-off' phenomenon (the effects of levodopa disappear or reduce before it is time for the following levodopa dose) and unpredictable 'on–off' fluctuations (motor fluctuations). To minimize the motor long-term side effects, the levodopa-sparing initial therapy may be recommended. It consists of starting the treatment with dopamine agonists or monoamine oxidase type B inhibitors. Other common side effects of PD treatments can be nausea, somnolence, oedema, orthostatic hypotension, sedation, confusion, sleep disturbance and hallucinations (Jankovic and Tan, 2020 for a review). Specially related to dopamine agonists are impulsive control disorders such as gambling and binge eating (Kalia and Lang, 2015 for a review; Strafella et al., 2018 for a review). Due to its side effects, levodopa is almost always combined with carbidopa or benserazide, which are aromatic acid decarboxylase inhibitors that significantly reduce nausea by avoiding dopamine peripheral metabolism (Jankovic and Tan, 2020 for a review).

The heterogeneity of symptomatology causes different patients to require different doses of levodopa combined with different types of drugs. To address this problem, the levodopa equivalent daily dose (LEDD) can be calculated by considering the quantity of levodopa that has a comparable effect to the other drugs taken (Tomlinson et al., 2010

for a review). Apart from the clinical advantages, LEDD also allows the comparison between patients in the research field.

DLB treatment, unlike PD, is focused on non-motor symptomatology. The use of medication targeting movement impairment, such as levodopa, is often restricted in DLB patients as they are less responsive than PD to this medication, and prone to mental deterioration involving cognition and behaviour that can lead to confusion, psychosis, and exacerbation of hallucinations (Boot, 2015 for a review). The use of cholinesterase inhibitors has been supported to improve cognition in DLB (Sezgin et al., 2019 for a review) as well as in PDD (Sasikumar and Strafella, 2020 for a review). The use of antipsychotics to treat symptomatology like visual hallucinations should be avoided as, in dementias, they are associated with mortality risk; while novel drugs targeting the serotoninergic system look promising to treat the neuropsychiatric symptoms (McKeith et al., 2017 for a review).

A comprehensive treatment plan can significantly improve the quality of life of PD and DLB patients; however, there is still no medication available that can alter the progression of the disease.

1.3. NEUROPATHOLOGY OF PARKINSON'S DISEASE & DEMENTIA WITH LEWY BODIES

Neurodegenerative disorders are the product of a complex interaction of genetic and environmental factors that ultimately compromise the proper functioning of neurons. The aggregation of misfolded proteins has been found to be a hallmark of neurodegenerative disorders, and potentially the main cause of neuronal death. An example of protein inclusions are the ones made of α-synuclein, which are known as Lewy bodies and are the main characteristic of α-synucleinopathies, such as PD and DLB.

1.3.1. Braak staging

Braak staging views the progression of the disease according to α-synuclein deposits in the brain. It consists of 6 stages (Braak et al., 2003; Braak et al., 2006a; Braak and Del Tredici, 2008); the beginning can be either in the olfactory bulb or the medulla oblongata (stages I and II), which could explain the non-motor symptomatology such as olfactory, and autonomic disfunctions that precede motor symptoms. Then, it would ascend to the pons and basal forebrain, which includes the ventral pallidum (stages III and IV). These intermediate stages are associated with sleep disturbances and the core motor symptomatology of parkinsonism. Consequently, it is usually in these stages when the diagnosis of PD is done. Lastly, it spreads to the neocortex (stages V and VI), from the prefrontal cortex and associative sensory regions, extending to the premotor and primary sensory cortex (Figure 3).

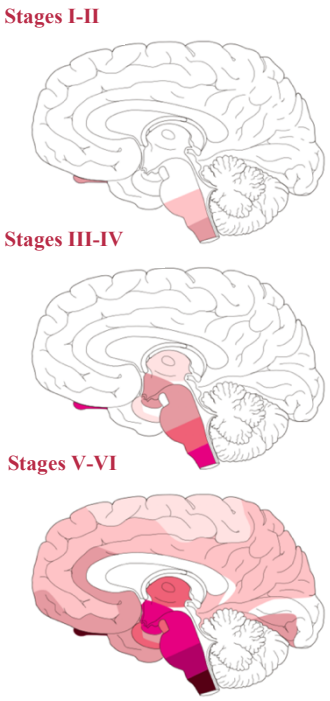

Figure 3: Propagation of α-synculein in the human brain following the Braak staging (Extracted from Goedert et al., 2015).

The last stages are related to severe motor symptoms as well as mood fluctuations, cognitive impairment, and dementia (Braak et al., 2006b).

Braak staging has not been without controversy, as some studies supported it while others rejected it (Jellinger, 2009 for a review). This hypothesis has appeared useful to describe the neuropathological evolution of PD (Jellinger, 2004; Halliday et al., 2008) but insufficient in most advanced stages (Jellinger, 2009), particularly in dementia (Jellinger, 2008) were β-amyloid and tau-containing neurofibrillary tangles coexist (Irwin et al., 2013). It has also failed to describe a PD phenotype characterized by late onset and fast progression of the disease (Halliday et al., 2008).

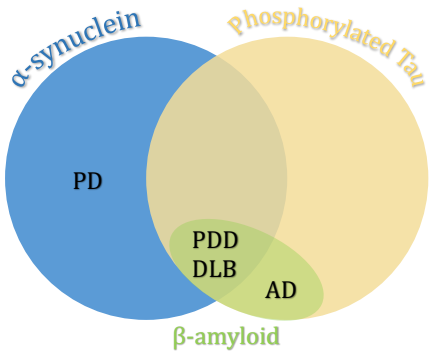

Figure 4: Biomarkers of Parkinson's disease (PD), Parkinson's disease dementia (PDD), Dementia with Lewy Bodies (DLB) and Alzheimer's disease (AD). Synucleinopathies are shown in blue, tauopathies in yellow and β-amyloid pathology is shown in green (Adapted from Zhang et al., 2017).

The validity of Braak staging according to α-synuclein deposits, is still to be established in DLB, and it will require the study of patients with different levels of severity in cognition and extrapyramidal symptoms (McKeith et al., 2005). DLB can course with Alzheimer's disease (AD) pathology (β-amyloid plaques and tau inclusions), leading to a PD/AD mixed pathology (Zhang et al., 2017) (Figure 4). In consequence, the current pathological assessment of DLB combines the Lewy Bodies related pathology categories (diffuse cortical, limbic, brainstem-predominant, amygdala-predominant, and olfactory bulb only) (McKeith et al., 2017 for a review) with AD categories related to the Braak staging of β-amyloid plaques and tau inclusions (Montine et al., 2012; McKeith et al., 2017 for a review).

1.3.2. Genetics

Genetic forms represent a low percentage of PD cases. However, they contribute to understand the neuropathological mechanisms underlying the disease. Autosomal dominant forms of PD had been linked to missense mutations as well as duplications and triplications of the SNCA gene (Kalia and Lang, 2015 for a review), which encodes for α-synuclein. The abnormalities in this protein can lead to aberrant soluble oligomeric conformations of the protein, causing the death of dopaminergic neurons by targeting different intracellular processes, including synaptic function. Additionally, secreted α-synuclein may be able to spread through prion-like transmission, contributing to disease propagation (Figure 5).

Mutations in the LRRK2, the gene encoding the leucine-rich repeat kinase-2, also known as PARK8 and Dardarin, have been associated with a higher risk of suffering from autosomal dominant, late-onset PD, clinically indistinguishable from idiopathic PD (Gandhi et al., 2009).

On the other hand, early-onset PD has been associated to mutations in Parkin (Lücking et al., 2000) and glucocerebrosidase (GBA) (Goker-Alpan et al., 2004). Parkin is a gene that encodes for E3 ubiquitin ligase, a widely expressed enzyme that links ubiquitins to a substrate protein which ultimately leads to its degradation in the proteosome, while GBA encodes a lysosomal protein that degrades glucocerebroside. Mutations in this gene may be contributing to PD pathogenesis by altering lysosomal homeostasis, endoplasmic reticulum stress, or mitochondrial damage (Do et al., 2019) (Figure 5).

Mutations in the microtubule-associated protein tau (MAPT), the protein responsible for the cell cytoskeleton stability, have been associated with several neurodegenerative disorders including PD. Interestingly, genome-wide association studies (GWAS) have shown that variability in SNCA, LRRK2, and MAPT are risk factors for sporadic PD, as well as the locus PARK16 (Simón-Sánchez et al., 2009).

DLB, as well as PD, is mostly sporadic, although rare autosomal dominant forms have also been associated with the most prevalent mutations in PD: SNCA, LRRK2 and GBA. Carrying the H1 haplotype of the MAPT is also a risk factor for DLB (Labbé et al., 2016). Additionally, *APOE* ε4 allele, a strong risk factor for AD, appears to be over-represented in DLB (Walker et al., 2015).

Figure 5: Cellular processes involved in the pathogenesis of Parkinson's disease

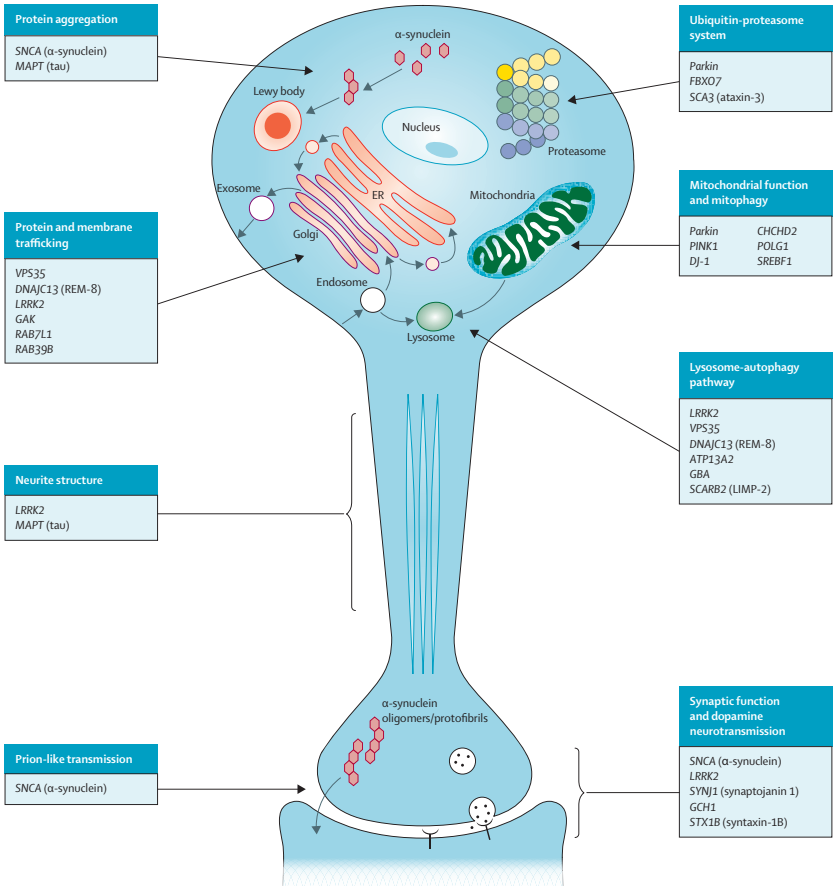

(Extracted from Kalia and Lang, 2015).

1.4. HETEROGENEITY IN PARKINSON'S DISEASE

PD is a complex neurodegenerative disorder characterized by a broad spectrum of motor and non-motor symptoms (Figure 2) that can differ in temporality and intensity among patients. In this context, many studies have focused on subtyping PD. The first subtyping approaches were based on a priori hypothesis using a single classification feature, moving to data-driven hypothesis-free approaches, such as clustering, to divide PD samples into subtypes.

1.4.1. Motor symptoms

In 1990, in a moment where researchers had started to study subsamples within PD, Jankovic et al., (1990) classified a PD sample of 800 patients from the DATATOP database, according to demographic and clinical characteristics, to study the potential subgroups that could be gathered in PD. They supported the clinical subtypes by giving evidence of at least 2 different PD trajectories according to the motor symptomatology: the tremor dominant subtype and the postural instability and gait difficulty predominant (PIGD) subtype. The tremor-dominant group is characterized by tremor that can be postural, akinetic or present at rest, the tremor at rest being the most common feature in PD that helps to distinguish it from essential tremor (Moustafa et al., 2016). On the other hand, the PIGD or akinetic/rigid subtype is characterized by significant axial rigidity and absence of tremor and can be accompanied by bradykinesia and rigidity (Nutt, 2016 for a review). PIGD has been related to a worse course of the disease compared to tremor predominant (Jankovic et al., 1990; Jankovic and Kapadia, 2001), as well as to more depression and difficulties in everyday activities (Jankovic et al., 1990; Burn et al., 2012) and dementia (Alves et al., 2006).

MRI has been used to study structural differences between the 2 motor profiles. The PIGD subtype has been seen to have reduced widespread GM volumes (Rosenberg-Katz et al., 2013), as well as altered structural connectivity in cortico-basal ganglia connections (Barbagallo et al., 2017) when compared to the tremor subtype.

Conversely, analyses based on WM found the tremor subtype to have increased mean diffusivity (MD) in motor areas (Vervoort et al., 2016).

It is worth noting that the stability of the motor subtypes has been questioned as higher percentages of subjects with tremor-dominant subtype have been seen to switch from tremor subtype to PIGD subtype over the years (Alves et al., 2006).

1.4.2. Age of onset

PD patients can be classified according to their age at disease onset in young-onset PD and late-onset PD. Young-onset PD comprises those patients diagnosed before the age of 40, although some studies established the onset at age 50 (Schrag and Schott, 2006 for a review). However, patients with an onset earlier than age 21 are considered juvenile PD and are commonly linked to gene mutations (Schrag and Schott, 2006 for a review). On the other hand, patients with an age at onset over 60 are considered late-onset PD. Early age at onset has been recurrently associated with slower disease progression (Jankovic and Kapadia, 2001; Ferguson et al., 2015) of motor symptoms (Jankovic and Kapadia, 2001), as well as non-motor symptoms, such as less sleep disturbances (Mahale et al., 2015), and slower progression of cognitive impairment (Kim et al., 2020). However, young-onset PD patients have higher depression and anxiety scores (Burn et al., 2012), and they rate their quality of life worse than do patients with older onset and comparable disease severity (Fereshtehnejad et al., 2014).

1.4.3. Non-motor symptoms

Different studies have focused on the additional prognosis implications linked to the presence or absence of specific non-motor features, beyond the motor classification. For example, PD with probable RBD is associated with a higher risk of developing dementia (Postuma et al., 2012; Anang et al., 2014), and the PIGD subtype (Kumru et al., 2007). Along this line, orthostatic hypotension has also been associated with dementia (Anang et al., 2014). While the presence of cognitive impairment has been related to more severe motor symptoms as well as higher H&Y scores (Baiano et al., 2019 for a review), and

visual hallucinations have been related to greater cognitive decline (Swann and O'Brien, 2019 for a review).

1.4.3.1. Visual hallucinations

Visual hallucinations (VH) are the most common psychotic symptomatology in PD, and in consequence, are included as part of its diagnosis (Ravina et al., 2007). A retrospective study of 445 PD patients, showed that 50% of the patients presented VH (Williams and Lees, 2005), and as the disease progress it occurs up to 60% of the patients (Forsaa et al., 2010).

VH consist of complex visual images of people, animals, buildings, or scenery, that take place when the patient is completely awake, and last for seconds or minutes (Barnes and David, 2001 for a review). Fully formed VH are usually seen at later stages of the disease; while, minor hallucinations, which have been defined as the presence of somebody in the room or a person/animal passing sideways (Fénelon et al., 2000) have been reported in 42% of early PD patients (Pagonabarraga et al., 2016).

The mechanisms underlying VH in PD are still unclear. Classically, one potential trigger for VH has been PD medication (Armstrong, 2007 for a review; Connolly and Lang, 2014 for a review). VH have a noticeable effect on the quality of life of patients (McKinlay et al., 2008); in consequence, numerous studies have evaluated the clinical associations that differentiate PD with and without VH, finding neuropsychological impairment as a major risk factor for VH (Barnes and David, 2001 for a review). To disentangle which changes the brain undergoes that might explain this symptomatology, studies have focused on structural and functional MRI (fMRI). Research based on structural MRI has reported reduced GM in the superior parietal lobe and the lingual gyrus (Ramírez-Ruiz et al., 2007) as well as in frontal regions (Gama et al., 2014). Reduced GM volume of the hippocampus has also been described in PD with VH (Ibarretxe-Bilbao et al., 2008) and PD with psychosis (Lenka et al., 2018). Specifically, patients with psychosis showed higher volume of the hippocampal fissure compared to PD without psychosis (Lenka et

al., 2018), which could be explained by a reduction of the hippocampal volume. Interestingly, a 2.5-year longitudinal study reported generalized GM loss of limbic and associative cortical regions in patients with VH while, PD without VH only had GM reductions in motor and cerebellar regions (Ibarretxe-Bilbao et al., 2010). A recent study has also found evidence of a potential contribution of the cerebellum in VH, as reduced GM volume of this region was found in PD with VH compared to PD without VH (Lawn and ffytche, 2021).

Brain activity alterations in PD with VH have been approached using task-based and resting-state functional MRI. Task-based studies have produced contradictory results. While Stebbins et al., (2004) described greater frontal and subcortical activation as well as less activation in the visual cortex in PD with VH compared to PD without VH, Ramírez-Ruiz et al., (2008) described reduced activation of frontal regions in PD with VH. Reduced functional connectivity in the dorsal attention network (DAN) has been described in PD with VH compared to PD without VH (Shine et al., 2015). Interestingly, visual misperceptions have been related to abnormal coupling of patterns involving the DAN, default mode network (DMN) and visual network (Shine et al., 2015). Resting-state functional MRI, on the other hand, has found higher functional connectivity in the DMN, including the right middle frontal gyrus, bilateral precuneus and bilateral posterior cingulate, in PD with VH compared to PD without VH (Yao et al., 2014).

Therefore, there are several structural and functional brain alterations associated with VH that explain this symptomatology beyond the levodopa side effects.

1.4.3.2. Cognition

Mild Cognitive Impairment

Cognitive impairment is a common non-motor symptom of PD that can even be present in newly diagnosed patients (Muslimović et al., 2005; Williams-Gray et al., 2007). The decline in cognitive functions starts with minimal impairment and can progress to mild cognitive impairment (MCI) which can end up in dementia. MCI is a condition

characterized by a more pronounced cognitive decline than that expected in normal ageing, but unlike PDD, it does not compromise the activities of daily living. MCI occurs in approximately 27% of PD patients (Litvan et al., 2011 for a review) and appears as a risk factor for the development of dementia (Pedersen et al., 2013). Non-tremor phenotype as well as impaired performance in neuropsychological tests with a posterior cortical basis, such as semantic fluency and pentagons copying presentations, have been defined as clinical predictors of global cognitive decline and dementia (Williams-Gray et al., 2007; Williams-Gray et al., 2013).

The description of the mechanisms underlying PD-MCI remains a challenge, as there is no uniform consensus about its diagnostic criteria. The Movement Disorder Society (MDS) task force proposed 2 levels of diagnostic criteria based on neuropsychological assessment (Litvan et al., 2012). Level I consists of an abbreviated cognitive assessment which makes it feasible for those cases in which it is not possible to use a long neuropsychological battery; however, it affords less certainty than level II. Level II consists of a more detailed assessment that requires, at least, the use of 2 tests for each of the 5 cognitive domains described in Litvan et al., (2012) (Panel 3).

Contrary to the original hypothesis that the degeneration of the nigro-striatal pathway led to the cognitive dysfunction described in PD, reduced GM in PD-MCI has been described in bilateral precentral and postcentral gyri, precuneus, superior and frontal gyri, superior lateral occipital cortex, superior and inferior temporal regions as well as subcortical regions (bilateral amygdala, hippocampus, and right putamen) (Melzer et al., 2012). When comparing PD-MCI with PD without MCI, GM reductions have been found in PD-MCI in the left insular, superior frontal and middle temporal areas (Mak et al., 2014a) as well as in subcortical structures: the thalamus and nucleus accumbens (Mak et al., 2014b).

Cortical thinning in PD-MCI has also been reported, mainly affecting the precentral cortex, and parietal regions including the bilateral supramarginal gyrus, left superior and inferior parietal (Segura et al., 2014; Baggio et al., 2015; Gasca-Salas et al., 2019),

precuneus as well as temporal (Segura et al., 2014; Gasca-Salas et al., 2019) and occipital cortices (Segura et al., 2014; Baggio et al., 2015; Gasca-Salas et al., 2019). When compared to healthy controls (HC), cortical thinning in early PD-MCI has also been described in the right inferior temporal, and left hemisphere including precentral, superior parietal and lingual gyrus (Pereira et al., 2014). Interestingly, in both early and advanced PD with MCI the thinning of the precuneus has been described when compared with PD without MCI (Segura et al., 2014; Pereira et al., 2014).

In a meta-analysis including both analyses based on GM volumes and on cortical thickness Mihaescu et al., (2019) reported that the regions that persistently appeared to have reduced GM in PD-MCI compared to PD without MCI, across the studies, were the right supramarginal gyrus, left posterior insula and the mid-cingulate cortex.

Impairment in the attentional performance of PD-MCI has been associated with atrophy of the putamen, nucleus accumbens (Mak et al., 2014b), left insular gyrus, left middle temporal gyrus and left superior frontal gyrus (Mak et al., 2014a). The language domain has been correlated with reduced GM volumes in the nucleus accumbens (Mak et al., 2014b), while the executive function has been related to the left insular and left middle temporal gyri (Mak et al., 2014a). Cortical thinning in PD-MCI has also been associated with impairment in the different cognitive domains (Segura et al., 2014).

Functional MRI has showed PD-MCI to have reduced functional connectivity (FC) between DAN and right fronto-insular regions which correlated with lower scores in attention/executive tests, whereas the DMN displayed increased connectivity with medial and lateral occipito-parietal regions (Baggio et al., 2015). Along the same lines, PD-MCI showed reduced within-DAN, within-DMN and DAN-frontoparietal connectivity, as well as loss of normal DAN-DMN anticorrelation in MCI patients (Baggio et al., 2015). Graph theory based on functional data has described altered graph measures in PD-MCI (Baggio et al., 2014; Díez-Cirarda et al., 2018). Going one step further, new studies have applied dynamic FC, which adds new information by capturing variations over a short time, and found impairment in temporal properties in PD-MCI (Díez-Cirarda et al., 2018; Fiorenzato et al., 2019) and more pronounced dysfunction as cognitive impairment increases towards the development of PDD (Fiorenzato et al., 2019).

Panel 3: Criteria for the diagnosis of PD-MCI *(Litvan et al., 2012)*

I. Inclusion criteria

- Diagnosis of Parkinson's disease as based on the UK PD Brain Bank Criteria.
- Gradual decline, in the context of established PD, in cognitive ability reported by either the patient or informant or observed by the clinician.
- Cognitive deficits on either formal neuropsychological testing or a scale of global cognitive abilities.
- Cognitive deficits are not sufficient to interfere significantly with functional independence, although subtle difficulties on complex functional tasks may be present.

II. Exclusion criteria

- Diagnosis of PD dementia based on MDS Task Force proposed criteria.
- Other primary explanations for cognitive impairment (e.g., delirium, stroke, major depression, metabolic abnormalities, adverse effects of medication, or head trauma).
- Other PD-associated comorbid conditions (e.g., motor impairment or severe anxiety, depression, excessive daytime sleepiness, or psychosis) that, in the opinion of the clinician, significantly influence cognitive testing.

III. Specific guidelines for PD-MCI level I and level II categories

A. Level I (abbreviated assessment)

- Impairment on a scale of global cognitive abilities validated for use in PD

Or

- Impairment on at least two tests, when a limited battery of neuropsychological tests is performed (i.e., the battery includes less than two tests within each of the five cognitive domains, or less than five cognitive domains are assessed).

B. Level II (comprehensive assessment)

- Neuropsychological testing that includes two tests within each of the five cognitive domains (i.e., attention and working memory, executive, language, memory, and visuospatial).
- Impairment on at least two neuropsychological tests, represented by either two impaired tests in one cognitive domain or one impaired test in two different cognitive domains.

Impairment on neuropsychological tests may be demonstrated by:

- Performance approximately 1 to 2 SDs below appropriate norms

Or

- Significant decline demonstrated on serial cognitive testing

Or

- Significant decline from estimated premorbid levels.

IV. Subtype classification for PD-MCI (optional, requires two tests for each of the five cognitive domains assessed and is strongly suggested for research purposes).

- PD-MCI single-domain—abnormalities on two tests within a single cognitive domain (specify the domain), with other domains unimpaired

Or

- PD-MCI multiple-domain—abnormalities on at least one test in two or more cognitive domains (specify the domains).

Parkinson's Disease Dementia

PDD is a common non-motor manifestation of PD associated with age and disease evolution (Williams-Gray et al., 2013) that occurs in 80% of PD patients (Christopher and Strafella, 2013 for a review). PDD appears in advanced stages of PD and is preceded by MCI, although MCI does not necessarily progress to dementia. It has been reported that 89% of PDD suffer from, at least, one neuropsychiatric symptom, depression being the most common followed by apathy and anxiety (Aarsland et al., 2007) (Figure 2). Interestingly, it has been described that PDD perform better than AD in memory tasks but worse in attentional (Noe et al., 2004) and visual perception tests (Mosimann et al., 2004). In terms of brain atrophy, PD-MCI converting to PDD showed reduced GM in the hippocampus when compared to PD-MCI non-converters (Kandiah et al., 2014), and reduced GM volume in the nucleus basalis of Meynert when compared to HC (Pereira et al., 2020). Cortical thinning in PD-MCI has been seen to predict the risk of developing dementia (Sasikumar and Strafella, 2020 for a review). Interestingly, Gasca-Salas et al., (2019) found PD-MCI converters to have thinner cortex in bilateral frontal regions, the insula, and the left middle cortex; however, the results did not survive multiple comparisons. In the meta-analysis of Mihaescu et al., (2019) the involvement of the left insula in PD-MCI, which expanded to the bilateral insula in PDD, was also described.

As expected, PDD has increased signs of brain atrophy, such as larger ventricles compared to HC and PD without cognitive impairment (Apostolova et al., 2010). Regionally, PDD seems to present cortical thinning in frontal, temporal and parietal areas when compared with HC, and to non-demented PD in the premotor cortex, posterior cingulate, supplementary motor, superior frontal and temporal areas (Zarei et al., 2013). Reductions in GM volumes have been described compared to non-demented PD and HC in the amygdala and the hippocampus (Zarei et al., 2013) as well as in the right caudate when compared to HC (Apostolova et al., 2010). In addition, reduced volume of the left caudate and the right putamen has been negatively correlated with the UPDRS-III score and the H&Y stages, respectively (Zarei et al., 2013).

1.5. HETEROGENEITY IN DEMENTIA WITH LEWY BODIES

DLB has been described as the second most common neurodegenerative form of dementia after AD (Lopez and Kuller, 2019 for a review), also accompanied by motor impairment, similar to PDD. DLB diagnosis appears as a challenge due to its clinical overlap with the aforementioned dementias.

The neuropsychological profile of prodromal DLB has been characterized by impaired memory, and impaired executive and visuoconstructive functions compared to HC (Kemp et al., 2017). Classically, the majority of studies have tried to differentiate DLB from AD, concluding that in early stages, DLB performs worse than AD in attentional and visuoperceptual/viusocontructive tasks, while coursing with better memory than AD (Oda et al., 2009 for a review). Additionally, other studies have compared DLB with PDD. Petrova et al., (2015) described DLB to perform worse than PDD in attentional/executive as well as visual tasks, while Smirnov et al., (2020) described PDD as the one with worse executive performance. When comparing PDD, DLB and AD, DLB and PDD have been observed to yield lower scores in visuospatial tasks compared to AD, but better scores than AD in the memory domain. In addition, over time, DLB has been described to decline faster than AD in the executive domain, but slower than PDD, while in the language domain DLB progression has been seen to be faster than in PDD (Smirnov et al., 2020).

1.5.1. Pattern of atrophy in Dementia with Lewy bodies

MRI analyses based on cortical thickness and GM volumetry have compared DLB patients with HC to define its pattern of atrophy (Table 2). A voxel-wise meta-analysis of GM that considered studies between 2000 and 2014, concluded that DLB showed reduced GM compared to HC in the lateral temporal lobe, the insula, and the putamen (Zhong et al., 2014). Additionally, other studies have described reductions in the parietal lobe (Ballmaier et al., 2004; Watson et al., 2015; van der Zande et al., 2018; Ye et al., 2020; Colloby et al., 2020), cingulate (Watson et al., 2015), the basal ganglia (Watson et al., 2016; van der Zande et al., 2018), the hippocampus (Watson et al., 2016; Elder et al.,

2017), the amygdala, and the thalamus (Watson et al., 2016), as well as in frontal regions (van der Zande et al., 2018; Ye et al., 2020) including the orbitofrontal and precentral gyrus (Colloby et al., 2020) and primary motor areas and fusiform (Ye et al., 2020). Interestingly, Blanc et al., (2016) studied prodromal DLB and described atrophy in specific clusters of the frontal cortex as well as the insula, the precuneus and the anterior cingulate compared to HC.

Studies based on structural MRI have also compared DLB with PD and AD due to its neuropathological overlap. DLB appears to be frequently misdiagnosed as AD in the clinics (Schneider et al., 2007); thus, finding differences in structural MRI between DLB and AD would help to its differential diagnosis.

DLB had been found to have greater GM volumes than AD in orbitofrontal, frontodorsal and temporal areas (Ballmaier et al., 2004) including the temporal giry, as well as the parietal cortex (Whitwell et al., 2007). The most recurrent finding has been DLB presenting greater GM volumes than AD in the medial temporal lobe (Whitwell et al., 2007, Watson et al., 2015, Chabran et al., 2020) including the hippocampus (Watson et al., 2012; Watson et al., 2016; Elder et al., 2017; van der Zande et al., 2018; Chabran et al., 2020), parahippocampal gyrus (Watson et al., 2012; Watson et al., 2015; Elder et al., 2017; Chabran et al., 2020) and the entorhinal cortex (Watson et al., 2015; Elder et al., 2017; Colloby et al., 2020) (Table 2). Interestingly, lower hippocampal volumes in DLB have been related to a more aggressive course of the disease (Graff-Radford et al., 2016).

When comparing DLB with PD, DLB has been found to have reduced GM in the right hippocampus and parahippocampal gyrus (De Schipper et al., 2019), as well as cortical thinning in the primary motor areas and fusiform gyri (Ye et al., 2020); however, no significant differences have been found when comparing DLB to cognitively impaired PD (Ye et al., 2020), including PDD (Ye at al., 2020; Colloby et al., 2020) (Table 2).

Table 2: Structural MRI studies in Dementia with Lewy bodies

Reference	Sample	Demographics (Age, Disease duration)	MRI analysis	Contrast (vs DLB)	Brain regions
Ballmaier 2004	16 DLB 29 AD 38 HC	76.4±6.7; 30±16.5 months 77.9(5.5);32.1±18 months 75.3±6.8; NA *Mean (SD)*	Cortical pattern matching	DLB < HC	L orbitofrontal Bilateral parietal Bilateral temporal
				DLB > AD	Bilateral orbitofrontal Bilateral frontodorsal Bilateral temporal
Whitwell 2007	72 DLB 72 AD 72 HC	73 (51-87); - 76 (52-88); - 74 (51-87); - *Median (range)*	VBM and VBM-based ROI analysis: Substantia innominata Dorsal midbrain Temporo-parietal cortex Sensori-motor cortex	DLB < HC	**Small loss involving:** Dorsal midbrain Substantia innominata Bilateral posterior Hippocampus Bilateral Insula Bilateral parietal lobe
				DLB > AD	Bilateral medial temporal lobe L inferior temporal gyri L middle temporal gyri L superior temporal gyri L parietal lobe
Sanchez-Castaneda 2009	12 DLB 16 PDD 16 HC	71.1(10.8);32.6(16.1) months 71.1(7.2);52.8(27.8) months 71.8(7.6); NA *Mean (SD)* *(Parkinsonism duration)*	VBM	DLB < HC	R inferior frontal L posterior cingulate L superior temporal L inferior parietal
				DLB < PDD	R superior frontal R premotor area R inferior frontal

Reference	Sample	Demographics (Age, Disease duration)	MRI analysis	Contrast (vs DLB)	Brain regions
Watson 2012	35 DLB 36 AD 35 HC	78.4±6.9; 41±21 months 78.3±5.8; 53±27 months 76.7±5.2; NA *Mean (SD)*	VBM	DLB < HC	Parahippocampal gyrus Amygadala Superior temporal gyrus Uncus R Caudate tail Parietal lobe
				DLB > AD	Parahippocampal gyrus L Hippocampus
Watson 2015	31 DLB 30 AD 33 HC	77.8±7.1; - 77.9±5.7; - 76.8± 5.3; NA *Mean (SD)*	CTh	DLB < HC	L inferior parietal L superior temporal L anterior cingulate L posterior cingulate
				DLB > AD	L medial temporal lobe (entorhinal cortex and parahippocampal gyrus)
Watson 2016	33 DLB 32 AD 35 HC	77.9±6.9; 40.9±21.0 months 77.6±5.7;53.0±27.3 months 76.7±5.7; NA *Mean (SD)*	GM subcortical volumetry	DLB < HC	Thalamus Putamen Pallidum Hippocampus Amygdala L Caudate Brainstem
				DLB > AD	Hippocampus

Reference	Sample	Demographics (Age, Disease duration)	MRI analysis	Contrast (vs DLB)	Brain regions
Blanc 2016	28 DLB 27 AD 33 HC (Prodromal DLB and prodromal AD)	67.5±9.2; - 69.3±7.8; - 72.4±10.4; NA *Mean (SD)*	VBM	DLB < HC	Insula Precuneus Medial Frontal L anterior cingulate L middle frontal R superior frontal R inferior frontal
				DLB > AD	R superior parietal
Elder 2017	65 DLB 76 AD 63 HC	78.4±40; 35.96 ± 27.74 months 77.99±7.51;32.61±21.83 76.81±6.05; NA *Mean (SD)*	CTh & GM subcortical volumetry ROIs: Hippocampal volume, and parahippocampal, entorhinal and temporal pole cortical thickness.	DLB < HC	Hippocampus Parahippocampal gyrus Entorhinal cortex Temporal pole
				DLB > AD	Hippocampus Parahippocampal gyrus Entorhinal cortex

Reference	Sample	Demographics (Age, Disease duration)	MRI analysis	Contrast (vs DLB)	Brain regions
van der Zande 2018	62 DLB/AD- 36 DLB/AD+ 84 AD 75 HC	67±8; 3.4±2.3 years 72±6.4; 2.7±1.8 years 69±7.8; 3.3±2.3 years 66±6.6; NA *Mean (SD)*	CTh Subcortical volumes (FSL-FIRST)	DLB/AD- < HC	**Small cortical loss in:** *Vertexwise analysis:* Parietal lobe Temporal lobe Cingulate gyrus *Subcortical volumes:* Caudate Nucleus Accumbens
				DLB/AD+ < HC	(Vertexwise analysis): Parietal lobe Temporal lobe Cingulate gyrus
				DLB/AD- > AD	Hippocampus
				DLB/AD+ > AD	n.s
				DLB/AD+ vs DLB/AD-	n.s
De Schipper 2019	14 DLB 62 PD	73.1±6.0; 5.5±3.4 years 71.9±4.1; 8.7±4.2 years	VBM	DLB <PD	**Small loss involving:** R Hippocampus R Parahippocampal

Reference	Sample	Demographics (Age, Disease duration)	MRI analysis	Contrast (vs DLB)	Brain regions
Ye 2020	21 DLB 24 PD 16 PD cognitively impaired 115 HC	71.6±7.1; 4.8±2.3 years 69.0±6.9; 9.3±5.4 years 73.1±7.2;9.4±4.7 years 69.4±7.4; 9.31±5.4 years *Mean (SD)*	CTh vertex based CTh ROI based: Medial temporal Inf. temporal gyrus Temporal pole Angular gyrus Superior frontal gyrus Supramarginal gyrus Precuneus Superior parietal lobe Inferior frontal sulcus Precentral Paracentral Fusiform	DLB< HC	Frontal Parietal Medial temporal
				DLB < HC, PD (ROIs)	Primary motor (precentral+paracentral) Fusiform
				DLB vs PD impaired (ROIs)	n.s
				DLB/AD- < HC	Dorsolateral prefrontal Precentral Temporal Lateral, medial parietal More restricted atrophy than in amyloid positive groups
				DLB/AD+ < HC	Dorsolateral prefrontal Precentral Temporal Lateral, medial parietal
Colloby 2020	65 DLB 75 AD 29 PDD 76 HC	78.2 ± 6.4; - 77.9 ± 7.5; - 74.5 ± 5.6; 8.9 ± 5.1 years 76.1 ± 5.8; NA *Mean (SD)*	CTh	DLB < HC	L middle temporal Medial orbitofrontal R inferior parietal R Precentral
				DLB vs PDD	n.s
				DLB > AD	Entorhinal cortex

Reference	Sample	Demographics (Age, Disease duration)	MRI analysis	Contrast (vs DLB)	Brain regions
Chabran 2020	92 DLB 70 AD 22 HC	70.1±9.4; - 74.4±8.3; - 66.5±7.8; - *Mean (SD)*	VBM	DLB < HC	Temporal lobes Insulae Frontal lobes
				DLB > AD	Medial temporal lobe (parahippocampal gyrus, hippocampus, amygdala)

1.5.2. Alzheimer's disease like pathology

The hypothesis that concomitant AD-type pathology could play a role in the heterogeneity described in DLB, has led several studies to classify DLB according to the presence or absence of β-amyloid and tau in order to study the influence of this neuropathological trait in the pattern of atrophy in DLB. Accordingly, Kantarci et al., (2012) investigated DLB based on the presence of concomitant AD pathology combined with the spatial location of Lewy body pathology (brainstem, limbic, or diffuse), and found that an increasing likelihood of neuropathologically confirmed DLB was associated with high GM volumes in the amygdala and the hippocampus. Along the same lines, a stepwise thinning from DLB/AD- to DLB/AD+ to AD when compared to HC has been described in parietal, temporal, and cingulate cortex (van der Zande et al., 2018). Ye et al., (2020) found cortical thinning in the DLB/AD- and DLB/AD+ groups compared to HC in dorsolateral prefrontal, precentral, temporal, and parietal cortex, the DLB/AD+ showing more widespread atrophy in the lateral and medial parietal cortex. Interestingly, while DLB/AD- showed higher volumes than AD in the hippocampus, DLB/AD+ did not show significant differences compared to AD (van der Zande et al., 2018) (Table 2). However, no significant differences between the two DLB subgroups have been described (van der Zande et al., 2018). A follow-up of approximately 2 years with autopsy confirmed DLB, described greater atrophy rates in DLB/AD+ compared to DLB/AD- and HC in temporo-parietal cortices, the hippocampus, and the amygdala, as well as larger ventricular volumes (Nedelska et al., 2015).

1.5.3. Non-motor symptoms

DLB, as well as PD, is characterized by a wide range of motor and non-motor symptoms (Panel 1) that make it a very heterogeneous disease. Unsurprisingly, many studies have approached the disease by focusing on its clinical presentation, the majority of which aim to understand the mechanisms underlying one symptom.

1.5.3.1. Visual hallucinations

VH in DLB have been described as similar to the ones described in PDD (Mosimann et al., 2006) *(See section 1.4.3.1. Visual hallucinations, page 28).* Studies focused on studying the differences in GM volumes between DLB with and without VH have described reduced GM volume in DLB with VH in the inferior frontal gyrus (Sanchez-Castaneda et al., 2010), left cuneus (Blanc et al., 2016), medial and superior frontal gyrus, as well as in the putamen, caudate and insula (Pezzoli et al., 2019). Furthermore, GM loss in the precuneus has been correlated to the severity of visual hallucinations (Sanchez-Castaneda et al., 2010) and the score of visuospatial tests with GM volumes of the right inferior temporal gyrus (Pezzoli et al., 2019). In a study based on FDG-PET, metabolic impairment in the prefrontal, parietal, and posterior cingulate cortex was described to be associated with VH in DLB (Morbelli et al., 2019).

1.5.3.2. Cognitive fluctuations

Cognitive fluctuations consist of spontaneous variations in cognition that can include short interruptions of consciousness, episodes of increased confusion and cognitive deficits, periods of reduced arousal, and periods of prolonged sleep. Although cognitive fluctuations are a core symptom of DLB, these are perhaps the most difficult symptom to characterize (McKeith et al., 2005). In DLB loss of GM in the substantia innominata has been associated with cognitive impairment and the severity of cognitive fluctuations (Colloby et al., 2016), while atrophy in the thalamus has been correlated with compromised attentional function (Watson et al., 2017) which, at the same time, has been associated with the clinical evaluation of cognitive fluctuations (Matar et al., 2020 for a review), thus showing convergence between neuropsychological tests and clinical scales in assessing this symptomatology. Interestingly, Peraza et al., (2014) did not find significant results for most of the cortex when comparing DLB with cognitive fluctuations to HC, as they described DLB to have reduced GM in only 2 voxels. Although some studies have provided some evidence of the involvement of GM loss in cognitive fluctuations, it seems that its dynamic nature appears to be better explained in terms of functional MRI

and nuclear imaging. Studies focused on DLB with cognitive fluctuations, have described reduced interhemispheric connectivity in frontal and parietal regions as well as reduced connectivity between frontal and parietal areas in the right hemisphere (Franciotti et al., 2013), and reduced within-network functional connectivity in the left fronto-parietal, temporal, and sensory-motor networks (Peraza et al., 2014) compared to HC. Correlations have been described between the severity of cognitive fluctuations and the right middle frontal gyrus and right lateral parietal cortex (Franciotti et al., 2013) as well as clusters from the fronto-parietal network involving frontal regions (Lowther et al., 2014; Peraza et al., 2014), the lingual gyrus, the putamen, and pallidum (Peraza et al., 2014). Nuclear imaging studies have offered evidence of the involvement of the occipital cortex, basal ganglia, and thalamus in cognitive fluctuations in DLB (Matar et al., 2020 for a review).

Atrophy in fronto-occipital cortices and basal ganglia seem to be involved in VH in DLB, while the dynamic nature of cognitive fluctuations may be better explained by functional and nuclear imaging.

1.6. DATA-DRIVEN SUBTYPING

The heterogeneity of PD symptomatology, together with the limitations that come with single-factor subtypes, has led to more advanced statistical methods for subtyping. The main idea is to let the data describe the different PD profiles within the sample without a priori hypothesis. In this context, the most common methodology is cluster analysis, which consists of grouping the input data (e.g., patients) into subsets or "clusters" in such a way that those within each cluster are more similar to one another than the ones allocated to other clusters (Hastie et al., 2008). Cluster analysis does not use labels to tag the input data (e.g., class), but explores it and makes inferences to disentangle hidden arrangements. This fact differentiates the clustering analysis (unsupervised learning) from classification or discriminant analysis (supervised learning).

Supervised, as opposed to unsupervised models, learn from a training set, which consists of using labeled observations to predict the new as yet un-labelled ones. There are 2 main types of supervised approaches: regression and classification (Alpaydin, 2010), depending on the target variable. In regressions the output is a numerical value such as the score of a neuropsychological test, whereas the output of a classification represents a category such as presenting (1) or not (0) MCI. In this regard, Random Forest (RF) is a flexible example of a supervised learning method that can be used for both, classification, and regression problems (Breiman, 2001). In brief, RF builds multiple decision trees and merges them together to get a more accurate and stable prediction. The RF training algorithm applies the bootstrap aggregating technique (or bagging) to train an ensemble of decision trees. The RF searches for the best feature among a random subset of features while it creates the trees. This strategy provides wide diversity to attempt to improve the model. However, many supervised methods can be turned into unsupervised methods. In RF this can be done by constructing a joint distribution based on the independent variables that describe the data. From this point forth, a number of observations are simulated using this distribution. Then, the RF classifier tries to distinguish the real from the simulated observations (Shi and Horvath, 2006). The quantification of the proximity between observations based on what RF estimates when

trying to assign the labels is the relevant information. This provides a description of how close/similar the observations are from each other, and these can be clustered based on many techniques (Poulakis et al., 2018).

Distance-based clustering uses a measure of distance to define how similar are the observations between them. Classically, k-means has been the most used method. This algorithm uses the squared Euclidean distance as the dissimilarity measure and requires setting the number of clusters (K) a priori; in consequence, the data is forced into the number of clusters previously chosen (Figure 6).

Another method is hierarchical clustering which, as opposed to k-means, does not require specifying the number of cluster but tells, pairwise, which 2 observations are most similar. This last method produces a hierarchy in which the clusters of each new level are the result of merging clusters from a lower level. It can be divided into 2 strategies: agglomerative (bottom-up) and divisive (top-down). The agglomerative model starts at the bottom, where each observation represents a cluster, and at each level a selected pair of clusters - the groups with the smallest intergroup dissimilarity - are merged into a new cluster. An example of this strategy is the Ward's method. On the other hand, divisive methods start at the top, with all the observations part of the same cluster, and at each level one of the existing clusters splits into two new ones, which are the ones with the largest dissimilarity (Figure 6).

Figure 6: Representation of Hierarchical and K-means clustering methods

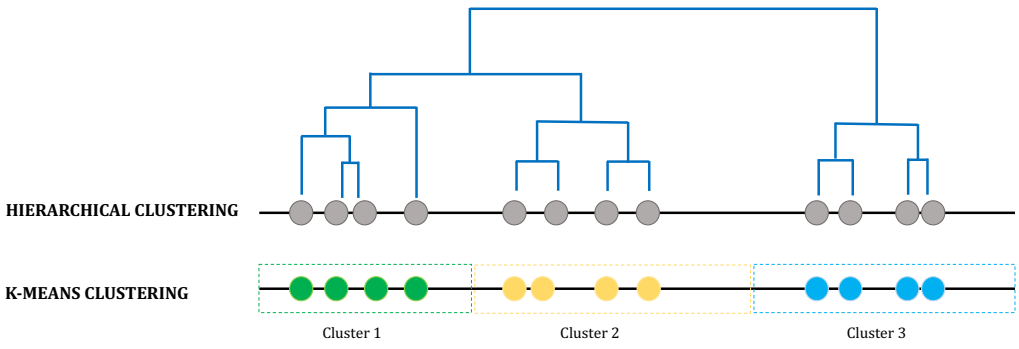

1.6.1. Data-driven subtyping in Parkinson's disease

Defining different subtypes is key to understanding the underlying mechanisms of PD which would lead to a personalized medicine. To that end, the National Institute of Health established identification of PD subtypes as one of the 3 main clinical goals (Sieber et al., 2014).

In the first decade of the 2000s, several studies focused on applying subtyping. In particular, the k-means method has been the clustering algorithm most commonly used. Those first cluster analyses looked for clinical subtypes and, used variables of motor severity, non-motor features, and age at onset (van Rooden et al., 2010 for a review) (Table 3).

In the second decade, cluster analyses incorporated a wider range of input data. Dujardin et al., (2013), undertook an extensive standardized cognitive assessment of a large group of patients, performing a cluster analysis based on data from 13 neuropsychological tests. They described 5 cognitive subtypes: 2 of them with preserved cognitive performance and the other 3 characterized by different levels of cognitive impairment. Fereshtehnejad et al., (2015) went a step forward by undertaking a follow-up of their subtypes. In this analysis 3 subtypes were described. A first subtype named *mainly motor/slow* because of its higher frequency of tremor dominant, combined with low frequency of non-motor symptoms and a slow progression of the disease. At the other extreme was the *diffuse/malignant,* in which all the patients had MCI, with a high number of them also suffering from RBD and other non-motor symptomatology. Moreover, it was characterized by gait disturbances and higher percentage of falls. This subtype had the most rapid and severe progression with 67% of patients presenting PDD in the follow-up. Interestingly, only 12% of the initial PD sample was classified in this group. The last subtype, the intermediate, was in between the other 2 clusters having an intermediate frequency of RBD, as well as intermediate scores in depression and anxiety. In a posterior study carried out in unmedicated early PD, Fereshtehnejad et al., (2017) identified the same 3 aforementioned subtypes (Fereshtehnejad et al., 2015) and complemented the

previous study by analysing β-amyloid and tau biomarkers post-hoc, facilitating the finding that the *diffuse/malignant* subtype presented an AD-like profile. This work also identified a greater decline in dopamine functional imaging in this subtype. In addition, the subtypes were also characterized in terms of brain atrophy, the *diffuse/malignant* subtype being the one with greater atrophy. In a recent study, the 3 subtypes previously established were associated with distinct patterns of diffusion tension imaging (DTI) properties (Abbasi et al., 2020). The *diffuse/malignant* subtype showed increased mean diffusivity (MD) in the basal ganglia. What is more, it had reduced efficiency in 2 small subnetworks compared to the mainly motor subtype: a first subnetwork connecting subcortical structures with the inferior frontal gyrus, and a second one connecting the insula with the superior temporal gyrus. The longitudinal approach showed that the differences became more accentuated over time (Abbasi et al., 2020). This study brought out the need to study PD subtypes also in terms of WM integrity and architecture.

Only a few key studies have performed unsupervised cluster analysis based on MRI data. Uribe et al., (2016) performed a hierarchical cluster analysis applying the Ward's linkage method in a sample of non-demented PD patients and found 3 subtypes: a first subtype with parieto-temporal atrophy with the worse cognitive performance; a second one characterized by frontal and occipital cortical atrophy and the younger age at disease onset; and a third subtype without detectable cortical atrophy. In a 4-year follow-up of these 3 subtypes, temporo-parietal thinning occurred in subtypes 2 and 3 over time, with subtype 3 showing a more pronounced thinning in occipital regions compared to subtype 2. Both subtypes experienced a decline in semantic fluency as well as in their attentional/working memory performance. Subtype 1 had a higher rate of attrition making the longitudinal analysis impossible (Uribe et al., 2019) (Figure 7). In a recent study, Guo et al., (2020) performed another hierarchical clustering applying the Ward's linkage method, in which the input data were 2 structural connectivity patterns: one related to limbic nodes, which explained depressive symptomatology, and a second one, the motor pattern, related to nodes close to the midline and accounted for motor symptomatology. This study led to the description of 3 PD subtypes: *severe depression-dominant, severe motor-dominant* and *mild* subtypes. The *depression-dominant* subtype

showed widespread dysfunction of functional connectivity and WM microstructure; the *motor-dominant* subtype showed moderate impairment of the 2 connectivity patterns; and the *mild* subtype was characterized by limited disconnection in the motor-related pattern.

Hierarchical clustering based on structural MRI has also been carried out in early unmedicated PD. Uribe et al., (2018) described 2 subtypes based on cortical thickness patterns: subtype 1 with cortical thinning in the bilateral orbitofrontal, the anterior cingulate, and the lateral and medial anterior temporal gyri, and subtype 2, which showed cortical thinning in the bilateral occipital gyrus, the cuneus, the superior parietal gyrus, and the left postcentral gyrus. In addition, subtype 2 appeared to perform worse than HC in neuropsychological tests evaluating memory and attention/working memory. Wang et al., (2020) estimated voxel-level neuroanatomic features with deformation-based morphometry (DBM) of T1-weighted MRI to perform a cluster analysis in early PD, and as had Uribe et al., (2018) they found 2 subtypes. However, while the first one had widespread smaller GM volumes compared to HC, the second one appeared to have larger volumes than HC. In addition, subtype 1 presented with worse motor symptomatology, higher frequency of RBD and faster disease progression compared to subtype 2 (Wang et al., 2020).

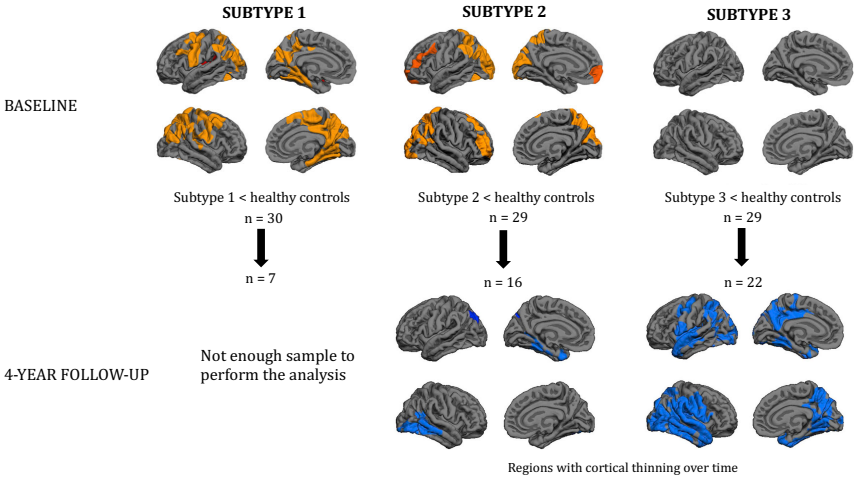

Figure 7: Cortical patterns of the 3 subtypes described in Uribe et al., 2016, and the longitudinal changes that took place after the 4-year follow-up (Uribe et al., 2019).

Altogether, these previous studies provide encouraging initial results favoring the existence of subtypes in PD, which are characterized by different clinical and neuropsychological profiles, as well as specific patterns of brain atrophy and progression. In this Thesis, we present, in Study 1, a multi-modal hierarchical cluster analysis that combines GM volumes and WM FA in order to better understand the heterogeneity found in PD.

Table 3: Parkinson's disease subtypes identified using cluster analyses based on clinical data

Reference	Sample	Cluster method	K	Cluster input	Description of the clusters (C)
Dujardin 2004	44 PD *(There was a follow-up)*	K-means	**2**	UPDRS-III Neuropsychological tests (7 variables)	**C1(n= 26)** Without cognitive impairment Less severe motor symptoms **C2 (n= 16)** Worse cognition More severe motor dysfunction (A cluster with 2 outliers with dementia was discarded)
Lewis 2005	120 early PD	K-means	**4**	Age of onset Disease progression L-DOPA dose UPDRS-III Depression (BDI) Global cognition (MMSE) Premorbid IQ Neuropsychological tests (2 variables)	**C1 (n=49): Young disease onset** Slow progression Mild motor symptoms No cognitive impairment ↓ Depression levels **C2 (n=20): Tremor dominant** Slow progression Modest motor symptoms No cognitive impairment Absence of depression **C3(n=31): Non-tremor dominant** Executive dysfunction Faster progression than C1 and C2 **C4 (n=20): Rapid disease progression** Aggressive course of the disease No cognitive impairment No severe motor disability

Reference	Sample	Cluster method	K	Cluster input	Description of the clusters (C)
Schrag 2006	124 PD	K-means	**2** **&** **3**	Age Age of onset Disease progression Fluctuations Dyskinesia Dementia	2-cluster solution: C1: Young-onset C2: Late-onset 3-cluster solution: **C1: Young-onset** ↓ Age ↑ Depression score ↑L-DOPA dose **C2: Late-onset (I)** ↑ Age, ↑ Age of onset ↑ Motor fluctuations, ↑ hallucinations No cognitive impairment Rapid progression but slower than C3 **C3: Late-onset (II)** ↑↑ Age, ↑↑ Age of onset ↓ Cognition, ↓ L-DOPA dose The most rapid disease progression ("n" not available)
Post 2008	131 early PD	K-means	**2** **&** **3**	Age Age of onset Disease progression L-DOPA responsive symptoms L-DOPA non-responsive symptoms Global cognition (MMSE) Affective disturbances	2-cluster solution: C1 (n=73): Young-onset C2 (n=58): Late-onset 3-cluster solution: **C1 (n=44): Young-onset** ↓ H&Y stages, less motor severity **C2 (n=35): Intermediate** ↑ Anxiety and depression Intermediate H&Y stages In-between motor severity **C3 (n=52): Late-onset** ↑ H&Y stages, Severe motor symptoms ↑ Rate of disease progression

Reference	Sample	Cluster method	K	Cluster input	Description of the clusters (C)
Reijnders 2009	2 PD samples (N=346): n=173 for clustering n= 173 for validation	K-means followed by a validation through a classification model	**4**	Age at onset Disease progression Tremor Hypokinesia/rigidity Postural instability gait difficulty L-DOPA complications Global cognition (MMSE) Depression Apathy Hallucinations	**C1 (n=11): Rapid disease progression** Non-tremor dominant ↓ Psychopathology, ↓ Cognition **C2 (n=51): Young-onset** ↑ L-DOPA complications **C3(n=29): Non- tremor-dominant & psychopathology** ↑ Hypokinetic rigid and PIGD symptoms ↑ H&Y average Worse activities of daily living (ADL) ↑ Psychopathology, ↓↓ Cognition **C4 (n=82): Tremor-dominant** ↓ H&Y average ↓ Psychopathology
Van Rooden 2011	2 PD samples: sample with follow-up (n=344) and validation sample (n=357)	Model-based clustering	**4**	Motor phenotypes Motor fluctuations Global cognition Autonomic dysfunction Psychotic symptoms RBD Daytime sleepiness Depression Anxiety	**C1 (n=169)** ↓ Age, ↓ Age of onset Mild severity in cognition ↓ L-DOPA intake, ↓ Exposure to L-DOPA **C2 (n=45)** ↑ % Women ↑ Motor complications Moderate sleep problems & depression ↑ Disease duration ↑ Exposure to L-DOPA **C3 (n=104)** ↑ Age, ↑ Age of onset Most domains severely affected Mild motor complications, less frequent **C4 (n=26)** ↑ Age, ↑ Age of onset, ↑ % Woman Mild tremor ↑Motor complications (but less than C2) ↑ Exposure to L-DOPA

Reference	Sample	Cluster method	K	Cluster input	Description of the clusters (C)
Dujardin 2013	557 PD	K-means	**5**	Neuropsychological tests (13 variables) including: Global cognition (MMSE) And the following domains: Attention/working Verbal episodic memory Executive functions Speed of processing Visuospatial abilities	**C1 (n=108)** ↓ Age, ↑ Educated, Cognitively intact **C2 (n=230)** Cognitively impaired but compared to C1: ↓ Working memory, ↓ Episodic memory ↓ Executive funcions **C3 (n=72)** Overall cognition slightly impaired except for recognition memory ↑ Performed slower Severe motor symptoms ↑ Disease duration ↑ Axial signs **C4 (n=133)** ↑ Age, ↑ Disease duration Impaired Cognition ↑ ↑ Performed slower Severe motor symptoms ↑ Axial signs ↑ Hallucinations, ↑ Blood pressure ↑ Apathy, ↑ Depression **C5 (n=14)** ↑ Age, ↑ Disease duration Severe impaired cognition ↑ ↑ ↑ Performed slower Severe motor symptoms ↑ Axial signs ↑ Hallucinations, ↑ Blood pressure ↑ Apathy, ↑ Depression ↑ % Demented

Reference	Sample	Cluster method	K	Cluster input	Description of the clusters (C)
Erro 2013	100 unmedicated early PD *(There was a follow-up)*	K-means	**4**	UPDRS-III (motor) Non-motor domains Global cognition (MMSE) Frontal assessment Anxiety Depression	**C1 (n=21): Benign Pure** ↓ Age Intermediate UPDRS-III Intermediate progression rate No depression, no anxiety No frontal cognitive impairment ↓↓ Non-motor score **C2 (n=32): Benign mixed motor-non-motor** ↓ UPDRS-III ↓ Progression rate Mild depression and anxiety Mild frontal cognitive impairment Intermediate non-motor score **C3 (n=27): Non-motor dominant** Intermediate UPDRS-III Intermediate progression rate Intermediate depression and anxiety Intermediate frontal cognitive impairment ↑ Non-motor score **C4 (n=20): Motor dominant** ↑ UPDRS-III ↑ Progression rate ↑ Depression and anxiety ↑ Frontal cognitive impairment Intermediate non-motor score

Reference	Sample	Cluster method	K	Cluster input	Description of the clusters (C)
Fereshtehnejad 2015	113 PD *(There was a follow-up)*	2-step cluster analysis	**3**	Motor severity Motor complications Motor subtypes Autonomic manifestations Psychiatric manifestations Olfaction Color vision Sleep parameters Neurocognitive testing The 7 most informative were: UPDRS-II (activities of the daily living) UPDRS-III (motor) RBD MCI Systolic blood pressure Depression Anxiety	**C1 (n=43): Mainly motor/slow progression** Intermediate motor severity Tremor subtype Slow progression rate ↓ RBD, Absence of orthostatic hypotension 44% MCI, ↓↓ Hallucinations Mild depression and anxiety Mild autonomic symptoms **C2 (n=30): Intermediate** ↓ Motor severity Intermediate progression rate 60% RBD Absence of MCI All PD with drop of systolic blood pressure Intermediate depression and anxiety **C3 (n=40): Diffuse/malignant** Rapid progression rate (follow-up) All PD with MCI All PD with orthostatic hypotension ↑↑ RBD, ↑ Depression and anxiety Severe motor symptoms Most severe gait disturbance More likely to develop dementia (at follow-up)

Reference	Sample	Cluster method	K	Cluster input	Description of the clusters (C)
Szeto 2015	209 early PD	K-means	**4**	Age of onset Disease progression Motor phenotype Global cognition (MMSE) Neurocognition (2 tests) Depression L-DOPA dose Premorbid IQ	**C1 (n=93): Young onset** ↑ L-DOPA ↓ MCI **C2 (n=24): Tremor dominant** ↓ L-DOPA Intermediate % of MCI **C3 (n=23): Non-tremor dominant** ↑ L-DOPA ↑ ↑ MCI ↑ Freezing gait ↑ Hallucinations ↑ Daytime somnolence ↑ RBD **C4 (n=44): Rapid disease progression** ↓ L-DOPA ↓ MCI No severe cognitive impairment
Erro 2016	398 unmedicated early PD	K-means	**3**	Global cognition (MoCA) Depression Anxiety Olfaction (UPSIT) RBD Autonomic symptomatology Motor phenotype Apathy Hallucinations Fatigue Pain	**C1 (n=179)** ↓ Motor symptomatology ↓ Neuropsychiatric symptomatology ↓ RBD, ↓ Pain Less nigral-striatal denervation (^{123}[I]-FP-CIT binding SPECT scan) **C2 (n=67)** ↑ Motor symptomatology ↑ Neuropsychiatric symptomatology ↑ RBD, ↑ Pain,↑↑ Hallucinations ↑↑ Apathy, ↑↑ Fatigue **C3 (n=152)** ↑ Motor symptomatology ↑ Neuropsychiatric symptomatology ↑ RBD, ↑ Pain, ↑ Hallucinations ↑Apathy, ↑ Fatigue

Reference	Sample	Cluster method	K	Cluster input	Description of the clusters (C)
Lopes 2017	An initial sample (N=156) to perform the cluster analysis, but only subjects with functional data available were used for the characterization (n=119)	K-means	**5**	Neuropsychological tests (18 variables) including: Global cognition (MMSE and Mattis DRS) And the following domains: Attention/working Memory Executive functions Language Visuospatial abilities	**C1 (n=31): Cognitive intact** ↓ Age, ↑ Education **C2 (n=31): Slight Mental Slowness** ↑ Education **C3 (n=43): Mild to moderate cognitive deficits** **C4+C5 (n=14): Severe cognitive deficits** Severe deficits in all domains ↑ Age, ↓ Educatio *Graph theory topological measures and connectivity, both derived from fMRI, showed to be progressively impaired as the cognitive deficits increased.*
Fereshtehnejad 2017	421 unmedicated early PD *(There was a follow-up)*	Agglomerative hierarchical clustering with Euclidean distance	**3**	Age Genetic risk score Orthostatic systolic Blood pressure drop Motor phenotype Olfaction (UPSIT) Neurophysiological tests (domains) RBD Depression Anxiety Impulse disorders Sleepiness Autonomic dysfunction Hallucinations Fatigue, Apathy Pain	**C1 (n=223): Mild motor predominant** ↓ Age ↓ Motor scores ↓ Non-motor scores Slow disease progression **C2 (n= 146): Intermediate** Intermediate motor scores Intermediate non-motor scores Intermediate disease progression **C3 (n=52): Diffuse malignant** ↑ Motor scores ↑ Non-motor scores Rapid disease progression Greater atrophy ↓ β-Amyloid and tau (CSF)

Reference	Sample	Cluster method	K	Cluster input	Description of the clusters (C)
LaBelle 2017	424 unmedicated early PD	Latent class analysis	**6**	Neuropsychological tests (6 variables): Semantic fluency SDMT JLO Working memory Verbal memory (x2)	**C1(n=20): Weak-Overall** ↑ Age Poor cognitive performance ↑ Depression, anxiety ↑ Autonomic dysfunction ↑ Anosmia, ↑ RBD **C2 (n=149): Typical-Overall** Average cognitive performance **C3 (n=134): Strong-Overall** ↓ Age, ↑ % Women ↑ Performance in all tests (verbal memory) ↓ Dysautonomia, ↓ Anosmia **C4 (n=23): Strong-Memory** ↓ Visuospatial score ↑ Learning & recall verbal memory scores **C5 (n=47): Weak-Visuospatial** ↑ Memory scores, ↓ Visuospatial scores **C6 (n=51): Amnestic** ↑ Tremor severity, ↑ Anosmia ↓↓ Verbal memory learning and recall scores, ↓ Verbal fluency score
Lawton 2018	2PD samples: n=1601 n=944 (validation)	K-means	**4**	Psychological well-being (apathy, fatigue, pain, neuroticism, anxiety, depression, QUIP (impulsive compulsive disorders)) Non-tremor motor (speech, rigidity, bradykinesia, postural)	**C1(n=307): Fast motor progression** ↑ Age at onset **C2(n=167): Mild motor and non-motor** ↓ Age at onset, ↑ % Women **C3(n=223): Severe motor disease, poor psychological well-being and poor sleep** ↑ PIGD, ↑ LEDD **C4(n=247): Slow motor progression** ↑ Tremor dominant

Reference	Sample	Cluster method	K	Cluster input	Description of the clusters (C)
Belvisi 2021	100 unmedicated early PD	2 cluster analyses: Agglomerative hierarchical clustering with Euclidean distance and k-means	**2**	Age Disease duration Motor domain Cognitive performance RBD Dysautonomia	**C1 (n=76): Mild motor predominant** ↓ Age ↓ UPDRS part II+ part III ↓ H&Y ↓ non-motor symptoms ↑ Cognition **C2 (n=24): Diffuse malignant** ↑ Age ↑ UPDRS part II+ part III ↑ H&Y ↑ non-motor symptoms ↓ Cognition *Transcranial magnetic stimulation:* ↑ Cortical excitability ↓ Plasticity *Kinematic analysis of motor performance*: Slower performance

1.6.2. Data-driven subtyping in Dementia with Lewy bodies

The heterogeneity described in DLB, as regards both clinical and neuroimaging features, leads to belief in the existence of different subtypes underlying the disease. Along this line, Morenas-Rodríguez et al., (2018) conducted a k-means cluster analysis based on longitudinal clinical data from the prodromal phase of the disease. Specifically, they calculated the time from the first symptom to fulfilment of DLB criteria, and the time from the presentation of hallucinations, as well as time from the presentation of parkinsonism to DLB diagnosis. This led to the description of the following 3 subtypes: the cognitive-predominant (57%), characterized by cognitive impairment as the earliest symptom; the neuropsychiatric-predominant (27%), which had the oldest age at disease onset and psychosis as the most common first symptom accompanied by an early onset of hallucinations; finally, the parkinsonism-predominant (16%), characterized by the presence of parkinsonism in all the patients and younger age at onset.

In a multicentre study, Oppedal et al., (2019) included 333 DLB patients as well as 352 AD patients and 233 HC and used visual rating scales to classify the DLB patients in 4 groups previously described in AD (Ferreira et al., 2017) (Figure 8). In the DLB group, the most common pattern of atrophy was the hippocampal-sparing, which is characterized by frontal and/or posterior atrophy, followed by the minimal-atrophy pattern (Figure 8). Interestingly, Caminiti et al., (2019), undertook a hierarchical cluster analysis based on FDG-PET of 14 ROIs known to be involved in DLB, and found 2 subtypes that slightly differed in occipital hypometabolism. The group with worse occipital involvement presented with worse global cognitive performance as well as a higher risk of developing VH.

In this Thesis, in Study 3, we present the first study using an unsupervised data-driven approach based on MRI data to find DLB subtypes.

Figure 8: AD subtypes based on atrophy patterns obtained from visual rating scales

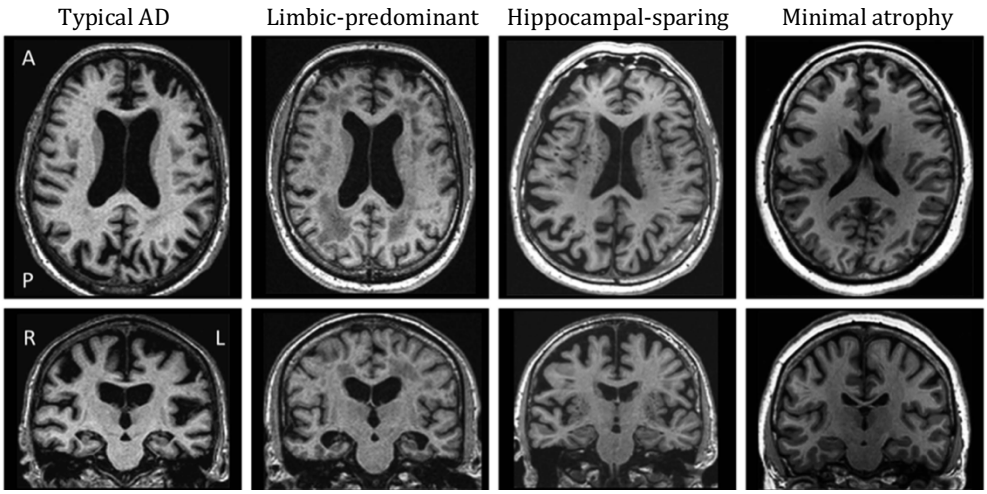

(Extracted from Ferreira et al., 2017)

1.7. THE BRAIN AS A NETWORK

In our day to day lives, we are involved in multiple networks, such as the Internet or social relationships, but among all these networks, the brain is probably the most complex one we deal with every day. A network is a system composed of a set of elements and the links connecting them. In the context of the brain, the elements could be the neurons, the connections the synapses. The human brain contains around 100 billion neurons, each linked by up to 15,000 connections, making the microscopic approach impossible. In this framework, MRI has made it feasible to approach the brain as a network with methods of acquisition and analysis, which allows the study of the different connections between brain regions by means of anatomical tracts and functional associations, as well as network properties using graph theory. Taken as a whole, it seems to be a promising way to better understand the mechanisms involved in neurodegenerative diseases.

1.7.1. Graph theory

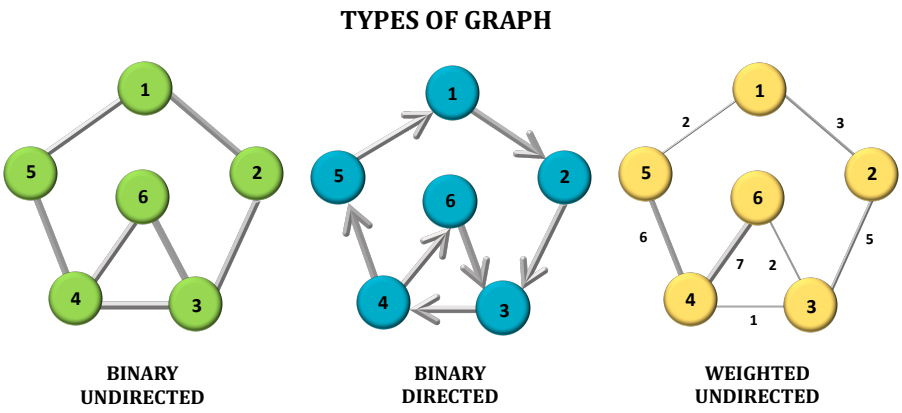

Figure 9: Different types of graphs according to the directionality and weight of their edges.

The first publications applying graph theory to network science appear at the end of the 20th century (Felleman and van Essen, 1991). However, the scene to understand the brain as a graph was previously set by Santiago Ramón y Cajal, when he undertook microscopic studies applying Golgi's staining technique, which allowed him to visualize the neurons. Ramón y Cajal then realized that neurons do not work alone, but rather make connections from one to another in order to form circuits.

In this context, we may wonder what a graph is exactly. A graph (G = (N, E)) consists of an adjacency matrix made of nodes (N) and the connections between them, which are called edges (E). Graphs can be defined as directed or undirected, depending on whether the edges have directionality or not. For instance, a directed graph would be a gene regulation network. They can also be described as binary, when the edges are defined as "0" (absence of connection) or "1" (presence of connection), or as weighted if the edges are linked to a value that reflects the strength of the connection (Figure 9).

Graph theory relies on several topological measures to describe the efficiency of a network and its nodes (Figure 10, Panel 4).

Figure 10: Measures of network topology

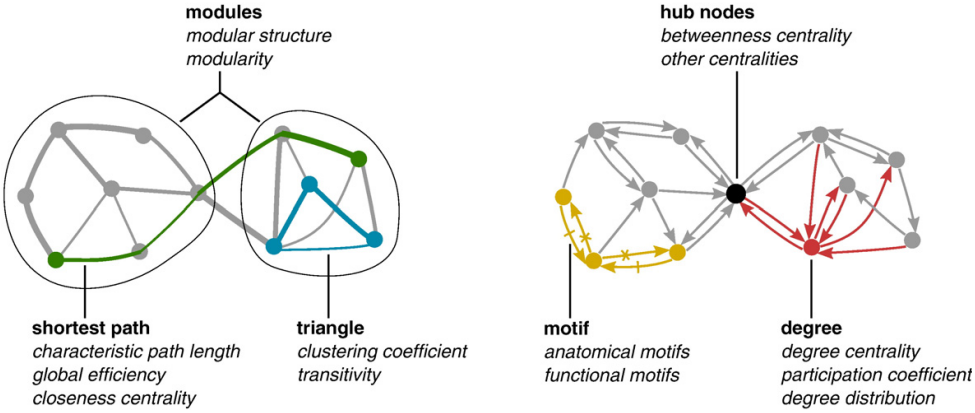

Illustration of key complex network measures (in italics). These measures are typically based on basic properties of network connectivity (in bold). Measures of integration are based on shortest path lengths (green), while measures of segregation are often based on triangle counts (blue) but also include more sophisticated decomposition into modules (ovals). Measures of centrality may be based on node degree (red) or on the length and number of shortest paths between nodes. Hub nodes (black) often lie on a high number of shortest paths and consequently often have high betweenness centrality. Patterns of local connectivity are quantified by network motifs (yellow). (Figure and text extracted from Rubinov and Sporns, 2010).

Panel 4: Brain network metrics

***Triangle*:** Number of neighbours of a node that are also neighbours of each other.

***Module*:** Subset of nodes.

***Path Length*:** Number of edges in a path, a path being a sequence of nodes connected by edges.

Clustering Coefficient: Measure of the density of connections between nearest neighbours of an index node.

***Motif*:** Pattern found in a network (subgraph) repeatedly.

***Hub Node*:** A node with more connections than the average.

***Degree*:** Total number of edges connected to a node.

1.7.1.1. Small world property

Most complex networks in the real world are small-world networks. The theory of 6 degrees of separation, which contends that we are just 6 introductions away from any person in the world, is a good example of the small-world property, as the network presents short paths between pairs of nodes (people) that can be far away, and the nodes allowing these connections are usually hubs (people with a lot of social relationships). The same happens with the brain, which is characterized by short average path length as well as high average clustering (Watts and Strogatz 1998), allowing a fast spread of the information through the network.

Figure 11: Types of networks according to path length and clustering coefficient measures

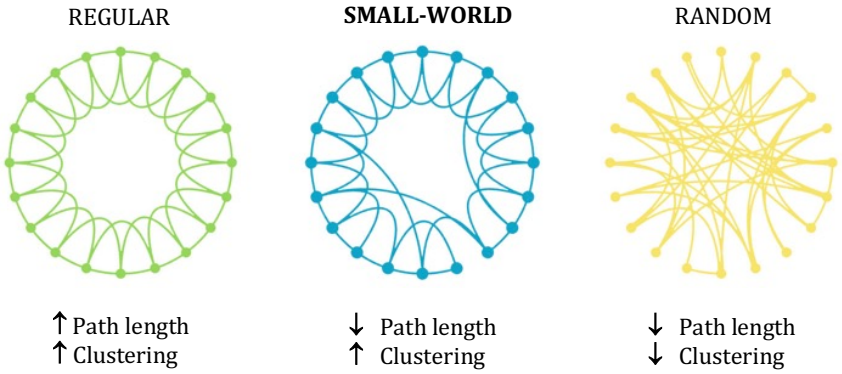

(Adapted from Watts and Strogatz, 1998)

The small-world property stands between regular and random networks. Regular networks have high average clustering, and high average path length; while, random networks show low average path length with low average clustering coefficient, thus implying that all nodes have a comparable number of edges, which does not adjust to what we see in real-world networks where hub nodes are commonly found (Figure 11). Networks can also be characterized according to the degree distribution - how many connections each node has - in decentralized or centralized networks. In decentralized networks there is a low level of diversity between the degree of the different nodes. However, what predominates in nature are the centralized networks, in particular the free scale networks, in which the degree distribution is very high, as there are many nodes with a low number of connections, while others have an exceptional number of edges (hubs). In this type of network there is an exponential relation between the number of connections of a node and the probability of having more connections. Free scale networks can be very robust and very weak at the same time, depending on the kind of node affected. If there are problems in random nodes the network would still work; however, if there is a problem in only one hub, it can have important negative effects in the whole network. Specifically, the brain network presents not only a small-world behaviour, but also the characteristics of a free scale network.

1.7.2. The Connectome

The comprehensive map of the structural connections that constitute the brain network is known as the connectome (Sporns et al., 2013). Along with the connectome comes a new field of science called connectomics, responsible for the study of the nodes and edges that constitute the brain connectivity, as well as the tools to analyse it (Hagmann et al., 2010). Brain connections can be captured by means of anatomical and physiological interactions using different neuroimaging techniques, leading to structural, functional and effective connectivity:

Structural connectivity defines anatomical connections associating different brain regions, and usually refers to WM projections connecting cortical and subcortical regions (Sporns, 2013).

Functional connectivity describes how different parts of the brain work together by looking at the statistical dependence of the BOLD signal between them. It arises from timeseries observations that can be obtained through techniques such as electroencephalography (EEG) or fMRI (Sporns, 2013).

Effective connectivity is based on causation and explains how activity in one region targets the physiological activity of another region (directed graph) (Sporns, 2013).

Figure 12: Structural and functional networks and the steps required before network analysis

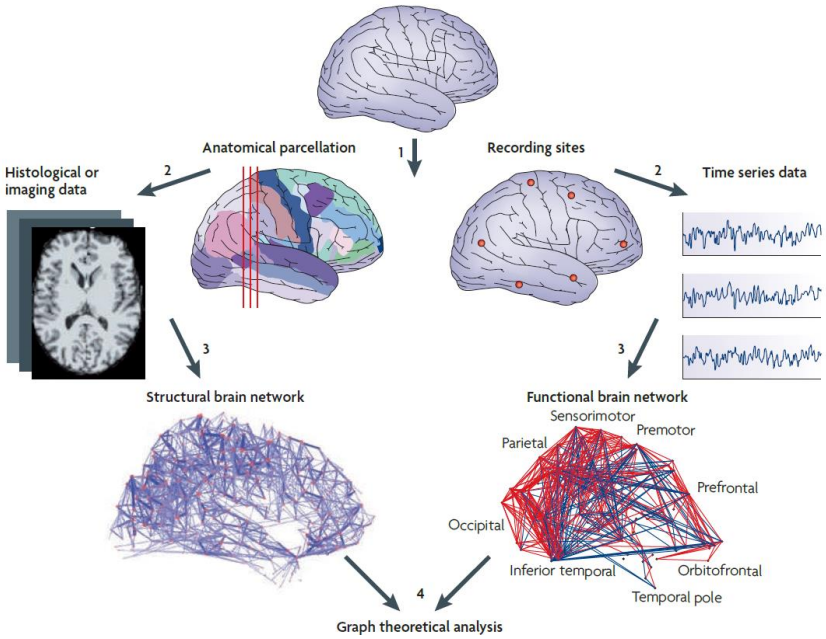

(Extracted from Medaglia and Bassett, 2017)

1.7.2.1. Structural MR connectomics

Diffusion weighted imaging (DWI) has allowed the mapping of the whole brain structural connectivity in vivo. Diffusion data provides indirect information about the structure surrounding water molecules by providing contrast associated to the degree of water diffusion in each voxel of the brain and, as WM presents anisotropic properties (Basser et al., 1994), it makes it possible to build connectivity matrices by inferring fibre tract trajectories based on FA and MD as well as the number of fibres.

DTI metrics

Diffusion Tensor Imaging (DTI) is a mathematical model that describes the diffusion at each voxel. Therefore, it provides information about microscopic changes in WM tissue. The principle of this imaging technique resides in the diffusion of water molecules in the brain and how its movement is restricted by membranes, fibres, and the macromolecules.

There are different metrics derived from DTI that are used to characterize WM integrity (Panel 5), by giving information about the shape and dimensions of the diffusion ellipsoid related to a particular voxel. These metrics are FA, MD, axial diffusivity (AxD) and radial diffusivity (RD), FA being the most broadly used metric to characterize WM (Mukherjee et al., 2008).

The eigenvectors are the three main axes that give information about the direction and magnitude of the diffusion ellipsoid. The primary eigenvector (λ_1) describes the direction of axonal fibre bundles, while the second and the third (λ_2, λ_3) give information about diffusion transversally to axonal bundles (Mukherjee et al., 2008). One of the most used methods to assess FA and the other metrics is the FSL tract-based spatial statistics (TBSS) tool (Smith et al., 2006), part of the FSL software (https: // fsl.fmrib.ox.ac.uk/ fsl/ fslwiki/TBSS).

DTI fibre tracking

Tractography is a method based on DTI data that allows us to infer the fibre bundles trajectories. It can be either deterministic, when it takes a unique orientation per voxel and, consequentially, generates one streamline for each seed voxel, or probabilistic, when it considers a distribution of fibre orientations creating multiple streamline samples per seed voxel based on a probability distribution of diffusion orientations within each voxel (Muller et al., 2018) (Figure 13).

Panel 5: White matter metrics derived from DTI

Fractional Anisotropy (FA): Degree of anisotropy with a value ranging between 0, in the case of isotropic (unrestricted diffusion), and up to 1 for anisotropic diffusion (preferential diffusion in one of the directions) (Mukherjee et al., 2008).

Mean Diffusivity (MD): Total diffusion within a voxel (mean of the three eigenvectors). Provides information about how the diffusion tensor is changing.

Axial Diffusivity (AxD): Direction of the long axis (λ_1). It is sensitive to axonal changes (Bennett et al., 2014).

Radial Diffusivity (RD): Amount of diffusion perpendicular to the long axis (mean of λ_2 and λ_3). It is sensitive to myelin changes (Bennett et al., 2014).

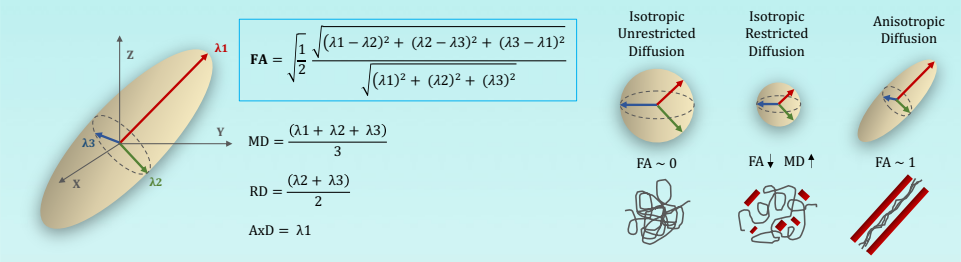

(Adapted from Mukherjee et al., 2008)

Figure 13: Pathway across voxels generated through deterministic and probabilistic tractography

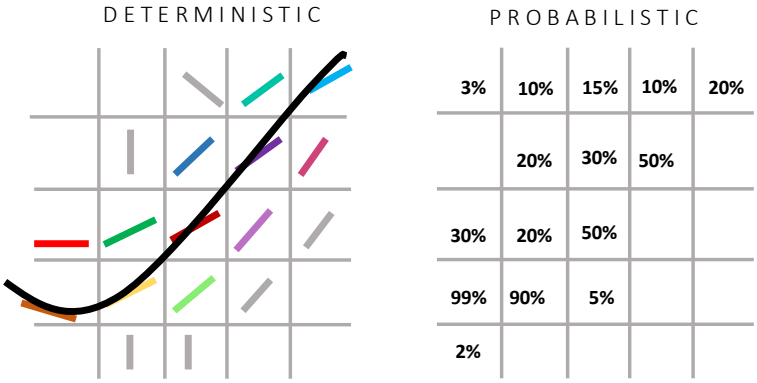

(Adapted from Muller et al., 2018)

Structural connectivity

Structural connectivity is frequently measured using tractography. The regions of interest (ROI) are defined as nodes and the reconstructed fibres that cross a pair of ROIs are considered the connections (Behrens et al., 2003). The strength of the connections (edges) can be established by the number of streamlines (NOS) between pairs of ROIs (Hagmann et al., 2007; Li et al., 2009). As has been previously described (*See section 1.7.1. Graph Theory, page 63*), this group of nodes and edges are going to constitute a weighted adjacency matrix that will be classified as symmetric, if its edges do not have directionality, or as asymmetric if the edges do have directionality (Figure 14).

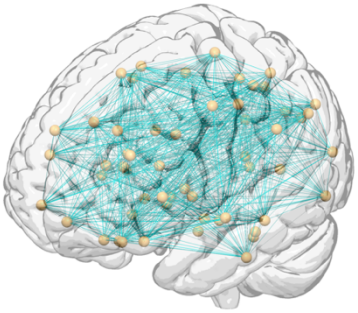

Figure 14: Structural connectivity of the human brain

Gold dots represent the nodes, while the turquois lines represent the edges. Surf Ice tool (www.nitrc.org) was used in combination with the Automated anatomical labelling atlas to draw the figure.

1.7.3. Structural findings in Parkinson's disease

In order to understand the role of WM in PD, DWI techniques have been used. Specifically, TBSS appears as a recurrently used method for this purpose; however, the results have not been conclusive. Whole-brain studies have found decreased FA in PD compared to HC in several tracts including the olfactory tract, hippocampal cingulate tract (Chen et al., 2018), the corpus callosum (Guimarães et al., 2018; Garcia-Diaz et al., 2018), internal and external capsule (Guimarães et al., 2018; Li et al., 2017), superior longitudinal fasciculus (Chen et al., 2018; Guimãraes et al., 2018), corona radiata, thalamic radiation, sagittal stratum (Guimarães et al., 2018), cingulum (Theilmann et al., 2013; Guimarães et al., 2018), forceps major and minor (Theilmann et al., 2013), and the uncinate fasciculus (Díez-Cirarda et al., 2015). Other studies did not find significant differences between PD and HC (Worker et al., 2014; Koshimori et al., 2015; Duncan et al., 2016), or even showed increased FA in PD in comparison to HC (Chen et al., 2018). On the other hand, ROI-based analyses have been mainly focused on the substantia nigra, reporting a reduction in FA in specific subregions (Schuff et al., 2015; Langley et al., 2016). There are studies that have specifically focused on PD-MCI. When comparing PD-MCI with HC they have found decreased FA in major associative tracts, the corona radiata and the corpus callosum (Hattori et al., 2012; Melzer et al., 2013; Agosta et al., 2014). However, studies looking for differences between PD with and without MCI did not find differences in FA (Galantucci et al., 2017) or found only a very small cluster with reduced FA (Melzer et al., 2013).

The reconstruction of the whole-brain structural connectome has been used to find abnormalities in PD connectivity compared to that of the HC. Reduced structural connectivity has been described in PD using deterministic (Nigro et al., 2016; Li et al., 2016) and probabilistic (Shah et al., 2017) approaches. Anomalies in PD connectivity have been found to involve frontal, temporal, parietal and occipital regions (Nigro et al., 2016; Li et al., 2016; Shah et al., 2017) as well as the basal ganglia (Nigro et al., 2016; Li et al., 2016). Global graph theory topological measures, such as cluster coefficient (Nigro et al., 2016; Shah et al., 2017), as well as nodal measures (Nigro et al., 2016; Li et al., 2016;

Shah et al., 2017) have been found to be reduced in PD. Controversially, Mishra et al., (2020) described greater connectivity in PD as well as greater values of nodal graph measures, while in line with previous studies, they also found reduced clustering coefficient.

Other studies based on ROIs have described reduced connectivity in connections involving the bilateral claustra (Arrigo et al., 2019) and subcortico-cortical connections of the sensorimotor circuitry (Sharman et al., 2012). While some have focused on describing abnormalities in PD subtypes, such as Abbasi et al., (2020), who described reduced connectivity in the diffuse malignant PD subtype compared to the mild motor predominant PD subtype (Fereshtehnejad et al., 2017) as well as reduced global efficiency and increased path length, others have focused on describing the structural connectivity of PD with different clinical characteristics. Galantucci et al., (2017) compared PD-MCI with HC and PD without MCI and found PD-MCI to have reduced structural connectivity in a bilateral principal connected component involving the basal ganglia and fronto-parietal regions. Wang et al., (2019) compared PD-MCI to PD without MCI and found reduced connectivity in several networks as well as reduced nodal efficiency, principally in orbitofrontal regions.

With the aim of finding particular patterns of connectivity alterations in PD, the previous studies used the network-based statistics (NBS), a statistical method that applies the FWE correction when analysing all the connections comprising the brain graph (Zalesky et al., 2010). In particular, the studies focused on PD-MCI based the NBS analyses on deterministic tractography. In Study 2 of this Thesis, structural networks of PD with and without MCI were reconstructed using probabilistic tractography and analysed by means of a novel technique, implemented by Baggio et al., (2018), the threshold-free network-based statistics (TFNBS), which combines threshold-free cluster enhancement (TFCE) and NBS, allowing us to obtain edge-wise p-values instead of thresholded cluster components. Moreover, the structural connectivity analysis presented in this Thesis was complemented with global and local graph topological measures, as well as with the analysis of FA and MD by means of TBSS.

CHAPTER 2

Hypotheses and Objectives

The present Doctoral Thesis is centered on the study of Parkinson's disease and Dementia with Lewy bodies heterogeneity. We aimed to identify subtypes in Parkinson's disease and Dementia with Lewy bodies based on structural MRI measures, as well as to characterize their clinical and cognitive profile. To this end, we performed subtyping analyses and structural connectivity analyses.

The general hypothesis is that there are different patterns of brain atrophy in Parkinson's disease as well as in Dementia with Lewy bodies, and that the heterogenous brain patterns could explain differences in cognitive impairment.

2.1. HYPOTHESES

1. Different Parkinson's disease subtypes are characterized by distinct patterns of brain atrophy. Grey matter atrophy is expected to be identified to a greater extent than white matter abnormalities in Parkinson's disease subtypes.
2. Brain atrophy patterns would be associated to different clinical and cognitive profiles. The Parkinson's disease subtype with later age at onset will display more atrophy than the other subtypes, as well as worse neuropsychological profile.
3. Parkinson's disease patients with mild cognitive impairment would be characterized by more prominent structural connectivity reduction than Parkinson's disease patients without mild cognitive impairment.
4. Structural connectivity abnormalities in Parkinson's disease patients are expected to be mild with major involvement of fronto-striatal connections, as well as in connections involving the posterior cortex that has been previously associated with cognitive impairment in nondemented PD patients.
5. We would detect different subtypes in Dementia with Lewy bodies that can be identified through data-driven subtyping based on MRI measures.
6. Different patterns of GM volume would be associated to different clinical and cognitive profiles in DLB, showing distinct neurodegeneration subtypes.

2.2. OBJECTIVES

1. To identify anatomical patterns involving grey and white matter variables of brain atrophy in Parkinson's disease through a multimodal MRI cluster analysis.
2. To identify the extent of white matter contribution to brain changes considering grey matter changes in the same sample.
3. To characterize the Parkinson's disease subtypes based on clinical and demographic data, as well as to their neuropsychological profile.
4. To describe whole-brain structural connectivity of Parkinson's disease patients with mild cognitive impairment.
5. To investigate complex structural brain networks in Parkinson's disease with mild cognitive impairment through complex structural brain networks in PD by means of global and regional graph-theory metrics.
6. To identify subtypes within Dementia with Lewy bodies based on different grey matter volumetric patterns by using a data-driven cluster analysis approach.
7. To characterize the Dementia with Lewy bodies subtypes based on clinical and demographic data as well as tau and β-amyloid biomarkers.

CHAPTER 3

Methods

The present Doctoral Thesis consists of three studies, listed below, comprising samples of patients with Parkinson's disease and Dementia with Lewy bodies, as well as healthy controls.

Study 1

Inguanzo A, Sala-Llonch R, Segura B, Erostarbe H, Abos A, Campabadal A, Uribe C, Baggio HC, Compta Y, Marti MJ, Valldeoriola F, Bargallo N, Junque C.

Hierarchical cluster analysis of multimodal imaging data identifies brain atrophy and cognitive patterns in Parkinson's disease. Parkinsonism & Related Disorders. 2021; 82: 16-23.

Study 2

Inguanzo A, Segura B, Sala-Llonch R, Monte-Rubio G, Abos A, Campabadal A, Uribe C, Baggio HC, Marti MJ, Valldeoriola F, Compta Y, Bargallo N, Junque C.

Impaired Structural Connectivity in Parkinson's Disease Patients with Mild Cognitive Impairment: A Study Based on Probabilistic Tractography. Brain Connectivity. 2021; 11(5): 380-392.

Study 3

Inguanzo A, Poulakis K, Mohanty R, Schwarz CG, Przybelski SA, Diaz-Galvan P, Lowe VJ, Boeve BF, Lemstra AW, van de Beek M, van der Flier W, Barkhof F, Blanc F, de Sousa PL, Philippi N, Cretin B, Demuynck C, Nedelska Z, Hort J, Segura S, Junque C, Oppedal K, Aarsland D, Westman E, Kantarci K, Ferreira D.

MRI data-driven clustering reveals different subtypes of Dementia with Lewy bodies. *Under review.*

3.1. STUDY SAMPLE

Below, a brief description of the principal methodological procedures for each study is provided. Further details are specified along this chapter and in the corresponding manuscripts attached in Chapter 4.

Inclusion and exclusion criteria for Studies 1 & 2

Inclusion criteria for patients were (i) fulfilling UK PD Society Brain Bank diagnostic criteria for PD and (ii) no surgical treatment with deep-brain stimulation. Exclusion criteria were (i) dementia according to Movement Disorders Society criteria, (ii) H&Y scale score > 3, (iii) severe psychiatric or neurological comorbidity, (iv) low global intelligence quotient estimated by the Vocabulary subtest of the Wechsler Adult Intelligence Scale 3rd edition (scalar score ≤ 7), (v) Mini Mental State Examination (MMSE) score below 25, (vi) claustrophobia, (vii) pathological MRI findings other than mild WM hyperintensities in the FLAIR sequence, and (viii) MRI artifacts.

Parkinson's disease patient sample - Studies 1 & 2

The sample included 69 PD patients recruited from the Parkinson's Disease and Movement Disorders Unit, Hospital Clínic (Barcelona, Spain). The following participants were excluded: 5 patients with MRI artifacts and 2 with claustrophobia. The final sample included participants with and without MCI. Motor symptoms were assessed with the UPDRS-III.

Healthy control sample – Study 1

The sample of HC in Study 1 included 36 volunteers from the Aging Institute in Barcelona. A total of 33 HC were selected, while 3 were excluded from the study: 2 with MRI artifacts and 1 with a cyst. The final sample included participants with and without MCI.

Healthy control sample – Study 2

The initial sample of HC in Study 2 included 54 volunteers from the Aging Institute in Barcelona. A total 51 HC were finally selected for the study. Three subjects were excluded: 2 HC with MRI artifacts, and one HC with a cyst. The inclusion criteria required absence of cognitive impairment.

Dementia with Lewy bodies patient sample – Study 3

A total of 165 subjects participated in this multicentre study. The data were a combination of the European DLB consortium (E-DLB) (n= 97) (Oppedal et al., 2019), including 29 subjects from the Motol University Hospital (Prague, Txec Republic), 34 from the Day Hospital of Geriatrics (Strasbourg, France), 34 from VU University Medical Centre (Amsterdam, the Netherlands) and 68 from the Mayo Clinic (Rochester, MN, United States). The diagnosis was made according to the 2005 International Consensus Criteria for probable DLB, based on history and clinical examinations performed by a licensed neurologist. Exclusion criteria were: (i) presence of acute delirium, (ii) terminal illness, (iii) previous stroke, (iv) psychotic or bipolar disorder, (v) craniocerebral trauma, and (vi) recent diagnosis of a major somatic illness. Presence or absence of clinical features was based on the 2005 International Consensus Criteria for probable DLB to allow harmonized diagnosis across all centers (McKeith et al., 2005).

Ethical statement of Studies 1 & 2

Written informed consent was obtained from all the participants of both studies after a full explanation of the procedures. The study was approved by the Institutional Ethics Committee from the University of Barcelona (IRB00003099).

Ethical statement of Study 3

Local ethics committee at each E-DLB centre and the Mayo Clinic Institutional Review Board approved the study. Informed consent on participation was obtained from all of the patients or an appropriate surrogate according to the Declaration of Helsinki.

3.2. CLINICAL AND NEUROPSYCHOLOGICAL ASSESSMENT

In Studies 1 and 2, neuropsychiatric and motor symptomatology was assessed, and a comprehensive battery of neuropsychological tests was administered. Further details are specified along the subsequent subsections.

3.2.1. Clinical assessment

Studies 1 & 2

Motor disease severity was evaluated using H&Y staging and UPDRS-III (Fahn and Elton, 1987). To study the presence of RBD-like symptomatology in both patients and controls the Innsbruck REM Sleep Behavior Disorder Inventory (RBD-I) was used (Frauscher et al., 2012). All PD patients were taking antiparkinsonian medication consisting of different combinations of L-DOPA, COMT inhibitors, MAO inhibitors, dopamine agonists, and amantadine. In order to standardize doses, LEDD was calculated (Tomlinson et al., 2010). All assessments were done in *on state*. Neuropsychiatric symptomatology was measured by means of Beck Depression Inventory II (BDI) (Beck et al., 1996), Starkstein's Apathy Scale (Starkstein et al., 1992), and the Neuropsychiatric Inventory (NPI) (Cummings et al., 1994). Additionally, in Study 1, olfaction was also assessed with the University of Pennsylvania Smell identification test (UPSIT) (Doty, 1995), and the Sniffin identification test (Hummel et al., 2007).

Study 3

All cardinal clinical features were assessed including presence of parkinsonism, VH, cognitive fluctuations, and a clinical history of probable RBD. MMSE was used as a measure of global cognitive performance.

3.2.2. Neuropsychological Assessment

Study 1 & 2

All participants underwent a comprehensive neuropsychological assessment addressing cognitive domains frequently impaired in PD (Table 4). Attention and working memory were assessed with the Trail Making Test (parts A and B), Digit Span Forward and Backward, Stroop Color and Word Test, Symbol Digit Modalities Test (SDMT)-Oral version. Executive functions were evaluated with phonemic and semantic fluencies. Language was assessed using the Boston Naming Test (BNT). Memory was assessed using Rey's Auditory Verbal Learning Test total learning recall, delayed recall and recognition abilities (RAVLT total, RAVLT recall, and RAVLT recognition, respectively). Visuospatial and visuoperceptual functions were assessed with Benton's Judgement of Line Orientation (JLO), Visual Form Discrimination (VFD), and Facial Recognition (FRT) tests.

Assessment of Mild Cognitive Impairment (MCI)

In Studies 1 and 2, the presence of MCI was defined using PD-MCI diagnostic criteria level II (Litvan et al., 2012). The z-scores for each test and for each subject were calculated based on the control group's means and standard deviations. Expected z scores adjusted for age, sex, and education were calculated based on a multiple regression analysis performed in the healthy control group (Aarsland et al., 2009). The presence of MCI was established if the z score for a minimum of 2 tests of the same domain, or one test of 2 different domains, were at least 1.5 below than the expected score (neuropsychological domains and tests are described in Table 4).

Table 4: Summary of neuropsychological tests

DOMAIN	TEST
Global cognition	Mini Mental State Examination (MMSE) (Folstein et al., 1975)
Attention & Working memory	Digit Span Forward and Backward (Wechsler, 1999) Symbol Digit Modalities Test (SDMT) (Smith, 2000) Trail Making Test (TMT, in seconds) part A and part B (Lezak et al., 2012) Stroop Color and Word Test (Stroop, 1935)
Executive functions	Phonetic Fluency (words beginning with "p" in 1 minute) (Lezak et al., 2012) Semantic fluency (animals in 1 minute) (Lezak et al., 2012)
Memory	Rey's Auditory Verbal Learning Test (RAVLT) (Lezak et al., 2012): · Total learning recall (sum of correct responses from trial I to trial V) · Delayed recall (total recall after 20min) · Recognition
Visuospatial & Visuoperceptual	Visual Form Discrimination (VFD) (Benton et al., 1994) Benton's Judgement of Line Orientation (JLO) (Benton et al., 1978) Short form of the Facial Recognition Test (FRT) (Benton et al., 1994)
Language	Short version of the Boston Naming Test (BNT) (Kaplan et al., 1983)

3.2.3. Statistical analyses for clinical and neuropsychological variables

Study 1 & 2

Demographic, neuropsychological, and clinical statistical analyses were conducted using IBM SPSS Statistics 25.0 (IBM Corp., Armonk, New York). To assess differences in demographic, clinical and neuropsychological quantitative variables, Kruskal-Wallis or Mann-Whitney U tests were used, while Pearson's chi-squared test was used for categorical variables. Additionally, in Study 2, correlations between the neuropsychological and clinical data with global FA measures and NOS were evaluated using Pearson correlation.

Study 3

Differences in demographic and clinical measures were assessed with one-way ANOVA for continuous variables and the Pearson's chi-square test for categorical variables. The analyses were performed using IBM SPSS Statistics 27.0 (IBM Corp., Armonk, New York).

3.3. MRI ACQUISITION

Figure 15: Summary of the MRI techniques used in each study

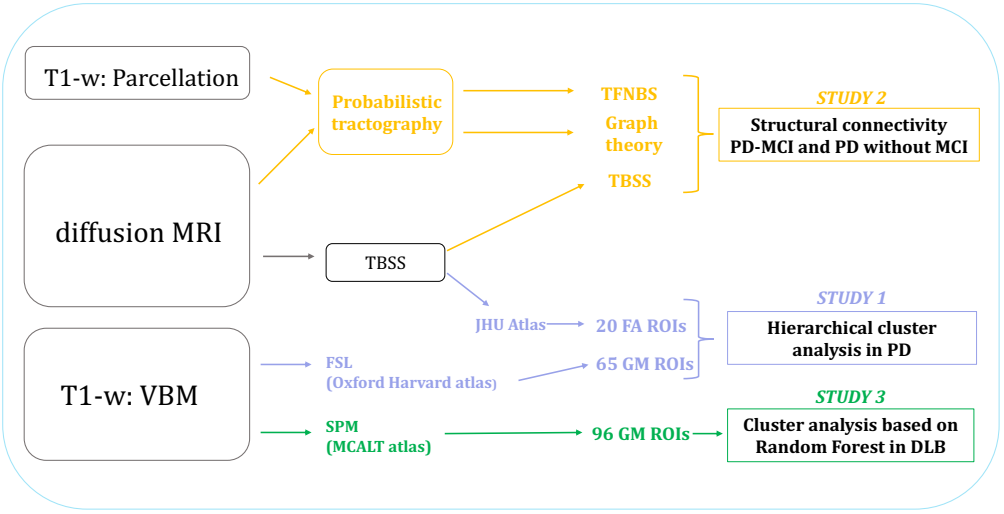

Studies 1 & 2

MRI data were acquired on a 3-Tesla SIEMENS MAGNETOM Trio Tim scanner. The scanning protocols included the following MRI sequences:

- Structural T1 images: high-resolution 3-dimensional T1-weighted images acquired in the sagittal plane (TR=2300 ms, TE=2.98 ms, TI=900 ms, 240 slices, FOV=256 mm, resolution= (1,1,1) mm).

- Diffusion-weighted images: two sets of single band spin-echo diffusion weighted images in the axial plane with opposite (anterior-posterior and posterior-anterior) phase encoding directions (TR=7700 ms, TE=89 ms, FOV=244 mm; resolution = (2,2,2) mm; number of directions=30, b-value=1000 s/mm2, b0=0 s/mm2).

- FLAIR: axial FLAIR sequence (TR = 9000 ms, TE = 96 ms).

Study 3

Structural T1 images were provided from 4 different centres:

- Images from Strasbourg were acquired on a 3-Tesla SIEMENS VERIO (TR=1900ms, TE=2.53ms, TI= 900ms, FA=9, resolution= (1,1,1) mm).
- Images from Prague were acquired on a 1.5-Tesla SIEMENS AVANTO (TR=2000ms, TE=3.08ms, TI=1100ms, FA=15, resolution= (0.98,0.98,1) mm).
- Images from Amsterdam were acquired on a 3-Tesla SIGNA (TR=8ms, TE=3ms, TI=450ms, FA= 12, resolution (0.98,0.98,1) mm).
- Images from Mayo Clinic were acquired on a 3-Tesla 3T General Electric (GE) Discovery SIGNA (TR=2300ms, TE= 3ms, TI= 900ms, resolution = (1,1,1.2) mm).

Table 5: Summary of the main MRI characteristics of the studies

Study	Study Description	Sample size	Age; disease duration	MRI data (images)	Analysis technique
Study 1	Data-driven analysis in PD	62 PD 33 HC	64.5 (15); 7(7) 66 (15); NA	T1-weighted DWI	VBM TBSS Hierarchical cluster analysis
Study 2	Structural connectivity in PD-MCI	62 PD 51 HC	64.5(15); 7(7) 66 (17); NA	T1-weighted DWI	TBSS TFNBS Graph theory
Study 3	Data-driven analysis in DLB	165 DLB	69 (8.57); 5.16 (4.62)	T1-weighted	Hierarchical cluster analysis based on Random Forest (VBM pipeline)

For Study 1 & 2 age and disease duration are shown as median (IQ), while in Study 3 are shown as mean (SD).

3.4. NEUROIMAGING TECHNIQUES

3.4.1. Structural MRI

3.4.1.1. Voxel-based morphometry

In Studies 1 and 3, voxel-based morphometry (VBM) was used to estimate the amount of GM in a voxel through its signal intensity (Good et al., 2001), which was then used for cluster analysis. Additionally, in Study 1, VBM was used for voxel-wise comparison of local GM volumes.

Data preprocessing

FSL-VBM pipeline (Douaud et al., 2007) was used in Study 1; while SPM12 (https://www.fil.ion.ucl.ac.uk/spm/) was used in Study 3 for the same purpose.

In Study 1, structural images were first brain-extracted and segmented into GM, WM and cerebrospinal fluid (CSF), then registered to the Montreal Neurological Institute (MNI) 152 standard space using non-linear registration. The resulting images were averaged to create a study-specific template, to which native GM images were nonlinearly registered. Second, native GM images were registered to this study specific template and modulated to correct for local expansion or contraction due to the nonlinear component of the spatial transformation. The modulated GM images were then smoothed with an isotropic Gaussian kernel with a sigma of 3 mm following the FSL guidelines (Douaud et al., 2007). GM volumes from 48 cortical regions and 17 subcortical regions of interest defined by the Harvard-Oxford atlases (https://fsl.fmrib.ox.ac.uk/fsl/fslwiki/Atlases) were obtained.

In Study 3, using ANTs (Avants et al., 2008), the Mayo Clinic Adult Lifespan Template (MCALT) atlas (https://www.nitrc.org/projects/mcalt/) was propagated to individuals' native MPRAGE space and regional estimations of volume across cortical and subcortical GM structures were calculated. Tissue probabilities were determined for each MPRAGE using the unified segmentation algorithm in SPM12 (Wellcome Trust Centre for

Neuroimaging, London, UK), with MCALT tissue priors and settings (Schwarz et al., 2017). The total intracranial volume (TIV) was calculated from the tissue probabilities. GM volume from 82 cortical, 12 subcortical and 2 brainstem ROIs were obtained.

3.4.1.2. Cortical segmentation

In Study 2, structural images were used to parcellate the cerebral cortex into gyral and sulcal structures based on the Desikan-Killiany atlas (Desikan et al., 2006), as well as for registration and normalization purposes.

Data preprocessing

Structural MRI preprocessing was performed using FreeSurfer (version 5.1; available at: https://surfer.nmr.mgh.harvard.edu/), an open-source software specialized in processing and analysing brain MRI images. FreeSurfer provides a full processing stream for structural MRI data: removal of non-brain tissue, automated Talairach transformation, intensity normalization (Sled et al., 1998), tessellation of the GM/WM boundary, automated topology correction (Ségonne et al., 2007), and accurate surface deformation to optimally place the GM/WM and GM/CSF boundaries (Fischl and Dale, 2000). The output of each step (registration, skull stripping, segmentation, and cortical surface reconstruction) was visually inspected to guarantee correct and accurate preprocessing.

3.4.2. Diffusion MRI

Diffusion MRI was employed in Study 1 and 2 to characterize WM abnormalities with diffusion tensor-derived measures and, additionally in Study 2, to reconstruct fibre tracts through probabilistic tractography.

Data preprocessing

Diffusion-weighted images were preprocessed with FSL version 5.08 using FDT (FMRIB's Diffusion Toolbox), a toolbox that includes data processing, local diffusion

modeling and tractography tools (Jbabdi et al., 2012). First, visual inspection of the images was done to identify motion and intensity artifacts. Followed by brain extraction using BET, susceptibility-induced distortion correction using top-up, and eddy-current distortion and subject motion correction with the eddy tool.

Diffusion analyses

TBSS: In Study 1 and 2, a voxel-wise statistical analysis of FA images was carried out using TBSS (Smith et al., 2006).
First, the preprocessed diffusion MRI images were analysed with FDT software from FSL. Then, individual FA maps were obtained using a Diffusion Tensor Model fit (DTIFIT). Voxel-wise statistical analysis of FA was carried through with TBSS (Smith et al., 2006), which performs nonlinear registration (using Nonlinear Image Registration Tool [FMRIB]) of FA images from DTIFIT to the MNI standard space and generates a mean FA skeleton that represents the centre of all WM tracts common to the whole group. Each subject's FA image was projected onto the skeleton and the resulting FA skeleton images were fed into a general linear model (GLM) to find vertex-wise differences in FA skeleton maps between groups. In addition, in Study 2, the same steps were used to obtain the MD maps.

Tractography: In Study 2, probabilistic tractography was used. First, the 86 ROIs previously obtained with FreeSurfer were linearly registered from native structural space to native diffusion space with FMRIB's Linear Image Registration Tool (Jenkinson et al., 2002) to be used as seeds. Next, Bedpostx was applied to calculate the probability distribution of fibre directions in each voxel (Behrens et al., 2007). Finally, the tractography was run with the Probrtarckx2 tool (Behrens et al., 2007) obtaining an 86x86 connectivity matrix per subject.

3.4.3. Graph Theory Connectivity

In Study 2, individual 86x86 connectivity matrices (68 cortical and 18 deep gray matter ROIs) were used for the connectome and graph theory analyses. The NOS between each pair of ROIs, was taken as a measure of the strength of structural connectivity between regions. To minimize false-positive connections, streamlines intersecting fewer than two regions were ignored, and those detected in at least 50% of the individuals were considered (Abos et al., 2019; Zalesky et al., 2010).

Connectome analysis: TFNBS was used to perform statistic inference in brain graph analyses.

Graph theory analysis: Graph theory topological parameters derived from the NOS matrices were obtained using the Brain Connectivity Toolbox from MATLAB. The graph metrics included global and local normalized clustering coefficient, global and local node degree, small worldness, normalized path length, modularity, local efficiency, and betweenness centrality. (*See Rubinov and Sporns, 2010 for detailed definitions and calculations of the graph metrics*).

3.5. DATA-DRIVEN SUBTYPING

In Studies 1 and 3, unsupervised data-driven approaches were used to find clusters within the PD and DLB sample, respectively. Calinski-Harabasz criterion was used in both studies to evaluate the optimal number of clusters.

3.5.1. Hierarchical cluster analysis

In Study 1, we performed a hierarchical cluster analysis using the Ward's linkage method, which combines pairs of clusters at each step while minimizing the sum of square errors from the cluster mean. First, we used the FSL command-line fslmeants to calculate the mean GM volume from 48 cortical and 17 subcortical ROIs defined by the Harvard-Oxford atlases (https://fsl.fmrib.ox.ac.uk/fsl/fslwiki/Atlases) in MNI standard space. Mean FA values were extracted from 20 tracts of interest defined in the JHU atlas (Wakana et al., 2007), also in the MNI standard space. The 85 resulting features were then merged into a single vector for each of the PD patients and used to perform a hierarchical cluster analysis with MATLAB (release 2014b, The MathWorks, Inc., Natick, Massachusetts).

3.5.2. Cluster analysis using Random Forest

In Study 3, we performed a cluster analysis with the RF method, which uses an ensemble classifier consisting of many decision trees (Breiman et al., 1996).

The analysis with the RF method was applied on the residuals of the 96 ROIs, from the MCALT atlas, which were adjusted by TIV and centre (Breiman et al., 2001). Then, through bootstrapping (Breiman et al., 1996), each tree was trained with a slightly different set of the data (Amit and Geman, 1997), which consisted of 70% of the original data, while the remaining 30% was used for validation. The RF method was implemented in R (The R Foundation for Statistical Computing; version 4.0.3). Cluster analysis using RF is based on the similarity (proximity) measure between pairs of observations (Shi and Horvath, 2006). First, each tree assigns the observations together on a certain class by directing them on the same terminal node, and each time the pair

of observations ends up on the same terminal node, the similarity measure increases by 1. Agglomerative hierarchical clustering with the average linkage method was then used in the output data from RF.

Ordering the cluster features according to their relevance

In Study 1, we used ANOVAs to determine which ROIs showed a greater difference between the 3 groups. Accordingly, features with higher F values were considered more relevant in differentiating the clusters.

In Study 3, the mean decrease in the Gini index was used to identify the ROIs with the highest contribution to the cluster analysis.

3.6. COMPLEMENTARY ANALYSES

3.6.1. Receiver Operating Characteristic (ROC) curve

In Study 2, we used the binomial logistic regression, which is based on a regression model to predict the probability that, for a given input data, each input belongs to a numeric category (0 or 1). It models data using a sigmoid function and becomes a classification technique when a threshold is established on the sigmoid (0.5). The receiver operating characteristic (ROC) curve was obtained from the probability estimations by the logistic regression as scores, as well as the corresponding area under the curve (AUC).

3.6.2. Supervised Random Forest

In Study 3, a supervised RF was performed using the 10 most relevant ROIs from the unsupervised RF (the ones with the lowest Gini values) as predictor variables, and the cluster number as the dependent variable. Hence, we obtained information on which ROIs better characterized each cluster.

3.6.3. Biomarkers of concomitant pathology

In Study 3, the presence of concomitant AD and cerebrovascular disease were evaluated.

In order to determine the presence of concomitant AD pathology, presence of both β-amyloid and tau biomarkers was required, as they are both needed for AD diagnosis (Jack et al., 2018). In the E-DLB consortium, the β-amyloid and tau pathologies were assessed with CSF β-amyloid 1-42 and phosphorylated tau biomarkers; while, in the Mayo Clinic, PET imaging with PiB and flortaucipir (AV-1451) tracers was used to assess β-amyloid and tau pathologies, respectively. Biomarker levels were classified as normal or abnormal based on centre-specific established cut points. For more detailed information on the biomarkers procedure please see Ferreira et al., (2020a) for the E-DLB, and Kantarci et al., (2017) for the Mayo Clinic.

For cerebrovascular disease, white matter hyperintensities (WMH) were defined as signal abnormalities of variable size in the WM using a semi-quantitative method described in Ferreira et al., (2021).

Differences in concomitant AD pathology and WMH between clusters were assessed with ANOVA.

3.6.4. Longitudinal analysis: linear mixed model

In Study 3, in order to evaluate the global cognitive decline in the DLB subtypes, a linear mixed model was implemented in R version 4.0.3. The linear mixed effects model design consisted of a random intercept per subject with the model reference set to the baseline and cluster 3. The outcome was the longitudinal MMSE scores (12-month, 24-month and 36-month follow-up). The fixed effects were time (categorical), cluster (categorical) and interaction between time and cluster. Post-hoc pairwise comparisons were done between clusters based on model estimates with multiple comparisons corrections with Tukey adjustment.

CHAPTER 4

Results

STUDY 1

Inguanzo A, Sala-Llonch R, Segura B, Erostarbe H, Abos A, Campabadal A, Uribe C, Baggio HC, Compta Y, Marti MJ, Valldeoriola F, Bargallo N, Junque C.

Hierarchical cluster analysis of multimodal imaging data identifies brain atrophy and cognitive patterns in Parkinson's disease. Parkinsonism & Related Disorders. 2021; 82: 16-23.

Parkinsonism and Related Disorders 82 (2021) 16–23

Contents lists available at ScienceDirect

Parkinsonism and Related Disorders

journal homepage: www.elsevier.com/locate/parkreldis

Hierarchical cluster analysis of multimodal imaging data identifies brain atrophy and cognitive patterns in Parkinson's disease

A. Inguanzo [a,b,c], R. Sala-Llonch [a,c,d,e], B. Segura [a,b,c,f,*], H. Erostarbe [a], A. Abos [a,b,c], A. Campabadal [a,b,c], C. Uribe [a,b], H.C. Baggio [a,b], Y. Compta [a,c,f,g], M.J. Marti [a,c,f,g], F. Valldeoriola [a,c,f,g], N. Bargallo [h,i], C. Junque [a,b,c,f]

[a] Institute of Neurosciences, University of Barcelona, Barcelona, Catalonia, Spain
[b] Medical Psychology Unit, Department of Medicine, University of Barcelona, Barcelona, Catalonia, Spain
[c] Institute of Biomedical Research August Pi i Sunyer (IDIBAPS), Barcelona, Catalonia, Spain
[d] Department of Biomedicine, University of Barcelona, Barcelona, Catalonia, Spain
[e] Centro de Investigación Biomédica en Red en Bioingeniería, Biomateriales y Nanomedicina (CIBER-BBN), Barcelona, Catalonia, Spain
[f] Centro de Investigación Biomédica en Red Sobre Enfermedades Neurodegenerativas (CIBERNED: CB06/05/0018-ISCIII), Barcelona, Catalonia, Spain
[g] Movement Disorders Unit, Neurology Service, Hospital Clínic de Barcelona, University of Barcelona, Barcelona, Catalonia, Spain
[h] Centre de Diagnostic per la imatge, Hospital Clínic de Barcelona, Barcelona, Catalonia, Spain
[i] Magnetic Resonance Core Facility, Institute of Biomedical Research August Pi i Sunyer (IDIBAPS). Barcelona, Catalonia, Spain

ARTICLE INFO

Keywords:
Parkinson disease
Cluster analysis
Magnetic resonance imaging
DTI
Gray matter volume

ABSTRACT

Background: Parkinson's disease (PD) is a heterogeneous condition. Cluster analysis based on cortical thickness has been used to define distinct patterns of brain atrophy in PD. However, the potential of other neuroimaging modalities, such as white matter (WM) fractional anisotropy (FA), which has also been demonstrated to be altered in PD, has not been investigated.

Objective: We aim to characterize PD subtypes using a multimodal clustering approach based on cortical and subcortical gray matter (GM) volumes and FA measures.

Methods: We included T1-weighted and diffusion-weighted MRI data from 62 PD patients and 33 healthy controls. We extracted mean GM volumes from 48 cortical and 17 subcortical regions using FSL-VBM, and the mean FA from 20 WM tracts using Tract-Based Spatial Statistics (TBSS). Hierarchical cluster analysis was performed with the PD sample using Ward's linkage method. Whole-brain voxel-wise intergroup comparisons of VBM and TBSS data were also performed using FSL. Neuropsychological and demographic statistical analyses were conducted using IBM SPSS Statistics 25.0.

Results: We identified three PD subtypes, with prominent differences in GM patterns and little WM involvement. One group (n = 15) with widespread cortical and subcortical GM volume and WM FA reductions and pronounced cognitive deficits; a second group (n = 21) with only cortical atrophy limited to frontal and temporal regions and more specific neuropsychological impairment, and a third group (n = 26) without detectable atrophy or cognition impairment.

Conclusion: Multimodal MRI data allows classifying PD patients into groups according to GM and WM patterns, which in turn are associated with the cognitive profile.

1. Introduction

Parkinson's disease (PD) is characterized by its clinical heterogeneity, which includes not only motor symptoms but also a wide range of non-motor manifestations [1,2]. Objective neuroimaging data obtained from magnetic resonance imaging (MRI) has been

* Corresponding author. Medical Psychology Unit, Department of Medicine, University of Barcelona, Casanova 143, 08036, Barcelona, Spain.
E-mail addresses: annainguanzo@ub.edu (A. Inguanzo), roser.sala@ub.edu (R. Sala-Llonch), bsegura@ub.edu (B. Segura), herostga7@alumnes.ub.edu (H. Erostarbe), alexandraabos@ub.edu (A. Abos), anna.campabadal@ub.edu (A. Campabadal), carme.uribe@ub.edu (C. Uribe), hbaggio@ub.edu (H.C. Baggio), ycompta@clinic.cat (Y. Compta), mjmarti@clinic.cat (M.J. Marti), fvallde@clinic.cat (F. Valldeoriola), bargallo@clinic.cat (N. Bargallo), cjunque@ub.edu (C. Junque).

https://doi.org/10.1016/j.parkreldis.2020.11.010
Received 17 January 2020; Received in revised form 15 September 2020; Accepted 10 November 2020
Available online 12 November 2020

demonstrated to be able to classify PD patients through cluster analysis. Uribe et al. [3] used cortical thickness from MRI data to define distinct anatomical subtypes in a non-demented PD sample, and found one group with frontal and occipital atrophy, a second group with parieto-temporal atrophy and a third with undetectable atrophy. These three patterns were then found to be associated with different clinical/cognitive profiles. Moreover, a follow up of this study concluded that the three patterns progressed differently over time, the pattern with the youngest age at onset being the one associated with the least structural degeneration [4].

These studies have used cortical thickness to define the clusters representing atrophy profiles. However, previous studies have also shown volumetric differences in cortical and subcortical GM regions [5] as well as microstructural white matter (WM) alterations in PD [6]. In addition, GM and WM changes have been widely shown to be associated with cognitive impairment [5,7–9]. Recently, disruption of integration of structural brain networks was observed in PD subtypes identified through clinical data and was correlated with motor and cognitive deficits [10].

To date, no previous studies have combined GM and WM information extracted from MRI to detect different disease subgroups in PD using a multimodal hypothesis-free data-driven approach. We hypothesized that multimodal clustering including FA measures would allow us to more accurately identify subgroups of patients characterized by different patterns of neurodegeneration, which at the same time would be associated with distinctive clinical and neuropsychological phenotypes. Accordingly, we aimed to combine measures of GM cortical and subcortical volumes, as well as measures of WM microstructure to determine (1) whether different anatomical profiles exist involving GM and WM patterns of brain atrophy; and (2) whether the different patterns are associated with distinct cognitive profiles.

2. Methods

2.1. Participants

The sample included 69 PD patients recruited from the Parkinson's Disease and Movement Disorders Unit, Hospital Clínic (Barcelona, Spain), and 36 healthy controls (HC) from the Aging Institute in Barcelona. Inclusion criteria for patients were (i) fulfilling UK PD Society Brain Bank diagnostic criteria for PD and (ii) no surgical treatment with deep-brain stimulation. Exclusion criteria for all participants were (i) dementia according to Movement Disorders Society criteria, (ii) Hoehn and Yahr (H&Y) scale score > 3, (iii) severe psychiatric or neurological comorbidity, (iv) low global intelligence quotient estimated by the Vocabulary subtest of the Wechsler Adult Intelligence Scale 3rd edition (scalar score ≤ 7), (v) Mini Mental State Examination (MMSE) score below 25, (vi) claustrophobia, (vii) pathological MRI findings other than mild WM hyperintensities in the FLAIR sequence, and (viii) MRI artifacts. A total of 62 PD patients and 33 HC were selected. The following participants were excluded from the study: five patients and two HC with MRI artifacts, two patients with claustrophobia and one HC with a cyst. The final sample included participants with and without mild cognitive impairment (MCI). Motor symptoms were assessed with the Unified Parkinson's Disease Rating Scale, motor section (UPDRS-III). All PD patients were taking antiparkinsonian drugs that consisted of different combinations of L-dopa, catechol-O-methyltransferase inhibitors, monoamine oxidase inhibitors, dopamine agonists, and amantadine. To standardize the doses, the L-dopa equivalent daily dose (LEDD) [11] was calculated. Written informed consent was obtained from all study participants after a full explanation of the procedures. The study was approved by the institutional Ethics Committee from the University of Barcelona (IRB00003099).

2.2. Neuropsychological tests

All participants underwent a comprehensive neuropsychological assessment in the *on state* addressing cognitive domains frequently impaired in PD [12]. Attention and working memory were assessed with the Trail Making Test (parts A and B), Digit Span Forward and Backward, Stroop Color-word Test, Symbol Digits Modalities Test (SDMT)-Oral version. Executive functions were evaluated with phonemic and semantic fluencies. Language was assessed using the Boston Naming Test (BNT). Memory was assessed using Rey's Auditory Verbal Learning Test total learning recall, delayed recall and recognition abilities (RAVLT total, RAVLT recall, and RAVLT recognition, respectively). Visuospatial and visuoperceptual functions were assessed with Benton's Judgement of Line Orientation (JLO), Visual Form Discrimination (VFD), and Facial Recognition (FRT) tests. Neuropsychiatric symptoms were evaluated with the Beck Depression Inventory-II, Starkstein's Apathy Scale and Cumming's Neuropsychiatric Inventory. Expected z scores adjusted for age, sex, and education were calculated for each test and subject based on a multiple regression analysis performed in the HC group [13]. The presence of MCI was defined using PD-MCI diagnostic criteria level II [12].

2.3. Neuroimaging data

2.3.1. MRI acquisition

MRI data were obtained with a 3T scanner (MAGNETOM Trio, Siemens, Germany). The scanning protocol included high-resolution 3-dimensional T1-weighted images acquired in the sagittal plane (TR: 2300 ms, TE: 2.98 ms, TI: 900 ms, 240 slices, FOV: 256 mm; 1 mm isotropic voxel), and diffusion-weighted images (DTI): two sets of single band spin-echo diffusion weighted images in the axial plane with opposite (anterior-posterior and posterior-anterior) phase encoding directions (TR: 7700 ms, TE: 89 ms, FOV: 244 mm; 2 mm isotropic voxel; number of directions: 30, b-value: 1000 s/mm^2, b0 value: 0 s/mm^2).

2.3.2. Structural MRI preprocessing

Structural data were analyzed with FSL-VBM [14]. First, structural images were brain-extracted and segmented into GM, WM and cerebrospinal fluid, then registered to the Montreal Neurological Institute (MNI) 152 standard space using non-linear registration. The resulting images were averaged to create a study-specific template, to which native GM images were nonlinearly re-registered. Second, native GM images were registered to this study specific template and modulated to correct for local expansion or contraction due to the nonlinear component of the spatial transformation. The modulated GM images were then smoothed with an isotropic Gaussian kernel with a sigma of 3 mm (FWHM = 6.9 mm) following the FSL guidelines [14].

2.3.3. Diffusion MRI preprocessing

Diffusion MRI images were analyzed with FMRIB's Diffusion Toolbox (FDT) software from FSL, (http://www.fmrib.ox.ac.uk/fsl). Individual fractional anisotropy (FA) maps were obtained using a Diffusion Tensor Model fit (DTIFIT) and introduced to group analysis using the Tract-Based Spatial Statistics (TBSS) protocol [15,16]. TBSS performs non-linear registration (FNIRT) of FA images to the MNI standard space and generates a mean FA skeleton that represents the center of all tracts common to the entire group. Then, the aligned FA image for each subject was projected onto the skeleton by filling the skeleton with FA values from the nearest relevant tract center.

2.4. Hierarchical cluster analysis

As described above, we obtained individual GM probability maps using a VBM approach and skeletonized FA maps from all subjects using a DTI approach with FSL. Using the FSL command-line fslmeants, we calculated the mean GM volume from 48 cortical regions and 17

subcortical regions of interest defined by the Harvard-Oxford atlases (https://fsl.fmrib.ox.ac.uk/fsl/fslwiki/Atlases) in MNI standard space. Mean FA values were extracted from 20 tracts of interest defined in the JHU atlas [17], also in the MNI standard space. The 85 resulting features were then merged into a single vector for each of the 62 PD patients subject and used to perform a hierarchical cluster analysis with MATLAB (release 2014b, The MathWorks, Inc., Natick, Massachusetts) (Fig. 1). We used Ward's clustering linkage method to combine pairs of clusters at each step while minimizing the sum of square errors from the cluster mean. Following the hierarchical structure of the analysis, each patient was first placed in his/her own cluster and then progressively clustered with others. Calinski-Harabasz criterion was used to evaluate the optimal number of clusters. Cluster analysis results are shown as a dendrogram with different levels of granularity. For each cluster, we defined a mean cluster vector of 85 features, calculated as the average of all features across the subjects included in the cluster.

2.5. Other statistical analyses

First, to quantify the differences between the groups identified through the clustering procedure, and to define their specific atrophy patterns compared with controls, we performed a set of t-tests using the GM and WM measures used as features. The results were corrected for multiple comparisons using false-discovery rate (FDR) correction across the 85 evaluated features, and the significance level was set at $p < 0.05$. To list the features according to their importance in forming the clusters, we used the F statistics obtained from ANOVAs.

We then performed voxel-wise analyses to obtain maps of GM and WM. For that purpose, we used a permutation-based general linear model (GLM) using the whole-brain VBM and FA maps [18]. In these analyses, we tested for differences between PD groups as well as differences between each group and controls. Age was considered as a covariate in the model. Results were corrected for multiple comparisons across space using family-wise error rate (FWE) correction, with a significance level of $p < 0.05$.

Demographic, neuropsychological, and clinical statistical analyses were conducted using IBM SPSS Statistics 25.0 (IBM Corp., Armonk, New York). To assess differences in demographic, clinical and neuropsychological quantitative variables, Kruskal-Wallis or Mann-Whitney U tests were used. Pearson's chi-squared test was used for categorical variables.

3. Results

The dendrogram resulting from the cluster analysis can be seen in the Supplementary material 1. Both two-cluster and three-cluster solutions had a high variance ratio of the Calinski-Harabasz values. The two-cluster solution (variance ratio: 11.58) identified one group without detectable brain atrophy; and a second group with widespread reduction of cortical and subcortical GM volume, decreased FA, late disease onset and higher prevalence of MCI. Detailed information about the two-cluster solution is shown in Supplementary material 2. The three-cluster solution (variance ratio: 8.59) divided the non-specific atrophy group from the two-cluster solution into two subgroups (Supplementary material 2 and 3). The sample size was too small for higher group solution, and the result would be considered too exploratory.

Ordering the features according to their importance for forming the clusters showed GM features were more relevant than the WM features (Supplementary material 4).

3.1. Whole-brain atrophy patterns in the three-cluster solution

Exploratory whole-brain analyses were first performed without covariates (Supplementary material 5, 6 and 7). Whole-brain analysis of VBM maps considering age in the model showed group 1 (PD1, N: 15) had lower GM volumes than HC mainly in occipital and medial temporal

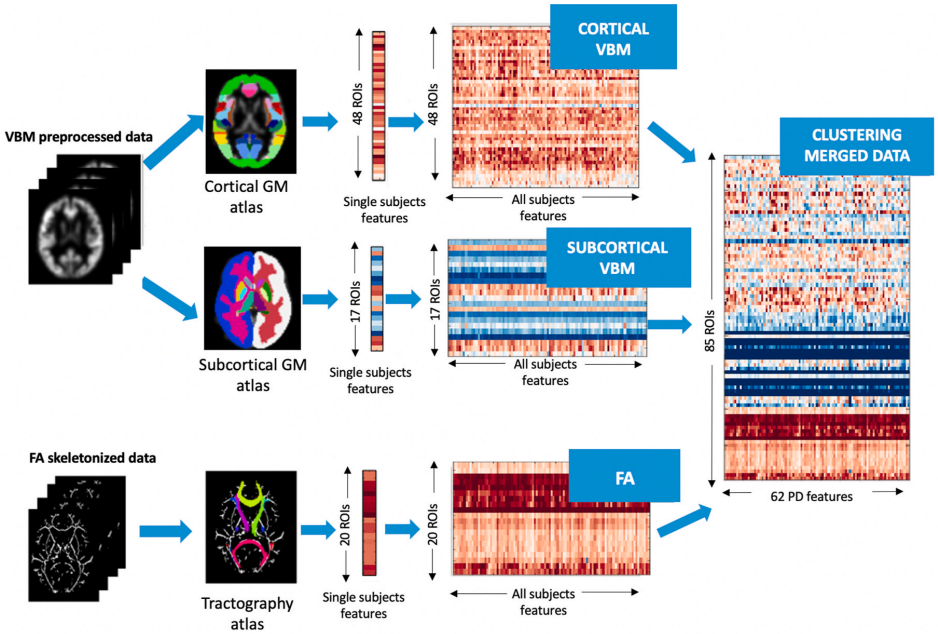

Fig. 1. Schematic representation of the pipeline followed to extract the features used in the classification procedure. Abbreviations: FA – fractional anisotropy, GM – gray matter, ROI – region of interest, VBM – Voxel-based morphometry analysis.

regions including the parahippocampal gyrus, temporal pole, cuneus, lingual gyrus, occipital fusiform gyrus and occipital pole. The atrophy pattern of PD1 also included the bilateral orbital and medial frontal cortex, paracingulate gyrus, superior parietal lobe, precuneus, and insula. Moreover, PD1 showed volume reductions in subcortical gray matter compared to HC in bilateral putamen, caudate, thalamus, and nucleus accumbens as well as the hippocampus (FWE-corrected, $p < 0.05$) (Fig. 2A and Supplementary material 8). Group 2 (PD2, N: 21) had GM atrophy compared with HC mainly in bilateral orbital and prefrontal cortical regions including the bilateral anterior cingulate gyrus, orbitofrontal cortex, medial prefrontal cortex, paracingulate gyri, frontal poles and the inferior and middle temporal gyri, as well as the right superior temporal gyrus (FWE-corrected, $p < 0.05$) (Fig. 2B and Supplementary material 8). Group 3 (PD3, N:26) did not show significant GM volume differences compared with HC (Fig. 2C).

Comparisons between patient groups showed that PD1 had reduced subcortical GM volume compared with PD2 in the thalamus, amygdala and right putamen bilaterally as well as in the hippocampus. PD1 also showed a characteristic posterior cortical atrophy including bilateral occipital poles, lingual gyri and cuneus, together with parahippocampal and fusiform gyri, as well as reductions in insular and cerebellar regions (Supplementary material 8 and 9). PD1 showed reduced cortical GM when compared with PD3 bilaterally in superior and middle temporal gyri, medial temporal lobe, occipital pole, the insular cortex, the

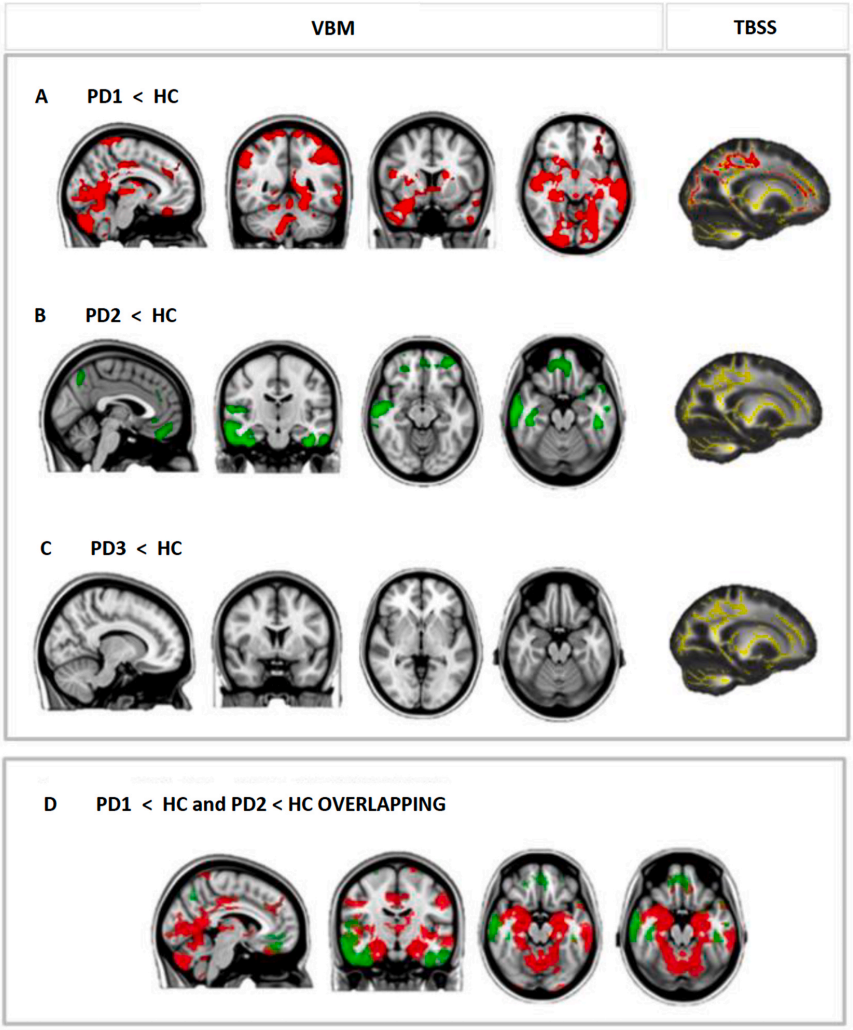

Fig. 2. Voxel-based morphometry (VBM) and tract-based spatial statistics (TBSS) analyses of the three-cluster solution. VBM: (A) regions in which PD1 showed less gray matter volume than HC are shown in red; (B) regions in which PD2 showed less gray matter volume than HC are shown in green; (C) absence of differences between PD3 and HC ($p < 0.05$, FWE-corrected). Results were adjusted by age. TBSS: FA skeleton (yellow) and white matter tracts in which PD1 showed lower FA than HC (red). Radiological convention is used. Abbreviations: HC – healthy controls; PD1 – Parkinson's disease patient subgroup 1; PD2 – Parkinson's disease patient subgroup 2; PD3 – Parkinson's disease patient subgroup 3. (For interpretation of the references to color in this figure legend, the reader is referred to the Web version of this article.)

intracalcarine cortex, and the hippocampus and significant reductions of the amygdala, thalamus, putamen, caudate and nucleus accumbens bilaterally (Supplementary material 8 and 9).

PD2 had less GM volume than PD3 in the right middle temporal gyrus. PD3 had less GM volume than PD2 in the cerebellum and the brainstem. HC had less GM than PD2 in the cerebellum (Supplementary material 8).

Whole-brain analyses of FA maps showed lower FA values in PD1 compared with HC in the corpus callosum and the following bilateral tracts: the inferior and superior longitudinal fasciculus, inferior fronto-occipital fasciculus, anterior thalamic radiation, uncinate fasciculus, corticospinal tract, and forceps major and minor (FWE-corrected, $p < 0.05$) (Fig. 2 and Supplementary material 10). There were no other significant differences between groups.

3.2. Demographic and clinical characteristics of PD subtypes

There were no differences in sex or years of education between groups. However, we did find significant differences in age between groups. PD3 was significantly younger than HC and the other PD groups, while PD1 tended to be older than HC ($p = 0.054$). PD groups did not differ in disease duration, motor disease severity as measured by the UPDRS-III, H&Y and LEDD, global cognition (MMSE), olfactory performance, or presence of neuropsychiatric symptoms. PD1 had a later disease onset compared with PD3 (Table 1).

3.3. Cognitive profiles of PD subtypes

Fig. 3 summarizes the cognitive profiles of patients in the three groups (see also Supplementary Table 11). PD1 and PD2 performed significantly worse than HC in the following tests: FRT, TMT Part A and Part B, and Stroop Color Test. Whereas PD3 did not show significant differences in cognitive performance in comparison with HC.

Moreover, PD1 performed significantly worse than HC and PD3 in RAVLT total and recognition scores, and in the semantic fluency test. PD1 also performed worse than HC in RAVLT recall. PD2 performed worse than HC in Stroop Words and SDMT.

PD1 showed a higher percentage of MCI (67%) when compared with PD3 (27%) and HC (Table 1).

4. Discussion

The main finding of this study is that a data-driven analysis based on multimodal MRI data can identify PD patient subtypes according to GM and WM degeneration patterns. Despite similar disease duration, our results distinguished (1) a group of patients with bilateral tempo-parieto-occipital loss of cortical GM as well as subcortical GM volume degeneration and widespread FA reductions mainly affecting fronto-occipital WM tracts; (2) a second group with reduction of GM volumes in bilateral orbital and medial prefrontal, but also in temporal cortical regions, and (3) a third group without detectable GM or WM alterations.

Patients grouped in PD1, which interestingly was the group with a higher percentage of MCI (67%), showed extensive atrophy similar to that previously reported using cortical thickness [3], as well as evident atrophy in bilateral hippocampus and subcortical structures, including the amygdala, thalamus, putamen and caudate. Similarly, the PD2 subgroup showed bilateral atrophy in orbitofrontal and temporal cortices, which partially overlapped with PD1. In this context, and without longitudinal evidence, these results could be indicative of different stages of evolution in our group. However, PD groups did not differ in the years of evolution of the disease, and although those in PD1 were older than in PD2, age of onset was also older. In addition, there were no differences in UPDRS part III or H&Y scores, or medication. Thus, our results reinforce the classical findings that late onset of the disease is associated with greater degree of atrophy and rapid disease progression [19].

Although most of the published results regarding loss of WM integrity in PD are based on analyses of regions of interest, whole-brain studies evidenced the involvement of the corpus callosum, cingulum and major association tracts in PD-MCI patients [7,9,20], but not in PD without MCI [9]. Nonetheless, these results are still scarce and less consistent than those reporting GM atrophy. In this regard, the existence

Table 1
Demographic and clinical characteristics of the three-cluster solution PD subtypes. Abbreviations: BDI – Beck Depression Inventory II; HC – healthy controls; IQ – interquartile range; LEDD – L-dopa equivalent daily dose; MCI – mild cognitive impairment; NA – not applicable; NPI – Neuropsychiatric Inventory; PD1 – Parkinson's disease group 1 patients; PD2 – Parkinson's disease group 2 patients; PD3 – Parkinson's disease group 3 patients; UPDRS – Unified Parkinson's Disease Rating Scale; UPSIT – University of Pennsylvania Smell Identification Test.[a] The chi- squared test was used;[b] The Kruskal-Wallis test was used.

	HC (N:33)	PD1 (N:15)	PD2 (N:21)	PD3 (N:26)	test-stats	p-value	Significant contrasts
sex (m/f)	18/15	13/2	14/7	19/7	5.4	0.145[a]	–
age, median (IQ)	66(15)	75(14)	68(9)	58.5(11)	29.273	<0.001[b]	PD3 vs HC PD3 vs PD2 PD3 vs PD1
Education, years, median (IQ)	12(8)	11(12)	13(9)	13(9)	1.171	0.768[b]	–
Disease duration, median (IQ)	NA	7(7.5)	9(9)	7(5.5)	1.302	0.521[b]	–
Age of onset, median (IQ)	NA	67(10)	57(11)	50(12.25)	20.097	<0.001[b]	PD1 vs PD3
LEDD, mg, median (IQ)	NA	650(415)	469(515)	593.75(324)	0.651	0.722[b]	–
UPDRS part III, median (IQ)	NA	30(1)	29(2)	30(2)	2.258	0.521[b]	–
Hoehn & Yahr, n, 1/2/2.5/3	NA	1/6/1/4	1/10/0/9	6/14/0/6	14.754	0.064[a]	–
MMSE, median (IQ)	0.102(3.32)	−0.96(4.32)	0.074(5.58)	−0.51(4.02)	1.908	0.592[b]	–
Total MCI, n (%)	3 (10%)	10 (67%)	10 (48%)	7(27%)	17.431	0.001[a]	PD1 vs HC PD1 vs PD3 PD2 vs HC
UPSIT (normosmia/hyposmia/anosmia)	5/26/0	0/2/12	1/11/8	1/13/11	34.998	<0.001[a]	PD1 vs HC PD2 vs HC PD3 vs HC
Sniffin (normosmia/hyposmia/anosmia)	20/9/0	0/4/7	1/14/3	3/13/6	53.56	<0.001[a]	PD1 vs HC PD2 vs HC PD3 vs HC
BDI, median (IQ)	5(8)	7(10)	9(12)	7(6)	4.5	0.212[b]	–
Apathy scale (apathy/normal)	5/25 (17%)	7/8 (47%)	10/9 (48%)	8/15 (31%)	9.757	0.135[a]	–
NPI, median (IQ)	1(4)	9(8)	7.5(19)	6(11)	19.047	<0.001[b]	PD1 vs HC PD2 vs HC PD3 vs HC
Visual hallucinations (no/yes), n (%)	29/0	11/4 (27%)	18/3 (14%)	21/5 (19%)	7.414	0.06[a]	–

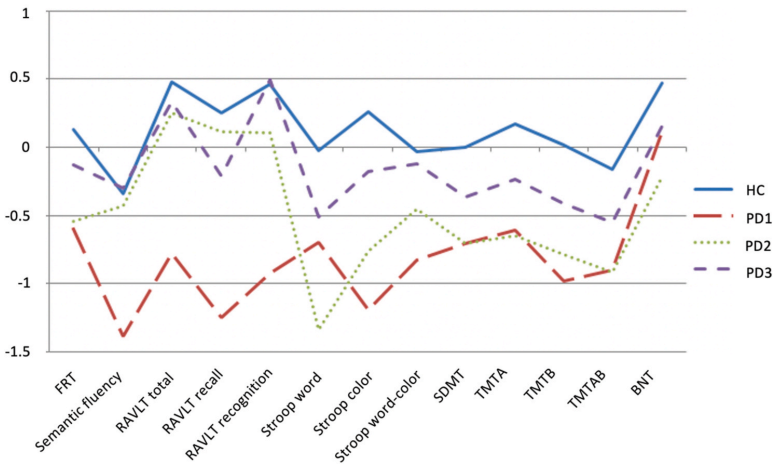

Fig. 3. Three-cluster solution – neuropsychological profiles. Neuropsychological profiles for healthy controls (blue), PD1 (red), PD2 (green) and PD3 (purple). Data are presented as z scores. The signs of TMTA, TMTB and TMTAB scores are flipped. In all cases, lower z scores indicate worse performance. Abbreviations: BNT – Boston Naming Test; FRT – Facial Recognition Test; HC – healthy controls; PD1 – Parkinson's disease patient subgroup 1; PD2 – Parkinson's disease patient subgroup 2; PD3 – Parkinson's disease patient group 3; RAVLT – Rey Auditory Verbal Learning Test; SDMT – Symbol Digits Modalities Test; Stroop color – Stroop color test; Stroop word – Stroop word test; Stroop word-color – Stroop word-color interference; TMTA – Trail Making Test Part A; TMTB – Trail Making Test Part B; TMTAB – Trail Making Test A minus B. Tests displayed are the ones showing significant differences between groups. (For interpretation of the references to color in this figure legend, the reader is referred to the Web version of this article.)

of different PD subtypes could help to elucidate previous controversial results on the study of WM abnormalities.

Our results suggest that only a subgroup with widespread GM atrophy showed WM alterations compared to HC, in line with the recent results of Abassi et al. [10] showing structural connectivity differences in PD subtypes. Unfortunately, in that study the authors did not report whole-brain FA differences in PD subtypes since the analyses were limited to the basal ganglia. Our results suggest that DTI abnormalities in PD patients could be understood as secondary to axonal degeneration after cortical and subcortical neuronal body damage, which consequently would be expected to be found alongside GM atrophy.

Our findings also revealed the existence of a third subgroup (PD3), which was the youngest group with earlier disease onset. Despite the similarity in other clinical variables between groups, PD3 patients did not show significant structural differences with HC neither in GM nor in WM, after controlling for age. Similarly, previous studies reported negative results when comparing PD patients without cognitive impairment and HC in cortical and subcortical GM using whole-brain VBM or WM methods [7,9]. Previous cortical thickness analyses also showed negative results when comparing PD and HC [21,22] or described differences that did not survive correction for multiple comparisons [23].

Regarding the neuropsychological performance of the PD subgroups, both PD1 and PD2 subtypes performed worse than HC in the Facial Recognition Test, TMT Part A and Part B, and Stroop Color Test; whereas PD3 performed similarly to HC. Moreover, PD1 also performed significantly worse than HC and PD3 in RAVLT and the semantic fluency test. It is noteworthy that the impairment in total learning and delayed recall verbal tasks characteristic of the PD1 subtype has been associated with future cognitive impairment in PD [24], the hippocampus being a key structure to understanding the memory changes in PD without dementia [25]. Additionally, PD1 had semantic memory impairment that agrees with the involvement of posterior cortical regions [4,26]. Specifically, posterior based cortical deficits, and semantic fluency in particular, have been shown to be a predictor of dementia in PD [27]. More precisely, the PD1 atrophy pattern also included the primary occipital cortex, just as it has been found before in early PD patients [28], and might be related to color perception deficits described in PD [29].

On the other hand, the PD2 subgroup did not show a detectable cognitive profile to distinguish it from other PD subgroups; however, the brain atrophy pattern in this group was clearly different. Despite a discreet overlap between PD1 and PD2, there is a dissociation between these groups: while the PD2 pattern consisted of a more prominent orbitofrontal atrophy including bilateral frontal medial regions, but also anterior areas, PD1 was characterized by extensive atrophic changes in bilateral temporo-parieto-occipital regions. This dissociation may have not only important cognitive but also behavioral and mood consequences. In this context, depression in PD has been related to decreased GM volume in orbitofrontal and temporal regions [30]. In the same way, apathy and recognition of emotions have been seen to correlate with GM volumes in the orbitofrontal cortex [31,32], the amygdala [31] and the temporal cortex [32]. Although we did not find significant differences between groups in BDI or the apathy scale, PD1 and PD2 yielded the highest percentage of subjects with apathy (close to 50%), while PD3 and HC showed lower percentages. In this regard, the inclusion of tests sensitive to orbitofrontal and posterior deficits in the neuropsychological batteries used to assess PD patients is of crucial interest as previously stated [3].

The need to better understand the heterogeneity seen in other neurodegenerative disorders, such as Alzheimer's disease (AD), has similarly led to the use of neuroimaging data and cluster analysis to assess the presence of potential subgroups [33]. Taking one step further, Jeon and colleagues recently used a multimodal cluster analysis based on cortical thickness, tau and amyloid depositions, which led to the characterization of three AD subgroups [34], mainly driven by the tau deposition and cortical atrophic pattern. However, multidimensionality remains a limitation of these studies, as well as of our work, despite our having managed to improve the high dimensionality problem compared with previous cluster analyses [3,34] through the use of only 85 features. Further progress in this issue will allow, for example, combining different diffusion measures in an optimal model in order to better characterize WM differences between PD subtypes. Another limitation would be that PD patients with a Hoehn and Yahr scale score above 3 were excluded from the study, which could have reduced the variability of the PD sample and, consequently, the probability of finding other PD groups. Finally, the wide confidence intervals of the neuropsychological data suggest that a larger sample would be required in order to more precisely identify cognitive differences between groups.

In conclusion, the use of unsupervised machine learning methods based on multimodal MRI data allows the classification of PD patients into the following subtypes: one group with cortical and subcortical GM atrophy, widespread WM abnormalities and worse cognition; a second group with mainly orbitofrontal and temporal cortical atrophy; and a third group without detectable GM or WM abnormalities, earlier disease onset and normal cognition. It is also worth noting that even though both WM and GM contributed to defining the different groups, GM

degeneration patterns were more relevant in the characterization of PD groups than WM alterations. Nevertheless, incorporating FA measures to the clustering algorithm implies moving one step closer to multimodal approaches. Moreover, these results add to recent evidence regarding different phenotypes in PD, which not only differ in cognitive performance but also in patterns of brain degeneration, thus lending further support to the hypothesis of distinct disease courses.

Appendix A. Supplementary data

Supplementary data to this article can be found online at https://doi.org/10.1016/j.parkreldis.2020.11.010.

Disclosures

This study was sponsored by the Spanish Ministry of Economy and Competitiveness (PSI2013-41393-P; PSI2017-86930-P cofinanced by Agencia Estatal de Investigación (AEI) and the European Regional Development Fund), by Generalitat de Catalunya (2017SGR748), Fundació La Marató de TV3 in Spain (20142310), and supported by María de Maeztu Unit of Excellence (Institute of Neurosciences, University of Barcelona) MDM-2017-0729, Ministry of Science, Innovation and Universities. AI and AC were supported by APIF predoctoral fellowship from the University of Barcelona (2017–2018). AA was supported by a fellowship from 2016, Departament d'Empresa i Coneixement de la Generalitat de Catalunya, AGAUR (2016FI_B00360). CU was supported by a fellowship from 2014, Spanish Ministry of Economy and Competitiveness (BES-2014-068173) and co-financed by the European Social Fund (ESF).

MJM received honoraria for advice and lecture from Abbvie, Bial and Merzt Pharma and grants from Michael J. Fox Foundation for Parkinson Disease (MJFF): MJF_PPMI_10_001, PI044024.

YC has received funding in the past five years from FIS/FEDER, H2020 programme, Union Chimique Belge (UCB pharma), Teva, Medtronic, Abbvie, Novartis, Merz, Piramal Imaging, and Esteve, Bial, and Zambon. YC is currently an associate editor for Parkinsonism and Related Disorders.

We are also indebted to the Magnetic Resonance Imaging core facility of the IDIBAPS for technical support (project IBPS15-EE-3688 cofunded by MCIU and by ERDF); and we acknowledge the CERCA Programme/Generalitat de Catalunya. We are especially grateful to all the participants in the study for their goodwill and generosity.

References

[1] K.R. Chaudhuri, G.G. Healy, A.H.V. Schapita, Non-motor symptoms of Parkinson's disease: diagnosis and management, Lancet Neurol. 5 (2006) 235–245. http://neurology.thelancet.com.

[2] L.V. Kalia, A.E. Lang, Parkinson's disease, Lancet 386 (2015) 896–912, https://doi.org/10.1016/S0140-6736(14)61393-3.

[3] C. Uribe, B. Segura, H.C. Baggio, A. Abos, M.J. Marti, F. Valldeoriola, et al., Patterns of cortical thinning in nondemented Parkinson's disease patients, Mov. Disord. 31 (2016) 699–708, https://doi.org/10.1002/mds.26590.

[4] C. Uribe, B. Segura, H.C. Baggio, A. Abos, A.I. Garcia-Diaz, A. Campabadal, et al., Progression of Parkinson's disease patients' subtypes based on cortical thinning: 4-year follow-up, Park. Relat. Disord. 64 (2019) 286–292, https://doi.org/10.1016/j.parkreldis.2019.05.012.

[5] N. Ibarretxe-Bilbao, E. Tolosa, C. Junque, M.J. Marti, MRI and cognitive impairment in Parkinson's disease, Mov. Disord. 24 (2009), https://doi.org/10.1002/mds.22670.

[6] C. Atkinson-Clement, S. Pinto, A. Eusebio, O. Coulon, Diffusion tensor imaging in Parkinson's disease: review and meta-analysis, NeuroImage Clin 16 (2017) 98–110, https://doi.org/10.1016/j.nicl.2017.07.011.

[7] T. Hattori, S. Orimo, S. Aoki, K. Ito, O. Abe, A. Amano, et al., Cognitive status correlates with white matter alteration in Parkinson's disease, Hum. Brain Mapp. 33 (2012) 727–739, https://doi.org/10.1002/hbm.21245.

[8] T.R. Melzer, R. Watts, M.R. MacAskill, T.L. Pitcher, L. Livingston, R.J. Keenan, J. C. Dalrymple-Alford, T.J. Anderson, White matter microstructure deteriorates across cognitive stages in Parkinson disease, Neurology 80 (2013) 1841–1849.

[9] F. Agosta, E. Canu, E. Stefanova, L. Sarro, A. Tomić, V. Špica, et al., Mild cognitive impairment in Parkinson's disease is associated with a distributed pattern of brain white matter damage, Hum. Brain Mapp. 35 (2014) 1921–1929, https://doi.org/10.1002/hbm.22302.

[10] N. Abbasi, S.M. Fereshtehnejad, Y. Zeighami, K.M.H. Larcher, R.B. Postuma, A. Dagher, Predicting severity and prognosis in Parkinson's disease from brain microstructure and connectivity, NeuroImage Clin 25 (2020), https://doi.org/10.1016/j.nicl.2019.102111.

[11] C.L. Tomlinson, R. Stowe, S. Patel, C. Rick, R. Gray, C.E. Clarke, Systematic review of levodopa dose equivalency reporting in Parkinson's disease, Mov. Disord. 25 (2010) 2649–2653, https://doi.org/10.1002/mds.23429.

[12] I. Litvan, J.G. Goldman, A.I. Tröster, B.A. Schmand, D. Weintraub, R.C. Petersen, et al., Diagnostic criteria for mild cognitive impairment in Parkinson's disease: Movement Disorder Society Task Force guidelines, Mov. Disord. 27 (2012) 349–356, https://doi.org/10.1002/mds.24893.

[13] D. Aarsland, K. Brønnick, J.P. Larsen, O.B. Tysnes, G. Alves, Cognitive impairment in incident, untreated Parkinson disease: the Norwegian ParkWest study, Neurology 72 (2009) 1121–1126, https://doi.org/10.1212/01.wnl.0000338632.00552.cb.

[14] G. Douaud, S. Smith, M. Jenkinson, T. Behrens, H. Johansen-Berg, J. Vickers, et al., Anatomically related grey and white matter abnormalities in adolescent-onset schizophrenia, Brain 130 (2007) 2375–2386, https://doi.org/10.1093/brain/awm184.

[15] S.M. Smith, M. Jenkinson, H. Johansen-Berg, D. Rueckert, T.E. Nichols, C. E. Mackay, et al., Tract-based spatial statistics: voxelwise analysis of multi-subject diffusion data, Neuroimage 31 (2006) 1487–1505, https://doi.org/10.1016/j.neuroimage.2006.02.024.

[16] M. Jenkinson, C.F. Beckmann, T.E.J. Behrens, M.W. Woolrich, S.M. Smith, Review FSL, Neuroimage 62 (2012) 782–790, https://doi.org/10.1016/j.neuroimage.2011.09.015.

[17] S. Wakana, A. Caprihan, M.M. Panzenboeck, J.H. Fallon, M. Perry, R.L. Gollub, K. Hua, J. Zhang, H. Jiang, P. Dubey, A. Blitz, P. van Zijl, S. Mori, Reproducibility of quantitative tractography methods applied to cerebral white matter, NeuroImage 36 (2007) 630–644, https://doi.org/10.1016/j.neuroimage.2007.02.049.

[18] A.M. Winkler, G.R. Ridgway, M.A. Webster, S.M. Smith, T.E. Nichols, Permutation inference for the general linear model, Neuroimage 92 (2014) 381–397, https://doi.org/10.1016/j.neuroimage.2014.01.060.

[19] S.M. Fereshtehnejad, Y. Zeighami, A. Dagher, R.B. Postuma, Clinical criteria for subtyping Parkinson's disease: biomarkers and longitudinal progression, Brain 140 (2017) 1959–1976, https://doi.org/10.1093/brain/awx118.

[20] F.X. Chen, D.Z. Kang, F.Y. Chen, Y. Liu, G. Wu, X. Li, et al., Gray matter atrophy associated with mild cognitive impairment in Parkinson's disease, Neurosci. Lett. 617 (2016) 160–165, https://doi.org/10.1016/j.neulet.2015.12.055.

[21] J.B. Pereira, D. Weintraub, K. Brønnick, A. Lebedev, E. Westman, D. Aarsland, Initial Cognitive Decline is Associated with Cortical Thinning in Early Parkinson Disease 82 (2014) 2017–2025. http://surfer.nmr.mgh.harvard.edu/fswiki, 2014.

[22] E. Mak, L. Su, G.B. Williams, M.J. Firbank, R.A. Lawson, A.J. Yarnall, et al., Baseline and longitudinal grey matter changes in newly diagnosed Parkinson's disease: ICICLE-PD study, Brain 138 (2015) 2974–2986, https://doi.org/10.1093/brain/awv211.

[23] J. Pagonabarraga, I. Corcuera-Solano, Y. Vives-Gilabert, G. Llebaria, C. García-Sánchez, B. Pascual-Sedano, et al., Pattern of regional cortical thinning associated with cognitive deterioration in Parkinson's disease, PloS One 8 (2013), e54980, https://doi.org/10.1371/journal.pone.0054980.

[24] G. Levy, D.M. Jacobs, M.X. Tang, L.J. Côté, E.D. Louis, B. Alfaro, et al., Memory and executive function impairment predict dementia in Parkinson's disease, Mov. Disord. 17 (2002) 1221–1226, https://doi.org/10.1002/mds.10280.

[25] C. Uribe, B. Segura, H.C. Baggio, A. Campabadal, A. Abos, Y. Compta, et al., Differential progression of regional hippocampal atrophy in aging and Parkinson's disease, Front. Aging Neurosci. 10 (2018) 1–9, https://doi.org/10.3389/fnagi.2018.00325.

[26] B. Segura, H.C. Baggio, M.J. Marti, F. Valldeoriola, Y. Compta, A.I. Garcia-Diaz, et al., Cortical thinning associated with mild cognitive impairment in Parkinson's disease, Mov. Disord. 29 (2014) 1495–1503, https://doi.org/10.1002/mds.25982.

[27] C.H. Williams-Gray, T. Foltynie, C.E.G. Brayne, T.W. Robbins, R.A. Barker, Evolution of cognitive dysfunction in an incident Parkinson's disease cohort, Brain 130 (2007) 1787–1798, https://doi.org/10.1093/brain/awm111.

[28] C. Uribe, B. Segura, H.C. Baggio, A. Abos, A.I. Garcia-Diaz, A. Campabadal, et al., Cortical atrophy patterns in early Parkinson's disease patients using hierarchical cluster analysis, Park. Relat. Disord. 50 (2018) 3–9, https://doi.org/10.1016/j.parkreldis.2018.02.006.

[29] R.B. Postuma, J Gagnon, J Bertrand, D.G Marchand, J.Y. Montplaisir, Parkinson risk in idiopathic REM sleep behavior disorder: preparing for neuroprotective trials, Neurology 84 (11) (2015) 1104–1113, https://doi.org/10.1212/WNL.0000000000001364.

[30] A. Feldmann, Z. Illes, P. Kosztolanyi, E. Illes, A. Mike, F. Kover, et al., Morphometric changes of gray matter in Parkinson's disease with depression: a voxel-based morphometry study, Mov. Disord. 23 (2008) 42–46, https://doi.org/10.1002/mds.21765.

[31] N. Ibarretxe-Bilbao, C. Junque, E. Tolosa, M.J. Marti, F. Valldeoriola, N. Bargallo, et al., Neuroanatomical correlates of impaired decision-making and facial emotion recognition in early Parkinson's disease, Eur. J. Neurosci. 30 (2009) 1162–1171, https://doi.org/10.1111/j.1460-9568.2009.06892.x.

[32] H. Alzahrani, A. Antonini, A. Venneri, Apathy in mild Parkinson's disease: neuropsychological and neuroimaging evidence, J. Parkinsons Dis. 6 (2016) 821–832, https://doi.org/10.3233/JPD-160809.
[33] Y. Noh, S. Jeon, J.M. Lee, S.W. Seo, G.H. Kim, H. Cho, et al., Anatomical heterogeneity of Alzheimer disease Based on cortical thickness on MRIs, Neurology 83 (2014) 1936–1944, https://doi.org/10.1212/WNL.0000000000001003.
[34] S. Jeon, J.M. Kang, S. Seo, H.J. Jeong, T. Funck, S.Y. Lee, et al., Topographical heterogeneity of Alzheimer's disease based on MR imaging, tau PET, and amyloid PET, Front. Aging Neurosci. 10 (2019) 1–10, https://doi.org/10.3389/fnagi.2019.00211.

SUPPLEMENTARY MATERIAL

Supplementary material 1

Dendrogram of the 62 PD patients clustered according to gray matter volume and fractional anisotropy values. PD patient subgroups 1 (PD1), 2 (PD2) and 3 (PD3) in red, blue and green, respectively.

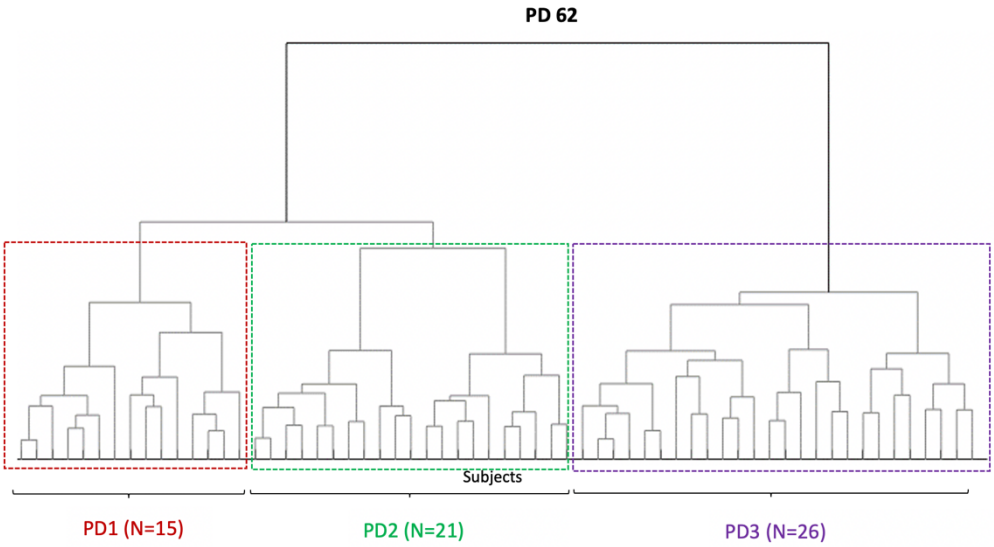

Supplementary material 2 (2-cluster solution)

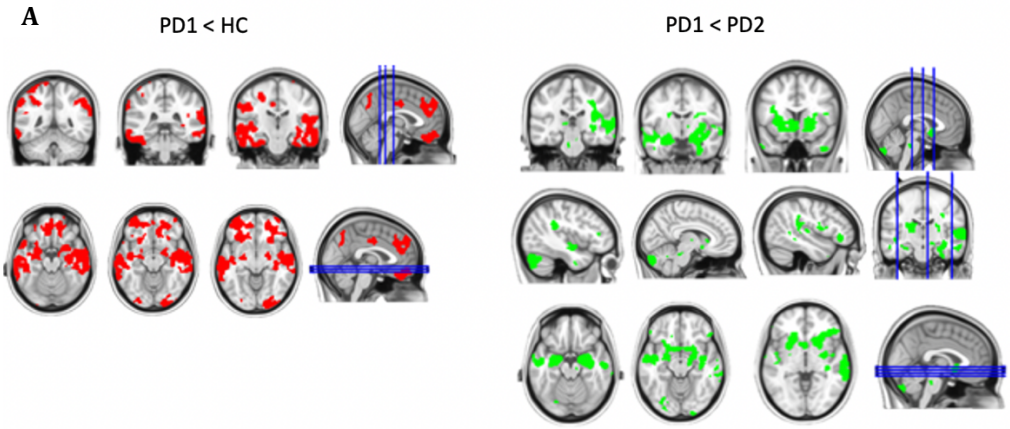

B	HC (N:33)	PD1 (N:36)	PD2 (N:26)	Test stats	p-value	Post hoc analysis
sex (m/f)	18/15	27/9	19/7	3.807[a]	.149	-
age, mean (SD)	66.03(10.88)	69.81(8.49)	57.88(7)	23.027[b]	<.001	PD2 vs HC PD2 vs PD1
Education, years, mean (SD)	12.56(4.70)	12.22(8.49)	13.54(4.77)	1.136[b]	.567	-
Disease duration, mean (SD)	NA	9(6.95)	7.96(4.51)	0.05[c]	.823	-
Age of onset, mean (SD)	NA	60.65(10.78)	50(8.84)	14.72[c]	<.001	-
UPDRS part III, mean (SD)	NA	17.69(9.65)	13.92(7.22)	1.815[c]	.178	-
Hoehn & Yahr, n, 1/2/2.5/3	NA	2/16/1/13	6/14/0/6	8.316[c]	.081	-
Total MCI, n (%)	27/3 (10%)	16/20 (55.55%)	19/7 (26.92%)	15.987[a]	<.001	PD1 vs HC PD1 vs PD2
LEDD, mg, mean (SD)	NA	655.96 (427.588)	591.79 (285.883)	446.5[c]	.946	-
UPSIT, n, normosmia/hiposmia/anosmia	5/26/0	1/13/20	1/13/11	48.672[a]	<.001	PD1 vs HC PD2 vs HC
Sniffin,n, normosmia/hiposmia/anosmia	20/9/0	1/18/10	3/13/6	42.611[a]	<.001	PD1 vs HC PD2 vs HC
Escala Apathy, n, normal/apatia	25/5	17/17	15/8	8.652[a]	.07	-
MMSE, median (IQ)	0.102(3.32)	-0.616(5.61)	-0.515 (4.02)	1.55[b]	.46	-

C

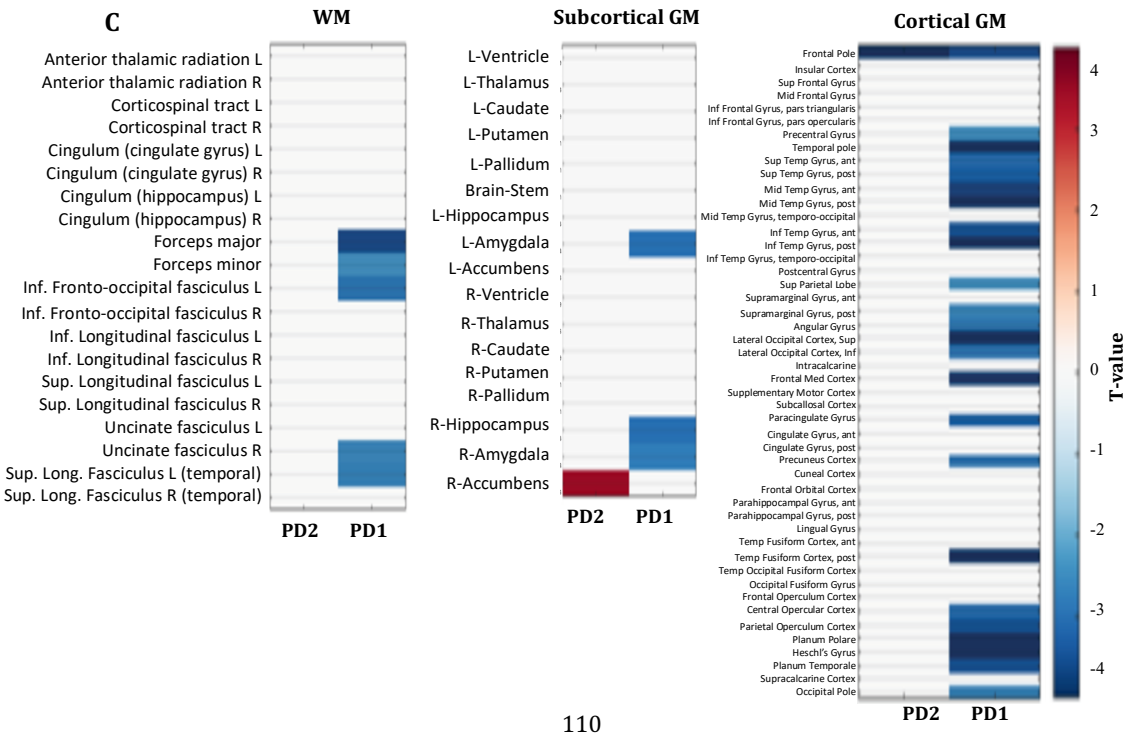

Results from the two-cluster solution. A. Voxel-based morphometry analysis. Regions in which PD1 showed less gray matter volume than HC are shown in red; regions in which PD1 showed less gray matter volume than PD2 are shown in green (p <0.05, FWE-corrected). B. Demographic and clinical characteristics of PD subtypes. C. Features used in the cluster analysis. Abbreviations: HC – healthy controls; IQ – interquartile range; LEDD – L-dopa equivalent daily dose; MCI – mild cognitive impairment; NA – not applicable; PD1 – Parkinson's disease group 1 patients; PD2 – Parkinson's disease group 2 patients; UPDRS – Unified Parkinson's Disease Rating Scale; UPSIT – University of Pennsylvania Smell Identification Test. [a] The chi-squared test was used. [b] The Kruskal-Wallis test was used. [C] The Mann-Whitney U test was used.

Supplementary material 3

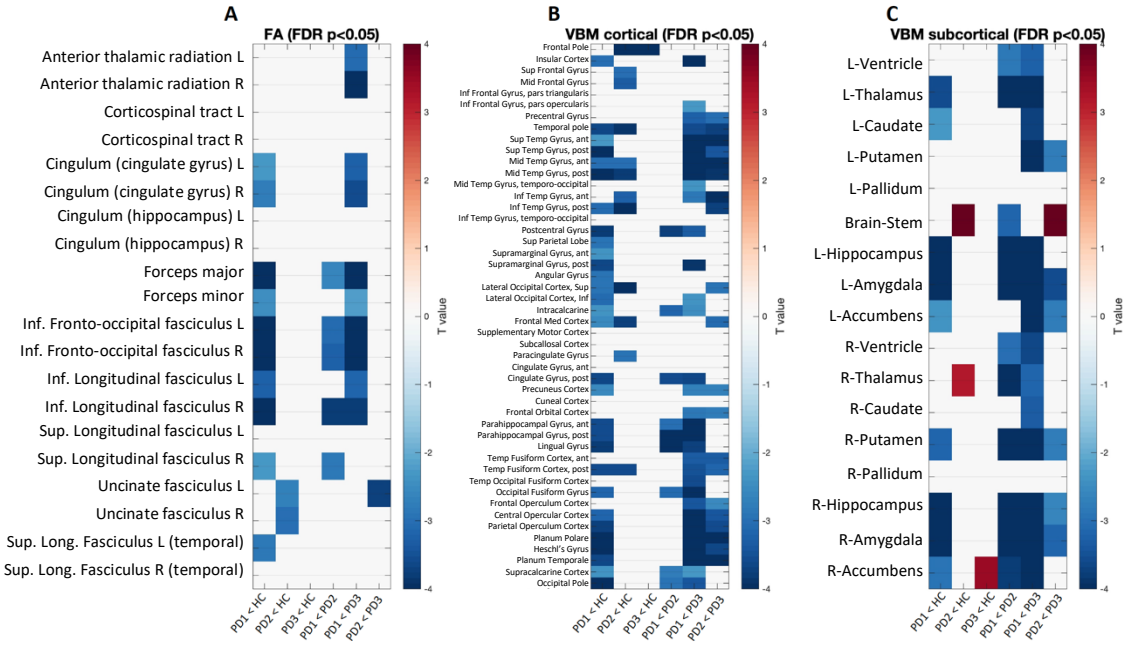

Supplementary material 4

Features ordered according to their importance in the cluster formation. F-scores of the ANOVAs above 5 are reported.

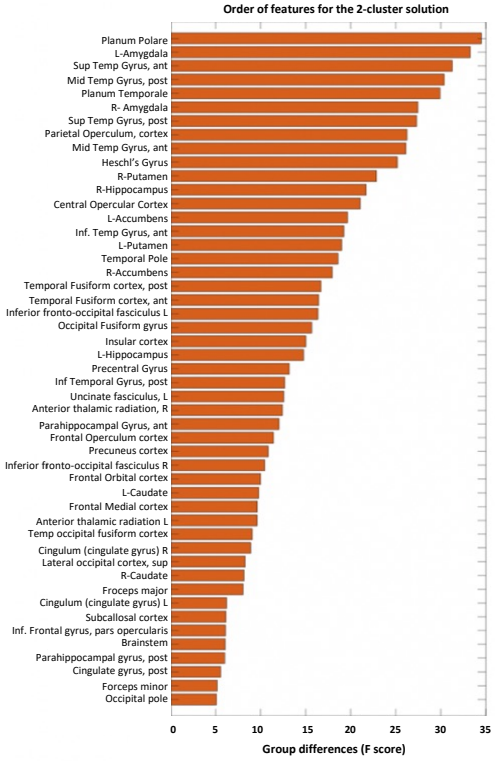

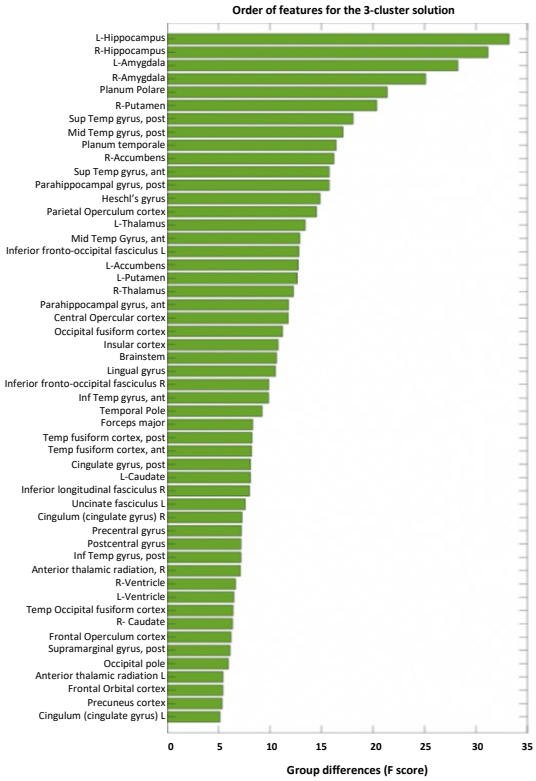

Supplementary material 5

VBM AND TBSS ANALYSES WITHOUT INTRODUCING AGE AS A COVARIATE.

Whole-brain analyses of VBM maps showed that PD1 had less GM volume than HC mainly in occipital and medial temporal regions as well as in subcortical structures. PD2 had reduced GM compared with HC mainly in bilateral orbital and medial prefrontal regions. PD3, in turn, showed lower GM volume than HC in a small right frontal region (Supplementary material 6) (FWE-corrected, $p < 0.05$). HC showed lower GM volume than PD2 in the cerebellum, and lower GM volume than PD3 in the putamen (Supplementary material 7). Comparisons between PD groups showed that PD1 had reduced GM volume in subcortical structures when compared with PD2 and PD3 as well as lower GM volume than PD3 in temporal, occipital and frontal regions (FWE-corrected, $p < 0.05$).

Whole-brain analyses of FA maps using TBSS showed extensive regions with lower FA values in PD1 compared with HC (Supplementary material 6) and PD3 (FWE-corrected, $p < 0.05$). PD1 also showed lower FA than PD2 in the bilateral inferior fronto-occipital fasciculus and corticospinal tract. In turn, PD2 showed lower FA than PD3 in some regions of these same tracts (Supplementary material 6 and 7).

Supplementary material 6

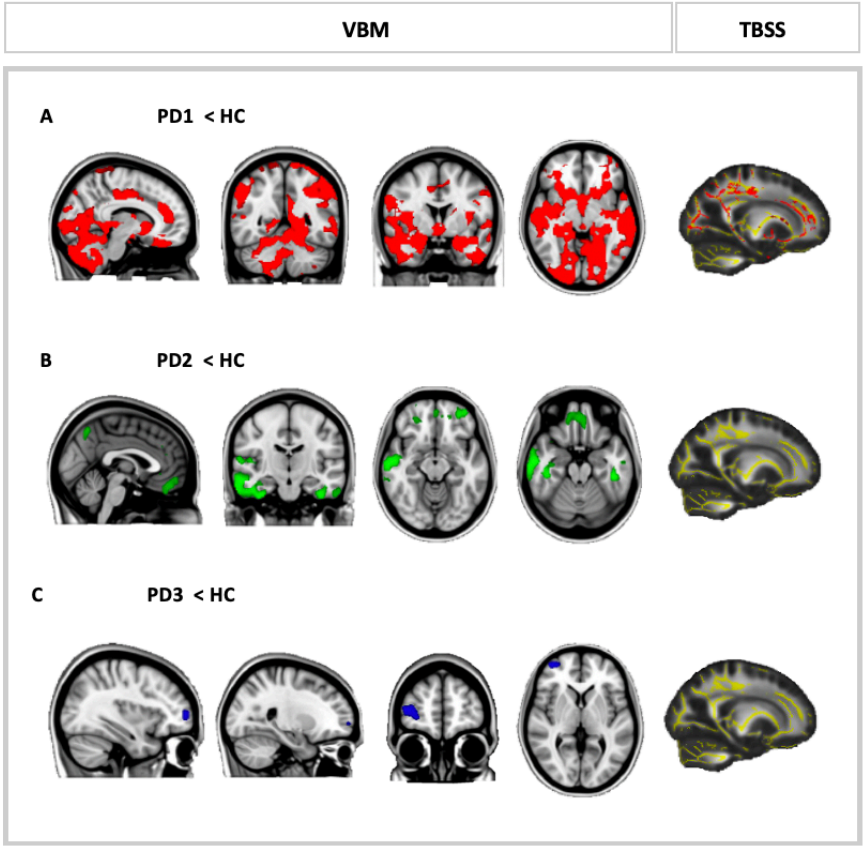

Voxel-based morphometry (VBM) and tract-based spatial statistics (TBSS) analyses of the three-cluster solution. VBM: regions in which PD1 showed less gray matter volume than HC are shown in red (A); regions in which PD2 showed less gray matter volume than HC are shown in green (B); (C) regions in which PD3 showed less gray matter volume than HC are shown in blue ($p < 0.05$, FWE-corrected). TBSS: FA skeleton (yellow) and white matter tracts in which PD1 showed less FA than HC (red). Radiological convention is used. Abbreviations: HC – healthy controls; PD1 – Parkinson's disease patient subgroup 1; PD2 – Parkinson's disease patient subgroup 2; PD3 – Parkinson's disease patient subgroup 3.

Supplementary material 7

		Cluster size (mm3)	Anatomical location	MNI coordinates			p-value
				x	y	z	
VBM							
	HC < PD2						
		84	L Cerebellum	-16	-46	-52	0.024
	HC < PD3						
		1280	L Putamen	-26	10	-6	0.002
		33	L Cerebellum	-48	-66	-42	0.042
	PD1< PD2						
		36289	R Cerebellum	12	-58	-64	<0.001
		753	R Cingulate gyrus	4	-22	42	0.02
		424	L Precentral gyrus	-46	-22	42	0.026
		79	R Superior Parietal lobe	32	-40	70	0.032
		32	R Postcentral gyrus	8	-36	78	0.045
		27	L Supramarginal gyrus	-52	-40	52	0.038
		14	L Postcentral gyrus	-38	-38	48	0.047
	PD1<PD3						
		81424	R Cerebellum	30	-62	-62	<0.001
	PD2>PD3						
		228	L Cerebelllum	-18	-44	-54	0.012
		137	Brain Stem	6	-30	-50	0.025
		13	Brain Stem	-2	-48	-48	0.044
	PD2<PD3						
		17426	L Inferior Temporal gyrus	-50	2	-44	<0.001
		1255	Precuneus	6	-64	-54	0.012
		647	R Precentral gyrus	20	-22	64	0.012
		635	L Planum Temporale	-50	-38	20	0.006
		207	L Precentral gyrus	-30	-20	50	0.023
		46	L Superior Parietal lobe	-24	-46	42	0.033
		44	R Inferior Frontal gyrus	32	14	26	0.045
		27	L Precentral gyrus	-28	-16	70	0.047
		15	L Lateral Occipital cortex	-34	-62	36	0.047
		11	L Supramarginal gyrus	-36	-42	34	0.045
TBSS							
	PD 1 < PD2						
		7481	R inferior fronto-occipital fasciculus	35	-56	-2	0.014
		3689	L inferior fronto-occipital fasciculus	122	62	72	0.018
		206	R inferior fronto-occipital fasciculus	27	33	10	0.042
		13	R inferior fronto-occipital fasciculus	19	42	-5	0.049
	PD1 < PD3						
		64867	L inferior fronto-occipital fasciculus	-24	33	-3	<0.001
	PD2 < PD3						
		4350	R Anterior thalamic radiation	3	-16	17	0.013
		1458	Corpus callosum	-13	-3	30	0.029
		12	L Cingulum	-19	-40	33	0.048

Location of significant clusters (>10 voxels) of the three-cluster solution without covariates. Harvard-Oxford Cortical Structural Atlas and JHU White-Matter Tractography Atlas were used to determine the anatomical locations. Abbreviations: HC – Healthy Controls; PD1 – Parkinson's disease patient subgroup 1; PD2 – Parkinson's disease patient subgroup 2; PD3 – Parkinson's disease patient subgroup 3; TBSS – tract-based spatial statistics, VBM – Voxel-based morphometry analysis, R – Right, L – Left.

Supplementary material 8

		Cluster size (mm3)	Anatomical location	MNI coordinates x	y	z	p-value
VBM							
	PD1<HC						
		43930	L Cerebellum	-16	-78	-54	<0.001
		1440	L Paracingulate gyrus	-10	34	30	0.011
		632	L Frontal Medial cortex	-4	38	-28	0.01
		191	L Frontal Pole	-22	48	6	0.031
		125	L Frontal Orbital cortex	-28	32	-6	0.03
		112	L Frontal Pole	-44	56	0	0.042
		48	R Frontal Pole	8	56	30	0.044
		11	L Frontal Orbital cortex	-20	20	14	0.048
	PD2<HC						
		4016	R Middle Temporal gyrus	60	-14	20	0.001
		2314	L Temporal Fusiform cortex	-40	-28	-30	0.001
		1807	L Frontal Pole	-30	50	-10	0.008
		747	L Superior Parietal lobe	-34	-58	48	0.024
		657	R Precuneus cortex	2	-64	54	0.015
		182	R Lateral Occipital cortex	36	-86	0	0.034
		132	R Precuneus cortex	18	-62	42	0.035
		58	L Middle Frontal cortex	-44	22	42	0.041
		57	R Superior Frontal gyrus	26	0	60	0.033
		48	L Paracingulate gyrus	-10	28	38	0.034
		42	R Precental gyrus	26	-10	72	0.037
		41	R Occipital pole	28	-94	24	0.04
		32	R Occipital pole	28	-90	24	0.04
		25	L Precental gyrus	-28	-14	74	0.037
		24	L Angular gyrus	-54	-52	46	0.044
		16	L Paracingulate gyrus	0	36	32	0.045
	HC < PD2						
		99	L Cerebellum	-16	-46	-52	0.019
	PD1<PD2						
		22969	R Cerebellum	12	-58	-64	<0.001
		99	R Supramarginal gyrus	48	-38	10	0.03
	PD1<PD3						
		32115	L Cerebelllum	-18	-76	-56	<0.001
		15	R Parietal Operculum cortex	50	-24	20	0.049
	PD2>PD3						
		278	L Cerebellum	-18	-42	-54	0.006
		117	Brain-stem	6	-30	-50	0.022
	PD2<PD3	261	R Superior Temporal gyrus	64	-30	4	0.023
TBSS							
	PD1<HC	32449	L Inferior Fronto-occipital fasciculus	-32	-64	-1	0.003

Location of significant clusters (>10 voxels) of the three-cluster solution. Harvard-Oxford Cortical Structural Atlas and JHU White-Matter Tractography Atlas were used to determine the anatomical locations. Abbreviations: HC – Healthy Controls; PD1 – Parkinson's disease patient subgroup 1; PD2 – Parkinson's disease patient subgroup 2; PD3 – Parkinson's disease patient subgroup 3; TBSS – Tract-based spatial statistics; VBM – Voxel-based morphometry Analysis; R – Right; L – Left.

Supplementary material 9

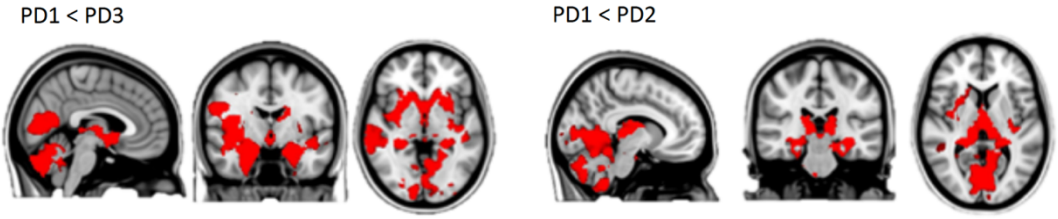

Voxel-based morphometry comparisons between three-cluster solution groups ($p<0.05$, FWE-corrected). Abbreviations: PD1 – Parkinson's disease patient subgroup 1; PD2 – Parkinson's disease patient subgroup 2; PD3 – Parkinson's disease patient subgroup 3.

Supplementary material 10

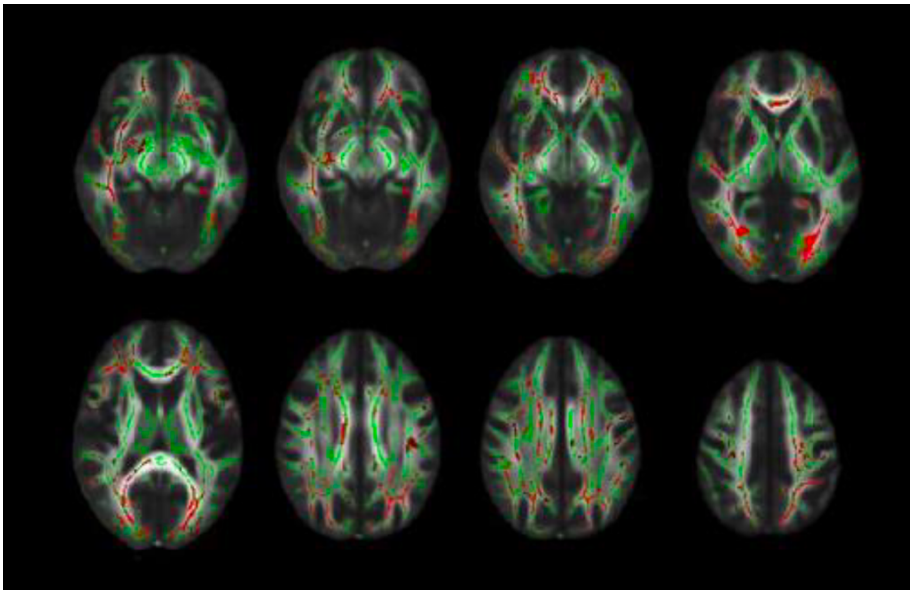

Tract-based spatial statistics (TBSS) analysis. The FA skeleton is shown in green and white matter tracts in which PD1 showed less FA than HC are shown in red. Radiological convention is used. Abbreviations: HC – healthy controls; PD1 – Parkinson's disease patient subgroup 1.

Supplementary material 11

	HC (N:33)	PD1 (N:15)	PD2 (N:21)	PD3 (N:26)	Test stats	p-value	Post-hoc analysis
VFD, median (IQ)	0.342(1.42)	-0.40(2.25)	-0.014(1.06)	-0.049(0.85)	6.273	0.099	-
JLO, median (IQ)	0.411(1.13)	0.185(2.11)	0.14(0.71)	0.077(0.72)	4.298	0.231	-
FRT (short version), median (IQ)	0.128(1.08)	-0.60(1.21)	-0.543(2.23)	-0.132(0.85)	13.564	0.004	PD1 vs HC
							PD2 vs HC
Phonemic fluency, median (IQ)	-0.284(1.01)	-0.47(0.89)	-0.43(1.46)	-0.126(0.72)	0.171	0.982	-
Semantic fluency, median (IQ)	-0.342(0.97)	-1.387(1.26)	-0.427(2.07)	-0.298(1.15)	10.682	0.014	PD1 vs HC
							PD1 vs PD3
RAVLT Total, median (IQ)	0.481(1.47)	-0.780(1.58)	0.252(1.8)	0.330(2.08)	14.911	0.002	PD1 vs HC
							PD1 vs PD3
RAVLT Delayed Recall, median (IQ)	0.251(1.68)	-1.247(2.06)	0.117(1.85)	-0.210(2.23)	15.471	0.001	PD1 vs HC
RAVLT True Recognition, median (IQ)	0.464(0.83)	-0.928(2.26)	0.105(1.20)	0.493(1.38)	10.989	0.012	PD1 vs HC
							PD1 vs PD3
Forward Digits Span, median (IQ)	-0.432(1.12)	-0.063(1.53)	-0.60(1.13)	-0.619(1.50)	2.190	0.534	-
Backward Digit Span, median (IQ)	-0.043(0.77)	-0.31(1.05)	-0.18(1.20)	-0.141(1.35)	1.5	0.682	-
Backward minus forward digits span	-0.415(1.58)	0.21(2.94)	-0.29(1.23)	-0.796(1.79)	6.133	0.105	-
Stroop word test, median (IQ)	-0.025(1.08)	-0.695(1.63)	-1.338(1.31)	-0.512(0.99)	19.627	<0.001	PD2 vs HC
Stroop color test, median (IQ)	0.261(1.09)	-1.193(1.5)	-0.764(1.41)	-0.18(0.64)	22.79	<0.001	PD1 vs HC
							PD2 vs HC
Stroop word-color, median (IQ)	-0.034(1.39)	-0.830(1.28)	-0.453(1.29)	-0.122(0.93)	10.952	0.012	-
SDMT, median (IQ)	-0.002(1.14)	-0.707(1.88)	-0.709(1.57)	-0.365(0.57)	9.61	0.022	PD2 vs HC
TMT A, median (IQ)	-0.167(0.71)	0.602(1.37)	0.651(1.40)	0.232(0.8)	18.237	<0.001	PD1 vs HC
							PD2 vs HC
TMTB, median (IQ)	-0.0167(1.19)	0.977(10.22)	0.783(2.49)	0.417(1.15)	11.994	0.007	PD1 vs HC
							PD2 vs HC
TMT AB, median (IQ)	-0.165(0.96)	-0.902(8.55)	-0.918(2.14)	-0.555(0.92)	7.218	0.065	-
BNT, median (IQ)	0.471(0.98)	0.11(0.90)	-0.22(1.49)	0.15(0.98)	8.130	0.043	-

Neuropsychological data presented as z-scores. For the statistical analyses Kruskal-Wallis test and Mann-Whitney U test were used. Outliers were excluded when required. Abbreviations: BNT – Boston Naming Test; FRT – Facial Recognition Test; HC – Healthy Controls; JLO – Judgment of Line Orientation Test; PD1 – Parkinson's disease patient subgroup 1; PD2 – Parkinson's disease patient subgroup 2; PD3 – Parkinson's disease patient subgroup 3; RAVLT – Rey's Auditory Verbal Learning Test; SDMT – Symbol Digit Modalities Test; TMTA- Trail Making test part A; TMTB – Trail Making Test.

STUDY 2

Inguanzo A, Segura B, Sala-Llonch R, Monte-Rubio G, Abos A, Campabadal A, Uribe C, Baggio HC, Marti MJ, Valldeoriola F, Compta Y, Bargallo N, Junque C.

Impaired Structural Connectivity in Parkinson's Disease Patients with Mild Cognitive Impairment: A Study Based on Probabilistic Tractography. Brain Connectivity. 2021; 11(5): 380-392.

BRAIN CONNECTIVITY
Volume 11, Number 5, 2021
Mary Ann Liebert, Inc.
DOI: 10.1089/brain.2020.0939

Impaired Structural Connectivity in Parkinson's Disease Patients with Mild Cognitive Impairment: A Study Based on Probabilistic Tractography

Anna Inguanzo,[1–3] Barbara Segura,[1–4] Roser Sala-Llonch,[1,3,5,6] Gemma Monte-Rubio,[1,2] Alexandra Abos,[1–3] Anna Campabadal,[1–3] Carme Uribe,[1–3,7] Hugo Cesar Baggio,[1,2] Maria Jose Marti,[1,3,4,8] Francesc Valldeoriola,[1,3,4,8] Yaroslau Compta,[1,3,4,8] Nuria Bargallo,[9,10] and Carme Junque[1–4]

Abstract

Background: Probabilistic tractography, in combination with graph theory, has been used to reconstruct the structural whole-brain connectome. Threshold-free network-based statistics (TFNBS) is a useful technique to study structural connectivity in neurodegenerative disorders; however, there are no previous studies using TFNBS in Parkinson's disease (PD) with and without mild cognitive impairment (MCI).
Materials and Methods: Sixty-two PD patients, 27 of whom classified as PD-MCI, and 51 healthy controls (HC) underwent diffusion-weighted 3T magnetic resonance imaging. Probabilistic tractography, using FMRIB Software Library (FSL), was used to compute the number of streamlines (NOS) between regions. NOS matrices were used to find group differences with TFNBS, and to calculate global and local measures of network integrity using graph theory. A binominal logistic regression was then used to assess the discrimination between PD with and without MCI using non-overlapping significant tracts. Tract-based spatial statistics were also performed with FSL to study changes in fractional anisotropy (FA) and mean diffusivity.
Results: PD-MCI showed 37 white matter connections with reduced connectivity strength compared with HC, mainly involving temporal/occipital regions. These were able to differentiate PD-MCI from PD without MCI with an area under the curve of 83–85%. PD without MCI showed disrupted connectivity in 18 connections involving frontal/temporal regions. No significant differences were found in graph measures. Only PD-MCI showed reduced FA compared with HC.
Discussion: TFNBS based on whole-brain probabilistic tractography can detect structural connectivity alterations in PD with and without MCI. Reduced structural connectivity in fronto-striatal and posterior cortico-cortical connections is associated with PD-MCI.

Keywords: DTI; magnetic resonance imaging; mild cognitive impairment; Parkinson's disease; probabilistic tractography; TFNBS

[1]Institute of Neurosciences, University of Barcelona, Barcelona, Catalonia, Spain.
[2]Medical Psychology Unit, Department of Medicine, University of Barcelona, Barcelona, Catalonia, Spain.
[3]Institute of Biomedical Research August Pi i Sunyer (IDIBAPS), Barcelona, Catalonia, Spain.
[4]Centro de Investigación Biomédica en Red sobre Enfermedades Neurodegenerativas (CIBERNED: CB06/05/0018-ISCIII), Barcelona, Catalonia, Spain.
[5]Department of Biomedicine, University of Barcelona, Barcelona, Catalonia, Spain.
[6]Centro de Investigación Biomédica en Red en Bioingeniería, Biomateriales y Nanomedicina (CIBER-BBN), Barcelona, Catalonia, Spain.
[7]Research Imaging Centre, Campbell Family Mental Health Research Institute, Centre for Addiction and Mental Health (CAMH), University of Toronto, Toronto, Canada.
[8]Movement Disorders Unit, Neurology Service, Institut de Neurociències, University of Barcelona, Hospital Clínic de Barcelona, Barcelona, Catalonia, Spain.
[9]Centre de Diagnostic per la Imatge, Hospital Clínic de Barcelona, Barcelona, Catalonia, Spain.
[10]Magnetic Resonance Core Facility, Institute of Biomedical Research August Pi i Sunyer (IDIBAPS), Barcelona, Catalonia, Spain.

Impact Statement

Our data help to clarify that whole-brain connectome analysis based on probabilistic tractography is a useful and sensitive approach to explore the role of white matter damages as a relevant pathological substrate of cognitive deficits in Parkinson's disease (PD). Our results might add some evidence regarding the involvement of mostly posterior cortical regions and their connections in PD patients with worse cognitive prognosis. Therefore, a threshold-free network-based statistics approach might indicate that structural connectivity abnormalities are not a global phenomenon, and suggests the implication of regional and predominantly posterior structural network disruption underlying cognitive impairment in PD.

Introduction

Parkinson's disease (PD) is a neurodegenerative disorder chiefly known for its motor symptoms; however, the course of PD is also accompanied by a broad range of nonmotor features, including cognitive decline (Kalia and Lang 2015). Mild cognitive impairment (MCI) is a common trait of PD that may be present in its earliest stages, gradually advancing with the progression of the disease and potentially leading to dementia, thus unfavorably affecting the patient's quality of life (Antonini et al. 2012).

Different neuroimaging approaches have been used to describe neuroanatomical correlates of MCI in PD. Previous studies comparing PD-MCI with healthy controls (HC) and PD without MCI have revealed global gray matter (GM) atrophy (Segura et al. 2014) and ventricular enlargement (Dalaker et al. 2010; Segura et al. 2014), as well as cortical thinning mainly involving posterior regions (Pereira et al. 2014; Segura et al. 2014). Nevertheless, little is known about the relevance of white matter (WM) microstructure degeneration in PD, or specifically in PD-MCI. Diffusion-weighted magnetic resonance imaging (MRI) (DWI) is a commonly used acquisition method to study the complex organization of WM tracts. However, tract-based spatial statistics (TBSS), a commonly used analysis method based on whole-brain voxel-based fractional anisotropy (FA) measures, have not been conclusive in characterizing WM alterations in PD, as some have found decreased FA in the corpus callosum (Garcia-Diaz et al. 2018), corona radiata, as well as in the internal and external capsule (Li et al. 2018) when comparing PD with HC, while others did not find significant results (Worker et al. 2014).

In addition, a few studies have focused on PD-MCI, showing decreased FA compared with HC in major associative tracts, the corona radiata and the corpus callosum (Agosta et al. 2014; Hattori et al. 2012; Melzer et al. 2013), but others did not find FA differences between PD-MCI patients and PD without MCI using TBSS (Galantucci et al. 2017).

Tractography is another DWI technique, which permits reconstruction of WM tracts and quantification of the local fiber density. This approach, in combination with graph theory, has been used to identify integration and segregation abnormalities in the reconstructed structural whole-brain connectome of PD patients (Abbasi et al. 2020; Mishra et al. 2020; Nigro et al. 2016).

Galantucci and colleagues (2017) studied structural connectivity across different brain systems and found PD-MCI to have reduced structural connectivity in networks, including the basal ganglia and fronto-parietal regions, when compared with HC and with PD patients without MCI. Wang and colleagues found decreased structural connectivity in PD-MCI patients in comparison with PD without MCI in several subnetworks, as well as reduced nodal efficiency, mostly involving orbitofrontal regions (Wang et al. 2019).

The two studies mentioned above have used a deterministic tractography approach (Galantucci et al. 2017; Wang et al. 2019). However, with this approach, estimating the true trajectories of WM tracts becomes a relevant problem in the context of crossing or kissing fibers (Mori and Van Zijl 2002). To surmount this limitation, and to account for uncertainty in the estimation of the models at each voxel, probabilistic tractography algorithms have been proposed (Behrens et al. 2007). Muller and colleagues (2019) used both types of tractography in the same PD sample and demonstrated the benefits of probabilistic tractography over the deterministic one.

Given this, other studies have opted for probabilistic tractography to study PD patients (Abbasi et al. 2020; Barbagallo et al. 2017; Shah et al. 2017). Some of the reported findings are decreased clustering coefficient (Shah et al. 2017), decreased global efficiency, and increased path length in PD, as well as disrupted networks, which were mainly subcortical and already present in the early stages of the disease (Abbasi et al. 2020). In addition, changes in brain network metrics, such as decreased global efficiency and increased characteristic path length, have been found to correlate with a decline in global cognition (Abbasi et al. 2020).

When aiming to describe specific patterns of connectivity alterations in an edge-wise manner, network-based statistic (NBS) (Zalesky et al. 2010) has been one of the most frequently used methods. Using NBS, many studies have described reduced connectivity in PD compared with HC (Barbagallo et al. 2017; Gou et al. 2018; Nigro et al. 2016; Shah et al. 2017). In the last years, the development of the threshold-free network-based statistics (TFNBS) method (Baggio et al. 2018), which, unlike NBS, does not require the *a priori* definition of a component-defining threshold and generates edge-wise significant values, has been proposed as a step forward. TFNBS has been proved to be able to detect alterations in the organization and topology of WM tracts, along with the potential to correctly distinguish between neurodegenerative motor disorders (Abos et al. 2019a, 2019b).

To the best of our knowledge, there is no previous work studying TFNBS based on probabilistic tractography and graph theory analysis to characterize whole-brain structural connectivity in PD-MCI. In this regard, the present study aims to investigate potential abnormalities associated with MCI in PD in the complex structural brain networks.

Materials and Methods

Participants

The initial sample included 69 PD patients recruited from the Parkinson's Disease and Movement Disorders Unit, Hospital Clínic (Barcelona, Spain), and 54 HC from the Institut d'Envelliment, Universitat Autònoma de Barcelona. Inclusion

criteria for patients were (1) fulfilling UK PD Society Brain Bank diagnostic criteria for PD and (2) no surgical treatment with deep-brain stimulation. Exclusion criteria for all participants were (1) dementia according to Movement Disorders Society criteria, (2) Hoehn and Yahr (H&Y) scale score >3, (3) severe psychiatric or neurological comorbidity, (4) low global intelligence quotient estimated by the vocabulary subtest of the Wechsler Adult Intelligence Scale 3rd edition (scalar score ≤7), (5) Mini Mental State Examination (MMSE) score below 25, (6) claustrophobia, (7) pathological MRI findings other than mild WM hyperintensities in the fluid attenuated inversion recovery (FLAIR) sequence, and (8) MRI artifacts. A total of 62 PD patients and 51 HC were finally selected. The following participants were excluded from the study: five patients and two HC with MRI artifacts, two patients with claustrophobia, and one HC with a cyst. Motor symptoms were assessed with the Unified Parkinson's Disease Rating Scale, motor section (UPDRS-III).

All PD patients were taking antiparkinsonian drugs that consisted of different combinations of L-dopa, catechol-O-methyltransferase inhibitors, monoamine oxidase inhibitors, dopamine agonists, and amantadine. To standardize the doses, the L-dopa equivalent daily dose (LEDD) (Tomlinson et al. 2010) was calculated. Written informed consent was obtained from all study participants after a full explanation of the procedures. The study was approved by the Institutional Ethics Committee from the University of Barcelona (IRB00003099).

Neuropsychological tests

All participants underwent a comprehensive neuropsychological assessment in the *on* state addressing cognitive domains frequently impaired in PD (Litvan et al. 2012). Attention and working memory were assessed with the Trail Making Test (parts A and B), Digit Span Forward and Backward, Stroop Color-Word Test, Symbol Digits Modalities Test—oral version. Executive functions were evaluated with phonemic and semantic fluencies. Language was assessed by the Boston Naming Test (BNT). Memory was assessed using Rey's Auditory Verbal Learning Test total learning recall, delayed recall, and recognition abilities (RAVLT total, RAVLT recall, and RAVLT recognition, respectively). Visuospatial and visuoperceptual functions were assessed with Benton's Judgment of Line Orientation, Visual Form Discrimination (VFD), and Facial Recognition (FRT) tests. Neuropsychiatric symptoms were evaluated with the Beck Depression Inventory-II, Starkstein's Apathy Scale, and Cumming's Neuropsychiatric Inventory. Expected z scores adjusted for age, sex, and education were calculated for each test and subject based on a multiple regression analysis performed in the HC (Aarsland et al. 2009). The presence of MCI was defined using PD-MCI diagnostic criteria level II (Litvan et al. 2012).

MRI acquisition

MRI data were acquired with a 3 T scanner (MAGNETOM Trio, Siemens, Germany). The scanning protocol included high-resolution, three-dimensional, T1-weighted images acquired in the sagittal plane (repetition time [TR] = 2300 ms, echo time [TE] = 2.98 ms, inversion time [TI] = 900 ms, 240 slices, field of view [FOV] = 256 mm; 1 mm isotropic voxel), two sets of single-band, spin-echo diffusion-weighted images in the axial plane with opposite (anterior-posterior and posterior-anterior) phase encoding directions (TR = 7700 ms, TE = 89 ms, FOV = 244 mm; 2 mm isotropic voxel; number of directions = 30, b-value = 1000 sec/mm^2, b_0 value = 0 sec/mm^2), and a T2-weighted axial FLAIR sequence (TR = 9000 ms, TE = 96 ms).

MRI preprocessing

Structural MRI preprocessing was performed using the automated FreeSurfer (version 5.1) pipeline. The cerebral cortex was parcellated into gyral and sulcal structures based on 68 cortical regions of interest (ROIs) from the Desikan/Killiany atlas (Desikan et al. 2006), and 18 deep gray matter (DGM) ROIs from the automated FreeSurfer segmentation step (Filipek et al. 1994; Fischl and Dale 2000; Seidman et al. 1997). DWI images were preprocessed with the FMRIB Software Library (FSL; version 5.08). The preprocessing steps included brain extraction using Brain Extraction Tool, susceptibility-induced distortion correction using topup, and eddy-current distortion and subject motion correction with eddy. FMRIB's Diffusion Toolbox (FDT) was used for data processing, local diffusion modeling, and tractography (Jbabdi et al. 2012).

Tract-based spatial statistics

Preprocessed diffusion MRI images were analyzed with FDT software from FSL. Individual FA maps were obtained using a Diffusion Tensor Model fit (DTIFIT), and the voxelwise statistical analysis of FA was carried through with TBSS (Smith et al. 2006). TBSS performs nonlinear registration (using Nonlinear Image Registration Tool [FMRIB]) of FA images from DTIFIT to the MNI standard space and generates a mean FA skeleton that represents the center of all WM tracts common to the whole group. Each subject's FA image was projected onto the skeleton and the resulting FA skeleton images were fed into a general linear model (GLM) modeling the three groups (HC, PD without MCI, PD-MCI) to find vertex-wise differences in FA skeleton maps. The same steps were used to obtain the mean diffusivity (MD) maps. The global mean FA and MD were also extracted.

Tractography and structural connectivity analysis

To run probabilistic tractography, the 86 ROIs previously obtained with FreeSurfer were linearly registered from native structural space to native diffusion space with FMRIB's Linear Image Registration Tool (Jenkinson et al. 2002) to be used as seeds. Next, Bedpostx was applied to calculate the probability distribution of fiber directions in each voxel (Behrens et al. 2007). Then, we ran the tractography with the Probrtarckx2 tool (Behrens et al. 2007) using 5000 streamlines from each ROI, and an ROI-by-ROI connectivity setting obtaining an 86 × 86 connectivity matrix per subject, which contained the number of reconstructed streamlines (number of streamlines [NOS]) between each pair of ROIs. NOS was taken as a measure of the strength of structural connectivity between these regions. To minimize false-positive connections, streamlines intersecting fewer than two regions were ignored, and those detected in at least 50% of the individuals were considered (Abos et al. 2019b; Zalesky et al. 2010). Finally, to test tract-wise differences between groups in

interregional NOS, we used TFNBS (Baggio et al. 2018), which performs statistical inference on the data matrix. Results were corrected using family-wise error rate (FWE) correction, with a significance level of $p < 0.05$. Whole-brain NOS was also calculated as the mean of all NOS values.

Graph theory computation

Graph theory topological parameters derived from the thresholded NOS matrices were obtained using the Brain Connectivity Toolbox from MATLAB. The graph metrics included global and local normalized clustering coefficient, global and local node degree, small worldness, normalized path length, modularity, local efficiency, and betweenness centrality (see Rubinov and Sporns [2010] for detailed definitions and calculations of the graph metrics).

Additional statistical analyses

Demographic, neuropsychological, and clinical statistical analyses were conducted using IBM SPSS Statistics 25.0 (IBM Corp., Armonk, NY). To assess differences in demographic, clinical, and neuropsychological quantitative variables, the Kruskal–Wallis or Mann–Whitney *U* tests were used. The chi-squared test was used for categorical variables. Intergroup comparisons for summary graph measures, as well as for global mean FA; MD and NOS were assessed with GLM using in-house MATLAB scripts and Monte Carlo simulations with 5,000 permutations. Results were corrected for multiple testing using FWE correction, with a significance level of $p < 0.05$. Correlations between neuropsychological test scores and clinic data with global FA measures and NOS were evaluated using Pearson correlation.

Additional analyses were conducted to explore differences between PD with and without MCI. For this purpose, the number of connections with significantly reduced connectivity strength in PD-MCI patients compared with HC was matched to those obtained in PD without MCI compared with HC, and the overlapping connections were excluded. The resulting non-overlapping connections were used to calculate their capacity to discern between both groups of PD patients. This set of connections was split into cortico-cortical and cortico-DGM. To observe if both sets of connections could separately discriminate between PD with and without MCI, a binomial logistic regression for classification was performed using MATLAB (The MathWorks, Inc.; R2019b). Binomial logistic regression is based on a regression model to predict the probability that, for a given input data, each input belongs to a numeric category (0 or 1). It models data using a sigmoid function and becomes a classification technique when a threshold is established on the sigmoid (0.5). The receiver operating characteristic (ROC) curve was obtained from the probability estimations by the logistic regression as scores, as well as the corresponding area under the curve (AUC).

Results

Demographic and clinical characteristics of PD

PD patients and the HC group did not differ significantly in age or years of education, but they did in gender (Supplementary Data S1). Twenty-seven PD patients were classified as PD-MCI, and 35 without MCI. Regarding the sociodemographic and clinical characteristics of the three groups (HC, PD without MCI, and PD-MCI), shown in Table 1, no significant differences between groups were observed for age, years of education, nor global cognition (MMSE). A significant effect was found in gender ($p = 0.006$). PD groups did not differ in disease duration, LEDD, nor in motor disease severity as measured by the UPDRS-III scale. There was a difference in H&Y scores ($p = 0.044$) between subgroups.

Neuropsychological differences between groups

Table 2 shows differences in neuropsychological performance between groups. PD-MCI patient scores were significantly worse than those of PD without MCI and HC in all tests except forward and backward digits, and BNT. PD-MCI patients also showed lower scores than HC in VFD and FRT.

TBSS analysis

The TBSS analysis did not show significant differences between PD and HC in FA nor in MD. However, when the PD sample was subdivided according to the presence of MCI, PD-MCI patients showed reduced FA compared with HC ($p = 0.031$) (Fig. 1). Concretely, decreased FA was detected

Table 1. Sociodemographic and Clinical Data

	HC (n = *51*)	*PD without MCI* (n = *35*)	*PD-MCI* (n = *27*)	*Stats* (p)
Sex (male/female)	23/28	27/8	19/8	10.26 (0.006)
Age, median (IQR)	66 (17)	63 (11)	68 (16)	2.54 (0.28)
Education (years), median (IQR)	12 (7)	14 (10)	11 (7)	2.70 (0.26)
Disease duration (years), median (IQR)	NA	7 (6.25)	8 (9.25)	537.5 (0.36)
Age of onset, median (IQR)	NA	55.5 (12)	55.5 (21)	477 (0.601)
LEDD (mg), median (IQR)	NA	526.75 (362.5)	575 (502.5)	495 (0.79)
UPDRS part III, median (IQR)	NA	15 (9.75)	15 (10)	446 (0.83)
Hoehn and Yahr, *n*, 1/2/2.5/3	NA	8/20/0/7	2/11/1/13	8.12 (0.04)
MMSE, median (IQR)	0.096 (1.33)	0.11 (1.43)	−0.85 (2.31)	3.43 (0.18)
IADL, median (IQR)	8 (0)	7 (2)	7 (3)	22.53 (<0.001)

Group differences were assessed using Kruskal–Wallis or Mann–Whitney *U* test according to the number of groups being compared. Categorical variables were analyzed with Pearson's chi-squared test.

HC, healthy controls; IADL, instrumental activities of the daily life; IQR, interquartile range; LEDD, L-dopa equivalent daily dose; MCI, mild cognitive impairment; MMSE, Mini Mental State Examination; NA, not applicable; PD, Parkinson's disease; UPDRS, Unified Parkinson's Disease Rating Scale.

TABLE 2. GROUP COMPARISON OF NEUROPSYCHOLOGICAL PERFORMANCE

	HC	*PD without MCI*	*PD-MCI*	*Stats* (p)	*Post hoc*
VFD	0.28 (0.95)	0.08 (0.82)	−0.34 (1.87)	11.53 (0.003)	HC vs. PD-MCI
JLO	0.25 (1.08)	0.23 (0.59)	−0.35 (1.84)	9.79 (0.007)	HC vs. PD-MCI PD without MCI vs. PD-MCI
FRT	0.01 (1.18)	−0.08 (1.17)	−0.80 (1.45)	13.9 (0.001)	HC vs. PD-MCI
Phonemic fluency	−0.60 (1.41)	−0.05 (1.42)	−0.47 (1.33)	3.83 (0.15)	—
Semantic fluency	−0.37 (1.18)	−0.15 (1.27)	−1.21 (1.27)	20.90 (<0.001)	HC vs. PD-MCI PD without MCI vs. PD-MCI
RAVLT total	0.11 (1.38)	0.32 (1.31)	−0.80 (2.12)	13.17 (0.001)	HC vs. PD-MCI PD without MCI vs. PD-MCI
RAVLT recuperation	0.03 (1.13)	0.02 (1.90)	−1.33 (2.36)	20.90 (<0.001)	HC vs. PD-MCI PD without MCI vs. PD-MCI
Forward digits span	−0.40 (0.90)	−0.27 (1.16)	−0.64 (1.44)	1.40 (0.50)	—
Backward digits span	−0.17 (0.76)	−0.09 (1.13)	−0.33 (1.06)	2.91 (0.23)	—
Stroop word	−0.23 (1.14)	−0.33 (0.95)	−1.62 (1.28)	26.78 (<0.001)	HC vs. PD-MCI PD without MCI vs. PD-MCI
Stroop color	0.14 (1.14)	−0.17 (0.65)	−1.40 (1.27)	33.34 (<0.001)	HC vs. PD-MCI no MCI vs. PD-MCI
Stroop word-color	−0.07 (1.18)	0.01 (0.93)	−1.07 (0.86)	24.17 (<0.001)	HC vs. PD-MCI PD without MCI vs. PD-MCI
SDMT	−0.08 (1.06)	−0.24 (1.08)	−1.15 (1.24)	24.42 (<0.001)	HC vs. PD-MCI PD without MCI vs. PD-MCI
TMTA	0.20 (1.17)	0.30 (0.91)	1.35 (1.92)	18.94 (<0.001)	HC vs. PD-MCI PD without MCI vs. PD-MCI
TMTB	0.32 (1.70)	0.36 (0.94)	1.98 (8.20)	20.82 (<0.001)	HC vs. PD-MCI PD without MCI vs. PD-MCI
TMTBA	2.18 (1.80)	1.73 (1.21)	2.50 (7.33)	9.55 (0.008)	PD without MCI vs. PD-MCI
BNT	0.10 (0.90)	−0.07 (0.94)	0.05 (1.37)	2.77 (0.25)	—

Neuropsychological data presented as *z*-scores. For the statistical analyses Kruskal–Wallis test and Mann–Whitney *U* test were used.

BNT, Boston Naming Test; FRT, Facial Recognition Test; JLO, Judgment of Line Orientation Test; RAVLT, Rey's Auditory Verbal Learning Test; SDMT, Symbol Digits Modality Test; TMTA, Trail Making Test part A; TMTB, Trail Making Test part B; TMTAB, Trail Making Test B minus A; VFD, Visual Form Discrimination.

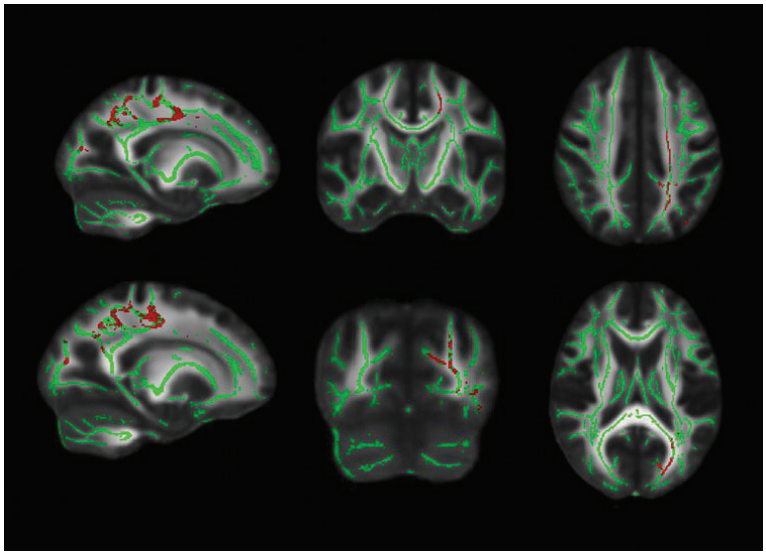

FIG. 1. White matter maps (in green) showing regions of significantly decreased FA in PD-MCI patients compared with HC (in red). Results were adjusted by gender ($p < 0.05$, FWE-corrected). Radiological convention is used. FA, fractional anisotropy; HC, healthy controls; MCI, mild cognitive impairment; PD, Parkinson's disease; WM, white matter. Color images are available online.

in the left inferior fronto-occipital fasciculus, corticospinal tract, inferior and superior longitudinal fasciculus, and forceps major. There were no differences between PD without MCI and HC, nor between PD subgroups. In contrast, TBSS analysis on MD maps did not show any significant results.

Comparisons in global mean FA did not show significant differences when comparing PD with HC ($F=1.102$; $p=0.323$) or when comparing PD-MCI or PD without MCI with HC ($F=1.104$; $p=0.339$).

No significant intergroup differences in global mean MD were found either between PD patients and HC ($F=0.126$; $p=0.723$) or when assessing the three previously mentioned groups ($F=0.546$; $p=0.588$).

TFNBS analysis

The PD patient group showed a reduced number of streamlines (NOS) compared with HC in 114 connections (FWE-corrected, $p<0.05$). From these 114 connections, 67 were found to be cortico-cortical (59%), 46 were cortico-DGM (40%), and only one was a DGM-DGM connection (1%). No connections showed significantly higher NOS in PD patients compared with HC. Figure 2 shows the violin plot distribution of the average NOS derived from the 114 connections.

When studying the two PD groups separately, we found that both PD-MCI and PD without MCI showed reduced NOS compared with HC; specifically, patients with PD-MCI showed a higher number of altered connections than PD without MCI (Fig. 3). However, differences between PD-MCI and PD without MCI did not reach statistical significance. PD-MCI showed reduced connectivity in 37 connections when compared with HC, 16 of which were cortico-cortical (43%), mainly involving temporal and occipital regions, and 21 were cortico-DGM (57%). At the same time, PD without MCI showed reduced structural connectivity compared with HC in 18 connections mainly involving frontal and temporal regions. Twelve connections were cortico-cortical (67%), five were cortico-DGM (28%), and only one was a DGM-DGM connection (5%). No connections showed significantly higher NOS in any of the PD groups compared with HC (Supplementary Data S2).

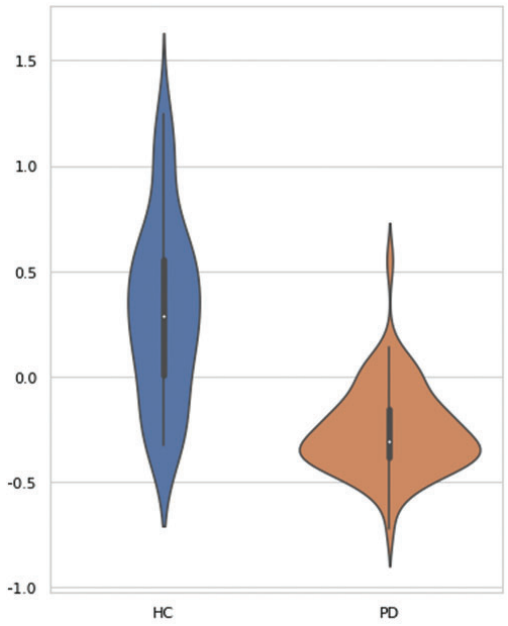

FIG. 2. Comparison of mean connectivity between HC and PD patients. Plots illustrate the distribution of average NOS derived from the 114 connections with significantly reduced connectivity in PD compared with HC. Significance of intergroup analyses (FWE-corrected, $p<0.05$) is shown. NOS, number of streamlines; TFNBS, threshold-free network-based statistics. Color images are available online.

Whole-brain mean NOS was significantly reduced in PD compared with HC ($T=2.78$, $p=0.003$). When divided into PD-MCI and PD without MCI, both subgroups showed decreased whole-brain mean NOS compared with HC ($T=2.56$, $p=0.008$ for PD-MCI and $T=2.13$, $p=0.022$ for PD without MCI; FWE-corrected).

We then selected the connections that were differentially altered in PD-MCI and did not overlap with the ones altered in PD without MCI, and we evaluated their discriminatory capabilities using classification metrics. The ROC analysis showed that cortico-cortical connections with reduced NOS in PD-MCI compared with HC determined a good AUC of 0.83 in distinguishing patients with MCI from those without MCI. In the same line, for DGM-cortical connections, we obtained an AUC of 0.85 (Supplementary Data S3 and Supplementary Figure S1).

NOS and FA values did not correlate with clinical variables nor with cognitive performance.

Graph analysis

No group effect was found for global graph parameters, which included the normalized clustering coefficient, mean node degree, small worldness, normalized path length, and modularity (Table 3). However, we found differences in local graph measures (FWE-corrected, $p<0.05$), which implied decreased local efficiency, node degree, and nodal clustering coefficient in both PD groups compared with HC (Table 4). Of note, we found differences between PD groups according to MCI presence. PD without MCI had higher nodal clustering coefficient in the left banks of the superior temporal sulcus, postcentral, transverse temporal cortices, as well as in the right superior parietal cortex in comparison with PD-MCI (Table 4). PD-MCI patients, on the contrary, showed higher local efficiency and nodal clustering coefficient in the right accumbens, as well as increased node degree in the left banks of the superior temporal sulcus, when compared with PD without MCI.

Discussion

We have studied structural connectivity alterations in PD and PD-MCI by assessing local changes in WM integrity with TBSS, pair-wise connectivity measures using TFNBS, and global as well as local measures of network integrity using graph theory. As far as we know, this is the first work investigating structural connectivity using TFNBS based on probabilistic tractography in PD-MCI.

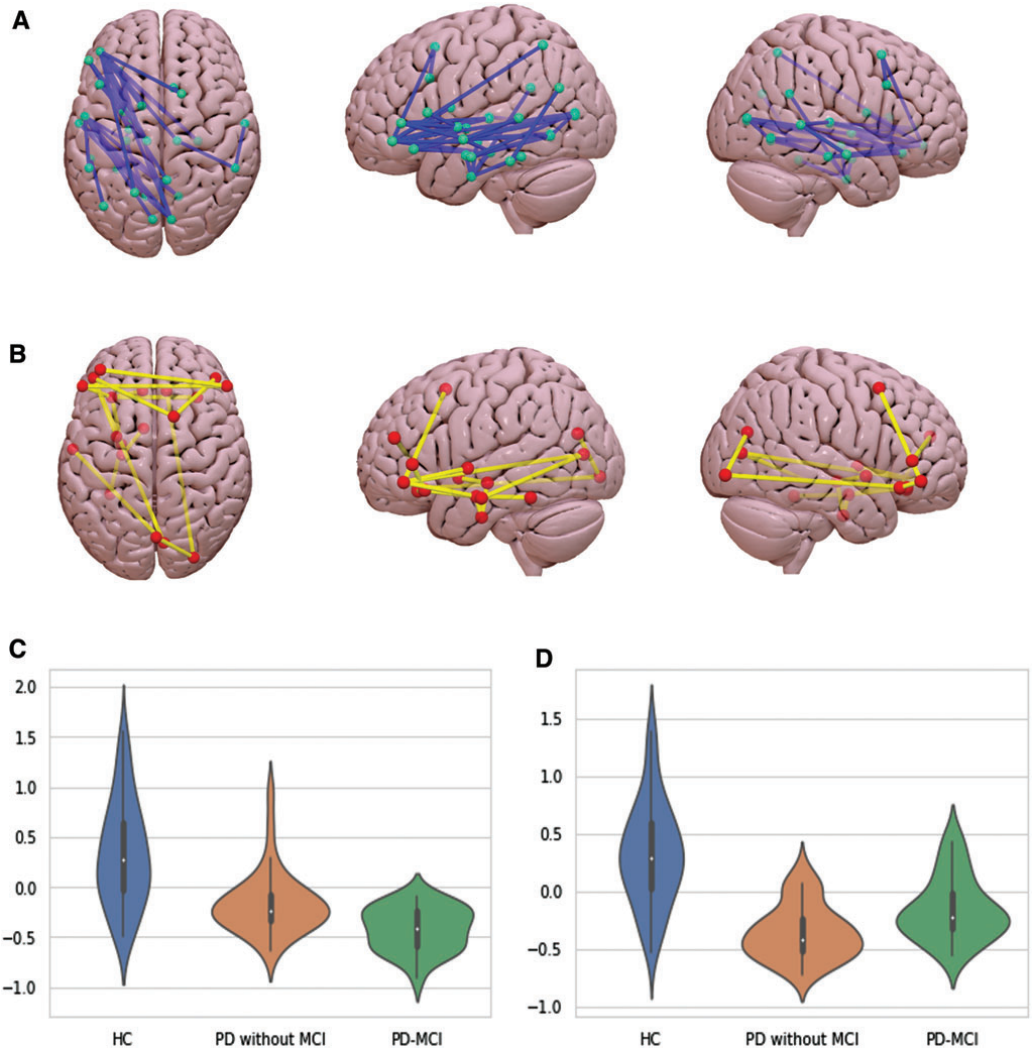

FIG. 3. Schematic representation of the structural connections with reduced structural connectivity strength in PD-MCI **(A)** and PD without MCI **(B)** compared with HC using TFNBS. Violin plots illustrate the distribution of the measures of average NOS obtained using TFNBS: connections derived from **(C)** the 37 significantly reduced tracts found in PD-MCI patients compared with HC and **(D)** the 18 significantly reduced tracts found in PD without MCI compared with HC. NOS values were z-transformed to allow better comparability. Connectivity figures were drawn using Surf Ice. Significance of intergroup analyses (FWE-corrected, $p < 0.05$) is shown. Neurological convention is used. Color images are available online.

PD patients showed reduced NOS compared with HC. Structural connectivity reduction was present in both PD-MCI and PD without MCI patients. Specifically, PD-MCI showed a higher number of abnormal connections involving cortico-DGM connections and mainly posterior cortico-cortical regions. PD patients without MCI, in turn, showed fewer impaired connections, mostly located in bilateral pre-frontal regions. Our data suggest that whole-brain connectome analysis based on probabilistic tractography is a useful and sensitive approach to explore the structural abnormalities related to cognitive decline in PD.

Whole-brain analysis of pair-wise connections showed reduced NOS in PD compared with HC in 114 connections. Particularly, PD-MCI showed reduced connectivity in a

Table 3. Global Graph Measures

	HC	*PD*	*Stat* (F)/p
Modularity	0.5260 (0.0176)	0.5244 (0.0133)	0.04/0.9978
Normalized clustering coefficient	1.4506 (0.1399)	1.4946 (0.1661)	1.34/0.5816
Mean node degree	68.0465 (3.5116)	68.0465 (3.5116)	3.38/0.1964
Small worldness	1.2687 (0.1423)	1.3248 (0.1580)	2.22/0.3608
Normalized path length	1.1284 (0.0169)	1.1284 (0.0169)	3.78/0.1564

	HC	*PD without MCI*	*PD-MCI*	*Stat* (F)/p
Modularity	0.5260 (0.0176)	0.5281 (0.0176)	0.5235 (0.0111)	0.96/0.773
Normalized clustering coefficient	1.4506 (0.1399)	1.5040 (0.1795)	1.4763 (0.1620)	0.81/0.833
Mean node degree	68.0465 (3.5116)	66.6744 (4.6977)	66.9070 (4.3721)	1.68/0.476
Small worldness	1.2687 (0.1423)	1.3397 (0.1602)	1.3130 (0.1650)	1.33/0.613
Normalized path length	1.1284 (0.0169)	1.123 (0.016)	1.1255 (0.0288)	2.16/0.322

Group differences were assessed using Monte Carlo simulations with 5,000 permutations (FWE-corrected, $p < 0.05$).
FWE, family-wise error rate.

higher number of connections than PD without MCI, which were mainly fronto-striatal and posterior cortico-cortical connections.

A previous study identified decreased global FA and increased global MD, as well as structural brain connectivity changes in certain subnetworks based on FA and MD values, which included basal ganglia as well as frontal and parietal nodes in PD-MCI patients in comparison with HC (Galantucci et al. 2017). Similarly, our results showed reduced NOS in fronto-striatal connections, which are known to be related to early cognitive deficits in PD, including those commonly described as dopaminergic fronto-striatal executive impairments (Schapira et al. 2017).

In agreement with our results, Galantucci and colleagues (2017) did not find differences in global NOS between PD patient subgroups; nonetheless, both PD-MCI and PD without MCI groups showed reduced global NOS in comparison with HC (Galantucci et al. 2017). In addition, in their study, initial FA NBS analyses showed no differences between PD patients. However, when more liberal statistical thresholds were used, FA connection changes were identified, and were similar to PD changes between controls and PD-MCI patients.

In contrast with the results of Galantucci et al. (2017) that found decreased FA in PD-MCI compared with HC in a bilateral principal connected component, we identified significant differences mainly in the left hemisphere. The differences could be due to the sample characteristics, as Galantucci et al. (2017) performed the analysis using matched PD samples. However, our results agree with those of Agosta et al. (2014) that reported decreased FA in PD-MCI compared with HC in several left tracts. A recent review of DTI in PD and other parkinsonism showed that although FA decreases are often bilateral, there are also different studies showing only left hemisphere decreases (Zhang et al. 2020). The origin of hemispheric asymmetries is unknown; however, the unilateral findings do not necessarily imply that the other hemisphere is not affected, the nonsignificant results may be a consequence of the specific threshold established for statistical significance.

In our study, moreover, PD-MCI patients showed reduced NOS in cortico-cortical connections mainly including temporal and occipital regions. In this context, posterior cortical-based neuropsychological deficits have been related to a higher risk of evolution to dementia (Williams-Gray et al. 2007). This hypothesis is supported by findings from other modalities: FDG-PET data have shown that posterior cortical hypometabolism may play an important role in the pathogenesis of cognitive impairment in PD (Garcia-Garcia et al. 2012; Wu et al. 2018). Moreover, regional cortical thinning in parieto-temporal regions, as well as increased global atrophy, has been suggested as structural neuroimaging markers of cognitive impairment in nondemented PD patients (Segura et al. 2014; Uribe et al. 2016).

Furthermore, based on pathological findings, the presence of cortical Lewy body pathology, as well as concomitant Alzheimer pathology, seems to be the most relevant factor in the development of cognitive impairment in PD (Halliday et al. 2014). A possible explanation is that neuronal cell bodies could be affected, with gradual loss of synaptic terminals, but dendritic arborization and neuronal connections could also be affected. Therefore, WM abnormalities observed in cognitively impaired patients may be understood as secondary to axonal degeneration after neuronal body damage. Within this framework, our results might add some evidence regarding the involvement of mostly posterior cortical regions and their connections in PD patients to worse cognitive prognosis.

In our work, logistic regression and ROC curve analysis showed that decreased cortico-cortical and cortico-DGM connections described in the group comparison between PD-MCI patients and HC can identify subgroups of patients with an AUC of 83% and 85%, respectively. Although our analyses were done to provide a quantification of the results obtained from the whole connectome, they are in accordance with results from recent approaches that have assessed the discriminant value of features extracted from MRI modalities. A previous study showed that structural connectivity data are relevant in distinguishing parkinsonian patients at the single-subject level with an overall accuracy of 82.23% (Abos et al. 2019b). In PD patients, these MRI data are also able to correctly discern PD patients from HC in longitudinal studies, obtaining similar accuracy results (83.6%) (Peña-Nogales et al. 2019). Only one previous study in PD-MCI (Galantucci et al. 2017) showed that structural abnormalities identified throughout the NBS approach could discriminate PD-MCI from those with PD without MCI with an 81% accuracy.

Table 4. Local Graph Measures

ROI	Post hoc p-value: HC vs. PD without MCI	Post hoc p-value: HC vs. PD-MCI	Post hoc p-value: PD without MCI vs. PD-MCI	Significant contrast
Local efficiency				
Left cuneus	n.s.	0.0418	n.s.	HC > PD-MCI
Left lateral orbitofrontal	0.0018	0.01	n.s.	HC > PD without MCI, HC > PD-MCI
Left lingual	n.s.	0.0186	n.s.	HC > PD-MCI
Left medial orbitofrontal	0.0486	n.s.	n.s.	HC > PD without MCI
Left pars orbitalis	0.0074	0.002	n.s.	HC > PD without MCI, HC > PD-MCI
Left pars triangularis	0.0108	0.0016	n.s.	HC > PD without MCI, HC > PD-MCI
Left pericalcarine	n.s.	0.03	n.s.	HC > PD-MCI
Left postcentral	n.s.	0.009	0.0144	HC > PD-MCI, PD without MCI > PD-MCI
Left rostral anterior cingulate	n.s.	0.035	n.s.	HC > PD-MCI
Left superior temporal	n.s.	0.0146	n.s.	HC > PD-MCI
Left temporal pole	0.0378	n.s.	n.s.	HC > PD without MCI
Right bankssts	n.s.	0.035	n.s.	HC > PD-MCI
Right inferior temporal	0.0124	n.s.	n.s.	HC > PD without MCI
Right lateral orbitofrontal	0.0134	n.s.	n.s.	HC > PD without MCI
Right medial orbitofrontal	0.0302	n.s.	n.s.	HC > PD without MCI
Right postcentral	n.s.	0.0036	n.s.	HC > PD-MCI
Right superior parietal	n.s.	0.0334	0.0244	HC > PD-MCI, PD without MCI > PD-MCI
Right temporal pole	0.0246	n.s.	n.s.	HC > PD without MCI
Left amygdala	0.033	n.s.	n.s.	HC > PD without MCI
Left hippocampus	n.s.	0.0176	n.s.	HC > PD-MCI
Left putamen	0.0496	n.s.	n.s.	HC > PD without MCI
Right accumbens	n.s.	n.s.	0.0366	PD-MCI > PD without MCI
Mean node degree				
Left bankssts	0.0216	n.s.	0.049	HC > PD without MCI, PD-MCI > PD without MCI
Left cuneus	n.s.	0.0446	n.s.	HC > PD-MCI
Left entorhinal	n.s.	0.0082	n.s.	HC > PD-MCI
Left frontal pole	n.s.	0.0144	n.s.	HC > PD-MCI
Left inferior temporal	0.0162	n.s.	n.s.	HC > PD without MCI
Left lateral orbitofrontal	0.0208	0.0338	n.s.	HC > PD without MCI, HC > PD-MCI
Left lingual	n.s.	0.0038	0.034	HC > PD-MCI, PD without MCI > PD-MCI
Left pars opercularis	0.0426	n.s.	n.s.	HC > PD without MCI
Left pars orbitalis	0.0014	0.0034	n.s.	HC > PD without MCI, HC > PD-MCI
Left pars triangularis	0.0136	0.0284	n.s.	HC > PD without MCI, HC > PD-MCI
Left rostral middle frontal	n.s.	0.0146	n.s.	HC > PD-MCI
Right frontal pole	n.s.	0.0406	n.s.	HC > PD-MCI
Right inferior parietal	n.s.	0.0412	0.0356	HC > PD-MCI, PD without MCI > PD-MCI
Right lateral orbitofrontal	0.0022	n.s.	n.s.	HC > PD without MCI
Right pars orbitalis	0.0028	n.s.	n.s.	HC > PD without MCI
Left hippocampus	0.0418	0.0014	n.s.	HC > PD without MCI, HC > PD-MCI
Right hippocampus	n.s.	0.0142	n.s.	HC > PD-MCI
Nodal clustering coefficient				
Left bankssts	n.s.	n.s.	0.0472	PD without MCI > PD-MCI
Left lateral orbitofrontal	0.0012	0.0032	n.s.	HC > PD without MCI, HC > PD-MCI
Left lingual	n.s.	0.0162	n.s.	HC > PD-MCI
Left medial orbitofrontal	0.0122	0.0382	n.s.	HC > PD without MCI, HC > PD-MCI
Left pars orbitalis	0.026	0.0024	n.s.	HC > PD without MCI, HC > PD-MCI
Left pars triangularis	0.01	0.0012	n.s.	HC > PD without MCI, HC > PD-MCI
Left pericalcarine	n.s.	0.0194	n.s.	HC > PD-MCI
Left postcentral	n.s.	0.0076	0.0342	HC > PD-MCI, PD without MCI > PD-MCI
Left rostral anterior cingulate	n.s.	0.0464	n.s.	HC > PD-MCI
Left rostral middle frontal	0.045	n.s.	n.s.	HC > PD without MCI
Left superior temporal	n.s.	0.009	n.s.	HC > PD-MCI
Left temporal pole	0.0246	n.s.	n.s.	HC > PD without MCI
Left transverse temporal	n.s.	n.s.	0.0336	PD without MCI > PD-MCI
Right bankssts	n.s.	0.0248	0.0516	HC > PD-MCI
Right inferior temporal	0.0084	n.s.	n.s.	HC > PD without MCI
Right lateral orbitofrontal	0.0146	n.s.	n.s.	HC > PD without MCI

(*continued*)

Table 4. (Continued)

ROI	Post hoc p-value: HC vs. PD without MCI	Post hoc p-value: HC vs. PD-MCI	Post hoc p-value: PD without MCI vs. PD-MCI	Significant contrast
Right medial orbitofrontal	0.0152	n.s.	n.s.	HC > PD without MCI
Right postcentral	n.s.	0.004	n.s.	HC > PD-MCI
Right superior parietal	n.s.	0.0266	0.0358	HC > PD-MCI, PD without MCI > PD-MCI
Right temporal pole	0.0298	n.s.	n.s.	HC > PD without MCI
Left accumbens	0.0248	n.s.	n.s.	HC > PD without MCI
Left amygdala	0.0328	n.s.	n.s.	HC > PD without MCI
Left hippocampus	n.s.	0.0164	n.s.	HC > PD-MCI
Left putamen	0.0448	n.s.	n.s.	HC > PD without MCI
Right accumbens	0.0124	n.s.	0.01	HC > PD without MCI, PD-MCI > PD without MCI

Group differences were assessed using Monte Carlo simulations with 5,000 permutations (FWE-corrected, $p < 0.05$).
n.s., not significant; ROI, regions of interest.

On the contrary, in our study, other measures derived from DTI showed lower sensitivity to WM abnormalities. We did not find significant differences between groups using mean global measures such as mean global FA and MD. Moreover, only PD-MCI patients compared with HC showed microstructural damage measured by TBSS. Previous literature using this methodological approach suggested that WM damage was emerging as a relevant pathological substrate of cognitive deficits in PD patients (Baggio et al. 2018; Hattori et al. 2012). While some studies identified widespread bilateral WM abnormalities in PD-MCI compared with PD without cognitive impairment in the left corticospinal tract, inferior longitudinal fasciculus, and forceps major (Agosta et al. 2014), others found more spatially restricted regions limited to the corona radiata (Melzer et al. 2013) and the posterior part of the corpus callosum (Garcia-Diaz et al. 2018), or did not find significant differences (Galantucci et al. 2017; Hattori et al. 2012).

Characterizing the structural connectome through graph theory provides information about the organization of the network (Griffa et al. 2013). Few studies have investigated the WM structural network connectome alterations in PD-MCI patients. In our study, graph analysis of global network properties did not show significant differences. Similarly, although Wang et al. (2019) reported decreased global efficiency and increased shortest path length in PD-MCI compared with HC, both important indicators of network interconnectivity, they did not find significant differences between PD subgroups or PD without MCI and HC. Contrarily, Galantucci et al. (2017), using FA and MD matrices, found increased assortativity—that is, the preference of a node to connect with similar nodes—and reduced clustering coefficient and global efficiency when comparing PD with and without MCI, suggesting global abnormalities in structural networks (Galantucci et al. 2017).

Moreover, our exploratory analysis brought noteworthy differences in local graph measures to light. PD patients showed less local efficiency, nodal degree, and clustering coefficient in several regions. Intergroup comparisons mostly suggested decreased nodal clustering coefficient, specifically in the left banks of the superior temporal sulcus, postcentral, transverse temporal cortices, as well as in the right superior parietal cortex in PD-MCI, in comparison with PD patients without cognitive impairment. The opposite trend was observed only in the right accumbens together with increased node degree in the left banks of the superior temporal sulcus. Widespread regions with decreased nodal efficiency have been previously observed between PD subgroups and HC. However, when PD-MCI and PD without MCI were compared, the reported regions only involved the left olfactory cortex and the left superior frontal gyrus, but not posterior regions (Wang et al. 2019).

In this sense, it should be pointed out that the reproducibility of network metrics can be affected by many factors. One relevant aspect would be that previous studies estimated structural connectivity using deterministic tractography, whereas our results were based on a probabilistic approach. Methodological differences as well as diversity in patient characteristics could be contributing to the heterogeneity of these results.

Previous results, taken altogether, highlighted the involvement of complex structural brain networks in PD-related cognitive impairment, rather than degeneration of individual WM tracts. Nevertheless, our TFNBS analysis, which allowed us to find a predominant reduction of NOS between PD patients and HC with no *a priori* selection of tracts, as well as the graph analysis results, might indicate that these structural abnormalities are not a global phenomenon and suggests the implication of regional and predominantly posterior structural network disruption underlying cognitive impairment in PD.

By combining the different methods, we aimed to surpass their individual limitations and give a more accurate vision of structural connectivity in PD-MCI. TBSS is a method that can detect changes in FA throughout the WM of the brain simultaneously. At the same time, although it is an approachable method that delivers comprehensive images, it may also cover relevant aspects of the data, as it only makes use of the FA map and discards the orientations' information.

This leads to complications when it comes to anatomical specificity in regions where paths of different structures merge (Bach et al. 2014). On the contrary, DTI fiber tracking measurements are derived from individual WM connections, and they do allow us to distinguish between adjacent connections.

However, they may also introduce spurious WM connections that do not exist, a limitation that we had tried to minimize by ignoring streamlines intersecting fewer than two regions and only considering the connections between pairs of regions that were detected in at least 50% of the individuals. While other approaches to the method, such as constrained spherical deconvolution, had managed to improve it (Jeurissen et al. 2011). In addition, graph theory facilitates study of topological properties of an entire network, instead of an individual analysis of large numbers of tracts. However it has its limitations as well, as these parameters are influenced by the number of nodes of the network, which are indeed arbitrarily chosen. For this reason, we selected well-implemented and standardized atlases.

As expected, in line with previous studies (Segura et al. 2014), our neuropsychological results showed a significantly worse performance in verbal memory, semantic fluency, visuospatial and visuoperceptive functions, and processing speed in PD-MCI compared with PD without MCI and HC. However, although altered WM has been recurrently associated with PD-MCI, we did not find significant correlations between cognition and WM measures in accordance with previous studies (Agosta et al. 2014). Although there are several authors who found significant correlations between neuropsychological performance and FA decreases (Zhang et al. 2020, review), they usually combine PD with and without MCI. Greater variability in the degree of cognitive impairment as well as in FA reductions favors the finding of correlations. It is probable that in our sample there is not enough variability within the PD-MCI group to provide statistical significance. Regarding the studies using NBS, only one reported significant correlations between the neuropsychological performance and graph measures, but they did not distinguish between PD with and without MCI (Wang et al. 2019).

On the contrary, it could also be considered that cognitive impairment is mainly explained by GM degeneration. For example, when both GM and WM changes are considered in the same sample, WM appears to be explaining just a small part of the degenerative pattern. In Inguanzo et al. (2021), we used GM and WM measures to perform a hierarchical cluster analysis, and we found three subgroups, of which only one presented WM alterations. Accordingly, cognitive performance in PD has been consistently seen to correlate with GM structural parameters (Garcia-Diaz et al. 2018; Mak et al. 2014), and with functional connectivity (Baggio et al. 2015).

Baggio and colleagues (2015) found that PD-MCI patients had reduced functional connectivity between the dorsal attention network and fronto-insular regions, as well as increased connectivity between posterior cortical regions and the default mode network, which in turn correlated with the attention/executive and visuospatial/visuoperceptual functions. Graph theory approaches also showed that PD-MCI had increased clustering coefficient, small-worldness, and modularity measures, which were negatively associated with visuospatial/visuoperceptual and memory scores (Baggio et al. 2014). All these taken together suggest that WM might be playing a secondary role in the cognitive impairment of PD.

Conversely, beyond the acceptance of MCI definition (Litvan et al. 2012) as useful clinical criteria to identify patients with worse cognitive profiles and dementia risk, recent evidence suggested the existence of a more complex picture, identifying PD subtypes based on neuropsychological, clinical, and MRI data (Dujardin et al. 2013; Uribe et al. 2016; Fereshtehnejad et al. 2017; Inguanzo et al. 2021). In light of our results, it could be suggested that the study of structural connectivity in PD subtypes might facilitate the study of different patterns of cognitive deterioration and shed light on their anatomical basis/substrates. Future studies should consider a whole-brain approach to better describe structural connectivity abnormalities in PD subtypes and its possible association with cognitive impairment. Moreover, combining neuroimaging with clinical data would allow for better precision in finding PD subgroups.

Conclusion

In conclusion, whole-brain structural connectivity techniques based on probabilistic tractography allow identification of reduced connectivity in fronto-striatal and posterior cortical connections related to cognitive decline in PD and are able to reveal potential structural connectivity indicators to classify PD disease phenotypes with high accuracy.

Authors' Contributions

C.J. and B.S. contributed to the research project conception and in the design of the study. A.A., A.C., and C.U. contributed to the acquisition of the data. A.I., R.S.-L., and G.M.-R. contributed to the analysis of the data and A.I., B.S., R.S.-L., G.M.-R., A.A., A.C., C.U., H.C.B., Y.C., M.J.M., F.V., N.B., and C.J. contributed to the interpretation of the data. A.I. and B.S. contributed to the draft of the article. A.I., B.S., R.S.-L., G.M.-R., A.A., A.C., C.U., H.C.B., Y.C., M.J.M., F.V., N.B., and C.J. revised the article critically for important intellectual content and approved the final version of the article.

Acknowledgments

We are grateful to all the participants in the study for their goodwill and generosity. We are also indebted to the Magnetic Resonance Imaging core facility of the IDIBAPS for technical support; and we acknowledge the CERCA Programme/Generalitat de Catalunya.

Author Disclosure Statement

No competing financial interests exist.

Funding Information

This study was sponsored by the Spanish Ministry of Economy and Competitiveness (PSI2013-41393-P; PSI2017-86930-P cofinanced by Agencia Estatal de Investigación [AEI] and the European Regional Development Fund), by Generalitat de Catalunya (2017SGR 748), Fundació La Marató de TV3 in Spain (20142310), and supported by María de Maeztu Unit of Excellence (Institute of Neurosciences, University of Barcelona) MDM-2017-0729, Ministry of Science, Innovation and Universities. A.I. and A.C. were supported by APIF predoctoral fellowship from the University of Barcelona (2017–2018). AA was supported by a fellowship from 2016, Departament d'Empresa i Coneixement de la Generalitat de Catalunya, AGAUR (2016FI_B 00360). C.U. was supported by the European

Union's Horizon 2020 research and innovation programme under the Marie Sklodowska-Curie fellowship (grant agreement 888692). M.J.M. received honoraria for advice and lecture from AbbVie, Bial, and Merz Pharma and grants from Michael J. Fox Foundation for Parkinson Disease (MJFF): MJF_PPMI_10_001, PI044024. Y.C. has received funding in the past 5 years from FIS/FEDER, H2020 programme, Union Chimique Belge (UCB pharma), Teva, Medtronic, AbbVie, Novartis, Merz, Piramal Imaging, and Esteve, Bial, and Zambon. Y.C. is currently an associate editor for Parkinsonism and Related Disorders.

Supplementary Material

Supplementary Data S1
Supplementary Data S2
Supplementary Data S3
Supplementary Figure S1

References

Aarsland D, Brønnick K, Larsen JP, et al. 2009. Cognitive impairment in incident, untreated Parkinson disease: the Norwegian ParkWest Study. Neurology 72:1121–1126.

Abbasi N, Fereshtehnejad SM, Zeighami Y, et al. 2020. Predicting severity and prognosis in Parkinson's disease from brain microstructure and connectivity. Neuroimage Clin 25:102111.

Abos A, Baggio HC, Segura B, et al. 2019a. Differentiation of multiple system atrophy from Parkinson's disease by structural connectivity derived from probabilistic tractography. Sci Rep 9:1–12.

Abos A, Segura B, Baggio HC, et al. 2019b. Disrupted structural connectivity of fronto-deep gray matter pathways in progressive supranuclear palsy. Neuroimage Clin 23:101899.

Agosta F, Canu E, Stefanova E, et al. 2014. Mild cognitive impairment in Parkinson's disease is associated with a distributed pattern of brain white matter damage. Hum Brain Mapp 35:1921–1929.

Antonini A, Barone P, Marconi R, et al. 2012. The progression of non-motor symptoms in Parkinson's disease and their contribution to motor disability and quality of life. J Neurol 259: 2621–2631.

Bach M, Laun BF, Leemans A, et al. 2014. Methodological considerations on tract-based spatial statistics (TBSS). Neuroimage 100:358–369.

Baggio HC, Abos A, Segura B, et al. 2018. Statistical inference in brain graphs using threshold-free network-based statistics. Hum Brain Mapp 39:2289–2302.

Baggio HC, Sala-Llonch R, Segura B, et al. 2014. Functional brain networks and cognitive deficits in Parkinson's disease. Hum Brain Mapp 35:4620–4634.

Baggio HC, Sala-Llonch R, Segura B. 2015. Cognitive impairment and resting-state network connectivity in Parkinson's disease. Hum Brain Mapp 36:199–212.

Barbagallo G, Caligiuri ME, Arabia G, et al. 2017. Structural connectivity differences in motor network between tremor-dominant and nontremor Parkinson's disease. Hum Brain Mapp 38:4716–4729.

Behrens TEJ, Berg HJ, Jbabdi S, et al. 2007. Probabilistic diffusion tractography with multiple fibre orientations: what can we gain? Neuroimage 34:144–155.

Dalaker TO, Zivadinov R, Larsen JP, et al. 2010. Gray matter correlations of cognition in incident Parkinson's disease. Mov Disord 25:629–633.

Desikan RS, Ségonne F, Fischl B, et al. 2006. An automated labeling system for subdividing the human cerebral cortex on MRI scans into gyral based regions of interest. Neuroimage 31:968–980.

Dujardin K, Leentjens AFG, Langlois C, et al. 2013. The spectrum of cognitive disorders in Parkinson's disease: a data-driven approach. Mov Disord 28:183–189.

Fereshtehnejad SM, Zeighami Y, Dagher A, et al. 2017. Clinical criteria for subtyping Parkinson's disease: biomarkers and longitudinal progression. Brain 140:1959–1976.

Filipek PA, Christian R, Kennedy DN, et al. 1994. The young adult human brain: an MRI-based morphometric analysis. Cereb Cortex 4:344–360.

Fischl B, Dale A. Measuring the thickness of the human cerebral cortex from magnetic resonance images. Proc Natl Acad Sci U S A 2000;97:11050–11055.

Galantucci S, Agosta F, Stefanova E, et al. 2017. Structural brain connectome and cognitive impairment in Parkinson disease. Radiology 283:515–525.

Garcia-Diaz AI, Segura B, Baggio HC, et al. 2018. Structural brain correlations of visuospatial and visuoperceptual tests in Parkinson's disease. J Int Neuropsychol Soc 24:33–44.

Garcia-Garcia D, Clavero P, Gasca-Salas C, et al. 2012. Posterior parietooccipital hypometabolism may differentiate mild cognitive impairment from dementia in Parkinson's disease. Eur J Nucl Med Imaging 39:1767–1777.

Gou L, Zhang W, Li C, et al. 2018. Structural brain network alteration and its correlation with structural impairments in patients with depression in de novo and drug-naïve Parkinson's disease. Front Neurol 9:1–9.

Griffa A, Baumann PS, Thiran JP, et al. 2013. Structural connectomics in brain diseases. Neuroimage 80:515–526.

Halliday GM, Leverenz JB, Schneider JS, et al. 2014. The neurobiological basis of cognitive impairment in Parkinson's disease. Mov Disord 29:634–650.

Hattori T, Orimo S, Aoki S, et al. 2012. Cognitive status correlates with white matter alteration in Parkinson's disease. Hum Brain Mapp 33:727–739.

Inguanzo A, Sala-Llonch R, Segura B, et al. 2021. Hierarchical cluster analysis of multimodal imaging data identifies brain atrophy and cognitive patterns of Parkinson's disease. Parkinsonism Relat Disord 82:16–23.

Jbabdi S, Sotiropoulos SN, Savio AM, et al. 2012. Model-based analysis of multishell diffusion MR data for tractography: how to get over fitting problems. Magn Reson Med 68: 1846–1855.

Jenkinson M, Bannister P, Brady M, et al. 2002. Improved optimization for the robust and accurate linear registration and motion correction of brain images. Neuroimage 17:825–841.

Jeurissen B, Leemans A, Jones, et al. 2011. Probabilistic fiber tracking using the residual bootstrap with constrained spherical deconvolution. Hum Brain Mapp 32:461–479.

Kalia LV, Lang AE. 2015. Parkinson's disease. Lancet 386:896–912.

Li XR, Ren YD, Cao B, et al. 2018. Analysis of white matter characteristics with tract-based spatial statistics according to diffusion tensor imaging in early Parkinson's disease. Neurosci Lett 675:127–132.

Litvan I, Goldman GJ, Tröster AI, et al. 2012. Diagnostic criteria for mild cognitive impairment in Parkinson's disease: movement disorder society task force guidelines. Mov Disord 27:349–356.

Mak E, Zhou J, Tan LCS, et al. 2014. Cognitive deficits in mild Parkinson's disease are associated with distinct areas of grey matter atrophy. J Neurol Neurosurg Psychiatry 85:576–580.

Melzer TR, Watts R, MacAskill MR, et al. 2013. White matter microstructure deteriorates across cognitive stages in Parkinson disease. Neurology 80:1841–1849.

Mishra VR, Sreenivasan KR, Yang Z, et al. 2020. Unique white matter structural connectivity in early-stage drug-naive Parkinson disease. Neurology 94:774–784.

Mori S, Van Zijl PCM. 2002. Fiber tracking: principles and strategies—a technical review. NMR Biomed 15:468–480.

Muller J, Alizadeh M, Mohamed FB, et al. 2019. Clinically applicable delineation of the pallidal sensorimotor region in patients with advanced Parkinson's disease: study of probabilistic and deterministic tractography. J Neurosurg 131:1520–1531.

Nigro S, Ricelli R, Passamonti L, et al. 2016. Characterizing structural neural networks in de novo parkinson disease patients using diffusion tensor imaging. Hum Brain Mapp 37: 4500–4510.

Peña-Nogales O, Ellmore TM, De Luis-García R, et al. 2019. Longitudinal connectomes as a candidate progression marker for prodromal Parkinson's disease. Front Neurol 13:1–13.

Pereira JB, Weintraub D, Brønnick K, et al. 2014. Initial cognitive decline is associated with cortical thinning in early Parkinson disease. Neurology 82:2017–2025.

Rubinov M, Sporns O. 2010. Complex network measures of brain connectivity: uses and interpretations. Neuroimage 52:1059–1069.

Schapira AHV, Chaudhuri KR, Jenner P. 2017. Non-motor features of Parkinson disease. Nat Rev Neurosci 18:435–450.

Segura B, Baggio HC, Marti MJ, et al. 2014. Cortical thinning associated with mild cognitive impairment in Parkinson's disease. Mov Disord 29:1495–1503.

Seidman LJ, Faraone SV, Goldstein J, et al. 1997. Reduced subcortical brain volumes in nonpsychotic siblings of schizophrenic patients: a pilot magnetic resonance imaging study. Am J Med Genet Neuropsychiatr Genet 74: 507–514.

Shah A, Lenka A, Saini J, et al. 2017. Altered brain wiring in Parkinson's disease: a structural connectome-based analysis. Brain Connect 7:347–356.

Smith SM, Jenkinson M, Johansen-Berg H, et al. 2006. Tract-based spatial statistics: voxelwise analysis of multi-subject diffusion data. Neuroimage 31:1487–1505.

Tomlinson CL, Stowe R, Patel S, et al. 2010. Systematic review of levodopa dose equivalency reporting in Parkinson's disease. Mov Disord 25:2649–2653.

Uribe C, Segura B, Baggio HC, et al. 2016. Patterns of cortical thinning in nondemented Parkinson's disease patients. Mov Disord 31:699–708.

Wang W, Mei M, Gao Y, et al. 2019. Changes of brain structural network connection in Parkinson's disease patients with mild cognitive dysfunction: a study based on diffusion tensor imaging. J Neurol 267:933–943.

Williams-Gray CH, Foltynie T, Brayne CEG, et al. 2007. Evolution of cognitive dysfunction in an incident Parkinson's disease cohort. Brain 130:1787–1798.

Worker A, Blain C, Jarosz J, et al. 2014. Diffusion tensor imaging of Parkinson's disease, multiple system atrophy and progressive supranuclear palsy: a tract-based spatial statistics study. PLoS One 9:e112638.

Wu L, Liu F, Ge J, et al. 2018. Clinical characteristics of cognitive impairment in patients with Parkinson's disease and its related pattern in 18F-FDG PET imaging. Hum Brain Mapp 39:4652–4662.

Zalesky A, Fornito A, Bullmore ET. 2010. Network-based statistic: identifying differences in brain networks. Neuroimage 53:1197–1207.

Zhang Y, Burock MA. 2020. Diffusion tensor imaging in Parkinson's disease and parkinsonian syndrome: a systematic review. Front Neurol 11:531993.

Address correspondence to:
Barbara Segura
Medical Psychology Unit
Department of Medicine
University of Barcelona
Casanova 143
Barcelona 08036
Spain

E-mail: bsegura@ub.edu

SUPPLEMENTARY MATERIAL

Supplementary Data S1

	HC (n=51)	PD (n=62)	Stats (p-value)
Age, median(IQ)	66 (17)	64.5 (15)	1485.5 (0.58)
Gender (m/f)	23/28	46/16	9.963 (0.002)
Years of education	12(7)	13(9)	1664.5 (0.48)
H&Y (1/2/2.5/3)	NA	10/31/1/20	-
UPDRS III	NA	15 (11)	-
LEDD	NA	526.75 (348.75)	-
Years of evolution	NA	7 (7)	-
IADL, median (IQ)	8 (0)	7 (3)	858 (<0.001)
MMSE, median (IQ)	0.096 (1.33)	0.094(1.33)	1393.5 (0.279)

Group differences were assessed using Mann-Whitney U test or Pearson's chi squared test. Abbreviations: HC – healthy controls; IQ – interquartile range; LEDD – L-dopa equivalent daily dose; NA – not applicable; PD – Parkinson's disease; UPDRS – Unified Parkinson's Disease Rating Scale.

Supplementary Data S2

PD-MCI < HC	PD without MCI < HC
Left entorhinal cortex - Left fusiform gyrus	Left lateral orbitofrontal cortex - Left medial orbitofrontal cortex
Left inferior parietal cortex - Left inferior temporal cortex	Left lateral orbitofrontal cortex - Left parstriangularis
Left bankssts - Left superior temporal cortex	Left lateral orbitofrontal cortex - Right lateral orbitofrontal cortex
Left lingual gyrus - Left superior temporal cortex	Left parsorbitalis - Right pericalcarine
Left pericalcarine cortex - Left superior temporal cortex	Left parsorbitalis - Right superior frontal cortex
Left entorhinal - Right isthmus cingulate	Left parstriangularis - Right parstriangularis
Left middle temporal cortex - Right lingual gyrus	Left rostral middle frontal cortex - Right pars triangularis
Left superior temporal cortex - Right lingual gyrus	Right parsorbitalis - Right superior frontal cortex
Right bankssts - Right middle temporal cortex	Left lateral orbitofrontal cortex - Left Amygdala
Left superior temporal cortex - Right pericalcarine cortex	Left parsorbitalis - Left Putamen
Left middle temporal cortex - Right pericalcarine	Left middle temporal cortex - Right pericalcarine
Left entorhinal cortex- Left Amygdala	Right cuneus - Right lateral occipital cortex
Left lingual gyrus- Right pericalcarine cortex	Right lateral orbitofrontal cortex - Right medial orbitofrontal cortex
Left entorhinal cortex - Left Hippocampus	Right lateral orbitofrontal cortex - Right parsorbitalis
Left lingual gyrus - Left Hippocampus	Left entorhinal - Left Amygdala
Left superior temporal cortex - Left Hippocampus	Left fusiform - Left Amygdala
Left entorhinal cortex - Left Ventral DC	Left entorhinal - Left Ventral DC
Right bankssts - Right Thalamus	Left Accumbens - Left Ventral DC
Left parsorbitalis - Right Hippocampus	
Left lateral orbitofrontal cortex - Right Hippocampus	
Left lateral orbitofrontal cortex - Right pericalcarine cortex	
Left parsorbitalis - Right pericalcarine cortex	
Right caudal anterior cingulate - Right superior frontal cortex	
Left parsorbitalis - Right superior frontal cortex	
Left parsorbitalis - Left Caudate	
Left lateral orbitofrontal cortex - Left Pallidum	
Left parsorbitalis - Left Pallidum	
Left parstriangularis - Left Pallidum	
Left parsopercularis - Left Putamen	
Left parsorbitalis - Left Putamen	
Left parstriangularis - Left Putamen	
Left parsorbitalis - Left Thalamus	
Left parstriangularis - Left Thalamus	
Left parsorbitalis - Left Ventral DC	
Left parstriangularis - Left Ventral DC	
Left parsorbitalis - Right Thalamus	

Structural connectivity connections with reduced number of streamlines in PD-MCI compared with HC and PD without MCI compared with HC. Abbreviations: HC – healthy controls; MCI – mild cognitive impairment; PD – Parkinson's disease patients.

Supplementary Data S3

CORTICO-CORTICAL CONNECTIONS	CORTICO-DGM CONNECTIONS
Left entorhinal cortex - Left fusiform	Left pars orbitalis - Left Caudate
Left inferior parietal cortex - Left inferior temporal cortex	Left entorhinal cortec - Left Hippocampus
Left pars orbitalis - Left superior parietal cortex	Left lingual gyrus - Left Hippocampus
Left bankssts - Left superior temporal cortex	Left superior temporal cortex - Left Hippocampus
Left lingual cortex - Left superior temporal cortex	Left lateral orbitofrontal cortex - Left Pallidum
Left pericalcarine cortex - Left superior temporal cortex	Left pars orbitalis - Left Pallidum
Left entorhinal cortex - Right isthmus cingulate	Left pars triangularis - Left Pallidum
Left middle temporal cortex - Right lingual gyrus	Left pars opercularis - Left Putamen
Left superior temporal cortex - Right lingual gyrus	Left parstriangularis - Left Putamen
Right bankssts - Right middle temporal cortex	Left pars orbitalis - Left Thalamus
Left lateral orbitofrontal cortex - Right pericalcarine cortex	Left pars triangularis - Left Thalamus
Left lingual gyrus - Right pericalcarine cortex	Left pars orbitalis - Left Ventra lDC
Left superior temporal - Right pericalcarine cortex	Left pars triangularis - Left Ventra lDC
Right caudal anterior cingulate - Right superiorfrontal cortex	Left lateral orbitofrontal - Right Hippocampus
	Left pars orbitalis - Right Hippocampus
	Left pars orbitalis - Right Thalamus
	Right bankssts - Right Thalamus

Set of cortico-cortical and cortico-DGM tracts used to obtain the ROC curves and corresponding AUC. Abbreviations: AUC – Area Under the Curve; ROC – Receiver Operating Characteristic.

Supplementary Figure S1

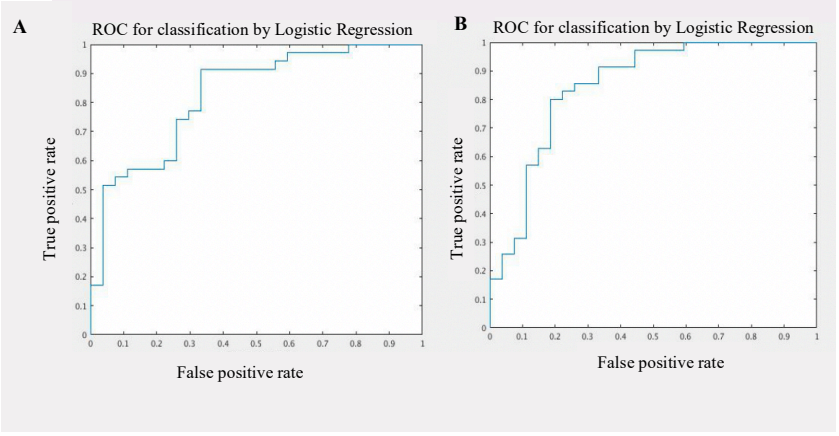

ROC curves obtained from the (A) cortico-cortical tracts and (B) DGM-cortical tracts. Abbreviations: ROC - Receiver Operating Characteristic.

STUDY 3

Inguanzo A, Poulakis K, Mohanty R, Schwarz CG, Przybelski SA, Diaz-Galvan P, Lowe VJ, Boeve BF, Lemstra AW, van de Beek M, van der Flier W, Barkhof F, Blanc F, de Sousa PL, Philippi N, Cretin B, Demuynck C, Nedelska Z, Hort J, Segura S, Junque C, Oppedal K, Aarsland D, Westman E, Kantarci K, Ferreira D.

MRI data-driven clustering reveals different subtypes of Dementia with Lewy bodies. *Under review.*

Under review

MRI data-driven clustering reveals different subtypes of Dementia with Lewy bodies

Anna Inguanzo, MSc [1,2,3], Konstantinos Poulakis, PhD[1], Rosaleena Mohanty, PhD [1], Christopher G. Schwarz, PhD [4], Scott Przybelski, PhD [5], Patricia Diaz-Galvan, PhD [1,4], Val J. Lowe, PhD, MD [4], Bradley F. Boeve, PhD, MD [4], Afina W. Lemstra, PhD, MD [6], Marleen van de Beek, PhD [6], Wiesje van der Flier, PhD, MD [6], Frederik Barkhof, PhD, MD [6,7], Frederic Blanc, PhD, MD [8,9], Paulo Loureiro de Sousa, PhD [8,9], Nathalie Philippi, PhD [8,9], Benjamin Cretin, PhD [8,9], Catherine Demuynck, PhD [8,9], Zuzana Nedelska, PhD, MD [4,10,11], Jakub Hort, PhD, MD [10,11], Barbara Segura, PhD [2,3], Carme Junque, PhD [2,3], Ketil Oppedal, PhD [12,13,14], Dag Aarsland, PhD, MD [15], Eric Westman, PhD [1,15], Kejal Kantarci, PhD, MD [4], and Daniel Ferreira, PhD[* 1,4]

[1] Division of Clinical Geriatrics, Center for Alzheimer Research, Department of Neurobiology, Care Sciences, and Society, Karolinska Institutet, Stockholm, Sweden.

[2] Medical Psychology Unit, Institute of Neurosciences, University of Barcelona, Barcelona, Spain.

[3] Institute of Biomedical Research August Pi i Sunyer (IDIBAPS), Barcelona, Spain.

[4] Department of Radiology, Mayo Clinic, Rochester, MN, United States.

[5] Quantitative Health Sciences, Mayo Clinic, Rochester, MN, United States.

[6] Department of Neurology and Alzheimer Center, VU University Medical Center, Amsterdam, Netherlands.

[7] UCL institutes of neurology and center for medical image computing, London, UK.

[8] Day Hospital of Geriatrics, Memory Resource and Research Center (CM2R) of Strasbourg, Department of Geriatrics, Hopitaux Universitaires de Strasbourg, Strasbourg, France.

[9] University of Strasbourg and French National Center for Scientific Research (CNRS), ICube Laboratory and Federation de Medecine Translationnelle de Strasbourg (FMTS), Team Imagerie Multimodale Integrative en Sante (IMIS)/ICONE, Strasbourg, France.

[10] Department of Neurology, Charles University, 2nd Faculty of Medicine, Motol University Hospital, Prague, Czech Republic.

[11] International Clinical Research Center, St. Anne's University Hospital Brno, Brno, Czech Republic.

[12] Center for Age-Related Medicine, Stavanger University Hospital, Stavanger, Norway.

[13] Stavanger Medical Imaging Laboratory (SMIL), Department of Radiology, Stavanger University Hospital, Stavanger, Norway.

[14] Department of Electrical Engineering and Computer Science, University of Stavanger, Stavanger, Norway.

[15] Department of Neuroimaging, Center for Neuroimaging Sciences, Institute of Psychiatry, Psychology and Neuroscience, King's College London, London, UK.

ARTICLE INFO

Keywords:
Dementia with Lewy bodies
Cluster analysis
Heterogeneity
Biomarkers
MRI

ABSTRACT

Background. Dementia with Lewy bodies (DLB) is a neurodegenerative disorder with a wide heterogeneity of symptoms. This heterogeneity has been disentangled using data-driven analysis on clinical data and hypothesis-driven analysis on magnetic resonance imaging (MRI). However, more research is needed to advance our understanding of the biology underlying this heterogeneity in DLB.

Objectives. We used a data-driven clustering approach on MRI data and characterized the resulting subtypes using demographic, clinical, and biomarker data.

Methods. We included 165 patients with probable DLB from the Mayo Clinic and 3 centers from the European DLB consortium. We used a random forest-based method to identify subtypes based on gray matter (GM) volumes from 82 cortical, 12 subcortical, and 2 brainstem regions. To characterize the subtypes, we assessed between-group differences in MRI volumes, demographic, and clinical data as well as tau, β-amyloid and cerebrovascular biomarkers.

Results. We identified 3 DLB subtypes with different patterns of GM volume and clinical profiles: a subtype with cortical predominant low GM volumes that included older patients with worse global cognition and faster cognitive decline over 3 years (n=49, 30%); a subtype with low GM volumes in fronto-occipital regions (n=76, 46%); and a subtype of younger patients with the highest cortical GM volumes, but proportionally lower GM volumes in basal ganglia and a higher frequency of cognitive fluctuations (n=40, 24%).

Conclusions. In this relatively large multi-center cohort, data-driven analysis on MRI revealed 3 distinct subtypes within probable DLB, which may have implications for clinical workout, research, and therapeutic decisions.

INTRODUCTION

Dementia with Lewy bodies (DLB) is a neurodegenerative disease clinically characterized by visual hallucinations (VH), cognitive fluctuations (CF), parkinsonism, and rapid eye movement sleep behavior disorder (RBD)[1]. These cardinal clinical features can course together with other symptomatology such as autonomic dysfunction, hyposmia, or anxiety, and vary in the frequency and temporal appearance across patients. This clinical complexity translates into a substantial clinical heterogeneity in probable DLB (pDLB) that has been approached through the investigation of disease subtypes[2].

Neuropathologically, DLB is characterized by abnormal accumulation of intraneuronal alpha-synuclein aggregates, similarly to Parkinson's disease (PD) with dementia. Additionally, DLB patients often have concomitant Alzheimer's disease (AD) pathology, including β-amyloid plaques and tau neurofibrillary tangles, which contributes to the heterogeneity within DLB. Structural magnetic resonance imaging (MRI) is recently emerging as a promising technique to aid differential diagnosis and investigate disease subtypes, both in pDLB[3] and AD[4]. Kantarci et al. (2012)[5] investigated 3 neuropathologically defined subtypes based on the presence of concomitant AD pathology and the spatial location of Lewy pathology (brainstem, limbic, or diffuse). An increasing likelihood of neuropathologically confirmed DLB was associated with high gray matter (GM) volumes in the amygdala and the hippocampus[5]. In contrast, lower hippocampal volumes in pDLB have been related to a more aggressive course of the disease[6]. These early studies focused on medial temporal areas have recently been extended to include posterior and frontal brain areas. Oppedal and Ferreira et al. (2019)[3] classified pDLB patients according to 4 brain atrophy subtypes previously described in AD[7]. The majority of pDLB patients were classified as hippocampal-sparing or minimal atrophy subtypes. These previous studies were all hypothesis-driven, while data-driven studies can reveal important aspects of the heterogeneity in neurodegenerative diseases[8]. For instance, in PD several data-driven studies have revealed that different brain atrophy subtypes drive part of the variability in clinical phenotype[9–11]. However, despite the preliminary evidence about the existence of DLB subtypes and the need for personalized medicine approaches, data-driven subtyping studies are still lacking in patients with pDLB.

The overall goal of this study was to advance our current understanding of the heterogeneity in DLB by expanding the previous research using a data-driven

clustering method to investigate MRI subtypes. The specific objectives were (1) to identify DLB subtypes based on different GM volumetric patterns, and (2) to characterize their clinical phenotypes at baseline and cognitive trajectories over three years of follow-up.

METHODS

1. *Participants*

A total of 165 pDLB patients participated in this multicenter study. The data were a combination of the E-DLB consortium (n= 97)[12] , including 29 subjects from Prague, 34 from Strasbourg, and 34 from VUmc Amsterdam, and the Mayo Clinic DLB cohort from Rochester, MN, United States (n= 68). Diagnosis and the presence/absence of cardinal clinical features were based on the 2005 International Consensus Criteria for pDLB[13], to allow harmonization among centers. All cardinal clinical features were assessed, including presence of parkinsonism, VH, CF, and a clinical history of probable RBD. The Mini-Mental State Examination (MMSE) was used as a measure of global cognition. Exclusion criteria were: (i) presence of acute delirium, (ii) terminal illness, (iii) previous stroke, (iv) psychotic or bipolar disorder, (v) craniocerebral trauma, and (vi) recent diagnosis of a major somatic illness.

2. β-*Amyloid and tau biomarkers*

β-amyloid and tau pathologies were assessed with cerebrospinal fluid (CSF) β-amyloid 1-42 and phosphorylated tau biomarkers in the E-DLB cohort, and with the positron emission tomography (PET) Pittsburgh compound B (PiB) and Flortaucipir (AV-1451) tracers in the Mayo Clinic. Biomarker levels were classified as normal or abnormal based on center-specific established cut points, as explained in detail in [14,15]. Currently, positivity in both β-amyloid and tau biomarkers is needed for the diagnosis of AD[16]. Hence, in the current study, we defined concomitant AD pathology when our pDLB patients showed positivity in both β-amyloid and tau biomarkers, in the subsample with available biomarkers (n = 122).

3. *Ethics*

Local ethics committee at each E-DLB center and the Mayo Clinic Institutional Review Board approved the study. Informed consent on participation was obtained from all patients or appropriate surrogates according to the Declaration of Helsinki.

4. *Neuroimaging data*

4.1. *MRI acquisition*

A high-resolution 3D T1-weigthed magnetization prepared rapid gradient echo (MPRAGE) sequence and a FLAIR sequence were acquired in 3T (The Day Hospital of

Geriatrics, Memory Resource and Research Center, CMRR, Strasbourg, France; the VU University Medical Center, VUmc, Amsterdam, the Netherlands; and the Mayo Clinic, Rochester, US) and 1.5T (Motol University Hospital, Prague, Czech Republic) scanners.

4.2. MRI preprocessing

Images from the E-DLB consortium were managed through the HiveDB database system[17]. All the data were preprocessed at the Mayo Clinic. Using ANTs[18], the Mayo Clinic Adult Lifespan Template (MCALT) (https://www.nitrc.org/projects/mcalt/) atlas was propagated to individuals' native MPRAGE space and regional estimations of volume across cortical and subcortical GM structures were calculated. Tissue probabilities were determined for each MPRAGE using the unified segmentation algorithm in SPM12 (Wellcome Trust Center for Neuroimaging, London, UK), with MCALT tissue priors and settings[19]. A total of 82 cortical ROIs, 12 subcortical ROIs and 2 brainstem ROIs were used in this study (Supplementary material 1). The total intracranial volume (TIV) was calculated from the tissue probabilities. To account for between-subject variability in GM volumes, a multiple linear regression model was fitted per each ROI (outcome variable), with TIV and center included as predictors. Residuals obtained from these regression models were used for the analyses. White matter hyperintensities (WMH) were defined as signal abnormalities of variable size in the white matter (WM), using a semi-quantitative method described in previous publications[20].

5. Subtypes of pDLB based on data-driven analysis

We performed a cluster analysis with the random forest method applied on the residuals of the 96 ROIs[21]. The random forest method is an ensemble classifier consisting of many decision trees[22]. Through bootstrapping[22], each tree was trained with a slightly different set of the data[23], which consisted of 70% of the original data, while the remaining 30% was used for validation. The random forest method was implemented in R (The R Foundation for Statistical Computing; version 4.0.3)[24].

Cluster analysis using random forest is based on the similarity (proximity) measure between pairs of observations[25]. Each tree assigns the observations together on a certain class by directing them on the same terminal node, and each time the pair of observations ends up on the same terminal node, the similarity measure increases by 1. At the end of the process, the similarities are symmetrized and divided by the number of trees. Agglomerative hierarchical clustering with the average linkage method[26] was then used in the output data from random forest. The Calinski-Harabasz index was used to

evaluate the optimal number of clusters, where 2 to 10 clusters were considered. The mean decrease in the Gini index was used to identify the ROIs with the highest contribution to the cluster analysis. The 10 most relevant ROIs were then used for a supervised random forest, in which the ROIs were the predictor variable and the cluster number the dependent variable. This supervised model was performed to identify the ROIs that best discriminate between the clusters.

6. Statistical analyses

Differences in demographic and clinical measures as well as biomarkers were assessed with one-way ANOVA for continuous variables and the Pearson's chi-square test for categorical variables. Differences between GM across ROIs were assessed with ANCOVA adjusting by age. These analyses were performed using IBM SPSS Statistics 27.0 (IBM Corp., Armonk, New York). The results from ANCOVA were corrected for multiple comparisons using the false-discovery rate (FDR) adjustment across the 96 ROIs, with the significance level set at $p < 0.05$. A linear mixed model was implemented in R to assess cognitive decline over 3 years as measured by MMSE scores (Supplementary material 2).

RESULTS

Cohort characteristics

The cohort included 165 patients with pDLB, 72% male, a mean age of 69 years (SD=8.57, range 45-88 years) and disease duration of 5.65 years (SD=4.34). The mean years of education was 13.63 years (SD=3.88). The mean MMSE score was 22.91 (SD=5.22), and the mean WMH burden was 16.12 cm^3 (SD=13.25), which roughly corresponds to a Fazekas score[27] of 2 (moderate WMH burden). Regarding the cardinal clinical features, 55% of the patients had VH, 83% had CF, 87% had parkinsonism, and 78% had probable RBD. 43% of the patients were *APOE* ε4 carriers and 11% were classified as having concomitant AD (CSF subsample, n=122).

Data-driven analysis using random forest

The three-cluster solution showed the highest Calinski-Harabasz index (CH=167.41), compared to the two-cluster solution (CH=105.14) and the four-cluster solution (CH=157.46). Based on this and visual inspection of the dendrogram (Supplementary material 3), we selected the three-cluster solution for subsequent analyses.

Morphological characterization of the MRI subtypes

Whole-brain GM patterns were characterized by comparing the subtypes across the 96 ROIs entered in the cluster analysis. ANCOVAs are shown in Supplementary material 4, and Figure 1 summarizes the regional differences between clusters. Cluster 1 (C1) was the subtype with overall lower GM volumes compared to cluster 2 (C2) and 3 (C3), while C1 showed GM volumes in the basal ganglia (BG) comparable to those in the other two clusters (Supplementary material 4). In consequence, we labeled C1 as the 'cortical predominant' subtype. C2 had intermediate GM volumes. However, C1 and C2 did not differ in frontal and occipital volumes (Figure 1A), suggesting that C2 had relative lower GM volumes in frontal and occipital areas. Hence, we labeled C2 as the 'fronto-occipital predominant' subtype. Finally, C3 had the highest cortical GM volumes but did not differ in BG GM volumes with the other two clusters. Hence, C3 was labeled as the 'subcortical predominant' subtype (Figure 1B and 1C). To further investigate these observations with regard to BG volumes in relation to cortical volumes, we computed a ratio by adding the bilateral volumes of the pallidum, putamen and caudate, and dividing them by the total sum of all cortical ROIs (Figure 2). The ratio was significantly lower in C3 compared with the other 2 subtypes, and it was significantly lower in C2 compared with C1 ($F(2,162) = 31.609$, $p<0.001$). Figure 3 shows the 10 most important ROIs in discriminating the 3 clusters (Supplementary material 5 and 6). GM volume in the left middle cingulum was the most important ROI in discriminating C1 and C2 from C3 (higher volume in C3); and the right olfactory cortex was the most important ROI in discriminating C2 from C1 (higher volume in C2).

Clinical characterization of the MRI subtypes

C3 included the youngest patients and C1 the oldest ones (Table 1). C1 had higher years of education than both C2 and C3 and had significantly worse MMSE scores at baseline compared with C3. The differences in MMSE remained when accounting for age and education ($F(2, 161)=5.936$, $p=0.005$). The longitudinal analysis of MMSE trajectories over 3 years showed that C1 had a more rapid cognitive decline over time compared to C3 (Figure 4). C1 also had a higher WMH burden than the other 2 subtypes (Table 1). However, differences in WMH burden disappeared after accounting for age ($F(2, 162)=2.643$, $p=0.074$).

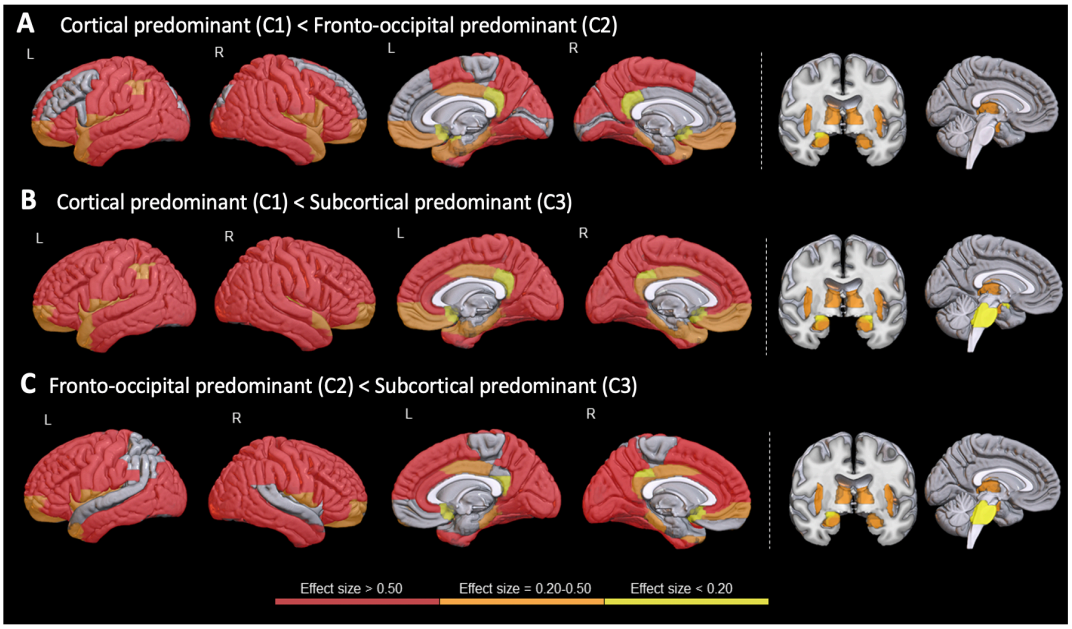

Figure 1: **Visualization of the effect sizes (Hedges' g) of the differences in GM volumes across pDLB clusters**. (A) Regions in which the cortical predominant cluster (C1) showed lower GM volumes than the fronto-occipital predominant cluster (C2); (B) Regions in which the cortical predominant cluster (C1) showed lower GM volumes than the subcortical predominant cluster (C3); (C) regions in which the fronto-occipital predominant cluster (C2) showed reduced GM volumes than the subcortical predominant cluster (C3). The cerebellum and vermis were not included in the analyses. Abbreviations: C – Cluster, GM – Gray matter, pDLB – probable Dementia with Lewy bodies.

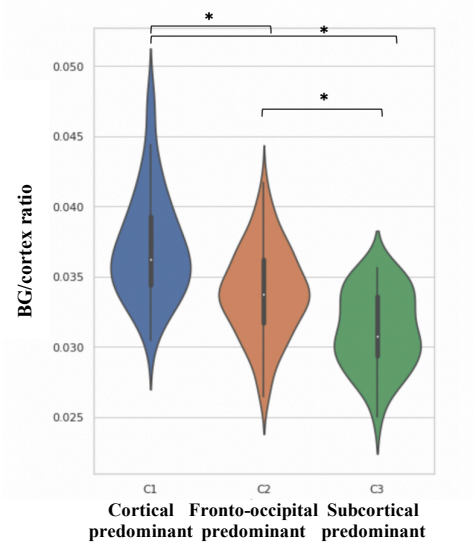

Figure 2: Ratio of basal ganglia (BG) to cortical GM volumes. The plot illustrates the distribution of the ratio across clusters. Significance for pair-wise comparisons is indicated with an asterisk ($p<0.05$).
Abbreviations: BG – basal ganglia;
C1 – cluster 1; C2 – cluster 2; C3 - cluster 3.

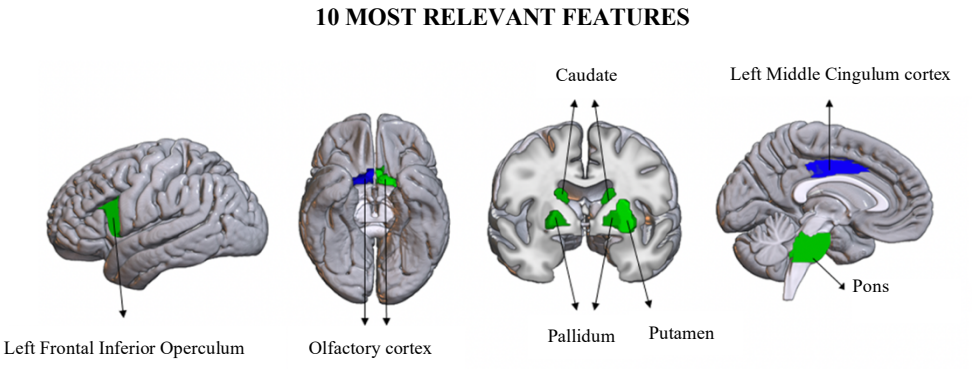

Figure 3: Visualization of the 10 most relevant regions in discriminating the 3 clusters. The supervised random forest model performed with the 10 most relevant ROIs showed that (in blue) the left middle cingulum discriminated the cortical predominant (C1) and fronto-occipital (C2) subtypes from the subcortical predominant (C3) subtype, while the right olfactory cortex discriminated the cortical predominant (C1) subtype from the fronto-occipital (C2) subtype.

	C1 (N=49) Cortical predominant	C2(N=76) Fronto-occipital	C3(N=40) Subcortical predominant	statistic (p-value)	post-hoc
Age, mean (SD)	73.43 (8.02)	69.05 (7.52)	63.68 (8.23)	17.048 (<0.001)[a]	C1 > C2, C1 > C3, C2 > C3
Years of education, mean (SD)	15.02 (3.61)	13.24 (3.90)	12.60 (3.80)	5.117 (0.007)[a]	C1 > C2, C1 > C3
MMSE, mean (SD)	21.57(5.49)	22.93(5.27)[1]	24.50 (4.38)	3.579 (0.030)[a]	C3 > C1
Sex, male (%)	71%	79%	60%	4.696 (0.096)[b]	
Disease duration (years), mean (SD)	5.109 (3.63)[2]	5.093 (3.46)[2]	7.25 (6)[3]	2.961 (0.056)[a]	
Visual hallucinations (presence)	66%[4]	52%[1]	48%	3.461 (0.177)[b]	
Cognitive fluctuations (presence)	71%[5]	85%[4]	95%[4]	8.614 (0.013)[b]	C3 > C1
Probable RBD (presence)	78%[5]	81%[7]	71%[6]	1.362 (0.506)[b]	
Parkinsonism (presence)	94%[4]	90%	78%	4.473 (0.107)[b]	
APOE genotype, ε4 carriers (presence)	37%	53%[5]	34%[4]	4.770 (0.092)[b]	
Concomitant AD pathology (presence)	7%[8]	15%[9]	6%[10]	2.352 (0.309)[b]	
White matter hyperintensities, mean (SD)	21.37 (15.41)	14.55 (13.13)	12.43 (7.958)	6.230 (0.002)[a]	C1 > C2, C1 > C3

Table 1: **Demographic, clinical, and biomarker characteristics of the pDLB clusters**. Abbreviations: AD – Alzheimer's disease; C – Cluster; DLB – Dementia with Lewy bodies; MMSE – Mini Mental State Examination; RBD – Rapid-eye movement behavior disorder; SD – Standard deviation. [a] One-way ANOVA was used; [b]The chi-squared test was used. [1] Missing data from 1 subject; [2] missing data from 17 subjects; [3] missing data from 8 subjects; [4] missing data from 2 subjects; [5] missing data from 4 subjects; [6] missing data from 5 subjects; [7] missing data from 6 subjects; [8] missing data from 20 subjects; [9] missing data from 16 subjects; [10] missing data from 7 subjects.

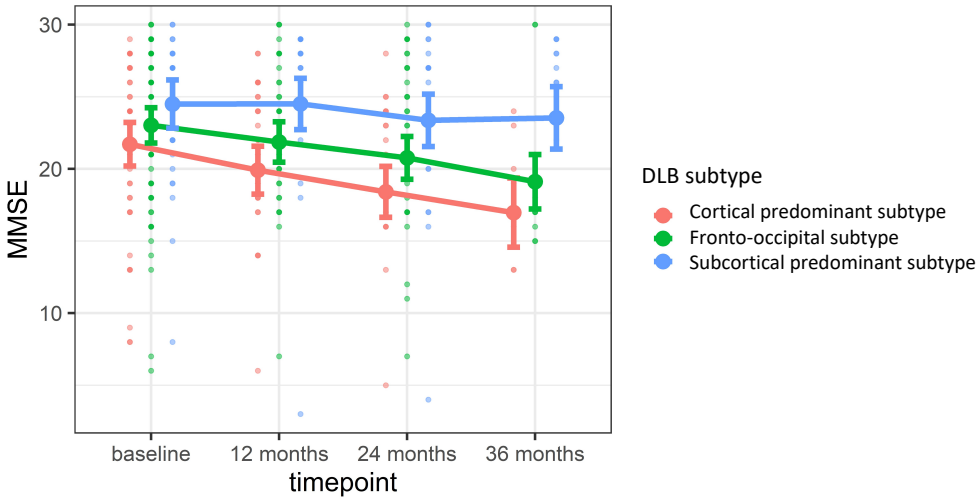

Figure 4: Cognitive decline over 3 years of follow-up as measured with the MMSE. Dots represent raw data in the background, the darker dots involve several individuals with the same score. Lines in the foreground represent estimated marginal means and error bars based on the standard error obtained from the linear mixed model. The cortical predominant subtype (C1) had significantly lower MMSE scores than the subcortical predominant subtype (C3) at baseline ($p=0.042$), with increasing magnitude of the differences over time as reflected by the lower MMSE scores at 12-month follow-up ($p<0.001$) the 24-month follow-up ($p<0.001$) and the 36-month follow-up ($p<0.001$). The fronto-occipital (C2) subtype had lower MMSE scores than the subcortical predominant (C3) subtype at the 36-month follow-up ($p=0.007$). The cortical predominant (C1) and fronto-occipital (C2) subtypes did not differ in MMSE scores over time. At baseline, MMSE scores were available for 49 (C1), 75 (C2), and 40 (C3) pDLB patients; at the 12-month follow-up, MMSE scores were available for 30 (C1), 38 (C2), and 29 (C3) pDLB patients; at the 24-month follow-up, MMSE scores were available for 22(C1), 29 (C2), and 25 (C3) pDLB patients; and at the 36-month follow-up MMSE scores were available for 7 (C1), 12 (C2), and 11 (C3) pDLB patients. Abbreviations: C1 – Cluster 1 (cortical predominant subtype); C2 - Cluster 2 (fronto-occipital subtype); C3 – Cluster 3 (subcortical predominant subtype); MMSE - Mini-Mental State Examination.

Regarding the cardinal clinical features, C3 showed a significantly higher frequency of CF (95%) compared with C1 (71%) (p=0.013). Although there were no significant differences between groups in the other clinical features, visual inspection showed that C1 had the highest frequency of VH (66%) and parkinsonism (94%); while C2 had the highest frequency of probable RBD (81%) (Table 1). The frequency of *APOE* ε4 carriers was statistically comparable across groups, although visual inspection showed that C2 had a higher frequency of *APOE* ε4 carriers (53%) than C1 (37%) and C3 (34%). Further, visual inspection showed a higher frequency of pDLB patients with concomitant AD pathology in C2 (15%) as compared with C1 (7%) and C3 (6%) (Table 1).

DISCUSSION

In this study, we expanded previous hypothesis-driven MRI subtyping studies in pDLB by conducting a data-driven MRI subtyping. We included a relatively large multi-center cohort including countries from Europe and the US. We found 3 subtypes within pDLB: (1) a cortical predominant subtype, which included older patients with lower GM volumes and worse global cognition; (2) a fronto-occipital subtype with intermediate GM volumes; and (3) a subcortical predominant subtype, which included younger patients with higher GM volumes and a higher frequency of CF. Differences in GM volumes and global cognition were independent of age.

C1 - the cortical predominant subtype - was the subtype with lowest GM volumes across all cortical regions and with the worst global cognitive performance. This subtype resembles the widespread cortical atrophy subtype with worst cognition previously reported in PD[11]. A similar widespread cortical atrophy subtype in AD has also been described to be the subtype with worst cognitive performance[4]. C2 - the fronto-occipital subtype - had intermediate age and GM volumes across many of the cortical regions, with particular involvement of fronto-occipital regions. This subtype resembles a subtype previously described in PD, which had reduced cortical thickness in fronto-occipital regions[9]. C3 -the subcortical predominant subtype - was the subtype with highest GM volumes, which is reminiscent of the minimal-atrophy subtype described by Oppedal., et al[3]. Similarly, clustering analyses in PD have repeatedly found a subtype with cortical thickness and GM volumes comparable to healthy controls[9,11].

An important finding in the current study is that despite the prominent differences in cortical GM volumes, we did not find any significant differences in the volume of BG GM across subtypes. Nonetheless, the

subcortical predominant subtype (C3) had lower subcortical GM volumes relative to cortical GM volumes as compared with cortical predominant (C1) and fronto-occipital (C2) subtypes. These observations suggest that the lack of differences in BG may reflect the same level of atrophy in our three subtypes, instead of preserved GM volumes. Previous studies showed that while pDLB patients can have a pattern of minimal cortical atrophy[3], on average they have reduced GM volumes in BG compared to healthy controls[28–30]. Reduced GM volumes in BG have been associated with attentional deficits in pDLB, which suggests that BG may be an early site of neurodegeneration[31]. This finding supports the idea that the 3 subtypes in our study do have some degree of neurodegeneration in the BG.

Altogether, our 3 subtypes show a gradient of neurodegeneration with low GM volumes in the cortical predominant subtype, intermediate GM volumes in the fronto-occipital subtype, and highest GM volumes in the subcortical predominant subtype. An important question is whether our DLB subtypes reflect different stages of the disease or distinct subtypes. The cortical predominant subtype could represent patients at a more advanced stage of the disease while the other 2 subtypes could represent less advanced stages. However, the different morphological patterns and the lower cognitive performance in the cortical predominant subtype remained after the statistical control for age, which suggests that the aforementioned subtype may represent a subtype with a more aggressive progression. This interpretation is further supported by two more findings. Firstly, the cortical predominant showed the most rapid cognitive decline over 3 years, while the subcortical predominant had relatively stable cognitive performance over time. Secondly, there were no significant differences in disease duration across subtypes, while the subcortical predominant subtype had, qualitatively, the longest disease duration. Hence, the late-onset form of pDLB seems to confer a more aggressive presentation, while the early-onset form seems to have a better prognosis, as it has been previously described in PD[32]. In other diseases such as AD, the cortical predominant subtype (our C1) is also a more aggressive presentation of the disease and is considered a distinct subtype rather than a disease stage[4,33,34]. In addition, the differences in clinical features described below further support this interpretation on different subtypes rather than subgroups at different stages of the disease.

It is worth noting that the olfactory cortex was the most important brain region to differentiate the cortical predominant from

the other subtypes, together with the different morphological patterns observed, this finding suggests different pathological pathways. We could speculate that the cortical predominant subtype reflects a variant with more intense neurodegeneration in olfactory cortex, perhaps reflecting origin of Lewy–related pathology in that area. Pathology in olfactory cortex is recognized in Braak's scheme for the progression of alpha-synuclein pathology[35] and in the revised diagnostic criteria of DLB[1], as a distinct subtype. In contrast, the subcortical subtype could reflect patients predominantly in the BG stage while the fronto-occipital subtype would have reached the cortex as predicted by Braak's scheme. The highest BG to cortical GM ratio in the cortical predominant also supports the idea that this subtype may deviate from a progression of the disease where Lewy pathology reaches BG before targeting olfactory and other cortices.

Clinically, the 3 subtypes only differed significantly in the presence of CF. Even though the subcortical predominant was the subtype with highest cortical GM volumes, it was also the subtype with the highest frequency of patients with CF. CF have been related to altered functional connectivity between the fronto-parietal network and subcortical regions such as pallidum and putamen[36]. This finding could explain the higher frequency of CF in the subcortical predominant, a subtype that has proportionally lower GM volumes in the BG. The dynamic nature of CF could be related to disconnection between cortical and subcortical GM structures in the aforementioned subtype. Brain disconnection has been suggested as one of the explanations for the minimal atrophy subtype of AD[37], a subtype that has the highest GM volumes, like our subcortical predominant subtype.

Concerning VH, despite no statistically significant differences between subtypes, visual inspection revealed that the cortical predominant subtype had the highest frequency (66%) of VH, especially when compared with the subcortical subtype (48%). Previous studies reported that pDLB patients with VH had reduced GM volumes in inferior frontal regions[38,39] and cuneus[40], when compared with pDLB patients without VH. In our study, the cortical predominant had lower GM volumes in inferior frontal regions and cuneus than both the fronto-occipital and subcortical predominant subtypes.

Regarding parkinsonism, the groups did not differ in this clinical feature, which could be explained by comparable GM volumes in BG across subtypes. Dysfunction of the BG is a well-known hallmark of DLB[1] and is often

related with motor impairment. Aberrant functional connectivity of the BG has been described in diseases with motor impairment such as PD[41] and is independent of cognitive status in PD[42].

In addition, comorbid brain pathologies could be one of the factors contributing to MRI subtypes in pDLB. We assessed WMHs as a common proxy of cerebrovascular disease, and β-amyloid and tau biomarkers to inform on concomitant AD. We found a higher WMH burden in the cortical predominant subtype in comparison with the other subtypes. However, this finding seemed to be primarily explained by the older age characteristic of this subtype. A recent study on pDLB showed the association of WMHs with GM in several cortical areas characteristic of the cortical predominant subtype, particularly, the olfactory cortex[20]. In the current study we included a measure of global WMH burden, and future studies investigating regional distributions of WMHs across MRI subtypes is warranted. Contrarily, the frequency of AD pathology (positive β-amyloid and tau biomarkers) did not reflect the age differences found in our subtypes. Rather, visual inspection suggests that the fronto-occipital subtype had the highest frequency of AD pathology. The interpretation of increased concomitant AD pathology in the fronto-occipital subtype is supported by its tendency to include a higher frequency (53%) of *APOE* ε4 carriers than the cortical predominant (37%) and subcortical predominant (34%) subtypes, since *APOE* ε4 is considered the strongest genetic risk factor for AD[43]. Further, the pattern of amyloid PET binding in DLB with concomitant AD[44] includes very similar cortical areas to those describing our fronto-occipital subtype.

Hippocampal volume is known to explain part of the heterogeneity in the clinical phenotype of DLB[5,6,45]. Further, although subtypes with higher hippocampal volume are the most common patterns in pDLB, hippocampal atrophy was reported in close to 40% of pDLB patients[3]. A novelty of our study is that by using a data-driven method to identify MRI subtypes of pDLB for the first time in the field, we observed that hippocampal volume was not among the regions that best reflected the heterogeneity in GM patterns in pDLB. Rather, cortically predominant, subcortical predominant, and fronto-occipital GM patterns illustrated the best mapping of morphological heterogeneity in our cohort of pDLB patients. A possible explanation for this finding is that hippocampal volume may have a more relevant role in DLB heterogeneity at more advanced stages of the disease, as in the cohorts often included in postmortem studies. In younger cohorts

at less advanced stages of the disease, the presence of concomitant AD pathology is lower[14], as reflected by the low proportion of pDLB patients with positive AD biomarkers in our current study, and the contribution of hippocampal volume to DLB heterogeneity may also be lower.

The current study has some limitations. Firstly, we did not have a group of healthy controls; while our main goal was to identify MRI subtypes in DLB and investigate demographic, clinical, and biomarker differences among them, having a control group could help to further characterize some aspects of our subtypes. However, the different centers included in this study had previously compared their DLB patients with their respective control groups; in consequence, our interpretations were built on previously established data. Secondly, we had some missing data for β-amyloid and tau biomarkers, giving a small subsample for statistical analysis. Still, we reported the proportion of biomarker-positive DLB patients along with group sizes due to the clinical interest of those data. Thirdly, the current study is cross-sectional, like virtually all current MRI subtyping studies[4,8]. The advent of new longitudinal clustering methods[46] will open the door to future longitudinal subtyping studies in DLB, helping to better characterize disease progression of our current DLB subtypes.

In conclusion, by using a data-driven approach on a relatively large cohort of pDLB patients, we found 3 MRI subtypes characterized by different patterns of GM volumes and clinical profiles: (1) a subtype with predominant cortical atrophy and worse global cognition, (2) a fronto-occipital subtype with intermediate GM volumes, and (3) a subcortical subtype with higher GM volumes and a higher frequency of CF. Our current findings shed some light in our endeavor to better understand the biology underlying the clinical heterogeneity in pDLB. Our approach is novel in DLB, and we hope it can inspire future works to help establish distinct neurodegeneration subtypes, as well as their links with close disorders such as PD and AD. The ultimate goal would be to leverage this knowledge to realize personalized medicine approaches, in which biomarkers and subtypes would guide therapeutic decisions in neurodegenerative diseases.

CONFLICT OF INTEREST

A Inguanzo, K Poulakis, R Mohanty, C.G. Schwarz, S.A. Przybelski, P Diaz-Galvan, B.F. Boeve, A.W. Lemstra, M van de Beek, W van der Flier, P Loureiro de Sousa, N Philippi, B Cretin, C Demuynck, Z Nedelska, Hort, B Segura, C Junque, K Oppedal, E Westman and D Ferreira report no disclosures relevant to the manuscript.

V Lowe consults for Bayer Schering Pharma, Piramal Life Sciences, Life Molecular Imaging, Eisai Inc., AVID Radiopharmaceuticals, and Merck Research and receives research support from GE Healthcare, Siemens Molecular Imaging, AVID Radiopharmaceuticals and the NIH (NIA, NCI). F Barkhof s supported by the NIHR biomedical research centre at UCLH. F Blanc has served as national coordinator and principal investigator for clinical trials sponsored by Biogen, Roche, Axovant and Eisai. D Aarsland has received research support and/or honoraria from AstraZeneca, H. Lundbeck, Novartis Pharmaceuticals and GE Health, and served as paid consultant for H. Lundbeck, Eisai and Evonik. K Kantarci serves on the data safety monitoring board for Takeda Global Research and Development Center, Inc.; receives research support from Avid Radiopharmaceuticals and Eli Lilly and receives funding from NIH and Alzheimer's Drug Discovery Foundation.

FUNDING

The authors particularly thank the patients and their family members for participating in this research. This work was supported by the National Institutes of Health (U01-NS100620, P50-AG016574, U01-AG006786, R37-AG011378, R01-AG041851, R01-AG040042, C06-RR018898 and R01-NS080820), Foundation Dr. Corinne Schuler, the Mangurian Foundation for Lewy Body Research, the Elsie and Marvin Dekelboum Family Foundation, the Little Family Foundation, the Robert H. and Clarice Smith and Abigail Van Buren Alzheimer's Disease Research Program, the Western Norway Regional Health Authority, the Swedish Foundation for Strategic Research (SSF), the Swedish Research Council (VR), Karolinska Institutet travel grants, Center for Innovative Medicine (CIMED), the Swedish Brain funding (Hjärnfonden), the Swedish Alzheimer's funding (Alzheimerfonden), ALF Medicine, the Swedish Dementia funding (Demensförbundet), the Foundation for Geriatric Diseases at Karolinska Institutet, and the Projet Hospitalier de Recherche Clinique (PHRC, IDCRB 2012-A00992-41) and fondation Université de Strasbourg. The sponsors played no role in study design; in the collection, analysis, and interpretation of data; in the writing of the report; or in the decision to submit the article for publication.

REFERENCES

1. McKeith IG. Diagnosis and managment of dementia with Lewy bodies: Fourth consensus report of the DLB Consortium. *Neurology*.2017;89(1):88-100. https://doi.org/10.1212/WNL.0000000000004058

2. Morenas-Rodríguez E, Sala I, Subirana A, Pascual-Goñi E, Sánchez-Saudinós MB, Alcolea D,

et al. Clinical Subtypes of Dementia with Lewy Bodies Based on the Initial Clinical Presentation. *J Alzheimer's Dis*. 2018;64(2):505-513. https://doi.org/10.3233/JAD-180167

3. Oppedal K, Ferreira D, Cavallin L, Lemstra AW, ten Kate M, Padovani A, et al. A signature pattern of cortical atrophy in dementia with Lewy bodies: A study on 333 patients from the European DLB consortium. *Alzheimer's Dement*. 2019;15(3):400-409. https://doi.org/10.1016/j.jalz.2018.09.011

4. Ferreira D, Nordberg A, Westman E. Biological subtypes of Alzheimer disease: A systematic review and meta-analysis. *Neurology*.2020;94(10):436-448. https://doi.org/10.1212/WNL.0000000000009058

5. Kantarci K, Ferman TJ, Boeve BF, Weigand SD, Przybelski S, Vemuri P, et al. Focal atrophy on MRI and neuropathologic classification of dementia with Lewy bodies. *Neurology*. 2012;79(6):553-560. https://doi.org/10.1212/WNL.0b013e31826357a5

6. Graff-Radford J, Lesnick T, Boeve BF, Przybelski SA, Jones DT, Senjem ML, et al. Predicting Survival in Dementia With Lewy Bodies With Hippocampal Volumetry. *Mov Disord*.2016;31(7):989-994. https://doi.org/10.1002/mds.26666

7. Ferreira D, Verhagen C, Hernández-Cabrera JA, Cavallin L, Guo CJ, Ekman U, et al. Distinct subtypes of Alzheimer's disease based on patterns of brain atrophy: Longitudinal trajectories and clinical applications. *Sci Rep*. 2017;7:1-13. https://doi.org/10.1038/srep46263

8. Habes M, Grothe MJ, Tunc B, McMillan C, Wolk DA, Davatzikos C. Disentangling Heterogeneity in Alzheimer's Disease and Related Dementias Using Data-Driven Methods. *Biol Psychiatry*. 2020;88(1):70-82. https://doi.org/10.1016/j.biopsych.2020.01.016

9. Uribe C, Segura B, Baggio HC, Abos A, Marti MJ, Valldeoriola F, et al. Patterns of cortical thinning in nondemented Parkinson's disease patients. *Mov Disord*. 2016;31(5):699-708. https://doi.org/10.1002/mds.26590

10. Uribe C, Segura B, Baggio HC, Abos A, Garcia-Diaz AI, Campabadal A, et al. Cortical atrophy patterns in early Parkinson's disease patients using hierarchical cluster analysis. *Park Relat Disord*.2018;50:3-9. https://doi.org/10.1016/j.parkreldis.2018.02.006

11. Inguanzo A, Sala-llonch R, Segura B, Erostarbe H, Abos A, Campabadal A, et al. Hierarchical cluster analysis of multimodal imaging data identifies brain atrophy and cognitive patterns in Parkinson ' s disease. *Parkinsonism and Related disorders*. 2021; 82: 16-23. https://doi.org/10.1016/j.parkreldis.2020.11.010

12. Oppedal K, Borda MG, Ferreira D, Westman E, Aarsland D & The European DLB Consortium. European DLB consortium: diagnostic and prognostic biomarkers in dementia with Lewy bodies, a multicenter international initiative. *Neurodegener Dis Manag*. 2019;9(5):247-250. https://doi.org/10.2217/nmt-2019-0016

13. Mckeith IG, Dickson DW, Lowe J, Emre M, O'Brien JT, Feldman H, et al. Diagnosis and management of dementia with Lewy bodies: Third report of the DLB Consortium. *Neurology*.

2005;66(9):1455.
https://doi.org/10.1212/01.wnl.0000224698.67660.45

14. Ferreira D, Przybelski SA, Lesnick TG, Lemstra AW, Londos E, Blanc F, et al. β-Amyloid and tau biomarkers and clinical phenotype in dementia with Lewy bodies. *Neurology*. 2020;95(24):e3257-e3268.
https://doi.org/10.1212/WNL.0000000000010943

15. Kantarci K, Lowe VJ, Boeve BF, Senjem ML, Tosakulwong N, Lesnick TG, et al. AV-1451 tau and β-amyloid positron emission tomography imaging in dementia with Lewy bodies. *Ann Neurol*. 2017;81(1):58-67.
https:// doi.org/10.1002/ana.24825

16. Jack CR, Bennett DA, Blennow K, Carrillo MC, Dunn B, Haeberlein SB, et al. NIA-AA Research Framework: Toward a biological definition of Alzheimer's disease. *Alzheimer's Dement*. 2018;14(4):535-562.
https://doi.org/10.1016/j.jalz.2018.02.018

17. Muehlboeck JS, Westman E, Simmons A. TheHiveDB image data management and analysis framework. *Front Neuroinform*. 2014;7:1-13. https://doi.org/10.3389/fninf.2013.00049

18. Avants BB, Epstein CL, Grossman M, Gee JC. Symmetric diffeomorphic image registration with cross-correlation: Evaluating automated labeling of elderly and neurodegenerative brain. *Med Image Anal*. 2008;12(2008):26-41. https://doi.org/10.1016/j.media.2007.06.004

19. Schwarz CG, Gunter JL, Ward CP, Vemuri P, Senjem ML, Wiste HJ. The Mayo Clinic Adult Lifespan Template: Better Quantification Across the Lifespan. *Alzheimer's Dement*. 2017;13:792. https://doi.org/10.1016/j.jalz.2017.06.1071

20. Ferreira D, Nedelska Z, Graff-Radford J, Przybelski SA, Lesnick TG, Schwarz CG, et al. Cerebrovascular disease, neurodegeneration, and clinical phenotype in dementia with Lewy bodies. *Neurobiol Aging*. 2021;105:252-261. https://doi.org/10.1016/j.neurobiolaging.2021.04.029

21. Breiman L. Random forests. *Mach Learn*. 2001;45:5-32.
https://doi.org/https://doi.org/10.1023/A:1010933404324

22. Breiman L. Bagging Predictors. *Mach Learn*. 1996;24(123-140).
https://doi.org/10.1007/BF00058655

23. Amit Y, Geman D. Shape Quantization and Recognition with Randomized Trees. *Neural Comput*. 1997;9(7):1545-1588. https://doi.org/10.1162/neco.1997.9.7.1545

24. Poulakis K, Pereira JB, Mecocci P, Vellas B, Tsolaki M, Kłoszewska I, et al. Heterogeneous patterns of brain atrophy in Alzheimer's disease. *Neurobiol Aging*. 2018;65:98-108. https://doi.org/10.1016/j.neurobiolaging.2018.01.009

25. Shi T, Horvath S. Unsupervised learning with random forest predictors. *J Comput Graph Stat*. 2006;15(1):118-138.
https://doi.org/10.1198/106186006X94072

26. Gray KR, Aljabara P, Heckemannc RA,

Hammers A, Rueckerta D. Random forest-based similarity measures for multi-modal classification of Alzheimer's disease. *Neuroimage*. 2013;65C:167-175. https://doi.org/10.1016/j.neuroimage.2012.09.065

27. Fazekas F, Chawluk JB, Alavi A. MR signal abnormalities at 1.5 T in Alzheimer's dementia and normal aging. *Am J Neuroradiol*. 1987;8(3):421-426.

28. Watson R, O'Brien JT, Barber R, Blamire AM. Patterns of gray matter atrophy in dementia with Lewy bodies: A voxel-based morphometry study. *Int Psychogeriatrics*. 2012;24(4):532-540. https://doi.org/10.1017/S1041610211002171

29. Watson R, Colloby SJ, Blamire AM, O'Brien JT. Subcortical volume changes in dementia with Lewy bodies and Alzheimer's disease. A comparison with healthy aging. *Int Psychogeriatrics*. 2016;28(4):529-536. https://doi.org/10.1017/S1041610215001805

30. van der Zande JJ, Steenwijk MD, ten Kate M, Wattjes MP, Scheltens P, Lemstra AW. Gray matter atrophy in dementia with Lewy bodies with and without concomitant Alzheimer's disease pathology. *Neurobiol Aging*. 2018;71:171-178. https://doi.org/10.1016/j.neurobiolaging.2018.07.005

31. Botzung A, Philippi N, Noblet V, Loureiro De Sousa P, Blanc F. Pay attention to the basal ganglia: A volumetric study in early dementia with Lewy bodies. *Alzheimer's Res Ther*. 2019;11(1):1-9. https://doi.org/10.1186/s13195-019-0568-y

32. Ferguson LW, Rajput AH, Rajput A. Early-onset vs. Late-onset Parkinson's disease: A Clinical-pathological Study. *Can J Neurol Sci*. 2015;43(1):113-119. https://doi.org/10.1017/cjn.2015.244

33. Murray ME, Graff-Radford NR, Ross OA, Petersen RC, Duara R, Dickson DW. Neuropathologically defined subtypes of Alzheimer's disease with distinct clinical characteristics : A retrospective study. *Lancet Neurol*. 2011;10(9):785-796. https://doi.org/10.1016/S1474-4422(11)70156-9

34. Na HK, Kang DR, Kim S, Seo SW, Heilman KM, Noh Y, Na DL. Malignant progression in parietal-dominant atrophy subtype of Alzheimer's disease occurs independent of onset age. *Neurobiol Aging*. 2016;47:149-156. https://doi.org/10.1016/j.neurobiolaging.2016.08.001

35. Braak H, Del Tredici K, Rüb U, De Vos RAI, Jansen Steur ENH, Braak E. Staging of brain pathology related to sporadic Parkinson's disease. *Neurobiol Aging*. 2003;24(2):197-211. https://doi.org/10.1016/S0197-4580(02)00065-9

36. Peraza LR, Kaiser M, Firbank M, Graziadio S, Bonanni L, Onofrj M, et al. fMRI resting state networks and their association with cognitive fluctuations in dementia with Lewy bodies. *NeuroImage Clin*. 2014;4:558-565. https://doi.org/10.1016/j.nicl.2014.03.013

37. Ferreira D, Pereira JB, Volpe G, Westman E. Subtypes of Alzheimer's disease display distinct network abnormalities extending beyond their pattern of brain atrophy. *Front Neurol*. 2019;10. https://doi.org/10.3389/fneur.2019.00524

38. Sanchez-Castaneda C, Rene R, Ramírez-Ruiz B, Campdelacreu J, Gascon J, Falcon C, et al. Frontal and associative visual areas related to visual hallucinations in dementia with lewy bodies and Parkinson's disease with dementia. *Mov Disord*. 2010;25(5):615-622. https://doi.org/10.1002/mds.22873

39. Pezzoli S, Cagnin A, Antonini A, Venneri A. Frontal and subcortical contribution to visual hallucinations in dementia with Lewy bodies and Parkinson's disease. *Postgrad Med*.2019;131(7):509-522. https://doi.org/10.1080/00325481.2019.1656515

40. Blanc F, Colloby SJ, Cretin B, De Sousa PL, Demuynck C, O'Brien JT, et al. Grey matter atrophy in prodromal stage of dementia with Lewy bodies and Alzheimer's disease. Alzheimer's Res Ther. 2016;8(1). http://dx.doi.org/10.1186/s13195-016-0198-6

41. Rolinski M, Griffanti L, Szewczyk-Krolikowski K, Menke RAL, Wilcock GK, Filippini N, et al. Aberrant functional connectivity within the basal ganglia of patients with Parkinson's disease. *NeuroImage Clin*. 2015;8:126-132. https://doi.org/10.1016/j.nicl.2015.04.003

42. Szewczyk-Krolikowski K, Menke RAL, Rolinski M, Duff E, Salimi-Khorshidi G, Filippini N, et al. Functional connectivity in the basal ganglia network differentiates PD patients from controls. *Neurology*. 2014;83:208-214. https://doi.org/10.1212/WNL.0000000000000592

43. Serrano-Pozo A, Das S, Hyman BT. APOE and Alzheimer's disease: advances in genetics, pathophysiology, and therapeutic approaches. *Lancet Neurol*. 2021;20(1):68-80. https://doi.org/10.1016/S1474-4422(20)30412-9

44. Kantarci K, Lowe VJ, Chen Q, Przybelski SA, Lesnick TG, Schwarz CG, et al. β-Amyloid PET and neuropathology in dementia with Lewy bodies. *Neurology*. 2020;94(3):e282-e291. https://doi.org/10.1212/WNL.0000000000008818

45. Elder GJ, Mactier K, Colloby SJ, Watson R, Blamire AM, O'Brien JT, et al. The influence of hippocampal atrophy on the cognitive phenotype of dementia with Lewy bodies. *Int J Geriatr Psychiatry*. 2017;32(11):1182-1189. https://doi.org/10.1002/gps.4719

46. Poulakis K, Ferreira D, Pereira JB, Smedby Ö, Vemuri P, Westman E. Fully Bayesian longitudinal unsupervised learning for the assessment and visualization of AD heterogeneity and progression. *Aging (Albany NY)*. 2020;12(13):12622-12647. https://doi.org/10.18632/aging.103623

SUPPLEMENTARY MATERIAL

Supplementary material 1

LIST OF ROIs ENTERED IN THE ANALYSIS	
Precentral bilateral	Occipital Inf bilateral
Frontal Sup bilateral	Fusiform bilateral
Frontal Sup Orb bilateral	Postcentral bilateral
Frontal Mid bilateral	Parietal Sup bilateral
Frontal Mid Orb bilateral	Parietal Inf bilateral
Frontal Inf Oper bilateral	Supramarginal bilateral
Frontal Inf Tri bilateral	Angular bilateral
Frontal Inf Orb bilateral	Precuneus bilateral
Rolandic Oper bilateral	Paracentral lobule bilateral
Supp Motor Area bilateral	Caudate bilateral
Olfactory bilateral	Pallidum bilateral
Frontal Sup Medial bilateral	Putamen bilateral
Frontal Med Orb bilateral	Thalamus bilateral
Rectus bilateral	Heschl bilateral
Insula bilateral	Temporal Sup bilateral
Cingulum Ant bilateral	Temporal Pole Sup bilateral
Cingulum Mid bilateral	Temporal Mid bilateral
Hippocampus bilateral	Temporal Pole Mid bilateral
Amygdala bilateral	Temporal Inf bilateral
Calcarine bilateral	Pons
Cuneus bilateral	Dorsal Mesopontine
Lingual bilateral	Entorhinal Cortex bilateral
Occipital Sup bilateral	ParaHippocampal bilateral
Occipital Mid bilateral	Cingulum Post bilateral
	Retrosplenial Cortex bilateral

Supplementary material 2

The linear mixed effects model was conducted in R version 4.0.3 using the lme4 package. The design consisted of a random intercept per subject with the model reference set to the baseline and cluster 3. The outcome was the longitudinal MMSE scores (12-month, 24-month and 36-month follow-up). The fixed effects were time (categorical), cluster (categorical) and interaction between time and cluster. Post-hoc pairwise comparisons were done between clusters based on model estimates with multiple comparisons corrections with Tukey adjustment (using emmeans package).

Supplementary material 3

Dendrogram from the cluster analysis

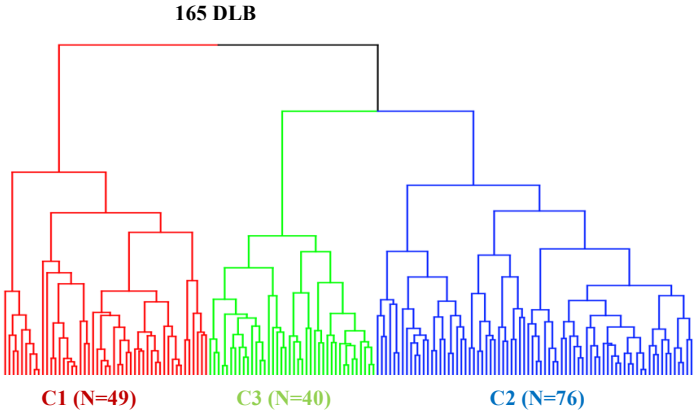

Figure 1: Dendrogram of the 165 patients with pDLB clustered according to gray matter volumes. Abbreviations: C1 – Cluster 1, C2 – Cluster 2, C3 – Cluster 3, DLB – Dementia with Lewy bodies.

Supplementary material 4

	C1(n=49)	C2(n=76)	C3(n=40)	F	p-value	post-hoc
Precentral_L	-0.717 (1.058)	0.081 (1.156)	0.723 (0.972)	24.943	1.37E-09	C1 < C2, C1 < C3, C2 < C3
Precentral_R	-0.613 (1.366)	0.038 (1.032)	0.679 (1.134)	17.002	3.56E-07	C1 < C2, C1 < C3, C2 < C3
Frontal_Sup_L	-0.471(0.944)	0.028 (0.983)	0.522 (1.024)	14.044	3.42E-06	C1 < C2, C1 < C3, C2 < C3
Frontal_Sup_R	-0.365 (0.995)	-0.138 (1.033)	0.709 (0.875)	17.731	2.11E-07	C1 < C3, C2 < C3
Frontal_Sup_Orb_L	-0.259 (0.307)	0.017 (0.298)	0.283 (0.262)	50.636	1.19E-16	C1 < C2, C1 < C3, C2 < C3
Frontal_Sup_Orb_R	-0.277 (0.328)	0.027 (0.310)	0.288 (0.384)	41.743	1.98E-14	C1 < C2, C1 < C3, C2 < C3
Frontal_Mid_L	-0.666 (1.946)	-0.053 (1.940)	0.917 (2.352)	8.104	0.000512632	C1 < C3, C2 < C3
Frontal_Mid_R	-0.858 (1.914)	0.076 (1.913)	0.906 (1.961)	11.519	2.70E-05	C1 < C2, C1 < C3, C2 < C3
Frontal_Mid_Orb_L	-0.381 (0.440)	0.028 (0.463)	0.412 (0.494)	42.525	1.42E-14	C1 < C2, C1 < C3, C2 < C3
Frontal_Mid_Orb_R	-0.382 (0.486)	0.104 (0.453)	0.270 (0.422)	32.574	7.04E-12	C1 < C2, C1 < C3, C2 < C3
Frontal_Inf_Oper_L	-0.169 (0.562)	-0.056 (0.529)	0.313 (0.629)	10.622	5.79E-05	C1 < C3, C2 < C3
Frontal_Inf_Oper_R	-0.369 (0.432)	0.034 (0.457)	0.387 (0.635)	32.956	5.65E-12	C1 < C2, C1 < C3, C2 < C3
Frontal_Inf_Tri_L	-0.337 (0.576)	0.062 (0.537)	0.293 (0.575)	18.469	1.23E-07	C1 < C2, C1 < C3, C2 < C3
Frontal_Inf_Tri_R	-0.328 (0.569)	0.003 (0.615)	0.395 (0.564)	20.859	2.22E-08	C1 < C2, C1 < C3, C2 < C3
Frontal_Inf_Orb_L	-0.525 (0.664)	0.152 (0.527)	0.352 (0.510)	39.274	9.45E-14	C1 < C2, C1 < C3, C2 < C3
Frontal_Inf_Orb_R	-0.462 (0.634)	0.094 (0.522)	0.387 (0.579)	33.306	4.71E-12	C1 < C2, C1 < C3, C2 < C3
Rolandic_Oper_L	-0.282 (0.354)	-0.014 (0.348)	0.374 (0.418)	46.489	1.23E-15	C1 < C2, C1 < C3, C2 < C3
Rolandic_Oper_R	-0.352 (0.487)	0.011 (0.422)	0.409 (0.518)	38.287	1.59E-13	C1 < C2, C1 < C3, C2 < C3
Supp_Motor_Area_L	-0.502 (0.563)	0.110 (0.710)	0.406 (0.894)	23.672	3.01E-09	C1 < C2, C1 < C3, C2 < C3
Supp_Motor_Area_R	-0.409 (0.627)	0.026 (0.886)	0.452 (0.902)	15.102	1.49E-06	C1 < C2, C1 < C3, C2 < C3
Olfactory_L	-0.037 (0.096)	0.001 (0.089)	0.0438 (0.105)	9.873	0.000109714	C1 < C2, C1 < C3, C2 < C3
Olfactory_R	-0.043 (0.104)	0.001(0.101)	0.051 (0.108)	11.3	3.23E-05	C1 < C2, C1 < C3, C2 < C3
Frontal_Sup_Medial_L	-0.345 (0.830)	-0.105 (0.839)	0.623 (0.923)	18.695	1.07E-07	C1 < C3, C2 < C3
Frontal_Sup_Medial_R	-0.297 (0.962)	-0.051 (1.130)	0.462 (1.064)	6.999	0.001342815	C1 < C3, C2 < C3
Frontal_Med_Orb_L	-0.332 (0.372)	0.055 (0.379)	0.302 (0.300)	47.162	9.07E-16	C1 < C2, C1 < C3, C2 < C3
Frontal_Med_Orb_R	-0.273 (0.445)	0.083 (0.438)	0.176 (0.297)	19.379	6.43E-08	C1 < C2, C1 < C3
Rectus_L	-0.1553 (0.285)	0.037 (0.238)	0.118 (0.324)	14.799	1.86E-06	C1 < C2, C1 < C3
Rectus_R	-0.154 (0.241)	0.053 (0.251)	0.087 (0.265)	15.736	9.16E-07	C1 < C2, C1 < C3
Insula_L	-0.454 (0.408)	0.043 (0.439)	0.473 (0.482)	67.639	1.14E-20	C1 < C2, C1 < C3, C2 < C3
Insula_R	-0.534 (0.477)	0.109 (0.419)	0.447 (0.536)	71.318	6.34E-21	C1 < C2, C1 < C3, C2 < C3
Cingulum_Ant_L	-0.163 (0.508)	-0.052 (0.555)	0.300 (0.578)	10.378	7.09E-05	C1 < C3, C2 < C3
Cingulum_Ant_R	-0.241 (0.650)	-0.094 (0.806)	0.476 (0.662)	14.444	2.47E-06	C1 < C3, C2 < C3
Cingulum_Mid_L	-0.109 (0.384)	-0.039 (0.304)	0.209 (0.408)	11.748	2.24E-05	C1 < C3, C2 < C3
Cingulum_Mid_R	-0.219 (0.368)	0.026 (0.398)	0.217 (0.403)	17.428	2.60E-07	C1 < C2, C1 < C3, C2 < C3
Hippocampus_L	-0.145 (0.354)	-0.010 (0.342)	0.199 (0.281)	14.798	1.86E-06	C1 < C2, C1 < C3, C2 < C3
Hippocampus_R	-0.152 (0.390)	0.011 (0.298)	0.165 (0.256)	13.513	5.23E-06	C1 < C2, C1 < C3, C2 < C3

	C1(n=49)	C2(n=76)	C3(n=40)	F	p-value	post-hoc
Amygdala_L	-0.034 (0.093)	0.001 (0.110)	0.040 (0.079)	7.723	0.001116279	C1 < C3
Amygdala_R	-0.059 (0.104)	0.010 (0.101)	0.051 (0.086)	18.038	1.71E-07	C1 < C2, C1 < C3, C2 < C3
Calcarine_L	-0.183 (0.814)	-0.188 (0.760)	0.582 (0.843)	16.618	4.80E-07	C1 < C3, C2 < C3
Calcarine_R	-0.290 (0.757)	-0.082 (0.724)	0.512 (0.895)	15.334	1.26E-06	C1 < C3, C2 < C3
Cuneus_L	-0.370 (0.7851)	-0.094 (0.742)	0.634 (0.917)	22.928	4.95E-09	C1 < C2, C1 < C3, C2 < C3
Cuneus_R	-0.405 (0.708)	0.001 (0.718)	0.494 (0.848)	19.939	4.39E-08	C1 < C2, C1 < C3, C2 < C3
Lingual_L	-0.547 (0.867)	0.008 (0.995)	0.655 (0.965)	22.166	8.75E-09	C1 < C2, C1 < C3, C2 < C3
Lingual_R	-0.577 (0.837)	0.062 (0.797)	0.588 (0.895)	27.829	1.66E-10	C1 < C2, C1 < C3, C2 < C3
Occipital_Sup_L	-0.214 (0.477)	-0.134 (0.500)	0.518 (0.640)	31.469	1.39E-11	C1 < C3, C2 < C3
Occipital_Sup_R	-0.180 (0.719)	-0.082 (0.579)	0.377 (0.594)	11.969	1.87E-05	C1 < C3, C2 < C3
Occipital_Mid_L	-0.666 (1.158)	-0.062 (1.346)	0.934 (1.141)	23.167	4.20E-09	C1 < C2, C1 < C3, C2 < C3
Occipital_Mid_R	-0.494 (0.913)	-0.022 (0.770)	0.648 (0.819)	26.807	3.43E-10	C1 < C2, C1 < C3, C2 < C3
Occipital_Inf_L	-0.270 (0.574)	-0.097 (0.583)	0.517 (0.445)	31.237	1.55E-11	C1 < C2, C1 < C3, C2 < C3
Occipital_Inf_R	-0.338 (0.706)	-0.032(0.670)	0.477 (0.629)	20.599	2.66E-08	C1 < C2, C1 < C3, C2 < C3
Fusiform_L	-0.631(0.988)	0.027 (0.977)	0.721 (0.795)	29.204	6.26E-11	C1 < C2, C1 < C3, C2 < C3
Fusiform_R	-0.726 (1.045)	0.160 (0.841)	0.584 (0.898)	30.798	2.06E-11	C1 < C2, C1 < C3, C2 < C3
Postcentral_L	-0.667 (1.061)	0.021 (1.003)	0.777(1.319)	23.889	2.63E-09	C1 < C2, C1 < C3, C2 < C3
Postcentral_R	-0.553 (1.011)	0.061 (1.024)	0.560 (1.190)	15.241	1.34E-06	C1 < C2, C1 < C3, C2 < C3
Parietal_Sup_L	-0.482 (0.881)	0.090 (0.995)	0.419 (0.869)	13.364	5.86E-06	C1 < C2, C1 < C3
Parietal_Sup_R	-0.531 (0.819)	0.069 (0.774)	0.518 (0.857)	24.013	2.32E-09	C1 < C2, C1 < C3, C2 < C3
Parietal_Inf_L	-0.318 (0.450)	0.121 (0.423)	0.160 (0.468)	21.436	1.49E-08	C1 < C2, C1 < C3
Parietal_Inf_R	-0.370 (0.508)	0.064 (0.706)	0.332 (0.714)	16.386	5.71E-07	C1 < C2, C1 < C3, C2 < C3
SupraMarginal_L	-0.489 (0.746)	0.061 (0.752)	0.482 (0.669)	25.151	1.15E-09	C1 < C2, C1 < C3, C2 < C3
SupraMarginal_R	-0.391 (0.696)	0.023 (0.687)	0.433 (0.698)	19.653	5.41E-08	C1 < C2, C1 < C3, C2 < C3
Angular_L	-0.329 (0.757)	0.075 (1.044)	0.261 (0.983)	5.587	0.005393258	C1 < C2, C1 < C3
Angular_R	-0.649 (0.963)	0.117 (1.209)	0.572 (1.101)	17.247	2.96E-07	C1 < C2, C1 < C3, C2 < C3
Precuneus_L	-0.938 (0.870)	0.054 (0.992)	1.045 (0.916)	67.966	1.14E-20	C1 < C2, C1 < C3, C2 < C3
Precuneus_R	-0.902 (0.986)	0.041 (0.971)	1.026 (1.100)	54.214	1.60E-17	C1 < C2, C1 < C3, C2 < C3
Paracentral_Lobule_L	-0.359 (1.050)	0.058 (0.854)	0.328 (0.972)	7.396	0.001116279	C1 < C2, C1 < C3
Paracentral_Lobule_R	-0.305 (1.058)	0.012 (0.791)	0.351 (0.955)	6.908	0.001116279	C1 < C3
Caudate_L	-0.0172 (0.335)	0.0001(0.278)	0.021 (0.288)	0.219	0.812463158	n.s
Caudate_R	-0.014 (0.387)	0.001(0.324)	0.016 (0.317)	0.109	0.897	n.s
Pallidum_L	-0.001 (0.049)	0.004 (0.059)	-0.007 (0.059)	0.668	0.536347826	n.s
Pallidum_R	-0.002 (0.040)	0.004 (0.055)	-0.005 (0.056)	0.562	0.589419355	n.s
Putamen_L	-0.036 (0.408)	0.001 (0.463)	0.042 (0.445)	0.428	0.666893617	n.s
Putamen_R	-0.094 (0.415)	0.019 (0.442)	0.080 (0.384)	2.436	0.096	n.s
Thalamus_L	-0.224 (0.288)	0.047 (0.247)	0.184 (0.322)	32.224	9.07E-21	C1 < C2, C1 < C3, C2 < C3
Thalamus_R	-0.182 (0.311)	0.028 (0.272)	0.169 (0.334)	19.548	5.74E-08	C1 < C2, C1 < C3, C2 < C3

	C1(n=49)	C2(n=76)	C3(n=40)	F	p-value	post-hoc
Heschl_L	-0.158 (0.186)	0.028 (0.240)	0.138 (0.310)	21.207	1.74E-08	C1 < C2, C1 < C3, C2 < C3
Heschl_R	-0.090 (0.146)	0.013 (0.170)	0.084 (0.220)	13.532	5.22E-06	C1 < C2, C1 < C3, C2 < C3
Temporal_Sup_L	-0.744 (1.003)	0.240 (1.150)	0.456 (1.219)	18.815	9.91E-08	C1 < C2, C1 < C3
Temporal_Sup_R	-0.666 (0.995)	0.171 (1.056)	0.490 (1.218)	17.501	2.50E-07	C1 < C2, C1 < C3
Temporal_Pole_Sup_L	-0.216 (0.446)	0.048 (0.424)	0.174 (0.351)	12.995	7.92E-06	C1 < C2, C1 < C3
Temporal_Pole_Sup_R	-0.232 (0.405)	0.057 (0.375)	0.176 (0.430)	15.902	8.11E-07	C1 < C2, C1 < C3
Temporal_Mid_L	-0.759 (1.385)	-0.152(1.295)	1.219 (1.356)	31.992	1.01E-11	C1 < C2, C1 < C3, C2 < C3
Temporal_Mid_R	-1.217 (1.566)	0.1202(1.505)	1.262 (1.477)	38.769	1.23E-13	C1 < C2, C1 < C3, C2 < C3
Temporal_Pole_Mid_L	-0.217 (0.404)	0.017 (0.512)	0.234 (0.474)	12.478	1.22E-05	C1 < C2, C1 < C3, C2 < C3
Temporal_Pole_Mid_R	-0.338 (0.440)	0.048 (0.502)	0.322 (0.567)	24.79	1.37E-09	C1 < C2, C1 < C3, C2 < C3
Temporal_Inf_L	-0.842 (1.073)	0.077 (0.990)	0.885 (0.994)	42.058	1.76E-14	C1 < C2, C1 < C3, C2 < C3
Temporal_Inf_R	-1.166 (1.040)	0.132 (1.144)	1.177 (1.213)	65.704	2.63E-20	C1 < C2, C1 < C3, C2 < C3
Pons	-0.013 (0.030)	-0.001(0.027)	0.018 (0.063)	8.84	0.000269776	C1 < C3, C2 < C3
Dorsal_Mesopontine	-0.002 (0.007)	- 0.0003(0.007)	0.003 (0.008)	6.622	0.002181818	C1 < C3, C2 < C3
Entorhinal_Cortex_L	-0.074 (0.279)	0.016 (0.282)	0.059 (0.244)	3.474	0.0352	C1 < C3
Entorhinal_Cortex_R	-0.103(0.195)	0.024 (0.262)	0.080 (0.2484)	8.599	0.000331248	C1 < C2, C1 < C3
ParaHippocampal_L	-0.092 (0.216)	0.003 (0.264)	0.1064 (0.218)	9.28	0.000184009	C1 < C2, C1 < C3, C2 < C3
ParaHippocampal_R	-0.135 (0.239)	0.022 (0.228)	0.122 (0.265)	16.249	6.29E-07	C1 < C2, C1 < C3, C2 < C3
Cingulum_Post_L	-0.078 (0.129)	0.004 (0.139)	0.087 (0.166)	18.559	1.17E-07	C1 < C2, C1 < C3, C2 < C3
Cingulum_Post_R	-0.100 (0.166)	0.026 (0.154)	0.072 (0.169)	17.744	2.11E-07	C1 < C2, C1 < C3
Retrosplenial_Cortex_L	-0.119 (0.151)	0.010 (0.192)	0.126 (0.243)	22.126	8.78E-09	C1 < C2, C1 < C3, C2 < C3
Retrosplenial_Cortex_R	-0.071 (0.126)	0.006 (0.135)	0.076 (0.150)	16.074	7.15E-07	C1 < C2, C1 < C3, C2 < C3

Mean(SD) of the residuals adjusted for centre, ICV and age. ANCOVAs and corrected p-values.

Supplementary material 5

The 10 ROIs with the lowest Gini Index values. The mean decrease in the Gini index was used to identify the ROIs with the highest contribution to the cluster analysis.

10 TOP ROIs	Gini Index
Right Pallidum	0.9521002
Left frontal inferior operculum	0.9675189
Left Olfactory cortex	0.9774211
Left Pallidum	0.9898548
Left middle cingulum	0.9928215
Pons	0.9928266
Left Caudate	0.9935472
Right Caudate	0.9976649
Right Olfactory cortex	1.0100825
Left Putamen	1.0108899

Supplementary material 6

Supervised classification tree showing the complete view of the variable discrimination rules for the DLB clusters. Among the 10 most relevant ROIs, the left middle cingulum, which showed greater volumes in C3 compared to C1 and C2, was placed on top of the tree, indicating that it was the most relevant ROI to discriminate between the DLB clusters. Then, the tree was divided into 2 branches: one that included C1 and C2, and another one for C3. The branch including C1 and C2 had the left opercular inferior frontal on top of the branch, which had a greater GM volume in C3 compared to C1 and C2, but it did not differ between C1 and C2. Next, the right olfactory cortex was able to discriminate between C1 and C2, with C2 showing larger GM volumes than C1.

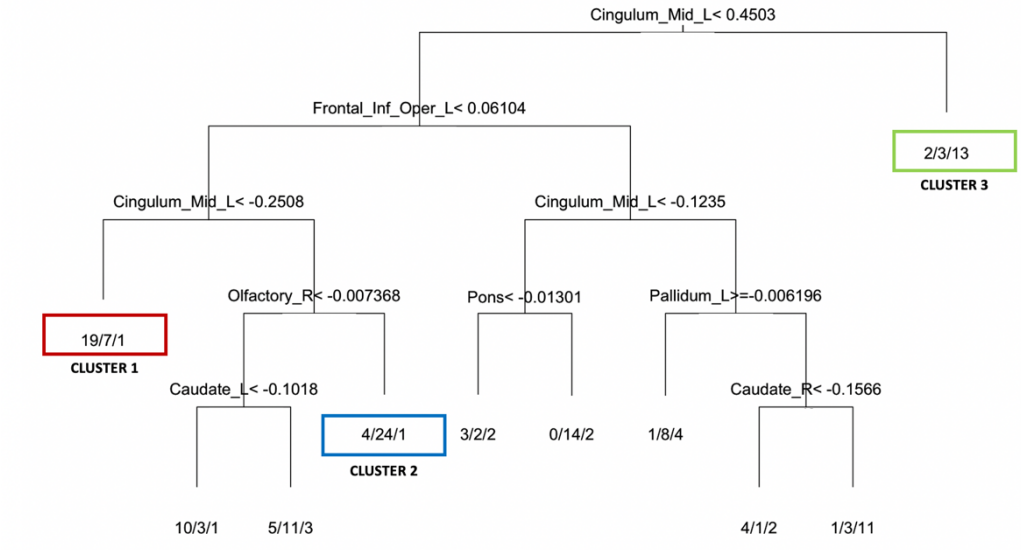

Supplementary material 7

timepoint = MMSE baseline							
contrast	estimate	SE	df	t-stat	p-value	Lower CL	Upper CL
1-2	-1.31	0.987	188	-1.33	0.3806	-3.64	1.0196
1-3	-2.79	1.145	188	-2.433	0.0419	-5.49	-0.0805
2-3	-1.47	1.052	188	-1.4	0.3428	-3.96	1.0122
timepoint = MMSE 12months							
contrast	estimate	SE	df	t-stat	p-value	Lower CL	Upper CL
1-2	-1.95	1.103	260	-1.766	0.1831	-4.55	0.6523
1-3	-4.59	1.234	236	-3.719	0.0007	-7.5	-1.6787
2-3	-2.64	1.148	244	-2.3	0.0577	-5.35	0.0672
timepoint = MMSE 24months							
contrast	estimate	SE	df	t-stat	p-value	Lower CL	Upper CL
1-2	-2.35	1.173	297	-2.006	0.1124	-5.11	0.4094
1-3	-4.96	1.288	265	-3.847	0.0004	-7.99	-1.9204
2-3	-2.6	1.193	270	-2.182	0.076	-5.42	0.208
timepoint = MMSE 36months							
contrast	estimate	SE	df	t-stat	p-value	Lower CL	Upper CL
1-2	-2.14	1.551	350	-1.382	0.3517	-5.8	1.5083
1-3	-6.57	1.643	355	-4	0.0002	-10.44	-2.7039
2-3	-4.43	1.46	352	-3.032	0.0073	-7.86	-0.9902

The method used for degrees of freedom was the Kenward-Roger method, and the p-value adjustment was carried out with the Tukey method for comparing a family of 3 estimates. A confidence level (CL) of 0.95 was used.

CHAPTER 5

General Discussion

The main objective of the current Doctoral Thesis was to find subtypes within Parkinson's disease and Dementia with Lewy bodies using data-driven approaches based on different neuroimaging modalities, as well as to characterize changes in brain architecture underlying mild cognitive impairment in Parkinson's disease.

In this Thesis we present the first clustering done in PD combining grey matter and fractional anisotropy, as well as the first clustering based on MRI data ever done in DLB. Also, in the study of mild cognitive impairment in PD, ours is the first analysis in structural connectivity based on probabilistic tractography and TFNBS.

Grey matter patterns in Parkinson's disease and Dementia with Lewy bodies subtypes

In Study 1 and 3, we described 3 subtypes within PD and DLB, respectively, by using different data-driven subtyping approaches.

In the first study, we identified a first subtype, PD1, with widespread GM atrophy, including cortical and subcortical regions, as well as WM FA reductions and the worse neuropsychological profile. PD1 had the worst performance in the memory and language domains. Along this line, impairment in memory tasks (Levy et al., 2002) as well as in semantic fluency (Williams-Gray et al., 2007) have been described as predictors of cognitive decline in PD. The second subtype, PD2, only presented with cortical atrophy limited to fronto-temporal regions. In our Study 1 there was a partial sample overlap with a 5-year gap with the sample used in Uribe et al., (2016), in which a hierarchical cluster analysis using the Ward's linkage method was also performed. However, in Uribe et al., (2016) the cluster analysis was based on vertex-wise cortical thickness measures. In that previous study, a PD subtype with neither detectable atrophy nor cognitive impairment was also found, as was described in our PD3.

In Study 3 we described 3 DLB subtypes, a first subtype with the lowest GM volumes across all cortical regions, worse cognitive performance and older age. This subtype was

named as cortical predominant subtype and resembled PD1 from Study 1, for its widespread pattern of reduced GM as well as for its impaired cognition. Despite having a different neuropathological basis, the cortical predominant DLB subtype presented similarities with the hippocampal-sparing subtype described in AD (Ferreira et al., 2020b for a review). The hippocampal-sparing AD subtype is characterized by neurodegeneration involving frontal, parietal and temporal cortices, the highest level of education, and an aggressive course of the disease (Ferreira et al., 2020b for a review), similar to the cortical predominant DLB subtype, which not only had more years of education compared to the other 2 subtypes but also presented a more aggressive course, as it showed widespread reductions of GM volumes compared to the other groups after the same years of disease duration, as well as the most pronounced cognitive decline over time. Qualitatively, the cortical predominant DLB subtype showed the highest percentage of individuals with VH, as well as the PD1 subtype described in Study 1. Reduced GM volumes in occipital regions could explain the slightly higher frequencies in the aforementioned subtypes. Specifically, the cuneus – the primary visual cortex - has been related to VH in DLB (Blanc et al., 2016), while in PD, VH have been related to GM atrophy in parieto-occipital areas, secondary visual cortex, and the hippocampus head (Ibarretxe-Bilbao et al., 2011 for a review). Along this line, in the DLB study (Study 3), the number of patients with VH in the cortical predominant and fronto-occipital subtypes were closer than they were between PD1 and PD2 (Study 1), perhaps due to the fact that, while in the PD cluster analysis, PD2 was characterized by fronto-temporal atrophy, in the DLB analysis, the second subtype was characterized by frontal and occipital atrophy. The second DLB subtype - the fronto-occipital subtype - had an age in between the cortical predominant and subcortical predominant subtypes, as well as reduced GM volumes across many of the cortical regions, with particular involvement of frontal and occipital regions. Interestingly, in a previous PD study, Uribe et al., (2016) also found a pattern of cortical thinning involving frontal and occipital regions. Finally, the third DLB subtype - the cortical predominant subtype - was the one with the highest GM volumes, resembling PD3 from Study 1, which did not present GM atrophy compared to healthy controls. Moreover, it is reminiscent of the PD subtype without detectable cortical thinning compared to controls described in Uribe et al., (2016) as well as to the

AD minimal-atrophy subtype recurrently described in AD MRI studies (Ferreira et al., 2020b for a review).

Age of onset and disease severity

Although there was the same disease duration among the PD subtypes described in Study 1 and the DLB subtypes described in Study 3, the youngest subtype from the PD sample (PD3), as well as the youngest subtype from the DLB study (subcortical predominant subtype), were the ones with preserved GM volumes and better cognitive performance. On the other hand, in Study 1, the subtype with the oldest onset of the disease (PD1) was characterized by GM atrophy affecting the largest number of cortical regions, as well as subcortical regions. Additionally, it had the worse neuropsychological profile. In Study 3, the older DLB subtype - the cortical predominant - also had widespread reduced GM volumes compared to the other subtypes and presented the lowest global cognition scores at baseline as well as faster cognitive decline over time.

Previous cluster studies based on clinical data had exclusively found 2 clusters corresponding to young and late-onset subtypes (Schrag et al., 2006; Post et al., 2008). Interestingly, in our 2-cluster solution from our PD study (Study 1), we also defined the young-onset group and the late-onset group, that with the highest percentage of patients with MCI *(Supplementary material from Study 1)*. Previous other clinical studies described more than 2 clusters but always finding the young and late-onset subtypes (van Rooden et al., 2011; Erro et al., 2013). Additional studies focusing on neuropsychological (Dujardin et al., 2013; Lopes et al., 2017; LaBelle et al., 2017) or combining both clinical and neuropsychological data (Fereshtehnejad et al., 2017) have also given evidence of 2 differentiated courses of the disease. Taking one step further, Uribe et al., (2016) performed a hierarchical cluster analysis and, in the 2-cluster solution, again described the subtypes as young and late-onset with worse cognition. It should be emphasized that, in AD as opposed to PD, early age of onset is related to worse progression of the disease, while late onset is associated with a better prognosis (Ferreira et al., 2020b for a review). All these studies give evidence of the importance of

considering age as a variable of interest, rather than a confounder, when performing subtyping analyses, as it has been demonstrated to be a specific characteristic that differs among subtypes. Here, the input data of the cluster analyses (Studies 1 and 3) was not adjusted by age, but we did account for it once the clusters were defined.

Studies 1 and 3 provide more evidence to the current knowledge of age-at-onset implications in PD, as well as in DLB prognosis, by showing that the subtypes with the latest onset suffer from a more aggressive course of the disease, characterized not only by a more pronounced cognitive decline but also by patterns of extensive reduced GM volumes.

The effect of ageing in neurodegenerative disorders

Brain ageing involves vascular injury and abnormal protein deposits that are able to produce cognitive deficits, leading to a greater comorbidity associated with ageing. In consequence, it appears as a primary risk factor for a variety of neurodegenerative disorders such as AD, PD and DLB (Hou et al., 2019). Additionally, the coexistence of cumulative effects of neuropathological changes, as well as the interaction among protein alterations, can have a relevant impact that should be considered.

Some brain regions appear to be more sensitive with the passage of time. In terms of atrophy, the prefrontal cortex appears as the most affected, followed by the striatum, and the temporal lobe, the cerebellum, and the hippocampus (Peters, 2006 for a review). Additionally, in PD-MCI, low hippocampal volume has been associated to the development of dementia (Kandiah et al., 2014), and the temporal lobe is known to be more affected in AD. White matter hyperintensities have been described to be more prominent in dementias (AD, DLB and PDD) than in PD, and have been associated to atrophy in the medial temporal lobes (Joki et al., 2018). Deposits of abnormal proteins are associated with ageing and can contribute to the final disease presentation. In Study 3, the oldest DLB subtype, the cortical predominant, was the one with higher number of WMH, a result that appeared to be associated with the older age characteristic of that

group. Additionally, there is overlap between diseases, DLB is an α-synucleinopathy that can also course with neurofibrillary tangles and β-amyloid plaques (Zhang et al., 2017 for a review) with a symptomatology that resembles AD, making its diagnosis challenging. In Study 3, we combined β-amyloid and tau biomarkers, although the number of DLB patients with both biomarkers was small in our study sample. The DLB subtype with reduced GM volumes in frontal and occipital regions appeared to have, qualitatively, a higher number of subjects with concomitant AD pathology and a higher number of APOE ε4 carriers, the genotype well-known to be the strongest risk factor for AD (Serrano-Pozo et al., 2021 for a review). Even more, although PD is another α-synucleinopathy, when involving dementia (PDD), it also courses with neurofibrillary tangles and β-amyloid plaques (Jellinger, 2018 for a review), which reinforces the association between the aforementioned protein deposits and ageing. In this context, accounting for ageing appears challenging and can prove to be a limitation, as it is difficult to discern between deviations of normal ageing and ageing itself. In this context, mediation methods are a statistical method with great potential to aid understanding of how ageing is mediating the effect of neurodegenerative disorders in the brain.

Age is also very important in cluster analyses. On the one hand, considering the effect of ageing before the analysis may cloud the finding of subtypes with different ages at onset. On the other, not accounting for age can lead to findings associated, to a certain degree, to the normal process of ageing. In a recent paper, a longitudinal cluster analysis, that incorporated the comparison with a control group in the cluster procedure itself, was applied in AD (Poulakis et al., 2020). In this context, longitudinal cluster analyses appear as a novel, promising technique to be used in large PD samples. For future studies, it would be also of interest for the patients included in the studies to have information regarding the different proteins associated to brain degeneration.

Structural connectivity related to cognition in Parkinson's disease

In Study 1, we combined WM changes measured with FA measures and GM volumes to perform a multimodal cluster analysis which allowed us to find different PD subtypes considered both grey and white matter degeneration. After finding 3 subtypes, we performed TBSS analysis to compare the PD subtypes with HC and found that only one of the 3 subtypes presented reduced FA. This subtype was also the subtype with more widespread GM atrophy and higher percentage of MCI. In Study 2, we approached the WM architecture underlying MCI in PD through different techniques. Again, TBSS only differentiated PD-MCI from HC, while PD without MCI did not show alterations in FA. Previous studies were also unable to detect alterations in FA in the PD without MCI group (Hattori et al., 2012; Agosta et al., 2014). Going a step further, we studied the structural connectivity in PD with and without MCI using TFNBS based on probabilistic tractography. TFNBS was able to show that PD without MCI had impaired structural connectivity compared to controls in cortico-deep grey matter and cortico-cortical connections involving bilateral fronto-temporal regions. On the other hand, PD-MCI doubled the number of connections with reduced NOS compared to controls, and in this case, the impaired connections were cortico-deep grey matter connections and cortico-cortical connections involving temporal and occipital regions. Along this line, posterior cortical-based neuropsychological deficits have been associated to a higher risk of developing dementia (Williams-Gray et al., 2007), and cortical thinning in parieto-temporal regions has been proposed as a structural neuroimaging marker of PD-MCI (Segura et al., 2014; Uribe et al., 2016). Conversely, Galantucci et al., (2017), found PD-MCI to have reduced structural connectivity in networks involving the basal ganglia and fronto-parietal regions by using NBS based on a deterministic approach. FA and MD values obtained from the networks were used to differentiate PD-MCI from PD without MCI with high accuracy. We also did a ROC curve analysis, which determined that cortico-cortical as well as cortico-deep grey matter connections with reduced NOS, in PD-MCI compared to controls, enabled us to distinguish between patients with and without MCI.

Taken as a whole, our results suggest that complex structural brain networks are involved in cognitive impairment in PD, rather than degenerations of individual WM tracts.

We highlight that results from Study 1 and 2 offer evidence that PD is not primarily a white matter disease. When entering WM as input of the cluster analysis (Study 1), WM was not able to provide specific WM patterns needed to discern the 3 subtypes. Additionally, in Study 2, although revealing clear differences in structural connectivity between PD with and without MCI, it lacked sufficient statistical power to significantly differentiate between the two aforementioned PD groups. Conversely, in demyelinating diseases, such as multiple sclerosis (MS), DTI has appeared as a useful technique to differentiate between MS types – primary progressive/relapsing remitting (Assaf and Pasternak, 2008 for a review). However, in PD, WM impairment may follow GM atrophy, which seems to play the relevant role in this disease. GM has been described to be able to differentiate PD from HC, PD with and without cognitive impairment, and to find predictors of MCI converting to dementia, as well as following progression over time, and even finding different PD subtypes based on cortical thickness measures (Krajcovicova et al., 2019 for a review).

Does white matter atrophy precede or follow grey matter atrophy?

Some studies have stated that WM alterations would take place previous to GM atrophy, a conclusion derived from the fact that they either found no GM atrophy (Agosta et al., 2014) or minimal GM differences (Rektor et al., 2018) in PD with and without MCI compared to controls, while TBSS showed PD-MCI to have reduced FA (Agosta et al., 2014; Rektor et al., 2018). However, these studies did not combine both modalities. In Study 1, through a multimodal approach in which GM and WM measures were considered together, we detected that the only PD subtype presenting reduced FA was PD1, the subtype with widespread GM atrophy. The other 2 subtypes did not show differences in WM compared to HC. Furthermore, PD1 was the subtype with a higher percentage of patients with MCI. Additionally, in Study 2, the TBSS analysis showed reduced FA in PD-MCI compared to controls, but PD without MCI showed no WM

alterations. This led to considering that WM atrophy appears after GM atrophy, and not the other way round. We also showed in Study 1 that GM features were more informative than WM features in the cluster analysis. In this context, we conclude that: WM is less informative than GM; WM alterations follow GM atrophy, and WM alone may not be informative enough to establish PD subtypes on its own, but combined with GM can provide a more detailed characterization of PD subtypes. The fact that some studies did not find differences in GM between PD and healthy controls may be due to disease duration heterogeneity within the sample, methodological issues, or a less accurate characterization of MCI.

Substrates of cognitive impairment

In Study 1, the subtype with the worst neuropsychological profile was the one with more GM atrophy as well as WM atrophy. In Study 2, PD-MCI presented reduced FA and structural connectivity impairment affecting more connections than PD without MCI. Delving deeper, in Study 3, the DLB subtype with the worst global cognition (cortical predominant subtype) was the one with the lower GM volumes. All the studies reflect that the global cognitive decline in PD and DLB is associated with widespread GM atrophy, and possibly to WM atrophy secondary to GM degeneration. However, cognitive fluctuations, a core symptom of DLB, were a characteristic of the subtype with highest GM volumes - the subcortical predominant. Interestingly, Peraza et al., (2014) performed a VBM analysis, to compare DLB with cognitive fluctuations to healthy controls, which did not show significant differences, except for just 2 voxels. The aforementioned evidence together with the dynamic nature of cognitive fluctuations suggests that cognitive fluctuations are not a consequence of GM atrophy, but rather the product of a functional connectivity disruption. In fact, cognitive fluctuations have been associated with impaired functional connectivity between the fronto-parietal network and subcortical regions (Peraza et al., 2014). Interestingly, brain disconnection has also been described as the potential cause of cognitive decline in the minimal atrophy subtype of AD (Ferreira et al., 2019). In PD, cognitive deficits have also been approached from the functional perspective. In PD-MCI, impairment in functional connectivity within and

between networks has been reported (Baggio et al., 2014; Baggio et al., 2015), as well as alterations in dynamic functional connectivity (Díez-Cirarda et al., 2018). This is in line with a later study that evaluated the progressive dysfunction in dynamic functional connectivity by studying a PD sample that ranged from PD without cognitive impairment to PDD (Fiorenzato et al., 2019).

Methodological implications of cluster analyses

Disentangling subtypes within neurodegenerative diseases seems to be a priority in current research, approached through both unsupervised and supervised methods. The supervised approaches make specific assumptions about the data, forcing the observations to fit into a specific number of clusters/subtypes. Consequently, it is biased towards prior knowledge. This fact makes unsupervised methods, which are guided by the data without *a priori* hypothesis, more suitable to investigate new subtypes (Feczko et al., 2019 for a review). There is evidence of data-driven analyses finding promising results within the study of neurodegenerative diseases (Habes et al., 2020 for a review). Similarly, when choosing specific ROIs as the input of the cluster analysis, we are working, to a certain level, with an hypothesis a priori. In Study 3, from previous literature, we could have chosen specific ROIs, such as the hippocampus, instead of performing a whole-brain analysis. However, the whole-brain approach revealed that the hippocampus was not among the 10 most relevant ROIs in discerning the subtypes. Interestingly, the hippocampus did not appear as one of the main regions to describe DLB. A possible explanation for this finding is that hippocampal volume may have a more relevant role in more advanced stages of DLB, as in the cohorts often included in postmortem studies. In younger cohorts at less advanced stages of the disease, the presence of concomitant AD pathology is lower (Ferreira et al., 2021), as reflected by the low proportion of DLB patients with positive AD biomarkers in Study 3. Thus, there is highly likelihood of DLB pathology, instead of AD-pathology, which has been associated with higher GM volumes in the hippocampus (Kantarci et al., 2012). Due to the aforementioned reasons and evidence, we used unsupervised whole-brain approaches in order to find new PD (Study 1) and DLB subtypes (Study 3). Particularly in Study 3, we present the first data-driven subtyping analysis based on MRI carried out in a DLB

sample. Nevertheless, there are some limitations that should be addressed for future improvements. On the one hand, most studies lack validation steps, while ideally, studies should have an independent cohort to ensure reproducibility (Feczko et al., 2019 for a review). Another aspect to consider is the input data used for the subtyping studies. Until now, the majority of analyses have opted for either focusing on high-dimensional data from one single modality or simplifying data from different modalities in order to be able to combine them (Habes et al., 2020 for a review). This leads to the curse of dimensionality, which when extrapolated to the biomedical field, implies that with the increase of the number of features - for example, cognitive, behavioural (neuropsychological tests, specific scales, etc.) or biological (genetic biomarkers, GM volumes, etc.) features **-** the number of observations (patients) required to generalize the model rises exponentially. In this context, two main problems can interfere with the reliability of the outcomes. One is the risk of overfitting, which occurs when we have more features than observations. The other is that the observations are complex to cluster, as these appear equidistant from each other. Generally, cluster analyses use the Euclidean distance to measure how similar the observations are; however, too many features force distances to be equal, which implies ending up without groups of observations similar among themselves, which makes finding relevant clusters impossible. In the PD cluster analysis (Study 1), we improved the problem of dimensionality compared to previous PD cluster analyses based on MRI data (Uribe et al., 2016; Uribe et al., 2018) by reducing the number of features entered in the analysis. Still, we wanted to go one step further in Study 3 and, in order to surpass this limitation, we opted for the Random Forest method, which overcomes this issue by building multiple decision trees. In each tree, only a subset of features is used, reducing the space over which each tree is minimizing. Regarding multimodality, it is necessary to perform complex cluster analyses that incorporate PET imaging data to MRI studies to better understand the subtypes. First approaches have worked on combining these different modalities. Jeon et al., (2019) performed a cluster analysis in AD combining cortical thickness, as well as tau and amyloid burden. PET imaging can help to disentangle which characteristics are due to a specific pathology, rather than a combination of pathologies, or ageing itself. As mentioned above, longitudinal cluster analyses (Poulakis et al., 2020)

seem to be a promising new technique that can help to clarify if the subtypes we recurrently find in different diseases, such as AD and PD, are differentiated entities, as it will facilitate the finding of subtypes based on their trajectories and emphasize the typicality dimension over the severity dimension (Ferreira et al., 2020b for a review), which is the main interest when performing subtyping analyses.

Final remarks

The present Doctoral Thesis has identified different patterns of atrophy in PD and DLB by applying unsupervised data-driven subtyping, which in turn has been associated with specific clinical and neuropsychological profiles. Specifically, our work has provided more evidence of the existence of subtypes within PD and DLB. In addition, we have studied cognition by thoroughly describing the neuropsychological profiles of the PD subtypes and by approaching structural connectivity in PD-MCI.

Our hope is that our research will help drive forward the identifying of neuroimaging and neuropsychological biomarkers that would assist in providing a specific diagnosis to DLB and PD patients resulting in a more personalized treatment.

CHAPTER 6

Conclusions

Through the combined analysis of the studies included in this Doctoral Thesis, we can conclude that:

1. Three subtypes were identified in Parkinson's disease based on GM and WM structural MRI data. One subtype characterized by loss of GM in bilateral tempo-parieto-occipital cortices and subcortical regions, as well as widespread FA reductions mainly affecting fronto-occipital WM tracts; a second subtype with loss of GM in bilateral orbital, medial prefrontal, and temporal cortical regions; and a third subtype without detectable GM or WM alterations.

2. Regarding the neuropsychological profile of these PD subtypes, the first subtype manifested pronounced cognitive deficits compared to healthy controls and the third PD subtype, while the third subtype did not show detectable cognitive impairment. The second subtype presented low scores in certain neuropsychological tests including Facial Recognition Test, Trail Making Test part A and part B, Stroop Color Test, Stroop Word Test and Symbol Digit Modalities Test compared to healthy controls but did not differ from any PD subtype.

3. The multimodal imaging cluster analysis revealed that the patterns of GM degeneration are more relevant in the characterization of PD subtypes than WM alterations. WM alterations are only observed in patients with widespread GM involvement.

4. Whole-brain structural connectivity based on probabilistic tractography revealed reduced fronto-striatal connectivity related to cognitive decline in PD, as well as impaired posterior cortical connections, mainly involving temporal and occipital regions.

5. Local graph measures including reduced local efficiency, node degree and nodal clustering coefficient are able to differentiate PD with and without MCI as well as both PD from controls.

6. Three DLB subtypes with different patterns of GM were identified through cluster analysis. The cortical predominant subtype was characterized by widespread reduced GM in cortical regions compared to the other subtypes; the fronto-occipital subtype had reduced GM volumes in frontal and occipital regions; finally, the subcortical predominant subtype was characterized by greater GM volumes than the other subtypes except for the basal ganglia, where it showed proportionally lower GM volumes than the other subtypes.

7. The cortical predominant DLB subtype was characterized by the worse global cognitive performance and fastest cognitive decline over time; while the subcortical predominant, although presenting with the greater GM volumes and global cognitive performance, included the highest number of patients with cognitive fluctuations.

ACKNOWLEDGEMENTS

Acaba una etapa important que ha estat plena de bons moments i d'altres més difícils, amb pandèmia inclosa. Una etapa que sens dubte no hauria estat possible superar si no hagués estat envoltada de gent com vosaltres, així que, que menys que dedicar-vos, com a mínim, unes paraules.

Primer de tot agrair a les meves directores de Tesi, les doctores Carme Junqué i Bàrbara Segura, per haver-me donat aquesta oportunitat. Carme, ha estat un honor poder formar part del teu grup i aprendre de tu, és impressionant tot el que saps, gràcies per haver-me guiat i donat els millors consells. Bàrbara, gràcies per tot el temps invertit i tota la feina feta juntes, després de tanta feina ho hem aconseguit! Roser, sense tu aquesta Tesi tampoc hagués estat possible, gràcies per tota la teva ajuda, idees i feina, ets increïble!

Les noies, Anna, Carme i Àlex gràcies per acollir-me des del primer moment, ha estat un plaer compartir lab amb vosaltres. Anna, gràcies per escoltar-me, i per compartir la meva primera experiència a un congrés. Carme, agraeixo moltíssim que sempre hagis estat disposada a ajudar-me, fins i tot des del Canadà! Àlex, m'ho vaig passar molt bé amb tu al lab, i se t'ha trobat a faltar.
Javi, el mejor compañero de proyecto! Lástima que el destino no quiso que reclutásemos demasiada muestra juntos. Gaudeix del que et queda i, si us plau, no aprenguis més català del que sé jo.

Vull agrair-li també a la Lídia, d'una manera molt especial, per tot el temps compartit juntes, tant dins com fora del lab. Des del nostre meravellós arbre de Nadal i les banderetes ideals que vam fer pel comiat de la Carme Uribe, fins als passejos i vermuts. Has estat una molt bona companya de lab, però sobre tot has estat una millor amiga. Gràcies per fer del lab més que un lloc de feina.

Els altres membres del BBSLab també heu contribuït en el bon ambient del lab. Gràcies al David, a la Cris i al Kilian, agraeixo molt haver estat rodejada per vosaltres.

Durant el temps que he estat al lab, he coincidit amb molta gent, alguns marxaven i altres començaven. Gràcies a l'Hugo, Pablo i Dídac, així com a les noves incorporacions, que han estat una sort. Gemma, gràcies per la teva ajuda, m'has transmès molts ànims, ets un sol! Marina, transmets un munt d'energia i entusiasme, és una alegria coincidir amb tu al lab. Lídia Mulet i María, sou encantadores, gràcies per animar-vos a compartir temps juntes fora del lab, segur que el que us queda de doctorat us aniré molt bé. Rubén, a tu també t'anirà molt bé, un cop passat l'entrebanc del confinament, tot anirà rodat.

I would also like to thank Daniel Ferreira and Eric Westman for giving me the great opportunity to work with them at Karolinska Institutet. Dani, muchas gracias por confiar en mi para el proyecto de DLB. También agradecerte tu amabilidad y todo el tiempo que me has dedicado, ha sido una suerte trabajar contigo. I would also like to thank my labmates from KI for making my stay a wonderful experience. Thank you Rosaleena, Giulia, Anna Canal and Konstantinos.

Família i amics, el doctorat mai hagués estat possible sense tots vosaltres. Gràcies per la vostra paciència, per animar-me a continuar i per omplir aquests anys de mil coses interessants. Gracias por estar siempre cerca a pesar de la distancia. A més, especial menció a l'Albert pel seu assessorament artístic en la Tesi i a l'avi per fer-me de model per la portada. Maureen, you are admirable, and this is only a small space that cannot reflect how much I want to thank you, thank you for checking my English, and above everything, for being my friend.

Finalment, m'agradaria agrair als voluntaris dels estudis i als seus familiars, que no han dubtat en regalar-nos el seu temps.

Moltíssimes gràcies a totes i a tots.

References

Aarsland D, Brønnick K, Larsen JP, Tysnes OB, Alves G. Cognitive impairment in incident, untreated Parkinson disease: the Norwegian ParkWest study. Neurology. 2009; 72(13):1121–1126.

Aarsland D, Brønnick K, Ehrt U, De Deyn PP, Tekin S, Emre M, et al. Neuropsychiatric symptoms in patients with Parkinson's disease and dementia: Frequency, profile and associated care giver stress. J Neurol Neurosurg Psychiatry. 2007;78(1):36–42.

Abbasi N, Fereshtehnejad SM, Zeighami Y, Larcher KMH, Postuma RB, Dagher A. Predicting severity and prognosis in Parkinson's disease from brain microstructure and connectivity. NeuroImage Clin. 2020;25:102111.

Abdo WF, van de Warrenburg BP, Burn DJ, Quinn NP, Bloem BR. The clinical approach to movement disorders. Nat Rev Neurol. 2010;6(1):29-37.

Abos A, Segura B, Baggio HC, Campabadal A, Uribe C, Garrido A, et al. Disrupted structural connectivity of fronto-deep gray matter pathways in progressive supranuclear palsy. NeuroImage Clin. 2019;23:101899.

Agosta F, Canu E, Stefanova E, Sarro L, Tomić A, Špica V, et al. Mild cognitive impairment in Parkinson's disease is associated with a distributed pattern of brain white matter damage. Hum Brain Mapp. 2014;35(5):1921–1929.

Alpaydin E. Introduction to machine learning. MIT Press. 2010.

Alves G, Larsen JP, Emre M, Wentzel-Larsen T, Aarsland D. Changes in motor subtype and risk for incident dementia in Parkinson's disease. Mov Disord. 2006;21(8):1123–1130.

Amit Y, Geman D; Shape Quantization and Recognition with Randomized Trees. Neural Comput. 1997; 9 (7): 1545–1588.

Anang JBM, Gagnon J, Bertrand J, Romentes SR, Latreille V, Passinet M, et al. Predictors of dementia in Parkinson disease. Neurology. 2014;83:1253–1260.

Apostolova LG, Beyer M, Green AE, Hwang KS, Morra JH, Chou YY, et al. Hippocampal, caudate, and ventricular changes in Parkinson's disease with and without dementia. Mov Disord. 2010;25(6):687–695.

Armstrong RA. Visual signs and symptoms of Parkinson's disease. Clin Exp Optom. 2007;91(2):129-38.

Arrigo A, Calamuneri A, Milardi D, Mormina E, Gaeta M, Corallo F, et al. Claustral structural connectivity and cognitive impairment in drug naïve Parkinson's disease. Brain Imaging Behav. 2019;13(4):933–944.

Assaf Y, Pasternak O. Diffusion tensor imaging (DTI)-based white matter mapping in brain research: a review. J Mol Neurosci. 2008;34(1):51-61.

Avants BB, Epstein CL, Grossman M, Gee JC. Symmetric diffeomorphic image registration with cross-correlation: Evaluating automated labeling of elderly and neurodegenerative brain. Med Image Anal. 2008;12(2008):26-41.

Baggio HC, Abos A, Segura B, Campabadal A, Garcia-Diaz A, Uribe C, et al. Statistical inference in brain graphs using threshold-free network-based statistics. Hum Brain Mapp. 2018;39(6):2289–2302.

Baggio HC, Segura B, Sala-Llonch R, Marti MJ, Valldeoriola F, Compta Y, et al. Cognitive impairment and resting-state network connectivity in Parkinson's disease. Hum Brain Mapp. 2015;36(1):199–212.

Baggio HC, Sala-Llonch R, Segura B, Marti MJ, Valldeoriola F, Compta Y, et al. Functional brain networks and cognitive deficits in Parkinson's disease. Hum Brain Mapp. 2014;35(9):4620–4634.

Baiano C, Barone P, Trojano L, Santangelo G. Prevalence and clinical aspects of mild cognitive impairment in Parkinson's disease: A meta-analysis. Mov Disord. 2019; 35 (1) : 45–54.

Ballmaier M, O'Brien JT, Burton EJ, Thompson PM, Rex DE, Narr KL, et al. Comparing gray matter loss profiles between dementia with Lewy bodies and Alzheimer's disease using cortical pattern matching: Diagnosis and gender effects. Neuroimage. 2004; 23 (1) : 325–335.

Barbagallo G, Caligiuri ME, Arabia G, Cherubini A, Lupo A, Nisticò R, et al. Structural connectivity differences in motor network between tremor-dominant and nontremor Parkinson's disease. Hum Brain Mapp. 2017;38(9):4716–4729.

Barnes J, David AS. Visual hallucinations in Parkinson's disease: a review and phenomenological survey. J Neurol Neurosurg Psychiatry. 2001;70(6):727-733.

Basser PJ, Mattiello J, LeBihan D. MR diffusion tensor spectroscopy and imaging. Biophys J. 1994;66(1):259–267.

Beck A, Steer R, Brown G. Manual for the Beck Depression Inventory-II. Psychological Corporation, San Antonio, Texas. 1996.

Behrens TEJ, Berg HJ, Jbabdi S, Rushworth MFS, Woolrich MW. Probabilistic diffusion tractography with multiple fibre orientations: What can we gain? Neuroimage. 2007;34(1):144–155.

Behrens TEJ, Woolrich MW, Jenkinson M, Johansen-Berg H, Nunes RG, Clare S, et al. Characterization and Propagation of Uncertainty in Diffusion-Weighted MR Imaging. Magn Reson Med. 2003;50(5):1077–1088.

Belvisi D, Fabbrini A, De Bartolo MI, Costanzo M, Manzo N, Fabbrini G, et al. The Pathophysiological Correlates of Parkinson's Disease Clinical Subtypes. Mov Disord. 2021;36(2):370–379.

Bennet IJ, Madden DJ. Disconnected aging: cerebral white matter integrity and age-related differences in cognition. Neuroscience. 2014;12(276):187-205.

Benton A, Sivan A, Hamsher K. Contributions to neuropsychological assessment. A clinical manual. 2nd ed. New York. 1994.

Benton A, Varney N, Hamsher K. Visuospatial judgment. A clinical test.

Arch Neurol. 1978;364–367.

Blamire AM. MR approaches in neurodegenerative disorders. Prog Nucl Magn Reson Spectrosc. 2018;108:1-16.

Blanc F, Colloby SJ, Cretin B, De Sousa PL, Demuynck C, O'Brien JT, et al. Grey matter atrophy in prodromal stage of dementia with Lewy bodies and Alzheimer's disease. Alzheimer's Res Ther. 2016;8(1).

Boot BP. Comprehensive treatment of dementia with Lewy bodies. Alzheimer's Res Ther. 2015;7(1):1–8.

Braak H, Del Tredici K. Cortico-basal ganglia-cortical circuitry in Parkinson's disease reconsidered. Exp Neurol. 2008;212(1):226-229.

Braak H, Rüb U, Schultz C, Del Tredici K. Vulnerability of cortical neurons to Alzheimer's and Parkinson's diseases. J Alzheimers Dis. 2006a;9:35-44.

Braak H, Rüb U, Del Tredici K. Cognitive decline correlates with neuropathological stage in Parkinson's disease. J Neurol Sci. 2006b;248(1-2):255-258.

Braak H, Del Tredici K, Rüb U, De Vos RAI, Jansen Steur ENH, Braak E. Staging of brain pathology related to sporadic Parkinson's disease. Neurobiol Aging. 2003;24(2):197–211.

Breiman, L. Random Forests. Mach Learn. 2001; 45: 5–32.

Breiman L. Bagging Predictors. Mach Learn. 1996;24(123–140).

Burn DJ, Landau S, Hindle J V., Samuel M, Wilson KC, Hurt CS, et al. Parkinson's disease motor subtypes and mood. Mov Disord. 2012;27(3):379–386.

Caminiti SP, Sala A, Iaccarino L, Beretta L, Pilotto A, Gianolli L, et al. Brain glucose metabolism in Lewy body dementia: Implications for diagnostic criteria. Alzheimer's Res Ther. 2019;11(1):1–14.

Chabran E, Noblet V, Loureiro De Sousa P, Demuynck C, Philippi N, Mutter C, et al. Changes in gray matter volume and functional connectivity in dementia with Lewy bodies compared to Alzheimer's disease and normal aging: Implications for fluctuations. Alzheimer's Res Ther. 2020;12(1):1–13.

Chen NK, Chou YH, Sundman M, Hickey P, Kasoff WS, Bernstein A, et al. Alteration of Diffusion-Tensor Magnetic Resonance Imaging Measures in Brain Regions Involved in Early Stages of Parkinson's Disease. Brain Connect. 2018;8(6):343–349.

Christopher L, Strafella AP. Neuroimaging of brain changes associated with cognitive impairment in Parkinson's disease. J Neuropsychol. 2013 ; 7 (2) : 225-240.

Cochrane CJ, Ebmeier KP. Diffusion tensor imaging in parkinsonian syndromes: a systematic review and meta-analysis. Neurology. 2013;80(9):857-64.

Colloby SJ, Watson R, Blamire AM, O'Brien JT, Taylor JP. Cortical thinning in dementia with Lewy bodies and Parkinson disease dementia. Aust N Z J Psychiatry. 2020;54(6):633–643.

Colloby SJ, Elder GJ, Rabee R, O'Brien JT, Taylor JP. Structural grey matter changes in the substantia innominata in Alzheimer's disease and dementia with Lewy bodies: a DARTEL-VBM study. Int J Geriatr Psychiatry. 2017;32(6):615-623.

Connolly BS, Lang AE. Pharmacological treatment of Parkinson disease: a review. JAMA. 2014; 311(16):1670-83.

Cummings J.L, Mega M, Gray K, Rosenberg-Thompson S, Carusi D.A, Gornbein J. The Neuropsychiatric Inventory: comprehensive assessment of psychopathology in dementia. Neurology. 1994; 44, 2308–2314.

De Schipper LJ, Hafkemeijer A, Van Der Grond J, Marinus J, Henselmans JML, Van Hilten JJ. Regional Structural Hippocampal Differences between Dementia with Lewy Bodies and Parkinson's Disease. J Parkinsons Dis. 2019;9(4):775–783.

Desikan RS, Ségonne F, Fischl B, Quinn BT, Dickerson BC, Blacker D, et al. An automated labeling system for subdividing the human cerebral cortex on MRI scans into gyral based regions of interest. Neuroimage. 2006;31(3):968-980.

Díez-Cirarda M, Strafella AP, Kim J, Peña J, Ojeda N, Cabrera-Zubizarretad A, et al. NeuroImage : Clinical Dynamic functional connectivity in Parkinson ' s disease patients with mild cognitive impairment and normal cognition. NeuroImage Clin. 2018;17:847–855.

Díez-Cirarda M, Ojeda N, Peña J, Cabrera-Zubizarreta A, Gómez-Beldarrain MÁ, Gómez-Esteban JC, Ibarretxe-Bilbao N. Neuroanatomical Correlates of Theory of Mind Deficit in Parkinson's Disease: A Multimodal Imaging Study. PLoS One. 2015;10(11):e0142234.

Do J, McKinney C, Sharma P, Sidransky E. Glucocerebrosidase and its relevance to Parkinson disease. Mol Neurodegener. 2019;14(1):1–16.

Doty RL. The Smell Identification Test. Administration Manual, 3rd ed. Sensonics, Haddon Hts. 1995.

Douaud G, Smith S, Jenkinson M, Behrens T, Johansen-Berg H, Vickers J, James S, Voets N, Watkins K, Matthews P.M, James A. Anatomically related grey and white matter abnormalities in adolescent-onset schizophrenia. Brain. 2007; 130: 2375–2386.

Dujardin K, Leentjens AFG, Langlois C, Moonen AJH, Duits AA, Carette AS, et al. The spectrum of cognitive disorders in Parkinson's disease: A data-driven approach. Mov Disord. 2013;28(2):183–189.

Dujardin K, Defebvre L, Duhamel A, Lecouffe P, Rogelet P, Steinling M, et al. Cognitive and SPECT characteristics predict progression of Parkinson's disease in newly diagnosed patients. J Neurol. 2004;251(11):1383–1392.

Duncan GW, Firbank MJ, Yarnall AJ, Khoo TK, Brooks DJ, Barker RA, et al. Gray and white matter imaging: A biomarker for cognitive impairment in early Parkinson's disease? Mov Disord. 2016;31(1):103–110.

Elder GJ, Mactier K, Colloby SJ, Watson R, Blamire AM, O'Brien JT, et al. The

influence of hippocampal atrophy on the cognitive phenotype of dementia with Lewy bodies. Int J Geriatr Psychiatry. 2017;32(11):1182–1189.

Erro R, Picillo M, Vitale C, Palladino R, Amboni M, Moccia M, et al. Clinical clusters and dopaminergic dysfunction in de-novo Parkinson disease. Park Relat Disord. 2016;28:137–140.

Erro R, Vitale C, Amboni M, Picillo M, Moccia M, Longo K, et al. The heterogeneity of early Parkinson's disease: a cluster analysis on newly diagnosed untreated patients. PLoS One. 2013, 8(8).

Fahn S, Elton R. UPDRS Program Member Unified Parkinson's Disease Rating Scale, Scale, in: Fahn, S, Marsden, CD, Goldstein, M, Calne, D. (Ed.). Recent Developments in Parkinson's Disease, Vol 2. Macmillan Health Care Information, Florham Park N, editor. 1987. 153-163,293-304.

Feczko E, Miranda-Dominguez O, Marr M, Graham AM, Nigg JT, Fair DA. The Heterogeneity Problem: Approaches to Identify Psychiatric Subtypes. Trends Cogn Sci. 2019;23(7):584–601.

Felleman DJ, Van Essen DC. Distributed hierarchical processing in the primate cerebral cortex. Cereb Cortex. 1991;1(1):1-47.

Fénelon G, Mahieux F, Huon R, Ziégler M. Hallucinations in Parkinson's disease: Prevalence, phenomenology and risk factors. Brain. 2000;123(4):733–745.

Fereshtehnejad SM, Zeighami Y, Dagher A, Postuma RB. Clinical criteria for subtyping Parkinson's disease: biomarkers and longitudinal progression. Brain. 2017 ; 140(7) : 1959-1976.

Fereshtehnejad S, Romenets SR, Anang JBM, Latreille V, Gagnon J, Postuma RB. New Clinical Subtypes of Parkinson Disease and Their Longitudinal Progression: A Prospective Cohort Comparison With Other Phenotypes. JAMA Neurol. 2015;72(8):863–873.

Fereshtehnejad SM, Hadizadeh H, Farhadi F, Shahidi GA, Delbari A, Lökk J. Comparison of the Psychological Symptoms and Disease-Specific Quality of Life between Early- and Typical-Onset Parkinson's Disease Patients. Parkinsons Dis. 2014;2014:819260.

Ferguson LW, Rajput AH, Rajput A. Early-onset vs. Late-onset Parkinson's disease: A Clinical-pathological Study. Can J Neurol Sci. 2015;43(1):113–119.

Ferreira D, Nedelska Z, Graff-Radford J, Przybelski SA, Lesnick TG, Schwarz CG, et al. Cerebrovascular disease, neurodegeneration, and clinical phenotype in dementia with Lewy bodies. Neurobiol Aging. 2021; 105: 252-261.

Ferreira D, Przybelski SA, Lesnick TG, Lemstra AW, Londos E, Blanc F, et al. β-Amyloid and tau biomarkers and clinical phenotype in dementia with Lewy bodies. Neurology. 2020a;95(24):e3257-e3268.

Ferreira D, Nordberg A, Westman E. Biological subtypes of Alzheimer disease: A systematic review and meta-

analysis. Neurology. 2020b;94(10):436-448.

Ferreira D, Pereira JB, Volpe G, Westman E. Subtypes of Alzheimer's disease display distinct network abnormalities extending beyond their pattern of atrophy. Front Neurol. 2019; 28;10:524.

Ferreira D, Verhagen C, Hernández-Cabrera JA, Cavallin L, Guo CJ, Ekman U, et al. Distinct subtypes of Alzheimer's disease based on patterns of brain atrophy: Longitudinal trajectories and clinical applications. Sci Rep. 2017;7:1–13.

Fiorenzato E, Strafella AP, Kim J, Schifano R, Weis L, Antonini A, et al. Dynamic functional connectivity changes associated with dementia in Parkinson's disease. Brain. 2019;142(9):2860–2872.

Fischl B, Dale AM. Measuring the thickness of the human cerebral cortex from magnetic resonance images. Proc Natl Acad Sci U S A. 2000;97(20):11050-5.

Folstein MF, Folstein SE, McHugh PR. "Mini-mental state". A practical method for grading the cognitive state of patients for the clinician. J. Psychiatr. Res. 1975; 12, 189–198.

Forsaa EB, Larsen JP, Wentzel-Larsen T, Goetz CG, Stebbins GT, Aarsland D, et al. A 12-year population-based study of psychosis in Parkinson disease. Arch Neurol. 2010;67(8):996–1001.

Franciotti R, Falasca NW, Bonanni L, Anzellotti F, Maruotti V, Comani S, et al. Default network is not hypoactive in dementia with fluctuating cognition: An Alzheimer disease/dementia with Lewy bodies comparison. Neurobiol Aging. 2013; 34(4):1148–1158.

Frauscher B, Ehrmann L, Zamarian L, Auer F, Mitterling T, Gabelia D, et al. Validation of the Innsbruck REM sleep behavior disorder inventory. Mov Disord. 2012;27:1673–1678.

Galantucci S, Agosta F, Stefanova E, Basaia S, Heuvel MP van den, Stojkovic T, et al. Structural Brain Connectome. Radiology. 2017;283(2):515-525.

Gama RL, Bruin VMS, Távora DGF, Duran FLS, Bittencourt L, Tufik S. Structural brain abnormalities in patients with Parkinson's disease with visual hallucinations: A comparative voxel-based analysis. Brain Cogn. 2014;87(1):97–103.

Gandhi PN, Chen SG, Wilson-Delfosse AL. Leucine-rich repeat kinase 2 (LRRK2): a key player in the pathogenesis of Parkinson's disease. J Neurosci Res. 2009;87(6):1283-95.

Garcia-Diaz AI, Segura B, Baggio HC, Uribe C, Campabadal A, Abos A, et al. Cortical thinning correlates of changes in visuospatial and visuoperceptual performance in Parkinson's disease: A 4-year follow-up. Park Relat Disord. 2018;46:62–8.

Gasca-Salas C, García-Lorenzo D, Garcia-Garcia D, Clavero P, Obeso JA, Lehericy S, et al. Parkinson's disease with mild cognitive impairment: severe cortical thinning antedates dementia. Brain Imaging Behav. 2019;13(1):180–8.

Gibb WR, Lees AJ. The relevance of the Lewy body to the pathogenesis of idiopathic Parkinson's disease. J Neurol Neurosurg Psychiatry. 1988;51(6):745-52.

Goedert M. Alzheimer's and Parkinson's diseases: The prion concept in relation to assembled Aβ, tau, and α-synuclein. Science. 2015; 349(6248): 61-69.

Goetz CG. The history of Parkinson's disease: Early clinical descriptions and neurological therapies. Cold Spring Harb Perspect Med. 2011;1(1):1–16.

Goker-Alpan O, Schiffmann R, LaMarca ME, Nussbaum RL, McInerney-Leo A, Sidransky E. Parkinsonism among Gaucher disease carriers. J Med Genet. 2004;41(12):937–40.

Good C.D, Johnsrude I.S, Ashburner J, Henson R.N.A, Friston K.J, Frackowiak R.S.J, A voxel-based morphometric study of ageing in 465 normal adult human brains. Neuroimage. 2001;14: 21–36.

Graff-Radford J, Lesnick TG, Boeve BF, Przybelski SA, Jones DT, Senjem ML, et al. Predicting Survival in Dementia With Lewy Bodies With Hippocampal Volumetry. Mov Disord. 2016;31(7):989-994.

Guimarães RP, Campos BM, de Rezende TJ, Piovesana L, Azevedo PC, Amato-Filho AC, et al. Is diffusion tensor imaging a good biomarker for early Parkinson's disease? Front Neurol. 2018;9:1–8.

Guo T, Guan X, Zhou C, Gao T, Wu J, Song Z, et al. Clinically relevant connectivity features define three subtypes of Parkinson's disease patients. Hum Brain Mapp. 2020;41(14):4077–4092.

Habes M, Grothe MJ, Tunc B, McMillan C, Wolk DA, Davatzikos C. Disentangling Heterogeneity in Alzheimer's Disease and Related Dementias Using Data-Driven Methods. Biol Psychiatry. 2020;88(1):70-82.

Hagmann P, Kurant M, Gigandet X, Thiran P, Wedeen VJ, Meuli R, et al. Mapping human whole-brain structural networks with diffusion MRI. PLoS One. 2007;2(7).

Halliday G, Hely M, Reid W, Morris J. The progression of pathology in longitudinally followed patients with Parkinson's disease. Acta Neuropathol. 2008; 115: 409–415.

Hastie T, Tibshirani R, Friedman J. The elements of statistical learning: data mining, inference, and prediction. 2017.

Hattori T, Orimo S, Aoki S, Ito K, Abe O, Amano A, et al. Cognitive status correlates with white matter alteration in Parkinson's disease. Hum Brain Mapp. 2012;33(3):727–739.

Hoehn MM, Yahr MD. Parkinsonism: Onset, progression, and mortality. Neurology. 1967; 17: 427–442.

Hou Y, Dan X, Babbar M, Wei Y, Hasselbalch SG, Croteau DL, et al. Ageing as a risk factor for neurodegenerative disease. Nat Rev Neurol. 2019;15(10):565–81.

Hummel T, Kobal G, Gudziol H, Mackay-Sim A. Normative data for the "Sniffin'' Sticks" including tests of odor identification, odor discrimination, and

olfactory thresholds: An upgrade based on a group of more than 3,000 subjects. Eur Arch Oto-Rhino-Laryngology. 2007;264:237–243.

Ibarretxe-Bilbao N, Junque C, Marti MJ, Tolosa E. Cerebral basis of visual hallucinations in Parkinson's disease: Structural and functional MRI studies. J Neurol Sci. 2011;310(1–2):79–81.

Ibarretxe-Bilbao N, Ramirez-Ruiz B, Junque C, Marti MJ, Valldeoriola F, Bargallo N, et al. Differential progression of brain atrophy in Parkinson's disease with and without visual hallucinations. J Neurol Neurosurg Psychiatry. 2010;81(6):650-657.

Ibarretxe-Bilbao N, Ramírez-Ruiz B, Tolosa E, Martí MJ, Valldeoriola F, Bargalló N, et al. Hippocampal head atrophy predominance in Parkinson's disease with hallucinations and with dementia. J Neurol. 2008; 255(9):1324–31.

Irwin DJ, Lee VM, Trojanowski JQ. Parkinson's disease dementia: convergence of α-synuclein, tau and amyloid-β pathologies. Nat Rev Neurosci. 2013;14(9):626–636.

Jack CR, Bennett DA, Blennow K, Carrillo MC, Dunn B, Haeberlein SB, et al. NIA-AA Research Framework: Toward a biological definition of Alzheimer's disease. Alzheimer's Dement. 2018;14(4):535–62.

Jankovic J, Tan EK. Parkinson's disease: etiopathogenesis and treatment. J Neurol Neurosurg Psychiatry. 2020;91(8):795–808.

Jankovic J, Kapadia AS. Functional decline in Parkinson disease. Arch Neurol. 2001;58(10):1611–5.

Jankovic J, McDermott M, Carter J, Gauthier S, Goetz C, Golbe L, et al. Variable expression of Parkinson's disease: A base-line analysis of the DATATOP cohort. The Parkinson Study Group. Neurol. 1990; 40(10): 1529-1534.

Jbabdi S, Sotiropoulos SN, Savio AM, Graña M, Behrens TE. Model-based analysis of multishell diffusion MR data for tractography: how to get over fitting problems. Magn Reson Med. 2012;68(6):1846-1855.

Jellinger KA. Dementia with Lewy bodies and Parkinson's disease-dementia: current concepts and controversies. Journal of Neural Transmission. Springer Vienna; 2018 (125): 615–650

Jellinger KA. A critical evaluation of current staging of alpha-synuclein pathology in Lewy body disorders. Biochim Biophys Acta. 2009;1792(7):730-740.

Jellinger KA. A critical reappraisal of current staging of Lewy-related pathology in human brain. Acta Neuropathol. 2008;116(1):1-16.

Jellinger KA. Lewy body-related alpha-synucleinopathy in the aged human brain. J Neural Transm. 2004;111(10-11):1219-35.

Jenkinson M, Bannister P, Brady M, Smith S. Improved optimization for the robust and accurate linear registration

and motion correction of brain images. Neuroimage. 2002;17: 825–841.

Jeon S, Kang JM, Seo S, Jeong HJ, Funck T, Lee SY, et al. Topographical Heterogeneity of Alzheimer's Disease Based on MR Imaging, Tau PET, and Amyloid PET. Front Aging Neurosci. 2019;11:211.

Joki H, Higashiyama Y, Nakae Y, Kugimoto C, Doi H, Kimura K, et al. White matter hyperintensities on MRI in dementia with Lewy bodies, Parkinson's disease with dementia, and Alzheimer's disease. J Neurol Sci 2018;385: 99–104.

Kalia LV, Lang AE. Parkinson's disease. Lancet. 2015; 386 (9996): 896–912.

Kandiah N, Zainal NH, Narasimhalu K, Chander RJ, Ng A, Mak E, et al. Hippocampal volume and white matter disease in the prediction of dementia in Parkinson's disease. Park Relat Disord. 2014;20(11):1203–8.

Kantarci K, Lowe VJ, Boeve BF, Senjem ML, Tosakulwong N, Lesnick TG, et al. AV-1451 tau and β-amyloid positron emission tomography imaging in dementia with Lewy bodies. Ann Neurol. 2017;81(1):58-67.

Kantarci K, Ferman TJ, Boeve BF, Weigand SD, Przybelski S, Vemuri P, et al. Focal atrophy on MRI and neuropathologic classification of dementia with Lewy bodies. Neurology. 2012;79(6):553-560.

Kaplan E, Goodglass H, Weintraub S. Boston Naming Test, in: The Corsini Encyclopedia of Psychology. John Wiley & Sons, Inc., Hoboken, NJ, USA. 1983.

Kemp J, Philippi N, Phillipps C, Demuynck C, Albasser T, Martin-Hunyadi C, et al. Cognitive profile in prodromal dementia with Lewy bodies. Alzheimer's Res Ther. 2017;9(1):1–10.

Kim R, Shin JH, Park S, Kim HJ, Jeon B. Longitudinal evolution of non-motor symptoms according to age at onset in early Parkinson's disease. J Neurol Sci. 2020;418: 117157.

Kosaka K. Lewy body disease and dementia with Lewy bodies. Proc Jpn Acad Ser B Phys Biol Sci. 2014;90(8):301-6.

Koshimori Y, Segura B, Christopher L, Lobaugh N, Duff-Canning S, Mizrahi R, et al. Imaging changes associated with cognitive abnormalities in Parkinson's disease. Brain Struct Funct. 2015;220(4):2249–61.

Krajcovicova L, Klobusiakova P, Rektorova I. Gray Matter Changes in Parkinson's and Alzheimer's Disease and Relation to Cognition. Curr Neurol Neurosci Rep. 2019;19(11).

Kumru H, Santamaria J, Tolosa E, Iranzo A. Relation between subtype of Parkinson's disease and REM sleep behavior disorder. Sleep Med. 2007;8(7–8):779–783.

Labbé C, Heckman MG, Lorenzo-Betancor O, Soto-Ortolaza AI, Walton RL, Murray ME, et al. MAPT haplotype H1G is associated with increased risk of dementia with Lewy bodies. Alzheimers Dement. 2016;12(12):1297-1304.

Labelle DR, Walsh RR, Banks SJ. Latent Cognitive Phenotypes in De Novo

Parkinson's Disease: A Person-Centered Approach. 2017;23(7):551–563.

Langley J, Huddleston DE, Merritt M, Chen X, McMurray R, Silver M, et al. Diffusion tensor imaging of the substantia nigra in Parkinson's disease revisited. Hum Brain Mapp. 2016;37(7):2547–2556.

Lawn T, ffytche D. Cerebellar correlates of visual hallucinations in Parkinson's disease and Charles Bonnet Syndrome. Cortex.2021;135:311–25.

Lawton M, Ben-Shlomo Y, May MT, Baig F, Barber TR, Klein JC, et al. Developing and validating Parkinson's disease subtypes and their motor and cognitive progression. J Neurol Neurosurg Psychiatry. 2018; 89(12):1279–1287.

Lee MH, Smyser CD, Shimony JS. Resting-state fMRI: a review of methods and clinical applications. AJNR Am J Neuroradiol. 2013;34(10):1866-1872.

Lenka A, Ingalhalikar M, Shah A, Saini J, Arumugham SS, Hegde S, et al. Hippocampal subfield atrophy in patients with Parkinson's disease and psychosis. J Neural Transm. 2018;125(9):1361–72.

Levin J, Kurz A, Arzberger T, Giese A, Höglinger GU. The Differential Diagnosis and Treatment of Atypical Parkinsonism. Dtsch Arztebl Int. 2016;113(5):61-9.

Levy G, Jacobs DM, Tang MX, Côté LJ, Louis ED, Alfaro B, et al. Memory and executive function impairment predict dementia in Parkinson's disease. Mov Disord. 2002;17(6):1221-1226.

Lewis SJG, Foltynie T, Blackwell AD, Robbins TW, Owen AM, Barker RA. Heterogeneity of Parkinson's disease in the early clinical stages using a data driven approach. J Neurol Neurosurg Psychiatry. 2005; 76(3):343–348.

Lezak, M.D. Neuropsychological assessment. Oxford University Press. 2012.

Li C, Huang B, Zhang R, Ma Q, Yang W, Wang L, et al. Impaired topological architecture of brain structural networks in idiopathic Parkinson's disease: a DTI study. Brain Imaging Behav. 2016;11(1):113–128.

Li Y, Liu Y, Li J, Qin W, Li K, Yu C, et al. Brain anatomical network and intelligence. PLoS Comput Biol. 2009;5(5).

Litvan I, Goldman JG, Tröster AI, Schmand BA, Weintraub D, Petersen RC, et al. Diagnostic criteria for mild cognitive impairment in Parkinson's disease: Movement Disorder Society Task Force guidelines. Mov Disord. 2012;27(3):349–356.

Litvan I, Aarsland D, Adler CH, Goldman JG, Kulisevsky J, Mollenhauer B, et al. MDS Task Force on mild cognitive impairment in Parkinson's disease: critical review of PD-MCI. Mov Disord. 2011;26(10):1814-24.

Lopes R, Delmaire C, Defebvre L, Moonen AJ, Duits AA, Hofman P, et al. Cognitive phenotypes in parkinson's disease differ in terms of brain-network organization and connectivity. Hum Brain Mapp. 2017; 38(3):1604–1621.

Lopez OL, Kuller LH. Epidemiology of aging and associated cognitive

disorders: Prevalence and incidence of Alzheimer's disease and other dementias. 1st ed. Handbook of Clinical Neurology. Elsevier B.V.; 2019; 167:139–148.

Lowther ER, O'Brien JT, Firbank MJ, Blamire AM. Lewy body compared with Alzheimer dementia is associated with decreased functional connectivity in resting state networks. Psychiatry Res – Neuroimaging. 2014;223(3):192–201.

Lücking CB, Dürr A, Bonifati V, Vaughan J, De Michele G, Gasser T, et al. Parkinson's Disease Genetics Study Group; European Consortium on Genetic Susceptibility in Parkinson's Disease. Association between early-onset Parkinson's disease and mutations in the parkin gene. N Engl J Med. 2000. 25;342(21):1560-1567.

Mahale R, Yadav R, Pal PK. Quality of sleep in young onset Parkinson's disease: Any difference from older onset Parkinson's disease. Park Relat Disord. 2015;21(5):461–464.

Mak E, Zhou J, Tan LCS, Au WL, Sitoh YY, Kandiah N. Cognitive deficits in mild Parkinson's disease are associated with distinct areas of grey matter atrophy. J Neurol Neurosurg Psychiatry. 2014a;85(5):576–580.

Mak E, Bergsland N, Dwyer MG, Zivadinov R, Kandiah N. Subcortical Atrophy Is Associated with Cognitive Impairment in Mild Parkinson Disease: A Combined Investigation of Volumetric Changes, Cortical Thickness, and Vertex-Based Shape Analysis. Am J Neuroradiol. 2014b; 35 (12): 2257–2264.

Matar E, Shine JM, Halliday GM, Lewis SJG. Cognitive fluctuations in Lewy body dementia: Towards a pathophysiological framework. Brain. 2020;143(1):31–46.

McKeith IG, Boeve BF, Dickson DW, Halliday G, Taylor JP, Weintraub D, et al. Diagnosis and management of dementia with Lewy bodies: Fourth consensus report of the DLB Consortium. Neurology. 2017 ;89(1):88-100.

Mckeith IG, Dickson DW, Lowe J, Emre M, O'Brien JT, Feldman H, et al. Diagnosis and management of dementia with Lewy bodies Third report of the DLB consortium. 2005; 65(12): 1863-1872.

McKinlay A, Grace RC, Dalrymple-Alford JC, Anderson T, Fink J, Roger D. A profile of neuropsychiatric problems and their relationship to quality of life for Parkinson's disease patients without dementia. Park Relat Disord. 2008;14(1):37–42.

Medaglia JD, Bassett DS. Network Analyses and Nervous System Disorders. Oxford Res Encycl Neurosci. 2018;1–43.

Mehra S, Sahay S, Maji SK. α-Synuclein misfolding and aggregation: Implications in Parkinson's disease pathogenesis. Biochim Biophys Acta Proteins Proteom. 2019;1867(10):890-908.

Melzer TR, Watts R, MacAskill MR, Pitcher TL, Livingston L, Keenan RJ, et al. White matter microstructure deteriorates across cognitive stages in Parkinson disease. Neurology. 2013; 80(20):1841–1849.

Melzer TR, Watts R, MacAskill MR, Pitcher TL, Livingston L, Keenan RJ, et al. Grey matter atrophy in cognitively impaired Parkinson's disease. J Neurol Neurosurg Psychiatry. 2012;83(2):188–194.

Mihaescu AS, Masellis M, Graff-Guerrero A, Kim J, Criaud M, Cho SS, et al. Brain degeneration in Parkinson's disease patients with cognitive decline: a coordinate-based meta-analysis. Brain Imaging Behav. 2019;13(4):1021–1034.

Mishra VR, Sreenivasan KR, Yang Z, Zhuang X, Cordes D, Mari Z, et al. Unique white matter structural connectivity in early-stage drug-naive Parkinson disease. Neurology. 2020;94(8):e774–784.

Montine T, Phelps C, Beach T, Bigio E, Cairns N, Dickson D, et al. National Institute on Aging-Alzheimer's Association guidelines for the neuropathologic assessment of Alzheimer's disease: a practical approach. Acta Neuropathol. 2012;123(1):1–11.

Morbelli S, Chincarini A, Brendel M, Rominger A, Bruffaerts R, Vandenberghe R, et al. Metabolic patterns across core features in dementia with lewy bodies. Ann Neurol. 2019;85(5):715–725.

Morenas-Rodríguez E, Sala I, Subirana A, Pascual-Goñi E, Sánchez-Saudinós MB, Alcolea D, et al. Clinical Subtypes of Dementia with Lewy Bodies Based on the Initial Clinical Presentation. J Alzheimer's Dis. 2018;64(2):505–513.

Mosimann UP, Rowan EN, Partington CE, Collerton D, Littlewood E, O'Brien JT, et al. Characteristics of visual hallucinations in Parkinson disease dementia and dementia with Lewy bodies. Am J Geriatr Psychiatry. 2006;14(2):153–160.

Mosimann UP, Mather G, Wesnes KA, O'Brien JT, Burn DJ, McKeith IG. Visual perception in Parkinson disease dementia and dementia with Lewy bodies. Neurology. 2004;63(11):2091–2096.

Moustafa AA, Chakravarthy S, Phillips JR, Gupta A, Keri S, Polner B, et al. Motor symptoms in Parkinson's disease: A unified framework. Neurosci Biobehav Rev. 2016; 68: 727–740.

Mukherjee P, Berman JI, Chung SW, Hess CP, Henry RG. Diffusion tensor MR imaging and fiber tractography: Theoretic underpinnings. Am J Neuroradiol. 2008;29(4):632–41.

Muller J, Alizadeh M, Mohamed FB, Riley J, Pearce JJ, Trieu B, et al. Clinically applicable delineation of the pallidal sensorimotor region in patients with advanced Parkinson's disease: Study of probabilistic and deterministic tractography. J Neurosurg. 2018;131(5):1520–1531.

Muslimović D, Post B, Speelman JD, Schmand B. Cognitive profile of patients with newly diagnosed Parkinson disease. Neurology. 2005;65(8):1239–1245.

Nedelska Z, Ferman TJ, Boeve BF, Przybelski SA, Lesnick TG, Murray ME, et al. Pattern of brain atrophy rates in autopsy-confirmed dementia with Lewy

bodies. Neurobiol Aging. 2015;36(1):452-461.

Nigro S, Riccelli R, Passamonti L, Arabia G, Morelli M, Nisticò R, et al. Characterizing structural neural networks in de novo Parkinson disease patients using diffusion tensor imaging. Hum Brain Mapp. 2016;37(12):4500–4510.

Noe E, Marder K, Bell KL, Jacobs DM, Manly JJ, Stern Y. Comparison of dementia with Lewy bodies to Alzheimer's disease and Parkinson's disease with dementia. Mov Disord. 2004;19(1):60–67.

Nutt JG. Motor subtype in Parkinson's disease: Different disorders or different stages of disease? Mov Disord. 2016;31(7):957–961.

Obeso JA, Stamelou M, Goetz CG, Poewe W, Lang AE, Weintraub D, Past, present, and future of Parkinson's disease: A special essay on the 200th Anniversary of the Shaking Palsy. Mov Disord. 2017;32(9):1264-1310.

Oda H, Yamamoto Y, Maeda K. Neuropsychological profile of dementia with Lewy bodies. Psychogeriatrics. 2009;9(2):85–90.

Oppedal K, Ferreira D, Cavallin L, Lemstra AW, ten Kate M, Padovani A, et al. A signature pattern of cortical atrophy in dementia with Lewy bodies: A study on 333 patients from the European DLB consortium. Alzheimer's Dement. 2019;15(3):400–409.

Ota M, Nakata Y, Ito K, Kamiya K, Ogawa M, Murata M, Obu S, et al. Differential diagnosis tool for parkinsonian syndrome using multiple structural brain measures. Comput Math Methods Med. 2013;2013:571289.

Pagano G, Niccolini F, Politis M. Imaging in Parkinson's disease. Clin Med. 2016;16(4):371-5.

Pagonabarraga J, Martinez-Horta S, Fernández de Bobadilla R, Pérez J, Ribosa-Nogué R, Marín J, et al. Minor hallucinations occur in drug-naive Parkinson's disease patients, even from the premotor phase. Mov Disord. 2016;31(1):45–52.

Pedersen KF, Larsen JP, Tysnes OB, Alves G. Prognosis of mild cognitive impairment in early Parkinson disease: The Norwegian ParkWest study. JAMA Neurol. 2013;70(5):580–6.

Peraza LR, Kaiser M, Firbank M, Graziadio S, Bonanni L, Onofrj M, et al. fMRI resting state networks and their association with cognitive fluctuations in dementia with Lewy bodies. Neuroimage Clin. 2014;4:558-565.

Pereira JB, Hall S, Jalakas M, Grothe MJ, Strandberg O, Stomrud E, et al. Longitudinal degeneration of the basal forebrain predicts subsequent dementia in Parkinson's disease. Neurobiol Dis. 2020.

Pereira JB, Weintraub D, Brønnick K, Lebedev A, Westman E, Aarsland D. Initial cognitive decline is associated with cortical thinning in early Parkinson disease. Neurol. 2014; 82(22):2017-2025.

Peters R. Ageing and the brain. Postgrad Med J. 2006; 82(964):84-88.

Petrova M, Mehrabian-Spasova S, Aarsland D, Raycheva M, Traykov L. Clinical and Neuropsychological Differences between Mild Parkinson's Disease Dementia and Dementia with Lewy Bodies. Dement Geriatr Cogn Dis Extra. 2015;5(2):212–220.

Pezzoli S, Cagnin A, Antonini A, Venneri A. Frontal and subcortical contribution to visual hallucinations in dementia with Lewy bodies and Parkinson's disease. Postgrad Med. 2019;131(7):509-522.

Pfeiffer RF. Non-motor symptoms in Parkinson's disease. Parkinsonism Relat Disord. 2016; 22(1):S119-122.

Poewe W, Seppi K, Tanner CM, Halliday GM, Brundin P, Volkmann J, et al. Parkinson disease. Nat Rev Dis Prim. 2017;3:1–21.

Post B, Speelman JD, De Haan RJ. Clinical heterogeneity in newly diagnosed Parkinson's disease. J Neurol. 2008;255(5):716–722.

Postuma RB, Berg D, Stern M, Poewe W, Olanow CW, Oertel W, et al. MDS clinical diagnostic criteria for Parkinson's disease. Mov Disord. 2015;30(12):1591–1601.

Postuma RB, Bertrand J, Montplaisir J, Desjardins C. Rapid Eye Movement Sleep Behavior Disorder and Risk of Dementia in Parkinson ' s Disease : A Prospective Study. 2012;27(6):720–726.

Poulakis K, Ferreira D, Pereira JB, Smedby Ö, Vemuri P, Westman E. Fully bayesian longitudinal unsupervised learning for the assessment and visualization of AD heterogeneity and progression. Aging (Albany NY). 2020;12(13):12622-12647.

Poulakis K, Pereira JB, Mecocci P, Vellas B, Tsolaki M, Kłoszewska I, et al. Heterogeneous patterns of brain atrophy in Alzheimer's disease. Neurobiol Aging. 2018;65:98-108.

Ramírez-Ruiz B, Martí MJ, Tolosa E, Falcón C, Bargalló N, Valldeoriola F, Junque C. Brain response to complex visual stimuli in Parkinson's patients with hallucinations: A functional magnetic resonance imaging study. Mov Disord. 2008;23(16):2335–2343.

Ramírez-Ruiz B, Martí MJ, Tolosa E, Giménez M, Bargalló N, Valldeoriola F, Junque C. Cerebral atrophy in Parkinson's disease patients with visual hallucinations. Eur J Neurol. 2007;14(7):750–756.

Ravina B, Marder K, Fernandez HH, Friedman JH, McDonald W, Murphy D, et al. Diagnostic criteria for psychosis in Parkinson's disease: Report of an NINDS, NIMH Work Group. Mov Disord. 2007;22(8):1061–1068.

Reijnders JSAM, Ehrt U, Lousberg R, Aarsland D, Leentjens AFG. The association between motor subtypes and psychopathology in Parkinson's disease. Park Relat Disord. 2009;15(5):379–382.

Rektor I, Svátková A, Vojtíšek L, Zikmundová I, Vaníček J, Király A, et al. White matter alterations in Parkinson's disease with normal cognition precede grey matter atrophy. PLoS One. 2018;13(1).

Rosenberg-Katz K, Herman T, Jacob Y, Giladi N, Hendler T, Hausdorff JM. Gray matter atrophy distinguishes between Parkinson disease motor subtypes. Neurology. 2013;80(16):1476–1484.

Rubinov M, Sporns O. Complex network measures of brain connectivity: Uses and interpretations. Neuroimage. 2010; 52(3):1059–1069.

Saeed U, Compagnone J, Aviv RI, Strafella AP, Black SE, Lang AE, Masellis M. Imaging biomarkers in Parkinson's disease and Parkinsonian syndromes: current and emerging concepts. Transl Neurodegener. 2017;6:8.

Sanchez-Castaneda C, Rene R, Ramírez-Ruiz B, Campdelacreu J, Gascon J, Falcon C, Calopa M, Jauma S, Juncadella M, Junque C. Frontal and associative visual areas related to visual hallucinations in dementia with Lewy bodies and Parkinson's disease with dementia. Mov Disord. 2010;25(5):615-622.

Sanchez-Castaneda C, Rene R, Ramírez-Ruiz B, Campdelacreu J, Gascon J, Falcon C, et al. Correlations between gray matter reductions and cognitive deficits in Dementia with Lewy bodies and Parkinson's disease with dementia. Mov Disord. 2009;24(12):1740–1746.

Sasikumar S, Strafella AP. Imaging Mild Cognitive Impairment and Dementia in Parkinson's Disease. Front Neurol. 2020;11(47):1–8.

Schneider JA, Arvanitakis Z, Bang W, Bennett DA. Mixed brain pathologies account for most dementia cases in community-dwelling older persons. Neurology. 2007;69(24):2197-204.

Schrag A, Schott JM. Epidemiological, clinical, and genetic characteristics of early-onset parkinsonism. Lancet Neurol. 2006;5(4):355–363.

Schuff N, Wu IW, Buckley S, Foster ED, Coffey CS, Gitelman DR, et al. Diffusion imaging of nigral alterations in early Parkinson's disease with dopaminergic deficits. Mov Disord. 2015;30(14):1885–1892.

Schwarz CG, Gunter JL , Ward CP, Vemuri P, Senjem ML, Wiste HJ. The Mayo Clinic Adult Life Span Template: Better Quantification Across the Lifespan. Alzheimers Dement. 2017; 13:792.

Ségonne F, Pacheco J, Fischl B. Geometrically accurate topology-correction of cortical surfaces using nonseparating loops. IEEE Trans Med Imaging. 2007; 26 (4) : 518-529.

Segura B, Baggio HC, Marti MJ, Valldeoriola F, Compta Y, Garcia-Diaz AI, et al. Cortical thinning associated with mild cognitive impairment in Parkinson's disease. Mov Disord. 2014;29(12):1495–1503.

Serrano-Pozo A, Das S, Hyman BT. APOE and Alzheimer's disease: advances in genetics, pathophysiology, and therapeutic approaches. Lancet Neurol. 2021;20(1):68-80.

Sezgin M, Bilgic B, Tinaz S, Emre M. Parkinson's Disease Dementia and Lewy Body Disease. Semin Neurol. 2019;39(2):274–282.

Shah A, Lenka A, Saini J, Wagle S, Naduthota RM, Yadav R, et al. Altered Brain Wiring in Parkinson's Disease: A

Structural Connectome-Based Analysis. Brain Connect. 2017;7(6):347–356.

Sharman M, Valabregue R, Perlbarg V, Marrakchi-Kacem L, Vidailhet M, Benali H, et al. Parkinson's disease patients show reduced cortical-subcortical sensorimotor connectivity. Mov Disord. 2012;28(4):447–454.

Shi T, Horvath S. Unsupervised learning with random forest predictors. J Comput Graph Stat. 2006;15(1):118–138.

Shine JM, Muller AJ, O'Callaghan C, Hornberger M, Halliday GM, Lewis SJG. Abnormal connectivity between the default mode and the visual system underlies the manifestation of visual hallucinations in Parkinson's disease: A task-based fMRI study. Parkinsons Dis. 2015;1:150003.

Sieber B-A, Landis S, Koroshetz W, Bateman R, Siderowf A, Galpern WR, et al. Prioritized research recommendations from the National Institute of Neurological Disorders and Stroke Parkinson's Disease 2014 conference. Ann Neurol. 2014; 76: 469–472.

Simón-Sánchez J, Schulte C, Bras JM, Sharma M, Gibbs JR, Berg D, et al. Genome-wide association study reveals genetic risk underlying Parkinson's disease. Nat Genet. 2009;41(12):1308–1312.

Sled JG, Zijdenbos AP, Evans AC. A nonparametric method for automatic correction of intensity nonuniformity in MRI data. IEEE Trans Med Imaging. 1998;17(1):87-97.

Smirnov DS, Galasko D, Edland SD, Filoteo JV, Hansen LA, Salmon DP. Cognitive decline profiles differ in Parkinson disease dementia and dementia with Lewy bodies. Neurology. 2020.

Smith A. Symbol digit modalities test: Manual, 8th ed. Western Psychological Services, Los Angeles. 2000.

Smith SM, Jenkinson M, Johansen-Berg H, Rueckert D, Nichols TE, Mackay CE, Watkins KE, Ciccarelli O, Cader MZ, Matthews PM, Behrens TE. Tract-based spatial statistics: voxelwise analysis of multi-subject diffusion data. Neuroimage. 2006;31(4):1487-1505.

Sporns O. Structure and function of complex brain networks. Dialogues Clin Neurosci. 2013;15(3):247–262.

Starkstein S.E, Mayberg, H.S, Preziosi T.J, Andrezejewski P, Leiguarda R., Robinson R.G. Reliability, validity, and clinical correlates of apathy in Parkinson's disease. J. Neuropsychiatry Clin. Neurosci. 1992; 4:134–139.

Stebbins GT, Goetz GG, Carrillo MC, Bangen KJ, Turner DA, Glover GH, et al. Altered cortical visual processing in PD with hallucinations: An fMRI study. Neurology. 2004;63(8):1409–1416.

Strafella AP, Bohnen NI, Pavese N, Vaillancourt DE, van Eimeren T, Politis M, Tessitore A, et al. IPMDS-Neuroimaging Study Group. Imaging Markers of Progression in Parkinson's Disease. Mov Disord Clin Pract. 2018;5(6):586-596.

Stroop JR. Studies of interference in serial verbal reactions. J Exp Psychol. 1935;18(6):643–662.

Swann P, O'Brien JT. Management of visual hallucinations in dementia and Parkinson's disease. Int Psychogeriatrics. 2019;31(6):815–836.

Szeto JYY, O'Callaghan C, Shine JM, Walton CC, Mowszowski L, Naismith SL, et al. The relationships between mild cognitive impairment and phenotype in Parkinson's disease. Parkinsons Dis. 2015;1:1–7.

Theilmann RJ, Reed JD, Song DD, Huang MX, Lee RR, Litvan I, et al. White-matter changes correlate with cognitive functioning in Parkinson's disease. Front Neurol. 2013;4:1–10.

Tomlinson CL, Stowe R, Patel S, Rick C, Gray R, Clarke CE. Systematic review of levodopa dose equivalency reporting in Parkinson's disease. Mov Disord. 2010;25(15):2649–2653.

Uribe C, Segura B, Baggio HC, Abos A, Garcia-Diaz AI, Campabadal A, et al. Progression of Parkinson's disease patients' subtypes based on cortical thinning: 4-year follow-up. Park Relat Disord. 2019;64:286–292.

Uribe C, Segura B, Baggio HC, Abos A, Garcia-Diaz AI, Campabadal A, et al. Cortical atrophy patterns in early Parkinson's disease patients using hierarchical cluster analysis. Park Relat Disord. 2018;50:3–9.

Uribe C, Segura B, Baggio HC, Abos A, Marti MJ, Valldeoriola F, et al. Patterns of cortical thinning in nondemented Parkinson's disease patients. Mov Disord. 2016;31(5):699–708.

van den Heuvel MP, Hulshoff Pol HE. Exploring the brain network: a review on resting-state fMRI functional connectivity. Eur Neuropsychopharmacol. 2010; 20 (8) : 519-534.

van der Zande JJ, Steenwijk MD, ten Kate M, Wattjes MP, Scheltens P, Lemstra AW. Gray matter atrophy in dementia with Lewy bodies with and without concomitant Alzheimer's disease pathology. Neurobiol Aging. 2018;71:171–178.

Van Rooden SM, Colas F, Martínez-Martín P, Visser M, Verbaan D, Marinus J, et al. Clinical subtypes of Parkinson's disease. Mov Disord. 2011;26(1):51–58.

Van Rooden SM, Heiser WJ, Kok JN, Verbaan D, Van Hilten JJ, Marinus J. The identification of Parkinson's disease subtypes using cluster analysis: A systematic review. Mov Disord. 2010;25(8):969–978.

Vervoort G, Leunissen I, Firbank M, Heremans E, Nackaerts E, Vandenberghe W, et al. Structural brain alterations in motor subtypes of Parkinson's disease: Evidence from probabilistic tractography and shape analysis. PLoS One. 2016;11(6):1–17.

Wakana S, Caprihan A, Panzenboeck MM, Fallon JH, Perry M, Gollub RL, et al. Reproducibility of quantitative tractography methods applied to cerebral white matter. Neuroimage. 2007;36(3):630–44.

Walker Z, Possin KL, Boeve BF, Aarsland D. Lewy body dementias. Lancet. 2015;386(10004):1683–1697.

Wang L, Cheng W, Rolls ET, Dai F, Gong W, Du J, et al. Association of specific biotypes in patients with Parkinson disease and disease progression. Neurology. 2020;95(11):e1445–60.

Wang W, Mei M, Gao Y, Huang B, Qiu Y, Zhang Y, et al. Changes of brain structural network connection in Parkinson's disease patients with mild cognitive dysfunction: a study based on diffusion tensor imaging. J Neurol. 2019;267(4):933–943.

Watson R, Colloby SJ, Blamire AM, Wesnes KA, Wood J, O'Brien JT. Does attentional dysfunction and thalamic atrophy predict decline in dementia with Lewy bodies? Parkinsonism Relat Disord. 2017;45:69-74.

Watson R, Colloby SJ, Blamire AM, O'Brien JT. Subcortical volume changes in dementia with Lewy bodies and Alzheimer's disease. A comparison with healthy aging. Int Psychogeriatrics. 2016;28(4):529–536.

Watson R, Colloby SJ, Blamire AM, O'Brien JT. Assessment of regional gray matter loss in dementia with lewy bodies: A surface-Based MRI analysis. Am J Geriatr Psychiatry. 2015;23(1):38–46.

Watson R, O'Brien JT, Barber R, Blamire AM. Patterns of gray matter atrophy in dementia with Lewy bodies: A voxel-based morphometry study. Int Psychogeriatrics. 2012;24(4):532–540.

Watts DJ, Strogatz SH. Collective dynamics of 'small-world' networks. Nature. 1998;393(6684):440–442.

Wechsler, D. Escala de inteligencia de Weschler para adultos-III. TEA, Madrid. 1999.

Whitwell JL. Voxel-based morphometry: an automated technique for assessing structural changes in the brain. J Neurosci. 2009;29(31):9661-9664.

Whitwell JL, Weigand SD, Shiung MM, Boeve BF, Ferman TJ, Smith GE, et al. Focal atrophy in dementia with Lewy bodies on MRI: A distinct pattern from Alzheimer's disease. Brain. 2007;130(3):708–719.

Williams DR, Lees AJ. Visual hallucinations in the diagnosis of idiopathic Parkinson's disease: A retrospective autopsy study. Lancet Neurol. 2005;4(10):605–610.

Williams-Gray CH, Mason SL, Evans JR, Foltynie T, Brayne C, Robbins TW, et al. The CamPaIGN study of Parkinson's disease: 10-year outlook in an incident population-based cohort. J Neurol Neurosurg Psychiatry. 2013;84(11):1258–1264.

Williams-Gray CH, Foltynie T, Brayne CEG, Robbins TW, Barker RA. Evolution of cognitive dysfunction in an incident Parkinson's disease cohort. Brain. 2007;130(7):1787–1798.

Worker A, Blain C, Jarosz J, Chaudhuri KR, Barker GJ, Williams SCR, et al. Diffusion tensor imaging of Parkinson's disease, multiple system atrophy and progressive supranuclear palsy: A tract-

based spatial statistics study. PLoS One. 2014;9(11).

Yao N, Shek-Kwan Chang R, Cheung C, Pang S, Lau KK, Suckling J, et al. The default mode network is disrupted in parkinson's disease with visual hallucinations. Hum Brain Mapp. 2014;35(11):5658–5666.

Ye R, Touroutoglou A, Brickhouse M, Katz S, Growdon JH, Johnson KA, et al. Topography of cortical thinning in the Lewy body diseases. NeuroImage Clin. 2020;26.

Zalesky A, Fornito A, Bullmore ET. Network-based statistic: Identifying differences in brain networks. Neuroimage. 2010;53(4):1197–1207.

Zarei M, Ibarretxe-Bilbao N, Compta Y, Hough M, Junque C, Bargallo N, et al. Cortical thinning is associated with disease stages and dementia in Parkinson's disease. J Neurol Neurosurg Psychiatry. 2013;84(8):875–881.

Zhang PL, Chen Y, Zhang CH, Wang YX, Fernandez-Funez P. Genetics of Parkinson's disease and related disorders. J Med Genet. 2017;55(2):73–80.

Zhong JG, Pan PL, Dai ZY, Shi HC. Voxelwise meta-analysis of gray matter abnormalities in dementia with Lewy bodies. Eur J Radiol. 2014;83(10):1870–1874.

Universitat de Barcelona
2021